UNIVERSITÀ DEGLI STUDI DI PADOVA

DIPARTIMENTO DI INGEGNERIA INDUSTRIALE
Corso di laurea Magistrale in Ingegneria Energetica

Tesi di laurea Magistrale in
Ingegneria Energetica

Simulation and performance evaluation of single and double pressure ORC systems on board a LNG carrier including off-design and transient operation

Relatore: ***Prof. Andrea Lazzaretto***

Correlatori: ***Prof. Christos A. Frangopoulos***

Ph.D. Sergio Rech

Laureando: ***Simone Zandarin***

ANNO ACCADEMICO 2014 – 2015

SOMMARIO

La propulsione di grandi navi è solitamente di tipo elettrico per avere libertà di posizionamento del motore a combustione interna (ICE, Internal Combustion Engine), riduzione di rumorosità, volume e peso della nave. Inoltre questo tipo di navi viaggia per lunghi periodi a velocità costante, di conseguenza il motore/i motori a combustione interna operano per lunghi periodi a carico costante. Con queste premesse risulta particolarmente interessante l'installazione a bordo di sistemi ORC (Organic Rankine Cycle) per la generazione di potenza elettrica addizionale e la conseguente riduzione del consumo di combustibile. Il progetto del sistema a ciclo combinato ICE-ORC deve essere effettuato in modo proprio al fine di massimizzare il lavoro prodotto e garantire un funzionamento stabile sia durante il funzionamento a carico costante sia nei transitori.

I modelli di simulazione sono degli strumenti convenienti per la valutazione delle prestazioni di un sistema: i modelli stazionari di fuori progetto possono fornire indicazioni precise sulla produttività del sistema in un determinato periodo, mentre i modelli dinamici di fuori progetto possono essere utilizzati per identificare possibili instabilità funzionali del sistema.

In questa Tesi vengono costruiti dei modelli dinamici e stazionari di fuori progetto di sistemi ORC a singolo livello di pressione e a due livelli di pressione che sfruttano il calore rigettato da quattro motori Diesel installati a bordo di una nave metaniera. Il calore disponibile proviene dall'acqua di raffreddamento della camicia, dal raffreddamento dell'olio e dell'aria di sovralimentazione. I gas di scarico dei motori non sono disponibili in quanto già sfruttati per altri usi interni alla nave. I modelli dinamici vengono utilizzati per simulare il comportamento del sistema durante i transitori e per individuare una strategia di controllo che garantisca la stabilità funzionale del sistema stesso. I modelli stazionari sono utilizzati per valutare la produttività del sistema ORC e per identificare le migliori condizioni di progetto considerando il reale funzionamento della nave. Vengono considerati tre configurazioni di sistemi ORC: a un livello di pressione, a due livelli di pressione con l'alta pressione subcritica e a due livelli di pressione con l'alta pressione supercritica.

Il miglior sistema ORC a singolo livello di pressione è risultato quello dimensionato per una velocità della nave pari a 16.5 nodi con nave senza carico e raggiunge una efficienza termica pari al 6.49% e una produttività annua di 1665.8 MWh. Tra i sistemi ORC a due livelli di pressione quello con alta pressione supercritica è risultato il migliore con un'efficienza termica pari al 12.64% e una produzione annua di 2306.6 MWh a 15.5 nodi con nave senza carico.

ABSTRACT

In large scale naval field, the propulsion system is usually electrical to allow a free placement of Internal Combustion Engines (ICEs), acoustically decouple engines and hull (this makes the ship less noisy), and reduce total weight and volume. Moreover, vessels travel for a long time period at a constant speed, so naval ICEs work at stationary conditions for most of the operation time. On that basis, ORCs (Organic Rankine Cycles) can be installed aboard to generate additional electric power and then reduce the ICEs fuel consumption. The ICEs-ORC combined cycle system is to be design properly to maximize the work production and guarantee a stable operation during both transient and stationary working conditions.

Mathematical simulation models are the most convenient tools to evaluate the performances of a system: steady-state off-design models can provide accurate estimation of the work production in a fixed period of time, while dynamic off-design models can identify possible instabilities among system components during operation.

In this thesis off-design dynamic and steady-state models of single-stage and two-stage ORC systems exploiting the waste heat of four dual fuel diesel ICEs on board a LNG carrier are built. The available heat is taken from the charge air, jacket and oil cooling system, while the exhaust gases are not available being used for other ship needs. The dynamic models are used to simulate the transient behaviour of the system and to define a proper control strategy to guarantee the system stability. The steady-state models are used to evaluate the ORC systems work production and to identify the best system design point considering the real ship operation. The following ORC layouts are taken into account: single-stage, two-stage with subcritical high pressure level and two-stage with supercritical high pressure level.

As results the best performing single-stage ORC is given by a design point corresponding to a ship velocity of 16.5 kn on laden voyage and achieves a thermal efficiency of 6.49% and an annual work production of 1665.8 MWh. Among the two-stage ORC systems the supercritical one is the best performing solution achieving a thermal efficiency of 12.64% and a work production of 2306.6 MWh at 15.5 kn laden.

TABLE OF CONTENTS

Nomenclature

A	Surface [m^2]
B_c	Baffle cut [%]
c_p	Specific heat at constant pressure [J/kg K]
c_v	Specific heat at constant volume [J/kg K]
D	Diameter [m]
f	Fouling factor [m^2K/W]
F_t	Temperature factor [-]
g	Gravitational acceleration [m/s^2]
h	Specific enthalpy [J/kg]
K	Stodola coefficient [m^2]
l	Off-design exponential factor [-]
L	Tube length [m]
layout	Tube layout [°]
$\dot{m}$	Mass flow rate [kg/s]
N_b	Number of baffles [-]
N_s	Number of shells in series [-]
N_{ss}	Number of pairs of sealing strips [-]
N_{tt}	Number of tubes [-]
p	Pressure [Pa]
P_T	Pitch distance [m]
$\dot{Q}$	Heat transfer rate [W]
R	Specific gas constant [J/kg K]
R_{sp}	Fouling resistance [m^2K/W]
s	Specific entropy [J/kg K]
s_g	Fluid specific gravity [-]
T	Temperature [K]
t	Time [s]
u	Specific internal energy [J/kg]
v	Fluid velocity [m/s]
U	Global heat transfer coefficient [W/m^2 K]
V	Volume [m^3]
$\dot{V}$	Volumetric flow rate [m^3/s]
$\dot{W}$	Power [W]
x	Vapour mass fraction [-]
y	Pump head [J/kg] [m^2/s^2]

Greek symbols

α	Heat transfer coefficient [W/m^2 K]
ε	Expansion ratio [-]
η	Efficiency [-]
λ	Thermal conductivity [W/m K]
μ	Dynamic viscosity [Pa s]
ρ	Density [kg/m^3]
φ	Viscosity correction factor [-]
ω	Rotational speed [rad/s]

Abbreviations, apexes and subscripts

‘	Hot
“	Cold
0	No flow rate allowed
B	Baffle
CC	Counter-current
conv	Convective
cr	Critical
D	Defined by literature
DP	Design point
Δ	Difference
δ	Differential
e	External
el	Electrical
f	Function
i	Internal
in	Inlet
is	Isentropic
l	liquid phase
LNG	Liquefied Natural Gas
ICE	Internal Combustion Engine
mec	Mechanical
m	Mean
ml	Mean log
n	Nozzle
ORC	Organic Rankine Cycle
out	Outlet
P	Pump
pipe	Pipe
s	Shell
sat	Saturation
t	Time (when apex)
tp	two phase
T	Temperature
	Turbine (when subscript)
v	vapour phase
wall	Wall

1 INTRODUCTION

Energy generation processes usually exploit fuels or high-grade heat to produce mechanical/electric power and reject low-grade heat to ambient. The waste low-grade heat may be use to feed another process downstream with a reduce the overall fuel consumption at constant product. Organic Rankine Cycle (ORC) systems are an efficient solution to exploit heat sources at low temperature, even below 100°C, with efficiencies (about 5% to 20% depending on the hot source/sources temperature) not achievable using conventional fluids as water and air in the same temperature range. Significant reviews of suitable heat sources and ORC applications have been proposed in [1, 2, 3].

A particular field in which ORC technology is being diffused is naval engineering, where ICEs are usually adopted for ship motion. Larsen et al. [4] and Shu et al. [5] present a review of WHR (Waste Heat Recovery) applications aboard ships, while reviews of ICEs (Internal Combustion Engine) exhaust WHR by ORCs are proposed by Sprouse et al. [6] and Wang et al. [7].

The ICEs-ORC combined cycle is to be design properly to maximize the work production and guarantee a stable operation during both transient and stationary working conditions. For this purpose, mathematical models are the most proper tools to define the system design and evaluate the system behaviour and performances.

Design models allow the system components to be sized at fixed design specifications and the performance at design point to be estimated. Many studies have been carried out for several configurations and organic working fluids. Ziviani et al. [8] propose an outline of the issues related to ORC modelling and guidelines to develop effective and powerful models. Quoilin et al. [9] present a design model of an ORC, used for WHR applications, for the cycle performance evaluation using different working fluids and different components sizes.

Steady-state off-design models are used to assess the system operation far from the nominal condition, by “passing” instantaneously from an equilibrium point to another. Calise et al. [10] carried out an energetic and economic performance evaluation of an ORC system, for different operating conditions and design criteria. In particular, the developed model allows geometrical parameters to be set and off-design performance to be evaluated.

Dynamic models are necessary to evaluate transient response of the system and verify its stability after variation in the heat sources characteristics, and to define a proper control strategy able to drive the system to an equilibrium point in the shortest possible time. Quoilin et al. [11] propose a dynamic model of a small-scale ORC used to recover energy from a variable waste heat source. The focus is on the time-varying performance of the heat exchangers (the dynamics of which are more important than other components) and on control strategies. Wei et al. [12] present two alternative approaches to dynamic modeling

for ORCs control and diagnostics systems definition. Manente et al. [13] developed a dynamic model for the analysis of an ORC system exploiting geothermal energy.

The aim of this thesis is to evaluate the work production, find the best performing design and define the control stability of single-stage and two-stage ORC systems exploiting the waste heat of four dual fuel diesel ICEs on board a LNG carrier. For this purpose off-design dynamic models and steady-state models of the systems are created taking into account the characteristic of the heat sources. The available heat is taken from the charge air, jacket and oil cooling system, while the exhaust gases are not available being used for other ship needs. The modelling approach is suggested by Vaja [14], and *MATLAB® Simulink* is used to implement the models. Particular attention is paid to the heat exchangers, their influence is crucial in determining off-design operation of the ORC. Three plant layouts are taken into consideration: single-stage, two-stage with subcritical high pressure level, two-stage with supercritical second high level.

2 ORGANIC RANKINE CYCLE SYSTEMS ON BOARD LNG CARRIERS

This chapter presents an Organic Rankine Cycle (ORC) systems technologies overview starting from basic concepts and main features and then focusing on the specific application case on board LNG carrier. In particular, a detailed summary of the works available in the literature is proposed at the end of the chapter.

2.1 ORCs OVERVIEW

The basic cycle of an Organic Rankine Cycle (ORC) system is the Rankine one, the purpose of which is to transform heat made available by an external source into mechanical power. Figure 2.1 shows a schematic a Rankine cycle and the related T-s diagram. The thermodynamic cycle is carried out by a low critical temperature fluid (e.g. organic fluid) and is composed by a close loop of the following transformations: compression, heat absorption (including vaporization), expansion, heat release (including condensation). Thus, the following four main devices are needed:

- a pump to increase the fluid pressure up to the desired value;
- an heat exchanger between hot source(s) and working fluid to preheat, evaporate and eventually superheat the fluid at high pressure;
- a vapour turbine to convert the fluid static and kinetic energies into mechanical one;
- an heat exchanger between cold source(s) and working fluid to de-superheat (if necessary) and condensate the fluid at low pressure (loop closure).

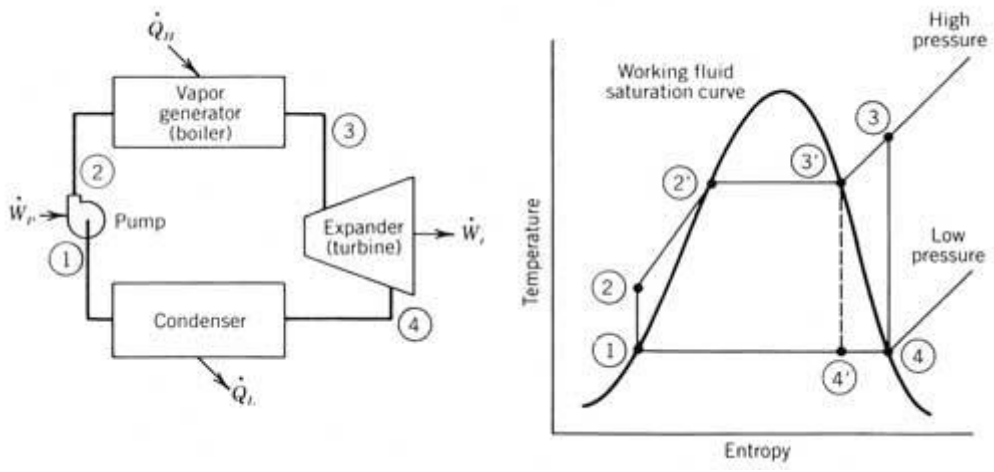

Figure 2.1 *Conceptual scheme of Rankine Cycle system and T-s diagram.*

2.1.1 Choice of the working fluids

The presented scheme is the basis to take into consideration to respect the operative sequence that characterizes Rankine cycles. From this starting point, the power plant's configuration can be developed according to the employed type of working fluid, the available heat source and other technical and economic considerations, in order to reach the best possible work production and cycle efficiency compatibly with required application and installation.

In particular, the fluid selection determines in a strong way the final form of the power plant. The optimal characteristics that the operative fluid should present to maximize the cycle efficiency are the following ones [15]:

- moderate maximum cycle pressure;
- condensation pressure higher than the atmospheric value;
- critical temperature higher than the maximum cycle temperature;
- low specific heat for the liquid phase, in order to possibly obtain a vertical saturated liquid line in the T-s diagram;
- a vertical saturated vapour line in the T-s diagram to avoid liquid or superheated vapour at the end of the expansion.

Other important features of the operative fluid and conditions that it should respect for its adoption in the Rankine cycle system:

- good characteristics of thermal exchange;
- chemical and thermal stability at the use conditions;
- solidification temperature lower than the lowest possible ambient temperature;
- low specific volume of the expanded vapour, to keep a small size for heat exchangers and the turbine's low pressure stage;
- for low temperature available sources, hence for low power applications, the fluid should present a high molecular mass in order to reduce rotational speed and number of turbine stages and increase mass flow rate and passage area in the blading;
- not flammable, not corrosive, not toxic, ozone-friendly, low global warming potential;
- compatibility with materials and fluids that could come in contact;
- not expensive.

An optimal working fluid, according to the proposed features, would be characterized by saturated liquid and vapour curves in Fig. 2.2.

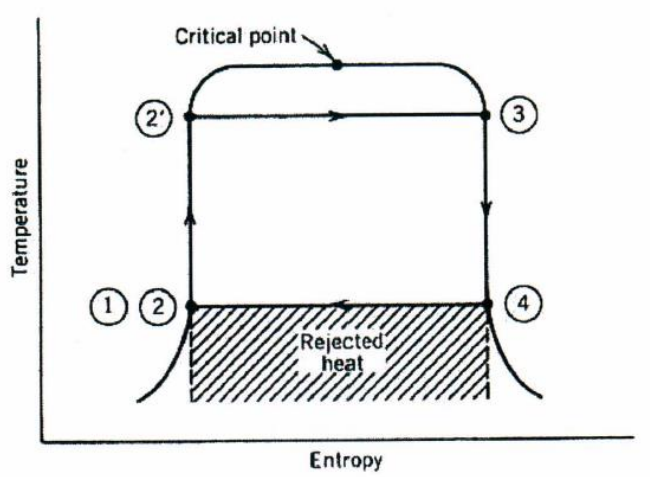

Figure 2.2 *Ideal T-s diagram for an organic fluid [15].*

There are not existing fluids able to meet every presented condition, hence it is necessary to select the proper operative fluid according to the application. An important distinction among real fluids regards the slope of the saturated vapour line in the T-s diagram, therefore the thermodynamic conditions at the end of expansion of saturated vapour (Fig. 2.3):

- *dry fluids*, characterized by a positive slope of the mentioned curve, that implies to find always superheated vapour at the end of the expansion, with the consequent necessity of de-superheating before condensation (it is achievable by the condenser device);
- *isentropic fluids*, presenting a nearly infinite slope of the saturated vapour line and hence saturated vapour at the exit of the expander;
- *wet fluids*, which negative slope of the curve in question implicates an expansion inside the two phase region, with formation of more and more liquid dropping the pressure, hence requiring vapour to be superheated before sending into the turbine to avoid this phenomenon.

The choice of working fluid is strongly influenced by the thermodynamic characteristics of the available heat source, in particular by its temperature level. The main distinction among applications that perform the Rankine cycle is the following one:

- for high temperature level of the heat source, the traditional Rankine cycle system usually employs water as operative fluid;
- for low temperature applications, below 320°C (geothermal, combustion of low quality fuel and waste heat recovery), the choice turns to organic fluids.

There are several organic fluids to choose for this kind of power plants. Wang et al. [16] propose a choice criterion based on the heat source temperature. This criterion was determined by the analysis of the relationship between operative fluids properties and thermal efficiency, optimal operation conditions and exergy destruction by means a thermal efficiency model of an ideal ORC system. The results are summarized in Figure 2.4 in which

the best fluids in terms of efficiency are related to the temperature level of the available heat source.

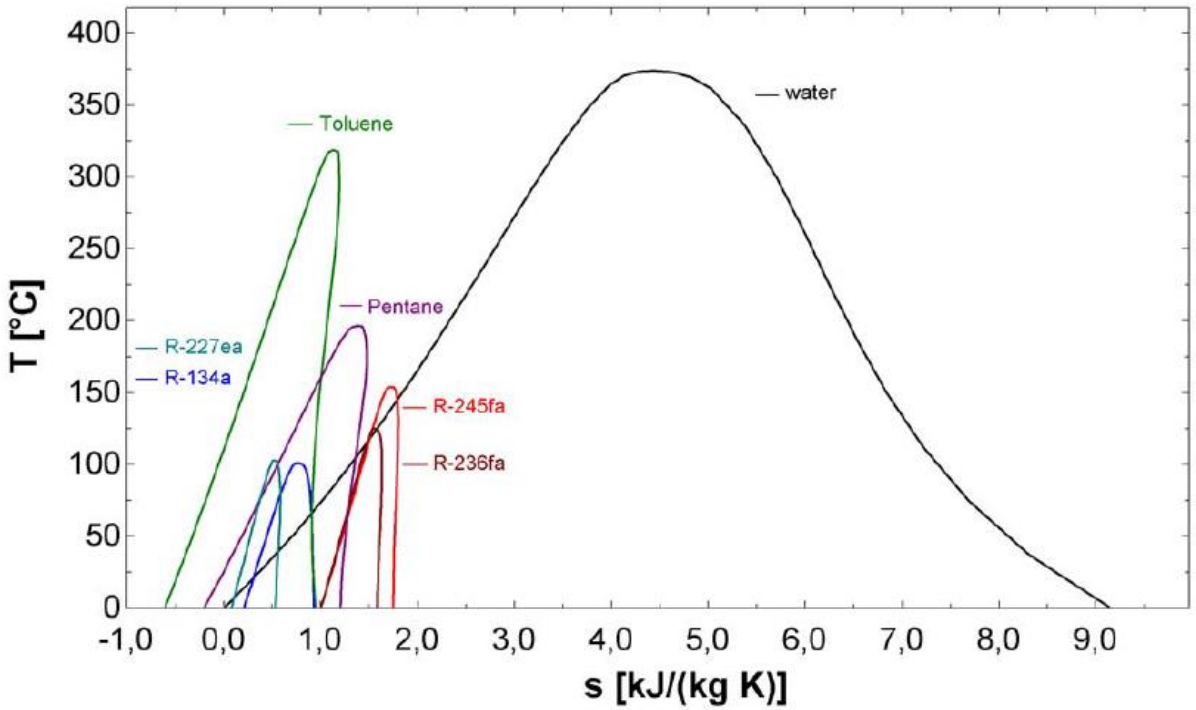

Figure 2.3 *T-s diagram of few organic fluids and water [16].*

Heat source T level [K]					
320-365	365-395	395-420	420-445	445-465	465-500
Critical T [K]					
R134a (346) R32 (351)	R22 (369) R290 (367) R134a (374) R227ea (375)	R152a(386) R124(395) CF_3I(396) R236fa(398)	R600a(408) R142b(410) R236ea(412)	R600(425) R245fa(427) R245ca(448)	R123(457) R601a(448) R601(470) R141b(478)

Figure 2.4 *Recommended working fluid selection for the ORC systems according to the corresponding temperature level of the available heat source, with relative critical temperature for the listed organic fluids [16].*

There may be limitation in the use of organic fluids depending on the application to which they are earmarked. In ships applications there is a regulation about the allowed fluids that refers to the international agreement for prevention and reduction of pollution from ships known as MARPOL 73/78 or to the European norm (EC) No. 1005/2009 [18], more restrictive than the first one because of the not given permission to the use of HCFCs (hydro-clorofluorocarbons). Furthermore, in case of transportation of high flammable and

eventually explosive wares (e.g. LNG carrier) the use of high flammables fluids (e.g., hydrocarbons) is not allowed for evident safety issues.

To summarize, the choice of working fluid for a ORC depends on several factors, the most important ones being compatibility and permission for the considered installation, temperature level of the available heat source, thermodynamic characteristics of the selected fluid for achievement of optimal cycle efficiency and work production, safety, technical and economic issues. There is not therefore an unique best solution for all Rankine power plants, but the fluid options must be analysed case by case.

2.1.2 Comparison between steam and organic Rankine cycles

As seen in the previous paragraph the main differences between ORC and steam Rankine cycle is the working fluid and the application field. The main differences about the characteristics of the two fluids are:

- the bigger entropy difference between saturated vapour and saturated liquid for water with respect to organic fluids, as it can be seen in Figure 2.3;
- water/steam has lower density while organic fluids are usually characterized by complex molecules, hence by high molecular weight;
- water is a wet fluid, that requires superheating to avoid or limit the presence of liquid droplets at the exit of the expander, while several dry and isentropic organic fluids can be found.

It is worth noting that while for steam power plants superheating is usually adopted for the efficiency optimization and often required for the cycle purposes, in case of ORC systems it is not only unnecessary for isentropic and dry fluids, but frequently not helpful in increasing thermal efficiency of the cycle. Moreover, the temperature level of the available heat source provided for an ORC may not be able to superheat the employed organic fluid.

About the power plant configuration, the operative pressures are different for the two types of system. For medium-small sized steam plants, evaporation pressure is usually set at about 60 ÷ 70 bar and condensation pressure at 0.1 bar absolute, while usually for ORC system the former is not more than 30 bar, the latter a little more than the atmospheric pressure. Consequently, evaporation temperature is much lower and condensation temperature is usually higher for ORC plants with respect to the steam Rankine cycle systems, allowing in this way the exploitation of low temperature heat sources.

Internal regeneration is often used by traditional Rankine cycles in order to increase thermal efficiency. It is performed by use of splits that connect the steam turbine in various points, at various stages with different pressure levels, for example to six preheaters and one degasser in the standard 320 MW group, taking in this way hot steam before expansion to preheat the liquid passing through the heat exchangers in the portion of circuit between pump and steam generator. In this way, part of the producible work is sacrificed thus making possible the increase of the average cycle temperature, hence the thermal efficiency. For the

ORC systems, internal regeneration is not so often adopted, for sure not with adoption of the presented solution, because it is not always helpful in increasing cycle efficiency, especially in WHR (Waste Heat Recovery) applications. Without an adequate increase of efficiency the use of an internal regenerator, a specific heat exchanger installed into the system for this purpose, results in a not justified raise of the plant costs, hence of the initial investment.

The ORC systems usually present the following main technical and operative advantages [15]:

- low grade heat exploitability;
- superheater is unnecessary for dry and isentropic fluids;
- compact devices, due to the high vapour density;
- high thermal efficiency, included during partial load operation;
- possibility to work at partial load until about 10% of the nominal power;
- high reliability, for a conspicuous amount of working hours;
- low maintenance;
- simple starting procedure;
- no licenced boiler operators required, thanks to use of thermal oil as intermediate fluid for the highest temperature level applications;
- personnel required for a low number of hours per week;
- automatic, continuous and silent operation;
- high efficiency for the vapour turbine (until 85%);
- possibility to adopt single or two stage turbine, for the low enthalpy drop due to the small difference between evaporation and condensation temperatures;
- low cost and simple design of the expander;
- low rounds per minute for the vapour turbine, that allow a direct connection with the electric generator without necessity of a speed reducer;
- low mechanical stress for the vapour turbine, for the low peripheral velocity;
- no erosion of the turbine blades, due to the absence of moisture to the nozzles.

The strengths of the traditional steam Rankine cycle systems are mainly:

- the higher producible work and electric efficiency, due to the larger plant size;
- the high specific heat and latent heat of the working fluid water, that make it a good energy carrier;
- water is chemically and thermally stable at every operating condition;
- water is not flammable nor toxic;
- water has low environmental impact;
- water is cheap and widely available.

The major differences between water and organic fluids are hence the following ones:

- organic fluids are usually toxic, flammable and thermally and chemically instable out of the right operative ranges; water does not present these critical issues;
- most of the organic fluids have high environmental impact;
- organic fluids are more expensive than water;
- water requires desalinization to reduce fouling and corrosiveness.

Main technical differences between traditional steam Rankine cycle systems and ORC power plants are summarized in the next points:

- electrical efficiency is lower for the ORC systems, but higher relatively to the available heat source (steam power plants would not achieve the same results with low temperature levels of the hot utility, in some cases they would not work at all); in the same way, with high grade heat available, producible work and electric efficiency are upper for traditional RC systems;
- superheaters are required by steam power plants, while often unnecessary for ORCs;
- internal regeneration is usually adopted in the traditional RC plants, whereas it is not frequently considered for ORCs;
- the higher pressure drop for the steam plants requires complex multi-stage turbines; in case of ORC, single stage or two stage vapour turbines are ordinarily adopted;
- size of ORCs is usually much smaller;
- in general, the layout is much more complex for traditional plants than ORCs: this aspect allows the last ones to be installed for local applications with little energy request, giving them a great prospect for a large scale diffusion.

2.1.3 Simple, regenerative, subcritical and supercritical cycles

A brief description of the possible thermodynamic cycles for the Organic Rankine Cycle systems is here provided.

- *Simple cycle*

The simple cycle presents only the basic components to run, arranged as discussed in the previous paragraphs. As aforementioned, for dry and isentropic fluids superheater is not necessary. After the expansion vapour is still superheated: the condenser desuperheats and condense it. An accumulator is usually installed downstream the condenser, with the double benefit of cycle stabilization and pressures control and sending of saturated liquid to the successive pump. Liquid is then compressed to the desired pressure value at which vaporizes inside the evaporator. The so produced vapour is sent to the turbine to run again the cycle. Figure 2.1 presents the schematic example of simple ORC with thermodynamic cycle.

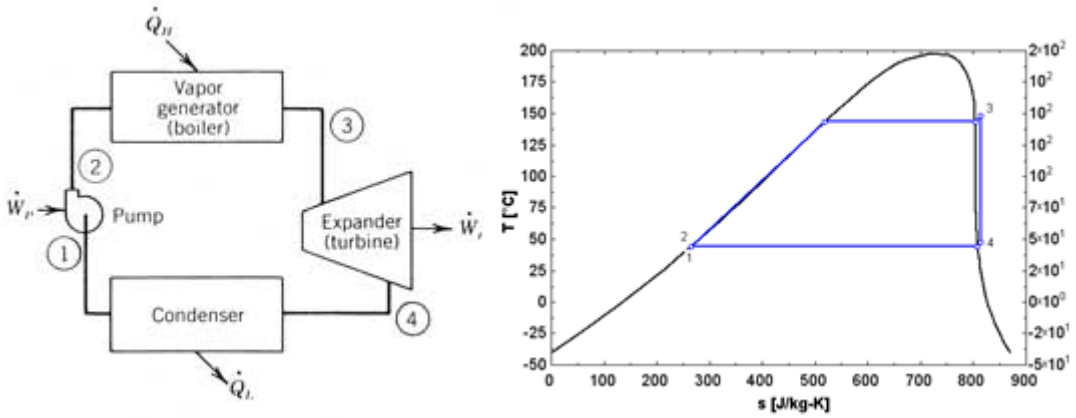

Figure 2.5 *Simple Organic Rankine Cycle system and T-s diagram.*

- *Regenerative cycle*

An additional heat exchanger, operating as regenerator, is installed in the ORC in order to receive the low pressure vapour at the turbine outlet to preheat the liquid coming from the pump. In this way, the cycle efficiency is increased. The cost-benefit ratio should be evaluated, to justify the raised initial investment which purpose is to achieve higher efficiency and work production. A simple regenerative cycle configuration is reported in Fig. 2.6, together to the relative curve in the T-s diagram.

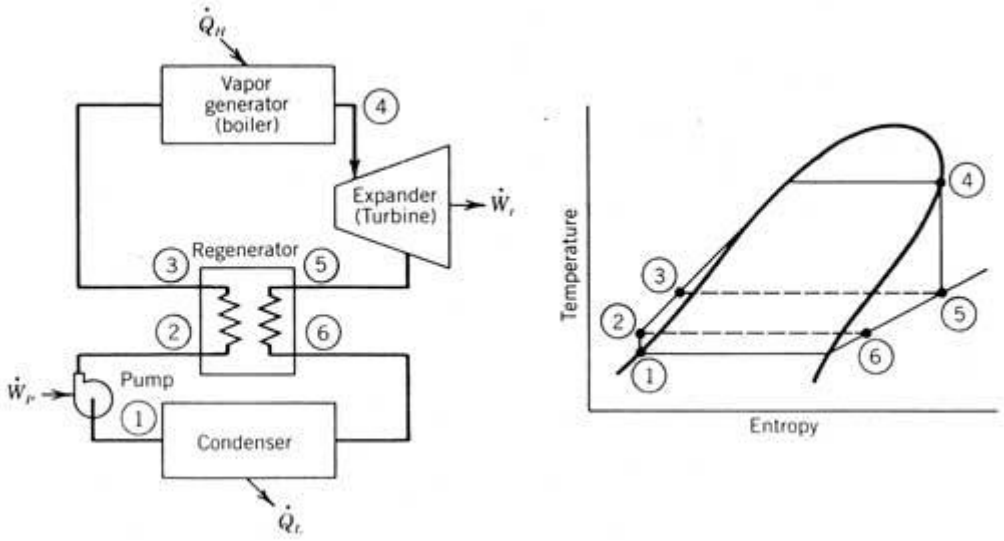

Figure 2.6 *Regenerative Organic Rankine Cycle system and T-s diagram.*

- *Subcritical and supercritical cycles*

Most of the ORC power plants perform a subcritical evaporation of the operative fluid at the evaporator. The subcritical evaporation is indeed very well known by the widely use in industrial applications. Several studies and correlations are available to design heat exchangers for this purpose, and most of the adopted organic fluids fits well in subcritical

Rankine cycles. Reliability and deep knowledge of these phenomena explain the wide diffusion of subcritical ORCs.

Differently, supercritical applications are conceived to guarantee higher work productions, by exploitation of higher enthalpy drops in vapour turbine. The shape of the Andrews' curve in the T-s diagrams of certain organic fluids can allow implementation of a supercritical cycle, compatibly with the available heat source. To achieve supercritical evaporation, the pump has to increase the fluid pressure over the critical value, with a sufficient margin to take into account of the pressure drop in the supercritical evaporator. In such heat exchanger, phase change occurs above the critical point and does not manifest with a clear separation of liquid and vapour phases as instead for subcritical evaporation. In particular, the transformation is continuous and the two phases do not present differences in their main thermodynamic properties, such as density, which makes impossible to clearly distinguish liquid from vapour.

Main advantages of adoption of supercritical cycles is the higher efficiency and work production, thanks to the larger enthalpy drop inside the expander at the cost of a little bigger energy expense in the pump component. Exergy losses result lower as well, for the better fitting of supercritical evaporation with the heat source profile. The phenomenon unfortunately is not deeply diffused in industrial applications yet, there are not many relevant studies and moreover there are still few available correlations to adopt.

Figure 2.7 shows a qualitative comparison between subcritical and supercritical ORCs.

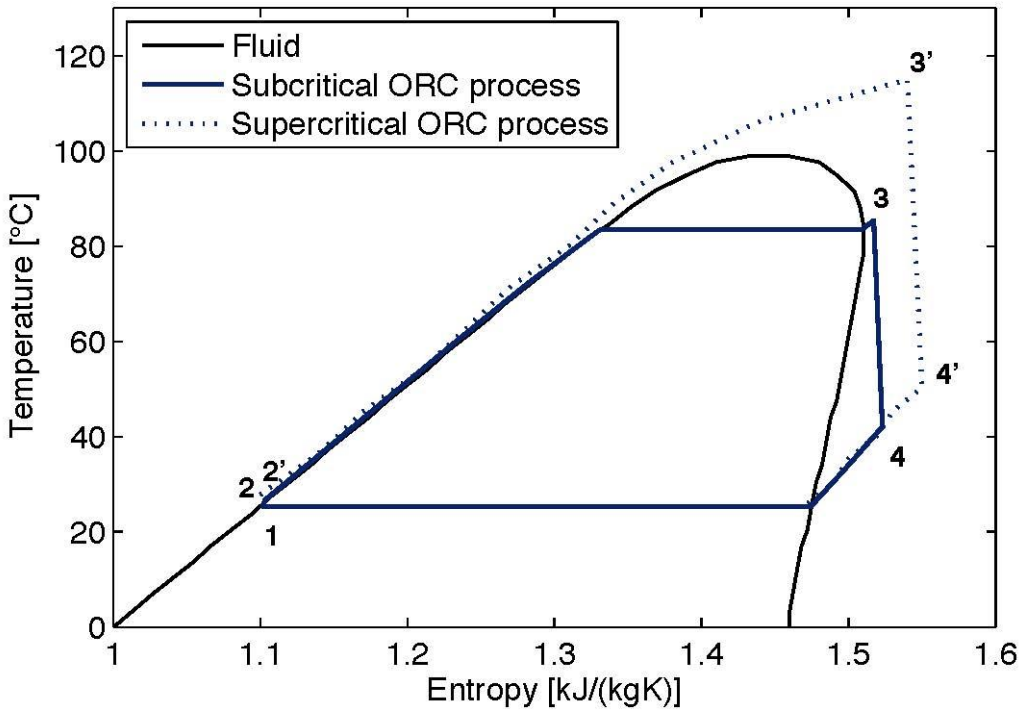

Figure 2.7 *T-s diagram for subcritical and supercritical cycles.*

- *Two stage cycles*

A second stage having a higher evaporation pressure level is added to the system. In this way, another possibly hotter source is exploitable by an additional heat exchanger, where to evaporate the working fluid at a higher pressure imposed by a second pump. The produced vapour is sent then to a second expander. The outlet fluid can be sent to a mixer valve or to a hot drum, to blend with the vapour of the first pressure level and proceed to the successive component, depending on the designed mixing point.

Critical issue for this kind of plant layout is the pressure control: it is crucial to verify if the selected configuration allows to reach equilibrium points by means a control system, both in design and in off-design operations.

There are several possible configurations for the two stage Rankine cycle systems, including both subcritical and supercritical second pressure levels. An example of two stage ORC design is proposed in Figure 2.8.

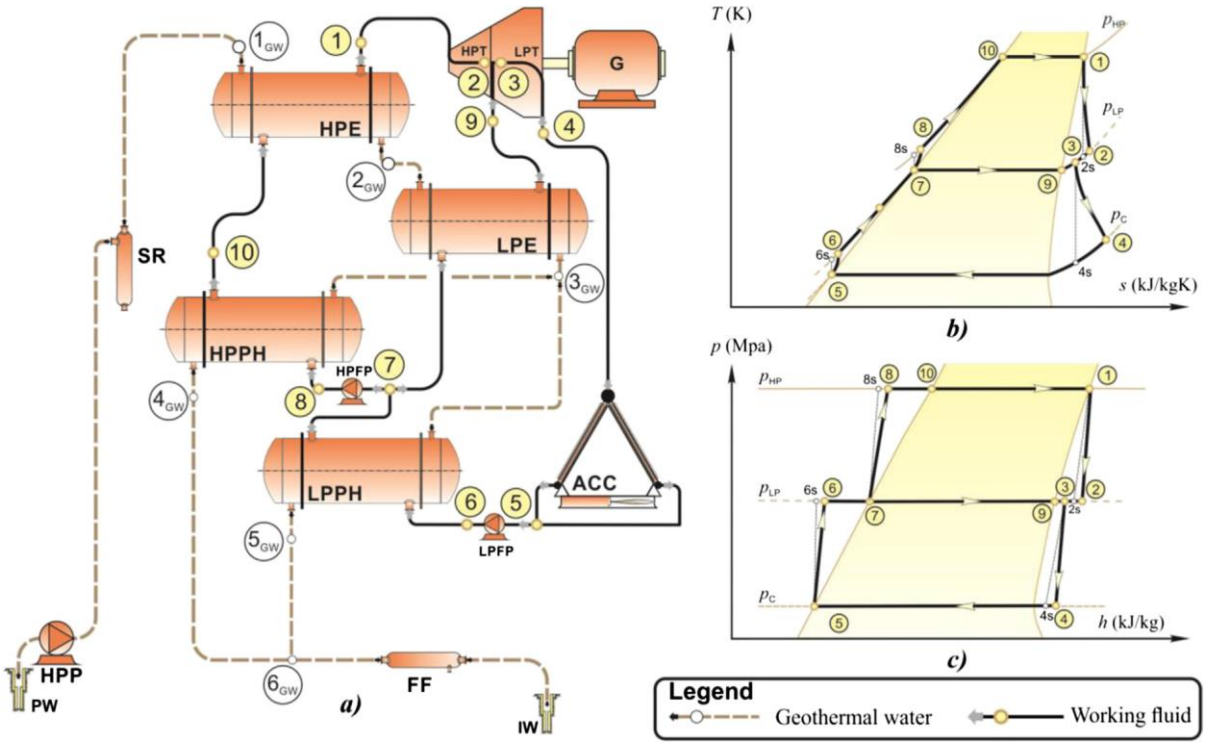

Figure 2.8 *Configuration scheme, T-s diagram and p-h diagram of dual pressure ORC [17].*

2.1.4 ORC applications

As aforementioned, the ORC technology matches at best with low grade heat sources, with respect to the traditional steam Rankine cycles. While the latter ones usually employ fossil fuels such as coal or oil, ORCs mainly exploit renewable sources, like geothermal energy, solar energy and biomass fuel, and waste heat from industry or other existing processes. A brief overview of the most frequent ORC applications is here presented.

- *Waste heat recovery (Fig. 2.9)*

Waste heat is heat rejected by processes that involve combustion, thermal and chemical reactions, usually findable at medium and low temperatures in industrial applications and during thermal engines operations. The basic idea is to exploit this source that represents a free supply for the power plant. Low grade waste heat can be recovered by ORC systems in order to generate additional electric energy, useful for example for a reuse into the process or to sell it to the electric market. Typical applications are recovery of waste heat from industrial process as plants for the cement, steel and glass production, and from ICEs (Internal Combustion Engines). In particular, the installation of an ORC system downstream engines, to form in this way a combined cycle, leads to an electric efficiency increase with consequent benefits about engine fuel consumption and electric energy production. The type of matching between ORC and the process that provides waste heat depends on the particular application, to evaluate case by case.

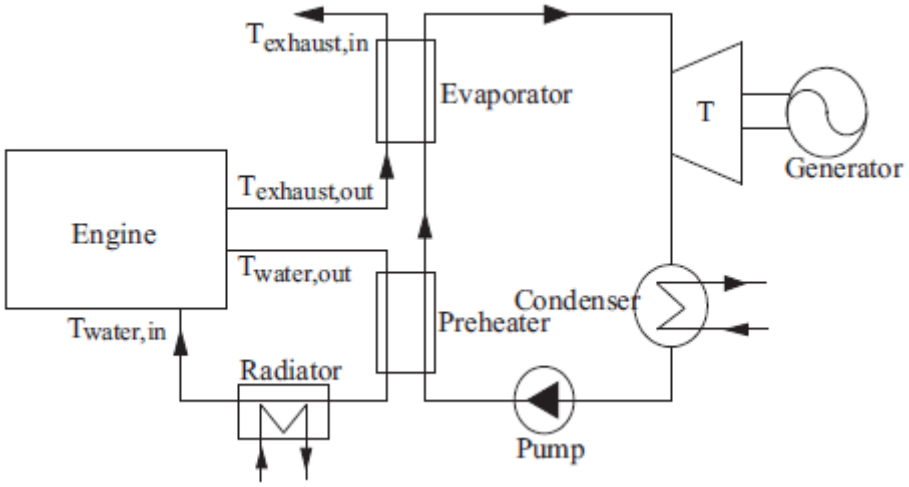

Figure 2.9 *ORC system exploiting waste heat from thermal engine [7].*

- *Biomass power plants (Fig. 2.10)*

Biomass fuel combustion allows to reach high temperature levels for the exhaust gases, in some cases sufficient to feed a traditional steam RC. Critical issue is the LHV (Low Heating Value) of the fuel, that is significant lower with respect to the fossil fuels one and implies high transportation costs and biomass growing area. For this reason, suitable applications are small scale CHP (Combined Heat and Power) plants, for sizes of $1 \div 2$ MW_{el}, more oriented for the ORC technology. These applications usually present an intermediate fluid, thermal oil, to avoid a direct connection between organic working fluid and hot exhaust gases, for safety reasons. Thermal oil allows indeed to run the Rankine cycle without supervision of licenced boiler operators, to make this technology attractive for a wide range of local applications. Adoption of this intermediate fluid is convenient for its thermodynamic properties and thermal inertia that allow to operate with low pressure in the oil-gas heat exchanger. Moreover, the best efficiency of thermal oil is usually at about 100°C, that matches well with the temperature of the considered heat source.

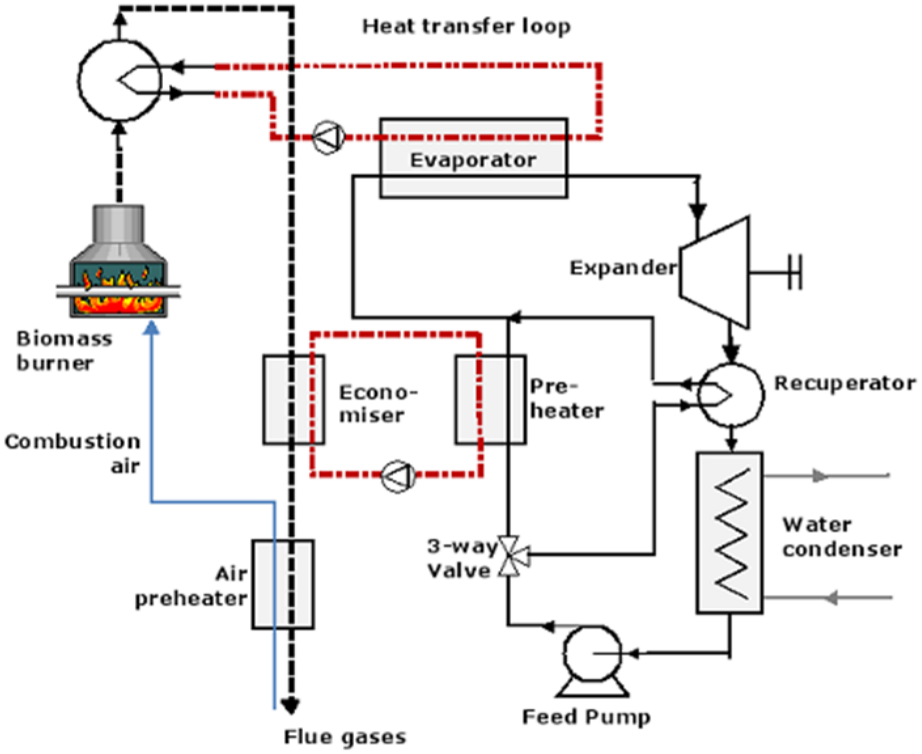

Figure 2.10 *Configuration example of a biomass CHP ORC power plant [1].*

- *Geothermal power plants (Fig. 2.11)*

Geothermal energy is a typical low grade heat source, which temperature range is from the ambient temperature to about 320°C. Binary power plants are actually used to perform the Rankine cycle by exploitation of the extracted geothermal vapour, to evaporate the working fluid before the reinjection into the ground. The basic binary systems usually operate within temperature levels between 125°C and 165°C. Organic fluids that present a low critical temperature, such as R245fa with its 154°C, are advisable for this kind of application.

- *Solar applications (Fig.2.12)*

Concentrating solar power plants represent another technology capable of providing low grade heat at temperature level high enough to feed an ORC system. Other possibilities are matches with Stirling engines, in case of lower sizes of the solar plant, and with traditional RC systems or combined cycle for the highest achievable heat grades. Modularity, low temperature operations, reduced capital and operation costs make ORC systems convenient for a matching with this kind of technology. Adoption of parabolic dishes and parabolic trough is advisable to collect and concentrate solar energy to feed an ORC power plant.

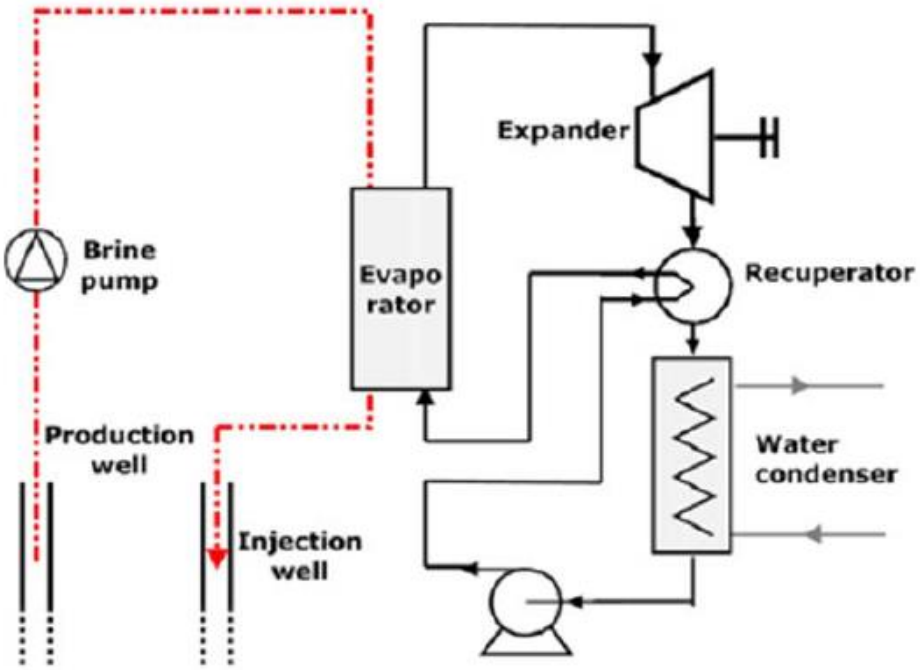

Figure 2.11 *Conceptual scheme of geothermal ORC power plant [1].*

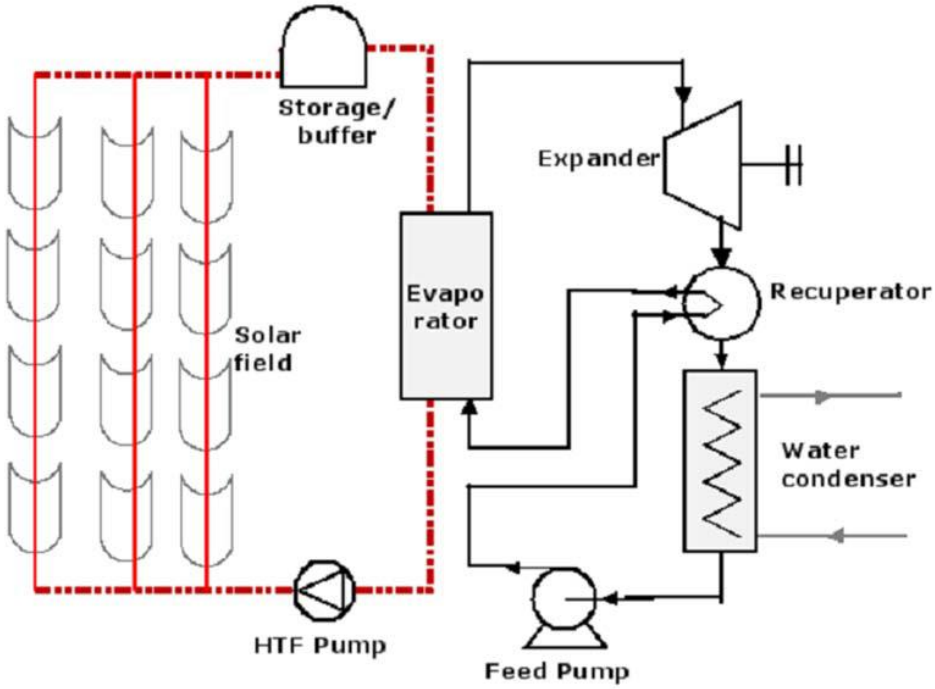

Figure 2.12 *Conceptual scheme of solar ORC system with parabolic trough solar field [1].*

2.2 CASE STUDY

In this work an LNG carrier characterised by an electric propulsion, generated by four Diesel engines, is analysed. Engines provides also heat for steam, hot water and fresh water generation. The load profile is variable depending on ship travel parameters, such as speed and load, that determine working conditions and the number of engines have to be active at the same time. In this context, an ORC (Organic Rankine Cycle) system will be considered installed in order to exploit the waste heat coming from the engines, in particular from charge air, cooling water and lubricating oil, to produce a supplement of electric energy and in this way reduce fuel consumption. There would be the possibility to use also exhaust gases for this purpose, that represent an hotter and hence more functional source for the ORC, but it is already employed for steam production in a recovery heat system for other utilizations in the ship. For this reason, further exploitation of exhaust gases is not considered in this work. Conversely the opportunity will be examined to effect some changes in the Diesel engines energy system configuration, in order to make possible and verify the potential about the implementation of a second pressure level, subcritical or supercritical, into ORC system, with the goal of increasing useful energy production. The aim of this work is to find the best ORC configuration for this particular LNG carrier with, as possible objectives, maximization of electric energy production, maximization of efficiency and minimization of engine fuel consumption, with all the related economic advantages. To do this, MATLAB Simulink is adopted as modelling tool to build an ORC model, to simulate its operation in order to find easily the best configuration for both design and off-design working conditions.

2.2.1 Energy system and energy demands of the ship

The four DFDG (Dual Fuel Diesel Generators) are four-stroke, turbocharged, inter-cooled and they are fuelled either with natural gas plus light fuel oil as pilot fuel or with HFO (Heavy Fuel Oil). Two different sizes of them are installed on the vessel:

- Wärtsilä 6L50DF, two engines, nominal electric power output of 5,500 kW, six cylinders in-line, from now onwards called “type A”;
- Wärtsilä 12V50DF, two engines, nominal electric power output of 11,000 kW, twelve cylinders V, from now onwards called “type B”.

The pumps of the cooling system are of the engine driven type. In the following, main characteristics and cross sections of the two types of engines are presented.

Table 2.1 *Main characteristics of the Diesel generator engines [18].*

	Unit	6L50DF	12V50DF
Mechanical output	kW	5700	11400
Cylinder bore	mm	500	500
Stroke	mm	580	580
Engine speed	rpm	500	500
Mean piston speed	m/s	9.7	9.7
Mean effective pressure	bar	20	20
Electrical output	kW	5500	11000
Generator efficiency	%	96.49	96.49

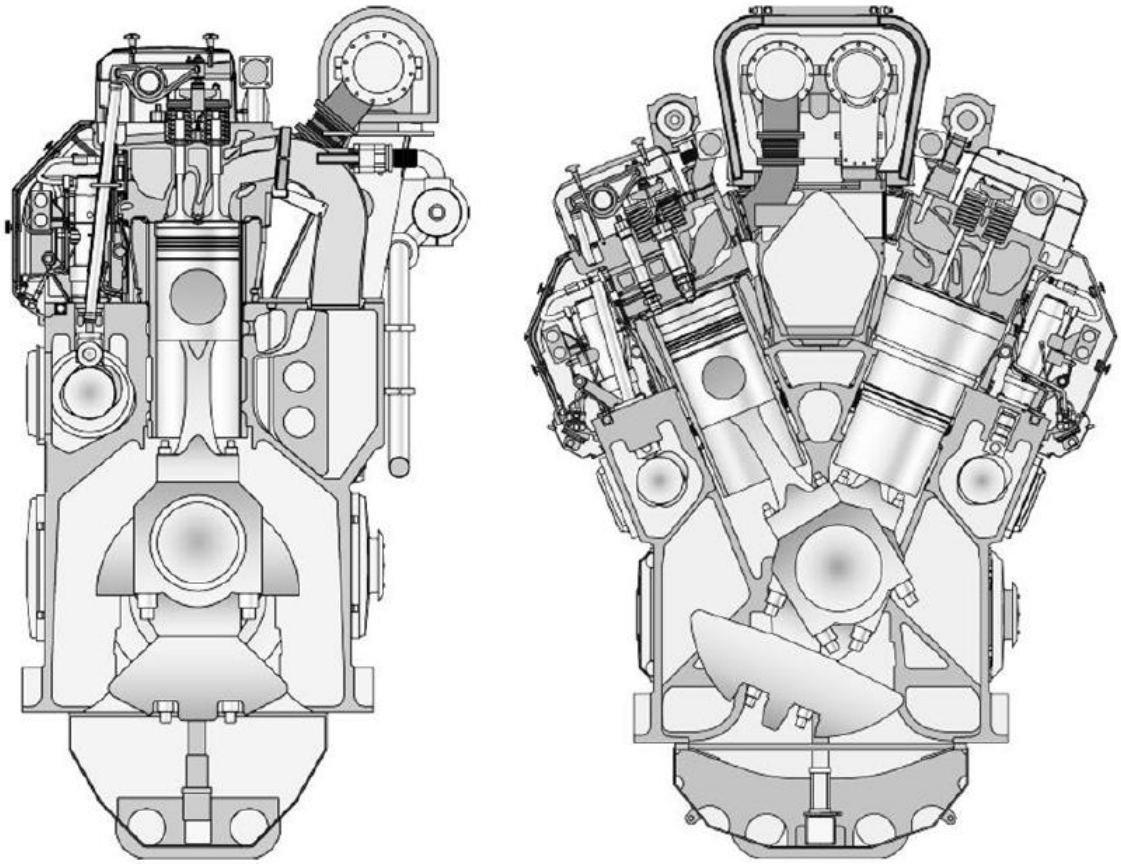

Figure 2.13 *Schematic cross section of the 6L50DF in-line engine (left) and of the 12V50DF V engine (right) [18].*

Soffiato [1, 2, 3] performed in his work a first law energy balance of the two presented types of engines, assuming an energy conversion from mechanical to electrical form included in the system's boundaries. The proposed balance describes the exploitation of the primary energy provided by the fuel and its transformation into the desired electric output. For this calculation, the following ISO conditions have been considered:

- reference temperature of 25°C;
- total barometric pressure of 1 bar;
- air relative humidity of 30%.

About the Wärtsilä engines, the charge air coolant temperature is 25°C. The engines are Dual Fuel type, but in this work the operating mode with Heavy Fuel Oil (HFO) will not be considered, but only the natural gas fuel case.

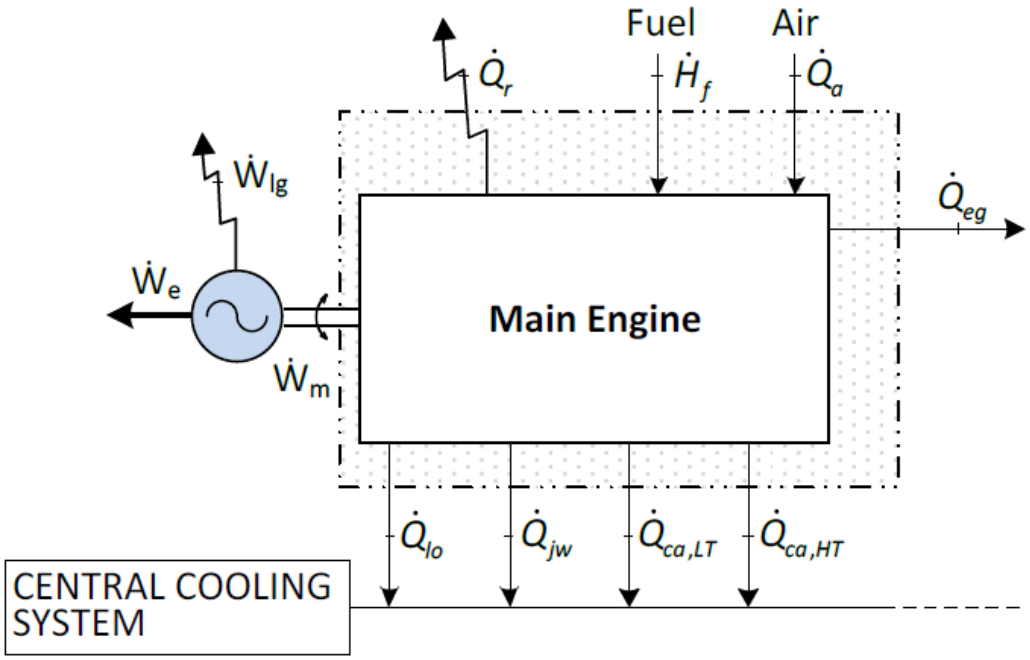

Figure 2.14 *ICE's control volume and schematic representation of the energy balance [18].*

The first law energy balance of a single engine is expressed as follows:

$$\dot{H}_f + \dot{Q}_a = \dot{W}_e + \dot{Q}_{lo} + \dot{Q}_w + \dot{Q}_{ca,HT} + \dot{Q}_{ca,LT} + \dot{Q}_{eg} + \dot{Q}_r + \dot{W}_{lg} \qquad (2.1)$$

where, referring to Figure (2.2)

$\dot{H}_f$	energy flow rate related to the fuel
$\dot{Q}_a$	energy flow rate of the air
$\dot{W}_e$	electric power
$\dot{Q}_{lo}$	heat flow rate rejected to the lubricating oil
$\dot{Q}_w$	heat flow rate rejected to the jacket water
$\dot{Q}_{ca,HT}$	heat flow rate at the high temperature charge air cooler
$\dot{Q}_{ca,LT}$	heat flow rate at the low temperature charge air cooler
$\dot{Q}_{eg}$	heat flow related to the exhaust gas
$\dot{Q}_r$	radiation and convection losses
$\dot{W}_{lg}$	electric generator losses

All main engines can work in temperature safety conditions thanks to a cooling system, similar for every unit, that operates with fresh water loops. Heat is collected inside the engines as well as at the two air coolers and at the lubricating oil cooler, therefore it is rejected at different temperature levels. To facilitate the heat exchange through the

generating power plant, the cooling system is split into two circuits, characterized by an higher and a lower temperature of cooling water. The fresh water, at the end of the path, is cooled by passing through a central cooler, mainly composed by heat exchangers that dissipate heat to a flow of sea water. The arrangement of main engines and fresh water cooling circuits is shown in Fig. 2.14. Note that the Fig. 2.14 refers to the operation of all the involved working engines at the considered operating point.

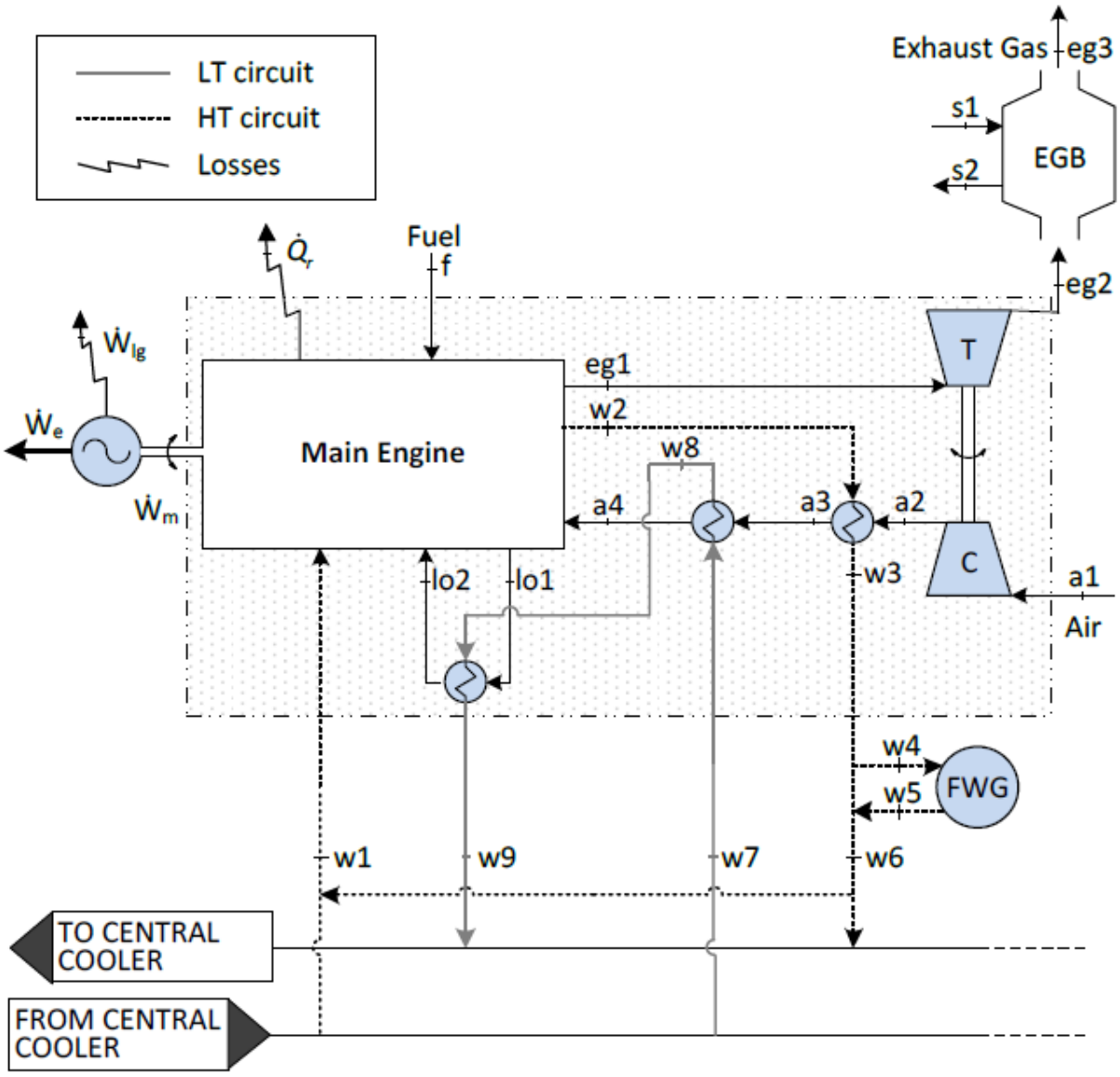

Figure 2.15 *Diesel engines and cooling system layout.*

The fresh water of the HT cooling circuit passes before through the engine and then through the first air cooler (AC1), while the LT cooling flow collects heat, in the order, from the second air cooler (AC2) and the lubricating oil cooler (LOC). Control valves are applied at the engines and the heat exchangers in order to maintain an appropriate temperature of the HT cooling water and of the air, by using recirculation if needed. Contrarily, the LT cooling

water is taken directly from the central cooler without any temperature control, therefore it is affected by its operating conditions.

The exhaust gas is exploited by an EGB (Exhaust Gas Boiler) to produce steam for internal utilizations in the ship, solution that impedes its use as additional source for the ORC system.

Soffiato gathered all available data of the main thermodynamic parameters of the ship energy system, with addition of the missing values calculated by application of mass and energy balance equations, into the following table. Data refer to the two types of engine.

Table 2.2 *Operating parameters of the two types of engine, type A on the left and type B on the right [18].*

		Wärtsilä 6L50DF					*Wärtsilä 12V50DF*				
Par.	Unit	100	90	85	75	50	100	90	85	75	50
T_{w1}	°C	74	74.6	75	76	78	76	76.4	76.6	77	78
T_{w2}	°C	79.4	78.3	78.6	79.5	81.0	80.1	79.8	79.9	80.5	81.0
T_{w3}	°C	83	82.2	82	82	82	85	83.3	83	83	82
T_{w7}	°C	36	36	36	38	38	36	36	36	36	36
T_{w8}	°C	45	43.7	43.1	43.9	41.4	45	43.7	43.1	41.9	39.4
T_{w9}	°C	54.2	52.6	51.9	52.6	49.7	54.2	52.6	51.9	50.6	47.2
T_{a2}	°C	187.0	177.6	170.5	151.9	113.1	183.3	176.8	169.6	151.9	113.1
T_{a3}	°C	97.8	95.2	94.1	91.1	79.3	96.3	94.9	93.7	91.1	79.6
T_{a4}	°C	44	44.6	45	46	50	45	44.2	44	45	51
T_{eg2}	°C	390	397	409.7	441	438	390	397	409.7	441	438
T_{lo1}	°C	76	75.4	75.3	75.1	73.6	76	75.4	75.3	75.1	73.6
T_{lo2}	°C	61	61	61	61	61	61	61	61	61	61
$\dot{m}_{lo}$	kg/s	18.1	18.1	18.1	18.1	18.1	36.2	36.2	36.2	36.2	36.2
$\dot{m}_{w1}$	kg/s	31.5	42.7	42.6	41.3	41.7	82.1	93.9	93.2	82.6	83.4
$\dot{m}_{w7}$	kg/s	13.3	13.3	13.3	13.3	13.3	26.6	26.6	26.6	26.6	26.6
$\dot{m}_{a}$	kg/s	9.15	8.27	7.78	6.9	5.26	18.3	16.64	15.67	13.81	10.52
$\dot{m}_{eg2}$	kg/s	9.4	8.5	8.0	7.1	5.4	18.8	17.1	16.1	14.2	10.8
p_{bar}	bar	1.028	1.028	1.028	1.030	1.031	1.015	1.015	1.015	1.016	1.016
p_{a2}	[bar-g]	2.4	2.14	2	1.7	1	2.3	2.16	2	1.6	0.9
p_{w1}	bar	3.15	3.15	3.15	3.15	3.15	3.15	3.15	3.15	3.15	3.15
p_{w7}	bar	3.15	3.15	3.15	3.15	3.15	3.15	3.15	3.15	3.15	3.15

Power demands are related to the propulsion of the ship, in particular, the electric power demand for propulsion and additional loads is function of the cube of the ship service

speed and it is given by the following two relations, determined by Soffiato [18], the first one valid for the laden voyage and the second one for the ballast voyage.

$$\dot{W}_{e,laden} = 89.5833\ V_s^3 - 4731.2500\ V_s^2 + 87060.4167\ V_s - 534918.7500 \quad (2.2)$$

$$\dot{W}_{e,ballast} = 84.7917\ V_s^3 - 4476.8750\ V_s^2 + 82365.2083\ V_s - 506033.125 \quad (2.3)$$

The available information about the working profile of the ship is divided into three main modes (Fig. 2.15): laden voyage (38.74% of the total time), ballast voyage (35.78% of the total time) and port operations (25.48% of the total time).

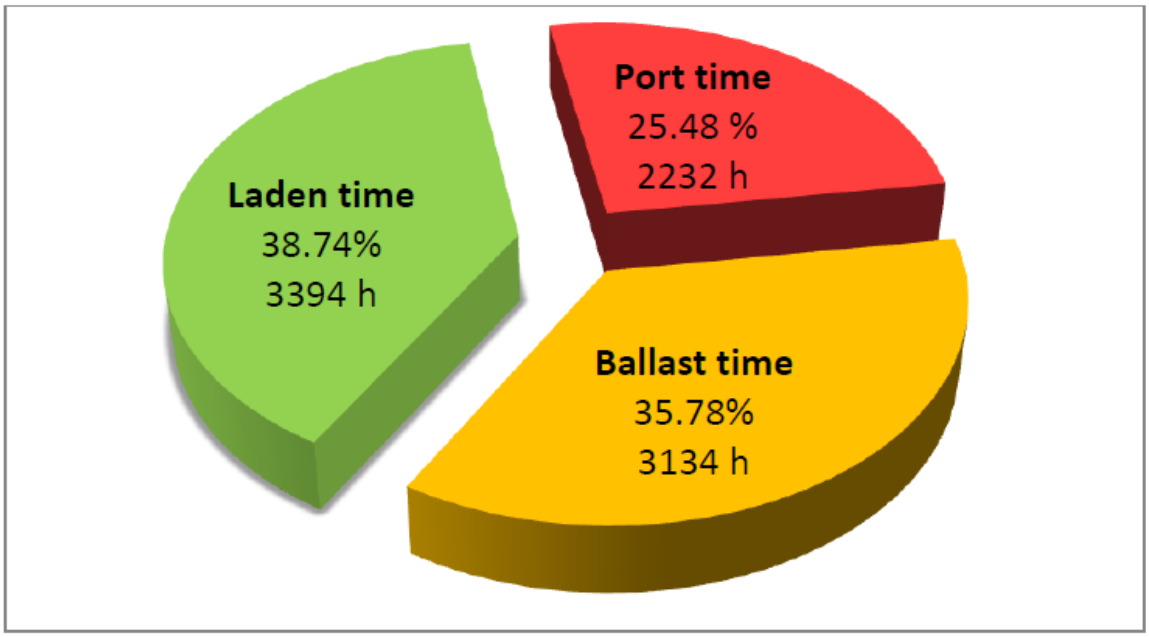

Figure 2.16 *Operating modes and relative working time of the vessel [18].*

All data were collected during 3.75 years of operation of the ship, to be averaged then in order to define a reference year. In this way, studies about annual operations are possible, especially to evaluate benefits in terms of electric energy production about the installation of an ORC system. The vessel speed distribution is given for laden and ballast voyages, the data of which are selected and provided for both of them in 13 different intervals, each one representing a velocity range of 1 kn. Every interval is described by the number of hours the ship travels at the related average speed.

All provided information about the ship speed distribution is reported in the two following tables, the first one (Tab. 2.3) is related to laden voyage, the second one (Tab. 2.4) to ballast voyage. Work production for every engine, and the relative load, is reported also to the number of operating engines.

Table 2.3 *Operating profile of the engines, laden mode [18].*

Average speed	Hours	Hours	W_e	12V50DF No.1	6L50DF No. 2	6L50DF No. 3	12V50DF No.4	Load
kn	%	-	kW	kW	kW	kW	kW	%
7.5	3.5	117.1	2823	0	0	2823	0	51
8.5	0.0	0.0	3517	-	-	-	-	-
9.5	1.3	43.8	4395	0	0	4395	0	80
10.5	3.7	125.2	5478	0	0	5478	0	100
11.5	6.2	211.8	6789	0	0	0	6789	62
12.5	5.3	180.6	8350	0	0	0	8350	76
13.5	11.4	386.6	10180	0	0	0	10180	93
14.5	10.5	357.7	12304	0	0	4101	8202	75
15.5	22.6	766.4	14741	0	0	4914	9827	89
16.5	14.2	483.3	17514	0	4378	4378	8757	80
17.5	9.6	326.5	20711	0	5178	5178	10355	94
18.5	4.3	146.6	24315	9726	0	4863	9726	88
19.5	7.3	248.1	28302	9434	4717	4717	9434	86

Table 2.4 *Operating profile of the engines, ballast mode [18].*

Average speed	Hours	Hours	W_e	12V50DF No.1	6L50DF No. 2	6L50DF No. 3	12V50DF No.4	Load
kn	%	-	kW	kW	kW	kW	kW	%
6.5	0.7	22.3	2112	0	0	2112	0	38
7.5	0.0	0.0	2617	-	-	-	-	-
8.5	0.0	0.0	3276	-	-	-	-	-
9.5	0.0	0.0	4110	-	-	-	-	-
10.5	0.5	14.7	5139	0	0	5139	0	93
11.5	6.2	192.8	6385	0	0	0	6385	58
12.5	7.4	232.3	7867	0	0	0	7867	72
13.5	14.2	444.1	9607	0	0	0	9607	87
14.5	5.6	175.5	11624	0	0	3875	7749	70
15.5	17.9	561.4	13939	0	0	4646	9293	84
16.5	34.5	1079.8	16573	8287	0	0	8287	75
17.5	10.1	317.5	19607	9804	0	0	9804	89
18.5	3.0	94.0	23027	9211	0	4605	9211	84

The number of operating engines and their load is evaluated a according to the two following rules:

- the electric power generation is generated by the lowest possible number of engines, in order to keep their efficiency high;
- the total electric power is subdivided to operating engines proportionally to their nominal power.

As an example in laden mode at 18.5 kn the required total power is 24315 kWe (Tab. 2.3) that correspond to the about the 74% of maximum total power. It may be generate by 3 engines (two 11 MWe sized and one 5.5 MWe sized) operating at about 88% of their maximum load. A lower number of operating engines cannot generate the required amount of total power, while the operation of all engines results in a lower load at which the engines work.

Tables 2.3 and 2.4 are used to determine the off-design operation of the ship during a typical year and then to evaluation of the annual consumption of the ship. In Fig. 2.16 it is easier to recognize the most adopted service speeds of the vessel during the year, useful information for design choices and off-design evaluations.

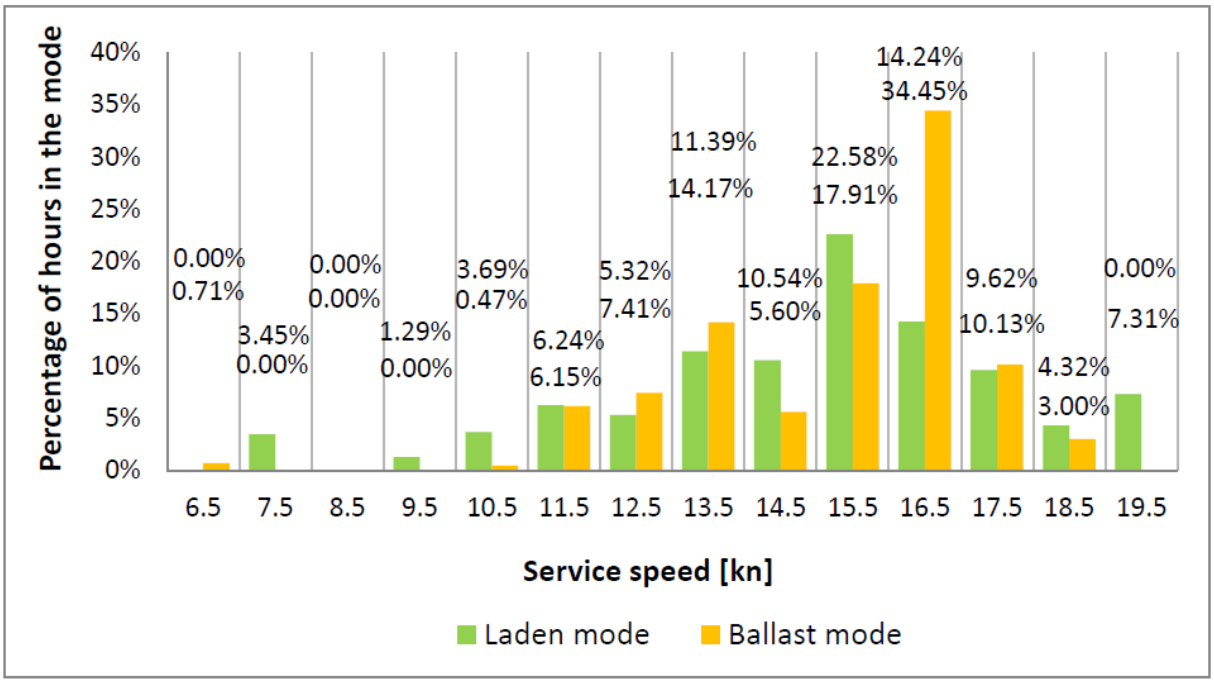

Figure 2.17 *Distribution profile of the vessel speed at laden and ballast voyage [18].*

It can be noticed that the most frequently encountered velocities of the vessel are in the range between 15 and 17 kn, for an amount of annual hours of 2890.9 of the total working hours of 6528.1. This is because the lower service speed leads to a significant reduction in power for propulsion compared to the higher velocities, hence in the fuel consumption, while the lower velocities could not be sufficient to satisfy the required travel times for the LNG carrier. This evaluation is very important to decide the design point of the ORC system, which affects also all the off-design operation. In particular, a proper choice of design conditions has to allow the exploitation of the biggest available range of velocities for the maximum possible working time of the ship.

Soffiato determined a nominal velocity based on the available statistic data about the ship's trips in the reference year, considering both the laden and the ballast voyage. The determined nominal speed of 18.40 kn in laden voyage corresponds to a load of 85% for

three Diesel engines, namely two of the more powerful type B and one of the type A, with the last engine not working. The covered power demand is in this way of 23,375 kW.

The found operating point is summarized in Tab. 2.4, where the produced electric power is related to the engines according to the assumptions made.

Table 2.5 *Operating point for the engines [18].*

W_e	12V50DF No.1	6L50DF No. 2	6L50DF No. 3	12V50DF No.4	Load
kW	kW	kW	kW	kW	%
23375	9350	0	4675	9350	85

2.2.2 Engines cooling system configurations

After the definition of an operating point for the vessel a preliminary estimation of the performances of the ORC system is performed. Its selection allows to determine the design conditions of the ship energy system, thanks to which it is possible to evaluate the best way to integrate the ORC and decide the most convenient configuration for the combined power plant. So it is possible to calculate the thermal flows that are rejected to the cooling system of the engines, and the heat related to the exhaust gas.

In order to make available the Diesel engines waste heat to the ORC system, Soffiato considered three different cooling system layouts for the ship:

- the *existing layout*, where the high temperature cooling flows coming from the three operating engines are mixed in a unique stream and sent to ORC heat exchangers (preheater, evaporator), and the same is done with the low temperature cooling flow, used in the ORC condenser; hot sources are so HT and LT cooling fluids;
- a *modified layout*, with a changing in low temperature cooling system, where a direct heat transfer between lubricating oil and ORC working fluid is adopted, with the consequent reduction of LT cooling fluid maximum temperature, still usable in ORC preheater; hot sources are HT and LT cooling fluids and lubricating oil;
- a *new design of engine cooling systems*, in order to optimize engines waste heat recovery and to exploit its better quality.

The selected configuration in this work for the single stage ORC system is the first one, the existing layout, because of its simplicity and that this choice does not need of an additional economic investment in Diesel engines cooling system modifications. For the two stage ORC system a modification in the layout is needed, in order to make available an hotter source for the second pressure level.

About the low pressure level, for both the ORC configurations, the employed heat comes from the fresh water cooling system. Regarding the high pressure level, it is powered

by the hottest available fluid, i.e., the charge air exiting from the compressor of the T-C system.

The resulting combined cycle, for both the configurations of the ORC system, is treated in the next paragraph. Fig. 2.17 show a simple scheme of the chosen layout.

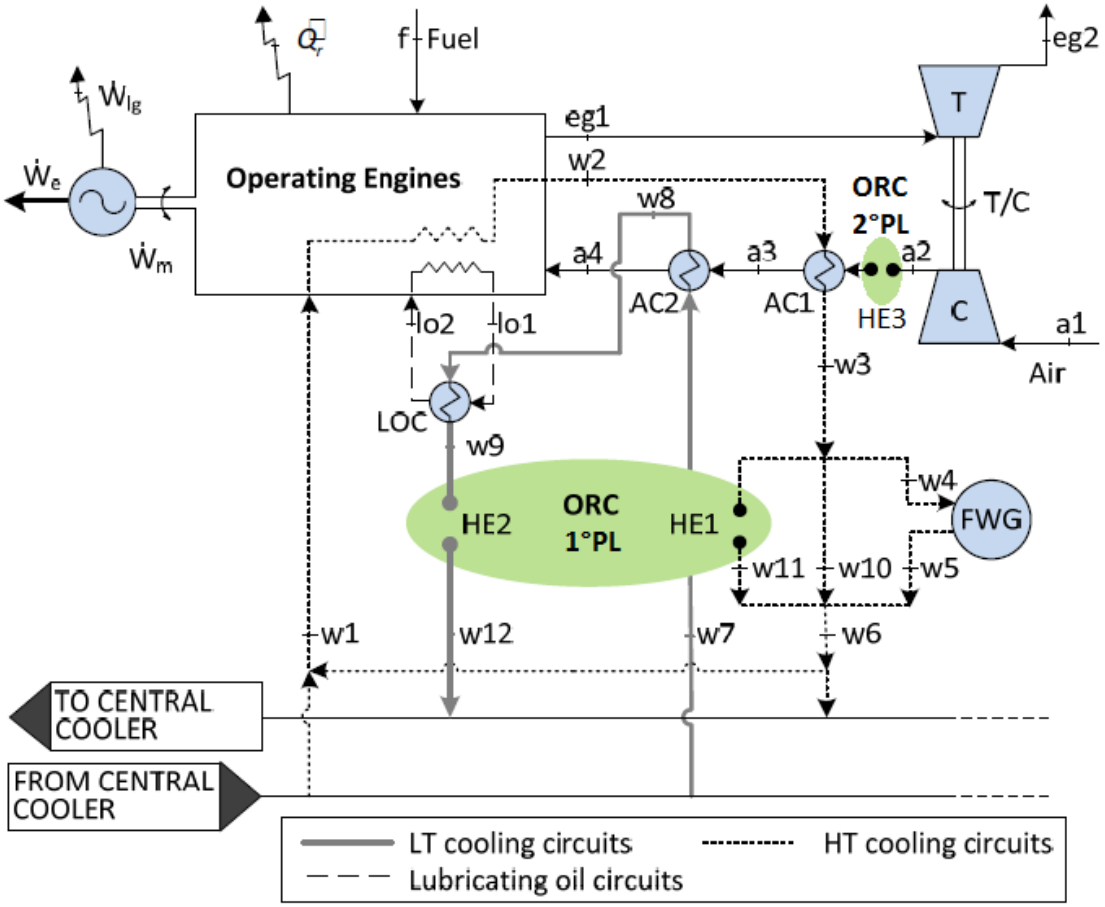

Figure 2.18 *Diesel engines – ORC configuration.*

There are two different available hot sources for the single stage ORC and the first pressure level of the two stage one, both taken just before being sent to the central cooler, one from the low temperature cooling circuits and one from the high temperature cooling circuits. The main function of these flows consists in cooling down:

- for the LT circuits, both the charge air, through the *air cooler* AC2, and the lubricating oil, using the *lubricating oil cooler* LOC;
- for the HT circuits, both the *cooling water* passing through the bodies of the engines, and the charge air again, through the *air cooler* AC1.

These circuits terminate at the *central cooler*, where the temperatures of the flows are decreased to allow them to restart the cooling cycle.

For the second pressure level, the useful available hot source is the charge air before it is cooled by the heat exchanger AC1.

2.2.3 Engines-ORC combined cycle

By inserting the first pressure level of the ORC system in the way shown in Figure 2.18, it can be noticed that the two hot sources are downstream the engines and upstream the central cooler. Thus, the ORC installation does not result in any variation of the engines, i.e. it is not actually influenced by the new installation. Rather, collecting the heated water after the cooling cycle and reducing its temperature again, the only important variation results in a lower cooling load of the central cooler. Hence there are no disadvantages in adopting this configuration for the Diesel engines system.

Contrarily, when the second pressure level is matched with the engines, an accurate design must be carried out in order to not compromise the main engines power plant operation. In particular, the outlet pressure and temperature of the charge air exiting the first air cooler (point *a3* in Fig.2.17) are to be maintained as closer as possible to the values without the ORC.

From the nominal velocity, hence from the vessel energy system's operating point, nominal conditions can be defined by checking the values of main parameters of the hot fluids coming from the engines and collected by ORC's heat exchangers. For every hot fluid these nominal parameters are: mass flow rate, pressure and inlet temperature in the exchanger.

From the design study of Soffiato, the interesting temperatures of the two cooling fluids, actually heated water and the charge air at the compressor outlet, that represent the available hot sources for the ORC system, are known both at nominal and partial load conditions of the Diesel engines. In particular, in Tabs. 2.5 and 2.6 the main values at design point of the mass flow rates and the state variables belonging to the three hot sources at the points of interest are reported, namely *w3* at the inlet of the first ORC's heat exchanger HE1, *w9* at the inlet of the second one HE2 and *a2* at the inlet of HE3.

Table 2.6 *Thermodynamic properties of the cooling water (hot sources) at the inlet of HE1 and HE2 for existing layout at design point of Soffiato [18].*

Hot source	Mass flow rate [kg/s]	Pressure [bar]	Temperature [°C]
w3 (HT cooling water)	196.36	3.15	82.8
w9 (LT cooling water)	66.5	3.15	51.9

Table 2.7 *Thermodynamic properties of the charge air (hot source) at the inlet of HE3 for modified layout at design point of Soffiato [18].*

Hot source	Mass flow rate [kg/s]	Pressure [bar]	Temperature [°C]
a2 (charge air)	39.12	3.015	169.78

Regarding the cold source that is used in the ORC's condenser in order to change the phase of the working fluid from vapour to liquid after the expansion in turbine, the adopted fluid is cold sea water, whose state variables are presented below. The inlet point can be

found in Figure 2.19, reporting the integration scheme between Diesel engines and ORC systems.

Table 2.8 *Thermodynamic properties of the cooling water (cold source) at the inlet of the condenser at design point of Soffiato [18].*

Cold source	Mass flow rate [kg/s]	Pressure [bar]	Temperature [°C]
c1 (cold water)	242.55	3.15	15.0

Soffiato investigated the possibility of implementation of three different ORC system configurations, optimized according to the selected organic fluid and the chosen cooling system layout:

- a *single pressure level ORC*, either subcritical or supercritical cycle;
- a *regenerative ORC*, with addition of a recuperator, a heat exchanger where working fluid coming from the pump is preheated by desuperheating the vapour exiting from the expander;
- a *two pressure level ORC*, with subcritical lower cycle and both subcritical and supercritical higher cycle.

Various simulations were carried out by Soffiato, selecting from available fluids the six best compatible choices with the use in a LNG carrier. Prerequisites for these fluids are: low flammability; low toxicity; ozone-friendly; permission for use in ship. Resulting fluids are so the following six: R-134a, R-125, R-236fa, R-245ca, R-245fa, R-227ea. Hydrocarbons are not allowed in LNG carrier, for obvious safety issues.

Optimization results, relatively to the three ORC configurations combined to the three engines cooling system layouts, show that the best performing fluids are different, depending on the whole considered ORC installation. In particular, according to Soffiato, for the single pressure level ORC inserted in the existing layout the best choices are R245fa and R245ca and their relatively low evaporation pressure makes them suitable for safety issues.

Malandrin [21] started from the results obtained by Soffiato to develop an off-design model of the single pressure level ORC system combined to the existing Diesel engines cooling system layout. He used MATLAB Simulink as modelling software and obtained a detailed off-design model that adopted to simulate two test cases in order to analyse the energy system's behaviour. He chose two possible working fluids from the list of six that Soffiato collected, R245fa and R134a, the use of the latter being now banned. For R245fa the adequate cycle is the saturated one, because of the shape of the Andrews curve in T-s diagram, whose saturated vapour line has positive slope and so superheating is not needed. For R134a superheating is necessary in order to avoid condensation inside the expander, due to the negative slope of saturated vapour line, typical of this particular refrigerant fluid.

In this work, focus will be on development of two ORC system off-design models: a single pressure level ORC and a two pressure level ORC with the higher one subcritical or supercritical. Selected fluid is one of the two chosen by Malandrin, R245fa. R134a is not considered anymore because of ban from market, ban that has been ruled for environmental safety issues. A different operating point is also defined: the previously

selected one indeed leads to a design of the ORC's heat exchangers that does not allow running the cycle in the off-design operation of 14 ÷ 16 kn. This is caused by the too low available heat with respect to the design one, with as consequence the impossibility for the operative fluid to reach an equilibrium point for the evaporation pressure inside the subcritical evaporator HE1. In this way, a large number of working hours is not exploitable for the ORC operation, making unattractive its installation. These problems are caused by the big difference in the available hot mass flow rate among the various ranges of velocities. For this reason, it is more convenient to select as new operating point a frequently adopted one by the vessel. After evaluations on four different choices, that will be presented in chapter 4, the selected new operating point in this work is corresponding for the single stage ORC to a service speed of 16.5 kn in laden voyage, for the two stage ORC to 15.5 kn again in laden voyage. The new design conditions, before for single stage and then for two stage ORC, are reported in next tables.

Table 2.9 *New selection of operating point for the engines (single stage and two stage ORCs).*

$\dot{W}_e$	12V50DF No.1	6L50DF No.2	GL50DF No.3	12V50DF No.4	Load
kW	kW	kW	kW	kW	%
17514	0	4378	4378	8757	80
14741	0	0	4914	9827	89

Table 2.10 *Thermodynamic properties at the new design point (single stage ORC).*

Source	Mass flow rate [kg/s]	Pressure [bar]	Temperature [°C]
w3 (HT cooling water)	137.80	3.15	82.41
w9 (LT cooling water)	53.20	3.15	51.46
c1 (cold water)	242.55	3.15	15.00

Table 2.11 *Thermodynamic properties at the new design point (subcritical two stage ORC).*

Source	Mass flow rate [kg/s]	Pressure [bar]	Temperature [°C]
w3 (HT cooling water)	106.10	3.15	80.65
w9 (LT cooling water)	39.90	3.15	52.47
a2 (charge air)	24.61	3.14	175.70
c1 (cold water)	242.55	3.15	15.00

Table 2.12 *Thermodynamic properties at the new design point (supercritical second stage).*

Source	Mass flow rate [kg/s]	Pressure [bar]	Temperature [°C]
w3 (HT cooling water)	106.10	3.15	79.70
w9 (LT cooling water)	39.90	3.15	52.47
a2 (charge air)	24.61	3.14	175.70
c1 (cold water)	242.55	3.15	15.00

2.2.3.1 Single stage ORC system

The optimal design operating characteristics determined by Soffiato, about all the six fluids he studied, are reported in Table 2.13. Green-shaded cells indicate the nominal values about the selected fluid for this work, the refrigerant R245fa. New designs of the ORC system have been carried out taking into account of the new selected operating points and the relative configurations to study, maintaining the original design choices only for condensation temperatures and pressures and the absence of superheating for the working fluid. The other results coming from this work will be shown in the next chapter, in Paragraph 3.3.3 regarding design operating characteristics.

In Figure 2.18 and Table 2.9 the simple scheme of the chosen layout and the thermodynamic properties of the hot sources are presented, to take the case of Soffiato as example, it must be noticed that only the heat exchanger HE1 is able to lead the fluid to evaporation, given the defined R245fa working fluid's pressure of 5.695 bar imposed by the pump in design conditions. The reason of this is that, at the fixed pressure, the R245fa evaporation temperature is at 67.436°C, higher than the temperature of 52.6°C of the available hot water at the point *w9*, where HE2 is placed. Consequently, the only correct choice is to exploit the LT cooling water hot source to preheat the working fluid through the heat exchanger HE2, while the HT cooling water is used into HE1 to evaporate it. Respecting this constraint, the installation of the single stage ORC in the existing layout of the Diesel engines system is possible.

Table 2.13 *Optimized operating characteristic for single stage ORC and ship existing layout.*

Fluid	unit	R134a	R125	R236fa	R245ca	R245fa	R227ea
p_{ev}	bar	20.132	35.197	9.327	4.054	5.695	14.288
p_{cond}	bar	7.702	15.685	3.210	1.217	1.778	5.284
T_{cond}	°C	30.0	30.0	30.0	30.0	30.0	30.0
ΔT_{sup}	°C	5.0	8.0	0.0	0.0	0.0	0.0
T_3	°C	72.8	72.8	67.8	67.4	67.4	68.2
T_4	°C	34.1	34.8	41.3	40.9	39.2	41.0
χ	-	1.02	1.05	1.07	1.05	1.05	1.09
sub/sup	-	sub	sub	sub	sub	sub	sub
w_{exp}	kJ/kg	14.968	8.923	12.395	17.153	16.133	9.547
w_{pump}	kJ/kg	1.658	2.651	0.722	0.328	0.469	1.044
w_{net}	kJ/kg	13.310	6.273	11.672	16.825	15.664	8.503
$q_{absorbed}$	kJ/kg	192.525	117.742	166.239	227.523	213.729	128.443
q_{cond}	kJ/kg	177.385	110.212	153.118	208.760	196.226	118.775

$\dot{m}_{wf}$	kg/s	30.388	51.517	35.450	25.372	27.109	44.699
W_{net}	kW	404.5	323.1	413.8	426.9	424.6	397.1
η_{th}	%	6.91	5.33	7.02	7.39	7.33	6.62
η_t	%	4.14	3.31	4.23	4.37	4.34	4.06
VR	-	2.801	2.657	3.136	3.323	3.234	3.153
SF	m	0.433	3.881	0.656	0.906	0.777	0.578
$\dot{Q}_{absorbed}$	kW	5850.4	6065.5	5893.2	5772.7	5749.0	5998.1
$\dot{Q}_{cond}$	kW	5390.4	5677.6	5428.0	5296.6	5319.5	5546.6

The adopted configuration of the first ORC version, the single stage one, is reported in Figure 2.19, overlaid to the Diesel engines system. In this layout one accumulator upstream the condenser is sufficient to dampen the variation in organic fluid density and pressure during start-up, shot-down and operation until an equilibrium point is reached.

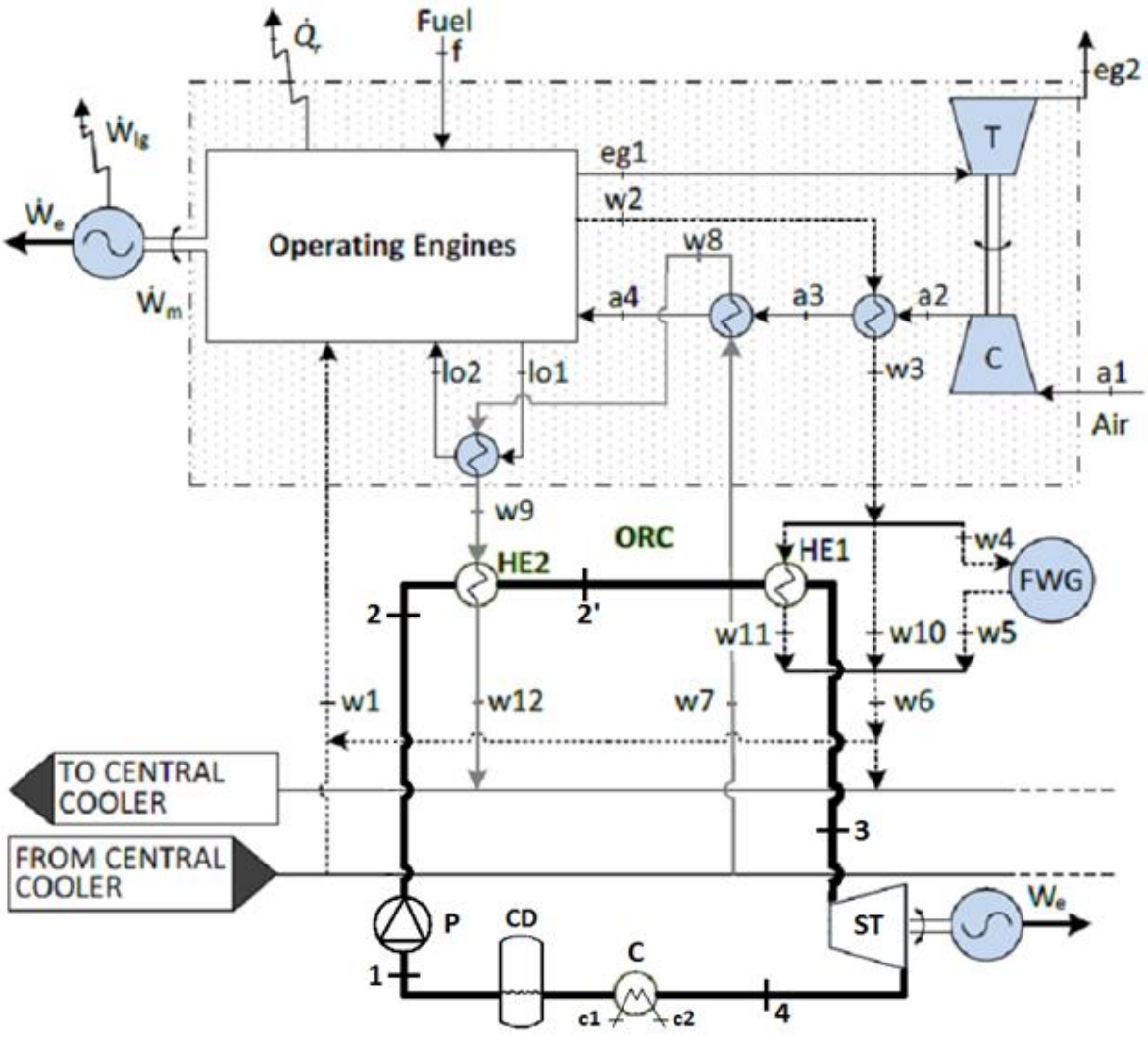

Figure 2.19 *Global configuration for the single stage ORC installation.*

The corresponding thermodynamic cycle is presented in Fig. 2.19 and the corresponding values of the main state variables of the working fluid R245fa at the various points is listed in Tab. 2.13.

Table 2.14 *Thermodynamic properties of the working fluid (R245fa) for the single stage Organic Rankine Cycle at design point.*

Cycle's point	Mass flow rate [kg/s]	Pressure [bar]	Temperature [°C]
1	28.00	1.778	29.80
2	28.00	5.236	29.92
2'	28.00	5.236	41.46
3	28.00	5.236	64.36
4	28.00	1.778	39.23

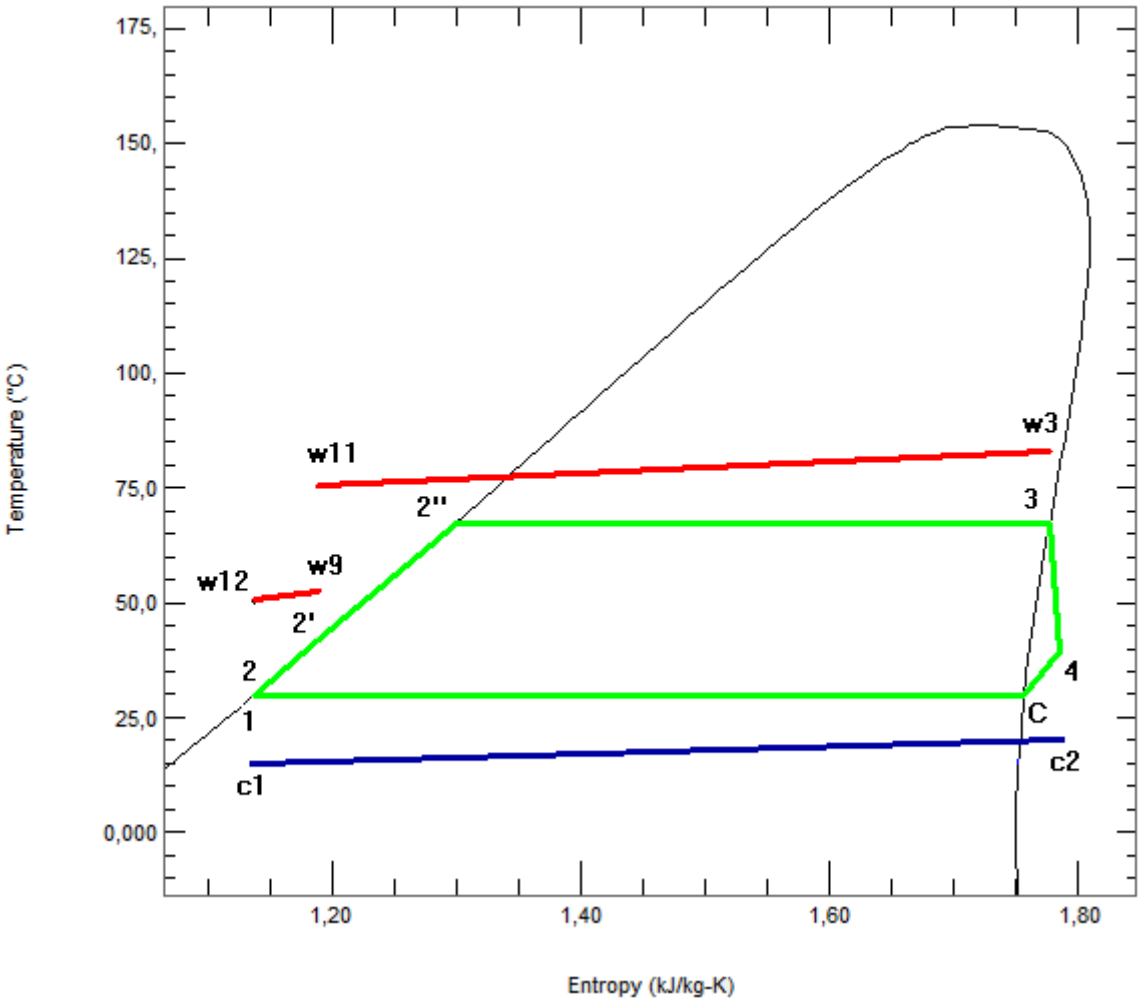

Figure 2.20 *Single stage ORC thermodynamic cycle.*

To determine the values of the characteristic parameters of the heat sources exploited by the ORC, mass and energy balance equations were applied. The contribution of all the working engines at the considered operating point must be taken into account. In the following, the adopted balances are presented. The subscript "A" will refer the parameter in

question to the engine type 6L50DF, while the subscript “B” will refer to the engine type 12V50DF.

Starting from the LT circuit, the cooling fluid providing heat for the preheater HE2, the inlet water temperature T_{w9} is obtained by the knowledge of pressure from available data and the evaluation of the respective enthalpy at point *w9*, by the application of the energy balance equation:

$$2\,\dot{m}_{w7,A}h_{w9,A} + \dot{m}_{w7,B}h_{w9,B} = \left(2\,\dot{m}_{w7,A} + \dot{m}_{w7,B}\right)h_{w9} \tag{2.4}$$

that can be rewritten in the following form, making explicit the parameter of interest

$$h_{w9} = \frac{2\,\dot{m}_{w7,A}h_{w9,A} + \dot{m}_{w7,B}h_{w9,B}}{2\,\dot{m}_{w7,A} + \dot{m}_{w7,B}} \tag{2.5}$$

The mass balance gives the water mass flow rate involved in the heat exchange, collected at the outlet of the LT circuit of the engines:

$$\dot{m}_{w7} = 2\,\dot{m}_{w7,A} + \dot{m}_{w7,B} \tag{2.6}$$

Once the values of h_{w9} and p_{w9} are available, the water temperature can be easily obtained by the use of NIST Refprop.

The presented procedure is also applied to calculate T_{w3}, by the use of the energy balance equation that follows:

$$2\,\dot{m}_{w1,A}h_{w3,A} + \dot{m}_{w1,B}h_{w3,B} = \left(2\,\dot{m}_{w1,A} + \dot{m}_{w1,B}\right)h_{w3} \tag{2.4}$$

which is solved for h_{w3}:

$$h_{w3} = \frac{2\,\dot{m}_{w1,A}h_{w3,A} + \dot{m}_{w1,B}h_{w3,B}}{2\,\dot{m}_{w1,A} + \dot{m}_{w1,B}} \tag{2.5}$$

The mass balance gives the water mass flow rate collected at the outlet of the HT circuit of the engines:

$$\dot{m}_{w1} = 2\,\dot{m}_{w1,A} + \dot{m}_{w1,B} \tag{2.6}$$

The involved flow rate in the heat exchange is $\dot{m}_{w11}$, to be obtained by the following mass balance:

$$\dot{m}_{w11} = \dot{m}_{w1} - \dot{m}_{w4} - \dot{m}_{w10} \tag{2.7}$$

The mass flow rate at point *w4* is the one required by the FWGs (Fresh Water Generators), models JWP-26-C100 and HWL 20-35. The operation at both design and off-design conditions is described by the relation below:

$$\dot{m}_{w4} = \frac{\dot{Q}_{FWG}}{h_{w4} - h_{w5}} \tag{2.8}$$

that can be rewritten in the following form

$$\dot{m}_{w4} = \frac{K\,\dot{V}_d}{\Delta T} \tag{2.9}$$

where K is a proportionality constant equal to 7.08 $\left[\frac{\text{kg}}{\text{s}}\frac{24\text{h}}{\text{m}^3}\text{K}\right]$, $\dot{V}_d$ the capacity of the fresh water generator $\left[\frac{\text{m}^3}{24\text{h}}\right]$, and ΔT the inlet-outlet temperature difference ($T_{w4} - T_{w5}$) of the feeding water. It is worth noting that, given the presented scheme of the engines-ORC configuration, the water temperature T_{w4} is equal to T_{w3}. It is assumed for the fresh water generators that the absorbed heat $\dot{Q}_{FWG}$ is constant in off-design conditions of the ship, thanks to a bypass valve that adjusts the feeding water $\dot{m}_{w4}$ for this purpose, and consequently the temperature T_{w5} is constant and equal to design conditions.

The remaining mass flow rate to define, $\dot{m}_{w10}$, is bypassed and mixed after the FWG in order to respect the constraint about T_{w5}. It is calculated by the following mass balance:

$$\dot{m}_{w3} = \dot{m}_{w5} + \dot{m}_{w10} + \dot{m}_{w11} \tag{2.10}$$

reformulated as follows

$$\dot{m}_{w10} = \dot{m}_{w1} - \dot{m}_{w4} - \dot{m}_{w11} \tag{2.11}$$

It is worth noting that the involved mass flow rate in the heat exchange with the evaporator of the ORC system, HE1, is imposed to be as high as possible. In this case, when there is the maximum exploitation of the heat related to the cooling water of the HT circuit, the temperature T_{w6} is equal to T_{w1}, and consequently T_{w11} is equal to T_{w1}. About the LT circuit, the maximum exploitation is pursued if the total flow rate $\dot{m}_{w7}$ is cooled down to the temperature T_{w7}.

The maximum amount of heat that can be absorbed from the low temperature circuit and the high temperature circuit of the cooling system is given by, respectively:

$$\dot{Q}_{LT,available} = 2\left(\dot{Q}_{ca,LT} + \dot{Q}_{lo}\right)_A + \left(\dot{Q}_{ca,LT} + \dot{Q}_{lo}\right)_B \tag{2.12}$$

$$\dot{Q}_{HT,available} = 2\left(\dot{Q}_{jw} + \dot{Q}_{ca,HT}\right)_A + \left(\dot{Q}_{jw} + \dot{Q}_{ca,HT}\right)_B - \dot{Q}_{FWG} \tag{2.13}$$

These energy balance equations can be rewritten as:

$$\dot{Q}_{LT,available} = \dot{m}_{w7}(h_{w9} - h_{w7}) \tag{2.14}$$

$$\dot{Q}_{HT,available} = \dot{m}_{w1}(h_{w3} - h_{w1}) - \dot{Q}_{FWG} \tag{2.15}$$

The assumed constant value of $\dot{Q}_{FWG}$ is:

$$\dot{Q}_{FWG} = 891.7\ kW$$

By the use of the available data in Table 2.2, it is possible to build the Hot Composite Curve, shown together with a table that collects the calculated values of the useful parameters.

Table 2.15 *Main parameters used for the construction of the HCC, single stage ORC system.*

Source	$\dot{Q}$	T_{max}	T_{min}	p
-	kW	°C	°C	bar
HT circuit	5555	82.4	72.8	3.15
LT circuit	3446	51.5	36	3.15

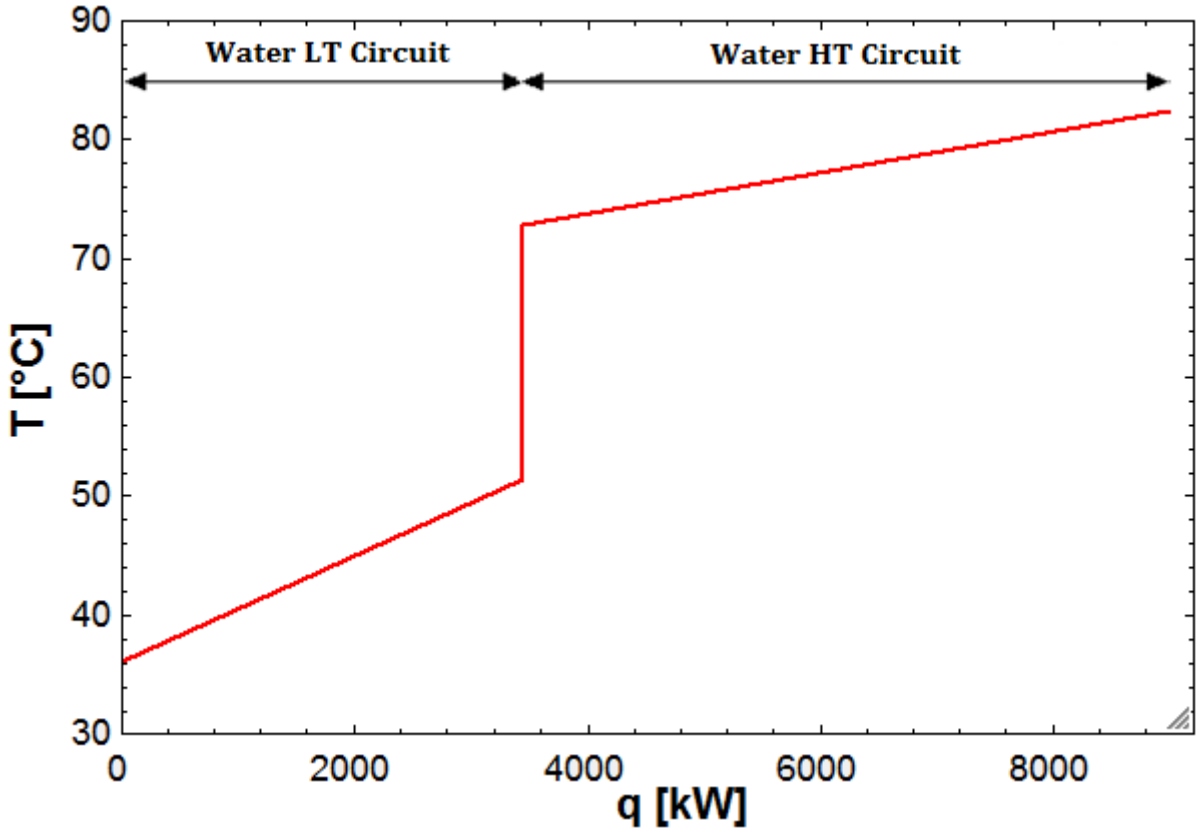

Figure 2.21 *Hot Composite Curve of the available heat and exchanging working fluid curve, single stage ORC system.*

2.2.3.2 Two stage ORC system

The only available hot source characterized by a temperature high enough to feed a second pressure level is the charge air at point *a2*, immediately after compression in the T-C system. The idea is hence to insert the evaporator HE3 (subcritical or supercritical) between the point *a2* and the heat exchanger AC1. A valve is added as well, to bypass the exchanger HE3 if the whole ORC or at its second pressure level, is not working.

To complete the second pressure level for the ORC system, a second pump and a second vapour turbine are included, according to Figure 2.19, as well as two three way valves. The valves are a diverter valve after the cold drum and two mixer valves after the two evaporators HE1 and HE3. It is worth noting that, in case of adoption of another subcritical evaporator for the second pressure level, an additional hot drum device both for the first

and the second pressure level is needed to dampen the mass flow rate and pressure fluctuation in the system during transient and normal operation. About the supercritical second stage, a hot drum device is still required for the first pressure level. The presence of these additional accumulators is necessary for the control system to fix and maintain the evaporation pressures, in order to find an equilibrium state in design and off-design stationary conditions for the whole cycle. In fact a control on the only cold drum device is not sufficient to stabilize all pressures in the cycle.

The values of the mass flow rate and the state variables at design point belonging to the hot source at the point *a2* are reported in Table 2.9.

The chosen configuration for the two stages ORC is shown in the Fig. 2.21. The corresponding subcritical and supercritical cycles is shown in Figs. 2.22 and 2.23, respectively. Tabs. 2.15 and 2.16 report the main values at design point of the working fluid in the two cases of study.

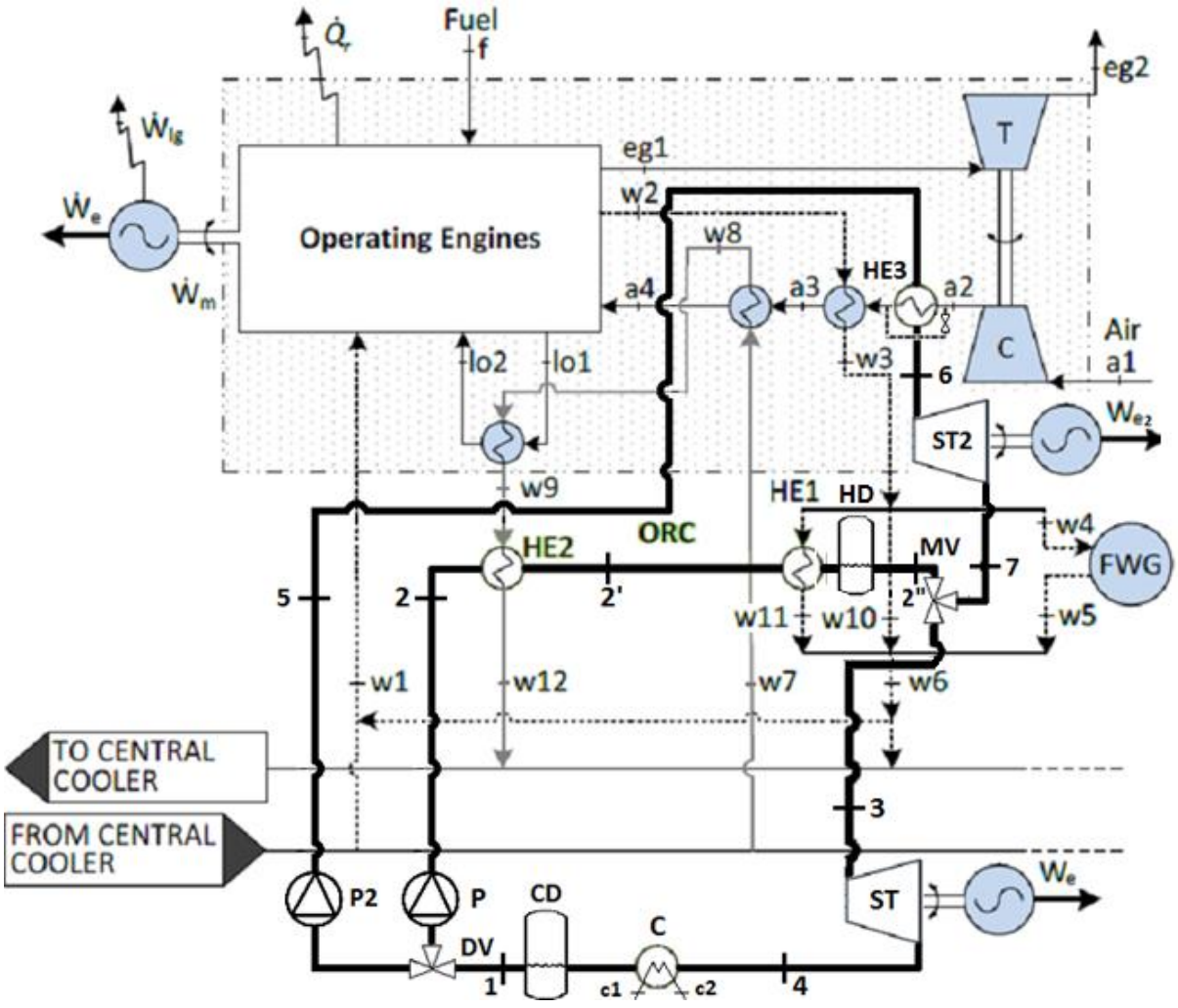

Figure 2.22 *Diesel engines – two stage ORC configuration (supercritical second stage).*

Table 2.16 *Thermodynamic properties of the working fluid (R245fa) for the two stage Organic Rankine Cycle at design point, case 1 (subcritical evaporator as HE3).*

Cycle's point	Mass flow rate [kg/s]	Pressure [bar]	Temperature [°C]
1	33.46	1.766	29.61
2	28.35	4.612	29.72
2'	28.35	4.612	42.57
2''	28.35	4.612	59.82
3	33.46	4.612	62.30
4	33.46	1.766	40.29
5	5.11	25.850	30.46
6	5.11	25.850	135.37
7	5.11	4.612	76.05

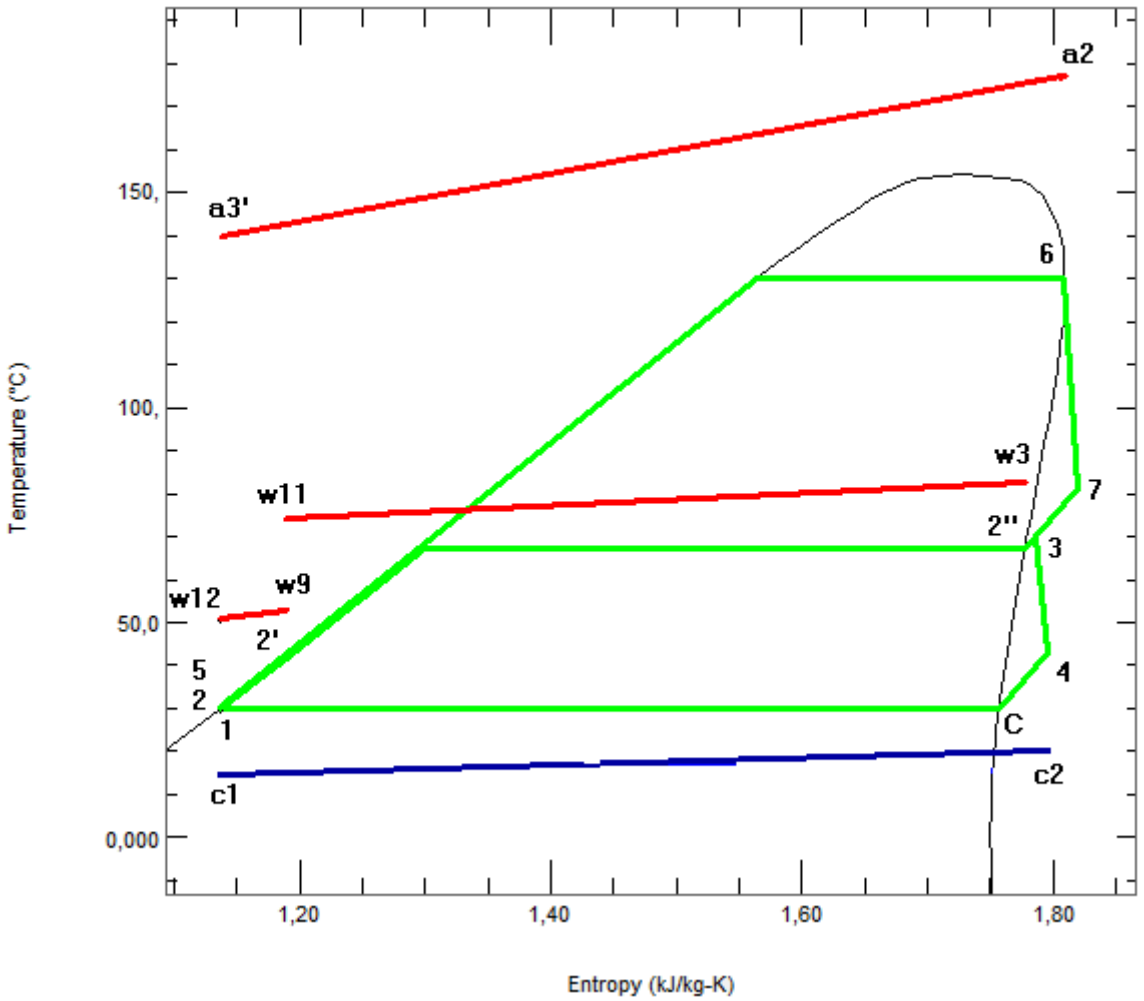

Figure 2.23 *Two stage ORC thermodynamic cycle (subcritical second pressure level).*

Table 2.17 *Thermodynamic properties of the working fluid (R245fa) for the two stage Organic Rankine Cycle at design point, case 2 (supercritical evaporator as HE3).*

Cycle's point	Mass flow rate [kg/s]	Pressure [bar]	Temperature [°C]
1	35.45	1.766	29.61
2	28.35	4.612	29.72
2'	28.35	4.612	42.47
2''	28.35	4.612	59.82
3	35.45	4.612	63.28
4	35.45	1.766	41.31
5	7.10	37.000	30.84
6	7.10	37.000	158.16
7	7.10	4.612	77.05

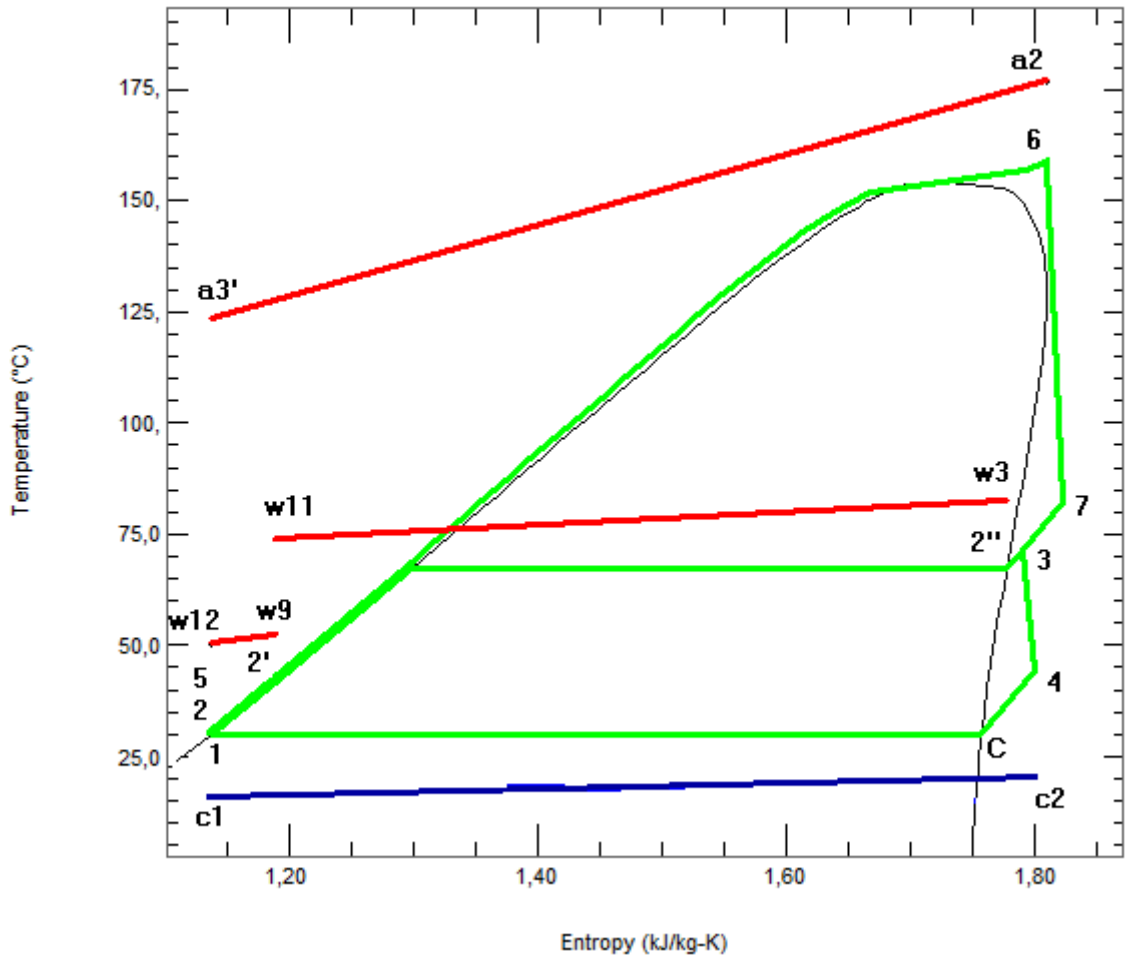

Figure 2.24 *Two stage ORC thermodynamic cycle (supercritical second pressure level).*

For the two stage ORC system, additional mass and energy balance equations have to be introduced in order to calculate the needed state parameters and flow rates for the second pressure level. The main difference about this calculation is the constraint coming from the assumption that the installation of the evaporator HE3 (subcritical or supercritical) must not affect the main engines energy system. For this reason, all the mass and energy balances are performed again, also for the first pressure level of the ORC, taking into account the variation of the heat exchange in the *air cooler* AC1. The equations about the LT and HT cooling circuits are the same presented in the previous paragraph (Eq. (2.4) to (2.11)).

As for the single stage ORC, the contribution of all the working engines at the considered operating point is taken into account. In the same way, the subscript "A" will refer the parameter in question to the engine type 6L50DF, while the subscript "B" will refer to the engine type 12V50DF.

To obtain the temperature T_{a2}, the next energy balance equation is applied:

$$2\,\dot{m}_{a,A} h_{a2,A} + \dot{m}_{a,B} h_{a2,B} = \left(2\,\dot{m}_{a,A} + \dot{m}_{a,B}\right) h_{a2} \tag{2.16}$$

which is solved for h_{a2}:

$$h_{a2} = \frac{2\,\dot{m}_{a,A} h_{a2,A} + \dot{m}_{a,B} h_{a2,B}}{2\,\dot{m}_{a,A} + \dot{m}_{a,B}} \tag{2.17}$$

The following mass balance equation gives the involved mass flow rate in heat exchange:

$$\dot{m}_a = 2\,\dot{m}_{a,A} + \dot{m}_{a,B} \tag{2.18}$$

Once the values of h_{a2} and p_{a2} are available, the charge air temperature can be easily obtained by the use of NIST Refprop. Note that in Table 2.2 the air pressure p_{a2} is expressed in [bar-g], hence the value refers to the relative pressure. For this reason, the absolute pressure must be determined, which given by p_{bar} in the table.

The maximum amount of heat that can be absorbed from the charge air circuit is expressed as follows:

$$\dot{Q}_{ca,HT,available} = 2\dot{Q}_{ca,_A} + \dot{Q}_{ca,_B} \tag{2.19}$$

$$\dot{Q}_{ca,HT,available} = \dot{m}_a (h_{a2} - h_{a3}) \tag{2.20}$$

By use of the available data in Table 2.2, also for this case the Hot Composite Curve is built and presented here together with a table that collects the calculated values of the characteristic parameters.

Table 2.18 *Main parameters used for the construction of the HCC, two stage ORC system.*

Source	$\dot{Q}$	T_{max}	T_{min}	p
-	kW	°C	°C	bar
Water HT circuit	5471	80.7	68.4	3.15
Water LT circuit	2747	52.5	36	3.15
Charge air	2040	175.7	94.2	3.14

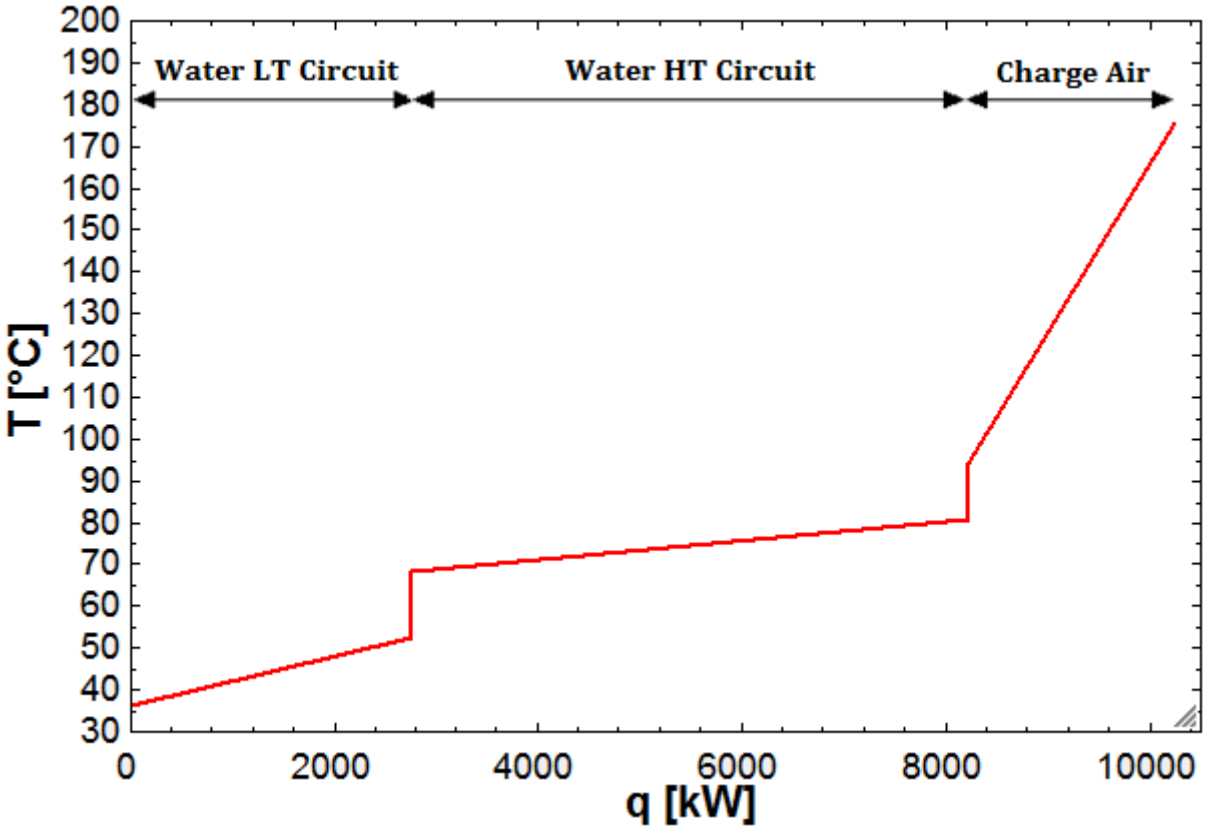

Figure 2.25 *Hot Composite Curve of the available heat, two stage ORC system.*

2.3 CONCLUSIONS

This chapter first presents the Organic Rankine Cycle technology, by evaluating thermodynamic cycle, optimal working conditions and features of the available operative fluids. A comparison between traditional steam Rankine cycle plants and ORC systems has been proposed, exposing advantages and limits of both technologies. Main ORC layouts have been then presented, in particular simple and regenerative cycles, subcritical and supercritical applications, and the possibility to implement a second stage into the system configuration. Typical usage of these power plants is discussed by reporting main exploited heat sources like biomass fuels, geothermal and solar energy and waste heat recovery (WHR).

The ORC system treated in this work belongs to the context of WHR applications: it collects waste heat from internal combustion engines, which generate electric energy for propulsion of a LNG carrier. The case study is presented, reporting operating conditions of the ship during a reference year, the engines cooling configuration, energy demands and all data at various working points. The ICEs-ORC coupling was hence analysed, by presenting the previous works of Soffiato [18, 19, 20] and Malandrin [21] first and then by discussing of possible configurations of the combined cycle on the basis of the available waste heat and design operating point selection. Three possible ORC layouts have been considered: single stage and two stage ORC having both subcritical and supercritical high pressure level. Chosen configurations and design points (thermodynamic cycles and hot sources composite curves) have been reported, including calculation of the main parameters.

3 MODELLING APPROACH

The selected modelling approach for the case study of this work is presented in this chapter. A brief introduction to the energy system dynamic modelling is firstly provided, to shift quickly to the discussion of the adopted modelling strategy for the ORC system to install on board the LNG carrier. Successively, design and off-design models of each component of the power plant in question are presented, together with the optimal design operating characteristics. Finally, the dynamic models and the steady-state models of the whole ORC systems, in the various considered configurations, are shown and explained at detail.

3.1 ORC MODELLING APPROACH

To explain the strategy about design and off-design model building, the selected modelling approach is introduced in order to fix some useful concepts to understand the choice made. The adopted method is suggested by Vaja [14], with addition of some important modifications that will be explained in the following.

The modelling approach starts from the definition of two variable categories to represent the fluid system:

- *Level variables*, indicating the amount of thermodynamic properties stored inside components, expression of the state variables in *state determined* systems; examples are mass, internal energy, kinetic energy;
- *Flow variables*, related to fluxes of extensive properties through boundary surfaces or components without mass or energy storage, they are outputs of *not state determined* systems; examples are mass flow rate, enthalpy flow rate.

Three types of system component are defined:

- *Reservoirs / Capacities*: these components receive flow variables and are characterized by states that represent the stored amount of level variables;
- *Flow control devices*: they receive as input the level variables leaving Capacities and determine the associated flows, typically as result of differences between Reservoir levels;
- *Heat exchangers*: their function consists in increasing or decreasing the working fluid temperature, or in changing its phase, by exchanging heat flux respectively with the hot or the cold source; the main relation with the previous categories is given by the decreasing of the fluid pressure by the pressure drops, when the heat exchange model is not assumed to be ideal. As it will be explained, pressure is an important thermodynamic parameter for this modelling approach, depending on which there may be different values of the level variables entering into flow control devices.

Typical examples of the first component category, capacities, are the hot and cold drums and the particular heat exchangers with phase change within possible internal mass and energy storage, such as subcritical evaporators and condensers. To give a precise example, a shell and tube heat exchanger type K, also known as Kettle Evaporator, belongs to this category because of the evaporation control inside the component. Basically, it works both as an evaporator and as an hot drum. On the contrary, typical flow control devices are turbomachinery, hence pumps and turbines, where there is a transformation of flow variables such as enthalpy flow rate, for these components respectively with its increase and decrease.

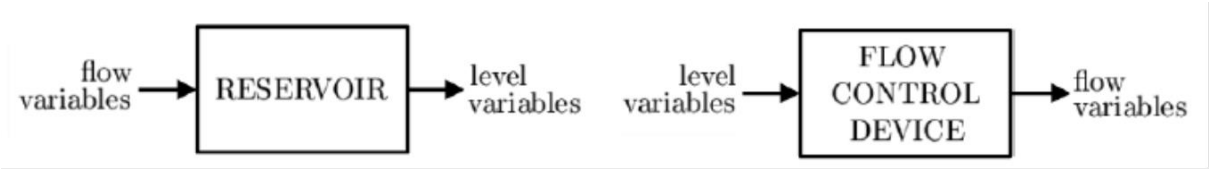

Figure 3.1 *Conceptual scheme of Reservoir and Flow Control Device [14].*

The simple conceptual scheme above is shown to fix in mind how these two types of components use to work. To make the right connections between capacities and flow control devices is fundamental in order to build an appropriate and working ORC model. Reservoirs must receive the flow variables coming from the previous and the following flow control devices, in order to carry out the simulation and produce a new level variable. Vice versa, level variables entering in a flow control device come from the preceding and the succeeding capacities, giving at the exit a new calculated flow variable. In this way, an alternation between these two types of components is set up, and it is worth noting that it is necessary also for making a reliable Rankine cycle. Hence, component models connection is ruled by the following conceptual scheme.

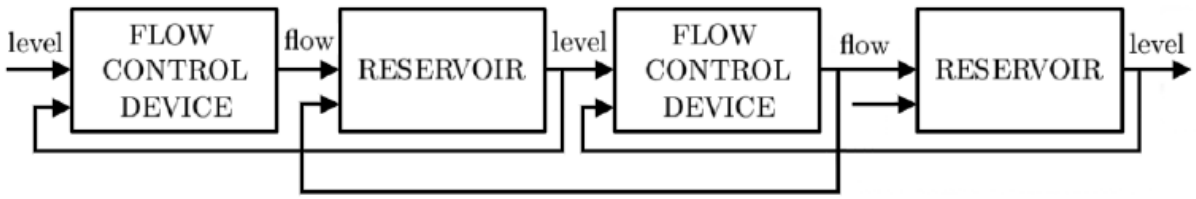

Figure 3.2 *Correct connections among Reservoirs and Flow Control Devices [14].*

It is important to clarify that these connections represent only signals, sent to the respective components according to the exposed scheme. They do not represent physical fluxes, they are rather information transmitted to the interested components in order to allow the whole model to work according to the set algebraic and differential equations.

In case of assumption of non-ideal heat exchanges, therefore if pressure drops are taken into account, the third component category called “Heat Exchangers” is introduced into the scheme according to the following figure.

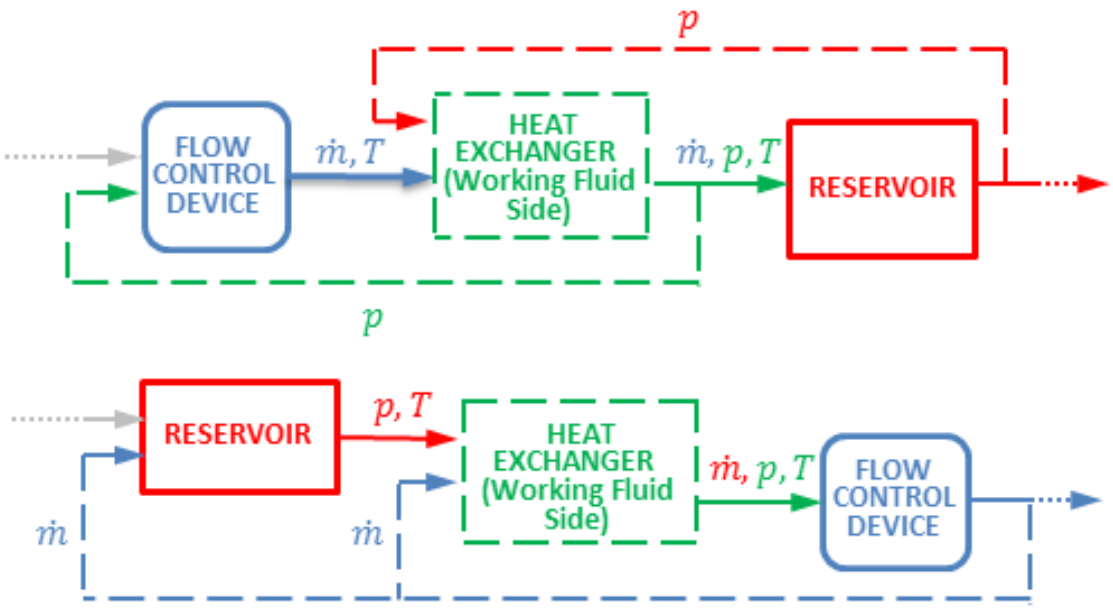

Figure 3.3 *Correct connections among the three categories of components.*

Focusing now on the Organic Rankine Cycle system of study, here the choices made about components selection are reported:

- *Heat exchangers with phase change*
  I. Shell and tube type F as Subcritical Evaporator
  II. Shell and tube type F as Condenser, with the possibility to choose between smooth tubes or finned tubes, the latter with the purpose to increase heat exchange
  III. Shell and tube type F as Supercritical Evaporator
- *Drums*
  I. Cold Drum, used as accumulator for the whole cycle, placed at the exit of the condenser in order to receive the working fluid and to send to the pump only saturated liquid
  II. Hot Drum, necessary in case of two stage ORC plant for stabilizing evaporation pressures for the two levels, it is installed at the outlet of subcritical evaporators and sends saturated vapour to the turbines;
- *Turbomachinery*
  I. Radial, single stage, variable rotational speed Pump, with rotational speed determined by a control system as function of liquid level inside cold drum
  II. Axial, single stage, fixed rotational speed Vapour Turbine
- *Heat exchangers without phase change*
  I. Shell and tube type E as Preheater / Economizer

Similarly to the above classification, these components belong to the following categories, relatively to this chosen modelling approach:

- *Reservoirs / Capacities*: Cold Drum, Hot Drum

- *Flow Control Devices*: Pumps, Vapour Turbines
- *Heat exchangers*: Preheater, Subcritical Evaporator, Supercritical Evaporator, Condenser

For the single stage ORC an hot drum is taken into consideration only for modelling purposes: it is assumed indeed that the subcritical evaporator operates, talking about the shown component categories, both as heat exchanger and capacity, in order to supply the drum function as well allowing to provide to the model the required differential equations that manage the dynamics, in particular by the calculation of the evaporation pressure p_{ev}. In this way, there may be mass and energy storage inside this component, depending on the evaporation rate that is function of the off-design condition of the ship, hence of the flowrate and thermodynamic values of the exchanging hot fluid.

Once definition of the components is completed, it is the turn of variables classification:

- *Level variables*: liquid and vapour mass, liquid and vapour volume, pressure
- *Flow variables*: mass flow rate, enthalpy flow rate

As explained above, level variables, hence organic fluid pressures leaving capacities, are sent to the previous and the following flow control devices, and the same happens to flow variables, as mass flow rates leaving flow control devices. In this way, the required alternation for the model is guaranteed.

In Figures 3.5 and 3.6 the single stage and a two stage ORC selected for the application into this LNG carrier of study are represented, the latter of which with saturated first stage and saturated or supercritical second stage.

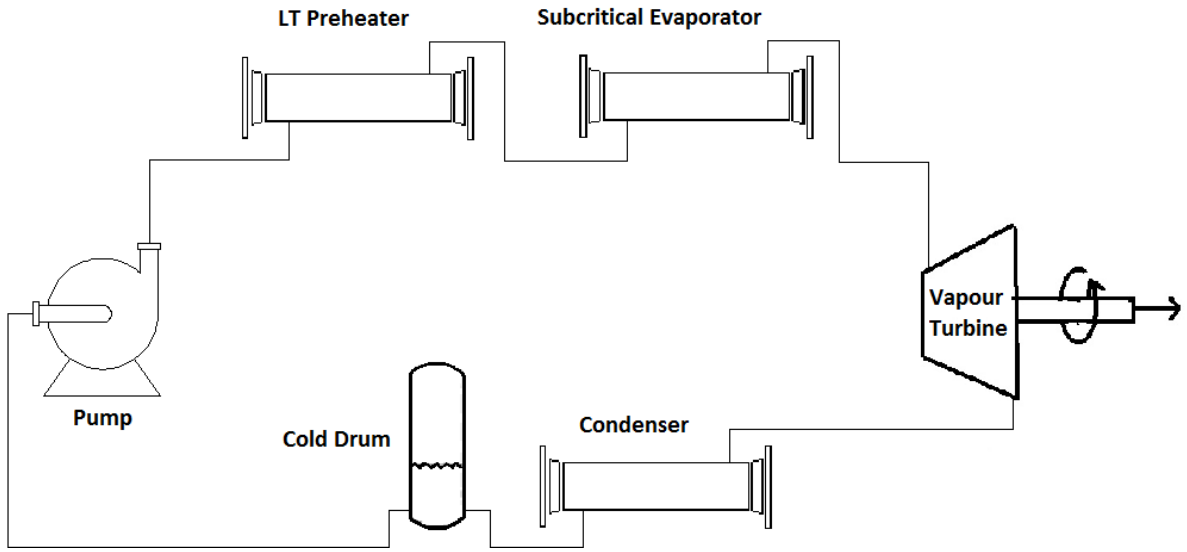

Figure 3.4 *Single pressure level ORC scheme.*

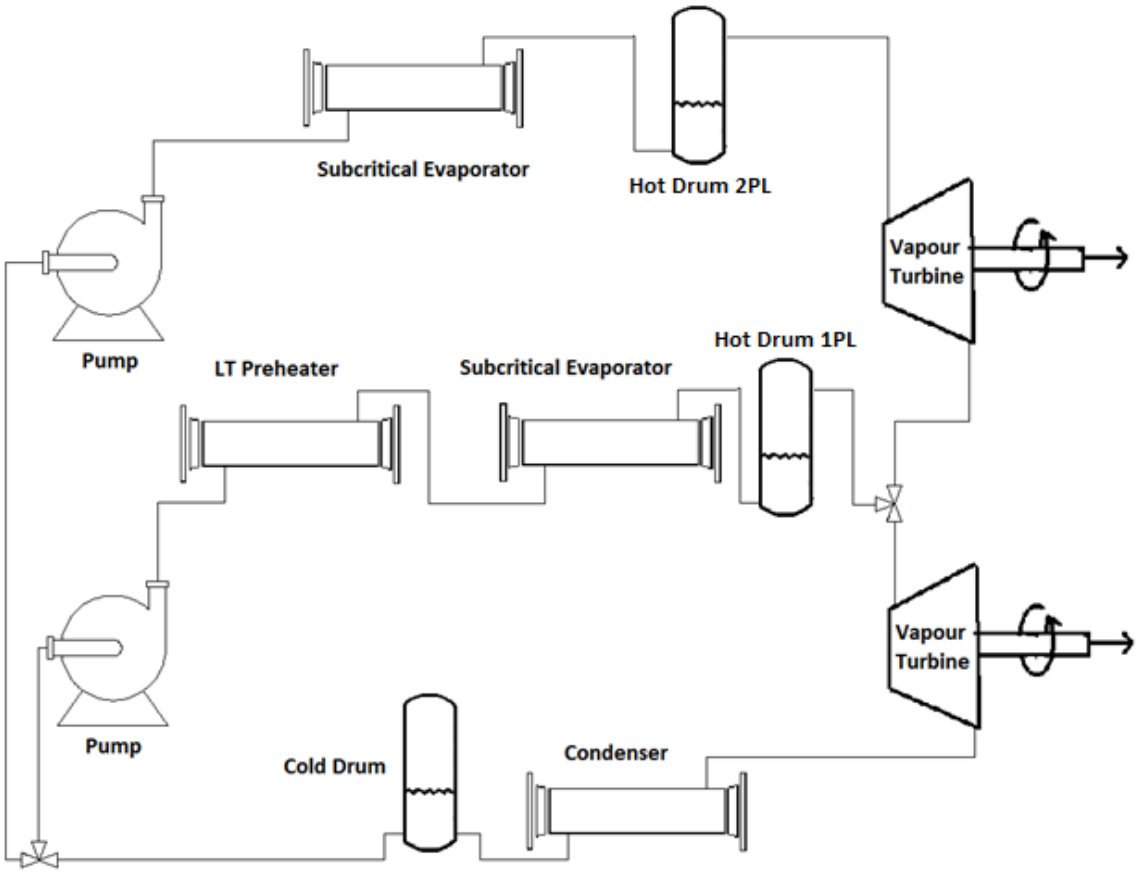

Figure 3.5 *Two pressure level ORC scheme (subcritical pressure levels).*

In the following figures, the same selected ORC systems are represented with overlaid the modelling signals of level variables and flow variables. The categories of components are also indicated.

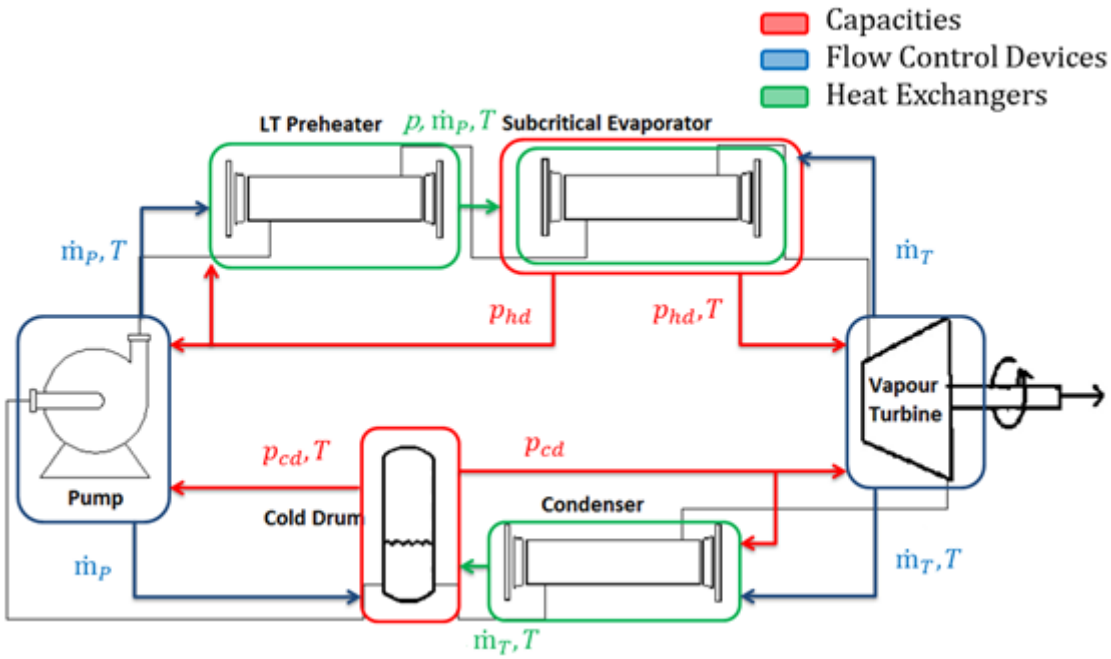

Figure 3.6 *Single pressure level ORC scheme with signal connections overlaid.*

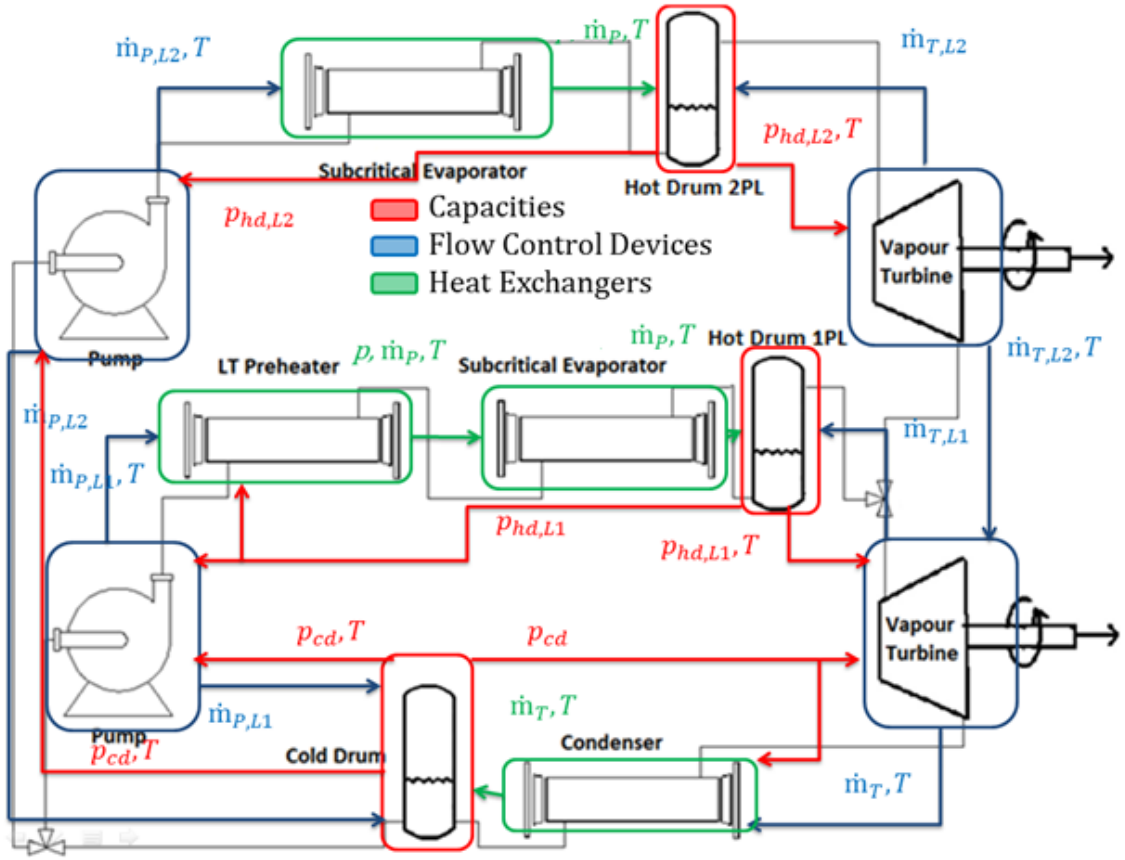

Figure 3.7 *Two pressure level ORC scheme with signal connections overlaid, subcritical case.*

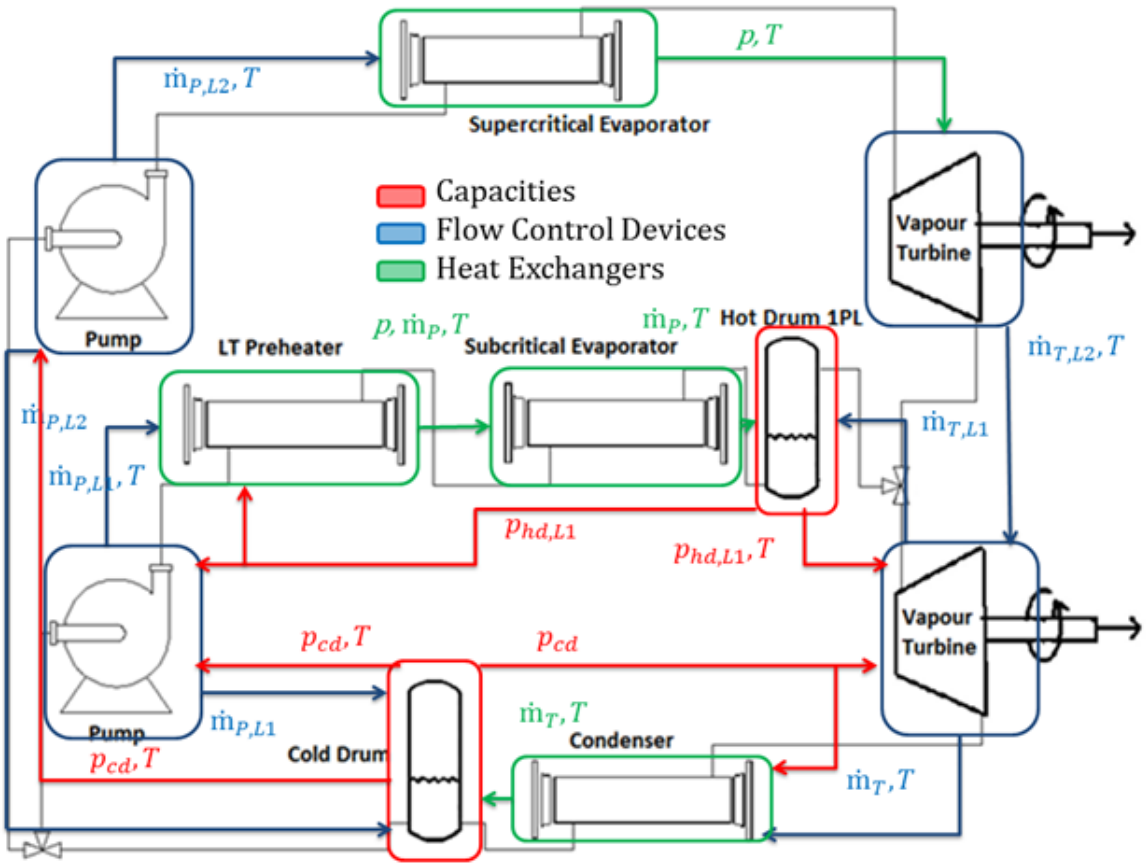

Figure 3.8 *Two stage ORC scheme with signal connections overlaid, supercritical case.*

Remember that these are signals, not representing the real physical fluxes. To be more precise, for example for the single pressure level ORC, mass flow rate leaving the pump is sent physically only to the preheater, while model's signals of the same physical quantity are sent both to evaporator and condenser. Another example: pressure of the organic fluid leaving the evaporator, which represents a level variable in this case, is an information that is sent to both vapour turbine and pump.

For the two stage ORC it must be noticed that, in case of supercritical second pressure level, the cycle does not present the required alternation: this happens because during supercritical evaporation the phase change manifests in continuous way, without a clear separation of the two phases. Instead of subcritical case, indeed, liquid and vapour phases have the same main thermodynamic properties, in particular the very same density, which leads to a complete vaporization of the fluid with about homogeneous characteristics along the component, but in liquid state at the inlet and vapour state at the outlet. For this reason, in the supercritical evaporator there cannot be mass or energy storage, it does not work in this way as capacity, and also there is no need for a hot drum at all. For this component, it is hence assumed directly to collect dry vapour at the outlet, without the necessity of dedicated phase separation inside drum.

At this point, the modelling strategy can be introduced in order to justify the proposed objectives. The aim of the work is to obtain an easy and "fast" ORC Simulink model, quick enough to allow to carry out several simulations without a great time expenditure, with as final purpose to obtain the best feasible solution. Obviously, the detail level of the model depends on assumptions adopted in building it, assumptions that will be presented in the next sections.

The modelling strategy of this work can be summarized in two steps:

1. Design models development for every single component;
2. Off-design models development for the *heat exchangers*, implementation of characteristic maps for the *flow control devices*:
    I. In case of heat exchangers a simple off-design behaviour law is integrated [22], adopted by Manente [13] as well in his study about the search of the optimal control strategy in a geothermal application of the ORC system, law that will appear as shown below:

$$UA = (UA)_{DP}\left(\frac{\dot{m}}{\dot{m}_{DP}}\right)^{l} \tag{3.1}$$

    II. Existing characteristic equations are found in literature and in previous works for the turbomachinery, and they will be presented in the following [5, 8]:
        - Pump:

$$h_{out,P} = h_{in,P} + \frac{(h_{,is,P} - h_{in,P})}{\eta_{is,P}} \tag{3.2}$$

$$y = \frac{y'_{DP} - y'_{0,DP}}{\dot{V}'^{2}_{DP}} \dot{V}^2 + y'_{0,DP} \tag{3.3}$$

$$\eta_{is,P} = 2\frac{\eta_{is,P,DP}}{\dot{V}_{P,DP}} \dot{V}_P - \frac{\eta_{is,P,DP}}{\dot{V}^2_{P,DP}} \dot{V}_P^2 \tag{3.4}$$

where $y_{0_{,DP}}$ is the head of the pump without flow rate allowed, at design point.

- Vapour turbine:

$$h_{out_{,T}} = h_{in,T} - \eta_{is,T}(h_{in,T} - h_{out,is_{,P}}) \tag{3.5}$$

$$\eta_{is,T} = \eta_{is,T,DP}\left[2\frac{\dot{m}_{R,T}}{\dot{m}_{R,T,DP}} - \left(\frac{\dot{m}_{R,T}}{\dot{m}_{R,T,DP}}\right)^2\right] \tag{3.6}$$

$$\dot{m}_R = \frac{\dot{m}(T)^{\frac{1}{2}}}{p} \tag{3.7}$$

where $\dot{m}_R$ is called *reduced flow rate*.

III. Several simulations are carried out in order to search for the best design and off-design results, related to the predefined goal (work production, efficiency), varying the main independent variables one by one.

A remark is done about the heat exchangers modelling. These components are described by two different steps, precisely by separating the design procedure and the off-design behaviour into two different model blocks. Heat exchangers modelling hence consists in the two following steps:

1) Starting from inlet mass flow rate, temperature and pressure of both fluids coming into the studied heat exchanger, the Simulink *design block* calculates:
   a. all geometric parameters, included the heat exchange surface, that will be fixed and used later in performing off-design behaviour;
   b. the global heat exchange coefficient U, at design point, using also the fluids properties and velocities, obtained by known information entering into the block (temperature and pressure to determine properties, mass flow rate for velocities);
   c. pressure drops in design conditions, for both hot and cold fluid;
2) The successive *off-design block* receives all the nominal parameters coming from design calculation, to use them with those variables that show variations when the ship leaves nominal conditions, in particular when it changes its speed respect to the nominal one, in order to obtain in the end the off-design values of U, q, T and Δp. To be more precise, mass flow rates and inlet temperatures belonging to both hot and cold fluid are variable input of working conditions.

As previously mentioned, the final purpose of this strategy is to find, by the use of the complete model to carry out simulations, changing time by time the design choices, the proper ORC configuration for this particular case of study, starting from the statistical data referred to one year for this given LNG carrier. After this work, all the obtained configurations should be compared in order to find in the end the best reliable and economical solution. Anyway, the result given out by this model is a good starting point.

In the following sections, design and off-design models for every component and the dynamics for the whole ORC model, with relative algebraic and differential equations, are shown.

3.2 DESIGN MODEL OF THE ORC SYSTEM

3.2.1 Turbomachinery

In this section, design models of pump and vapour turbine are presented. Their purpose consists in determining all required nominal values, to introduce them into the characteristic equations performed by the off-design models. Only the few needed operative parameters are calculated, none related to the geometry of these components.

3.2.1.1 Pump

The proposed design model refers to a single stage radial pump. Its main features are versatility and flexibility, because of necessity to fit well into ORC system and allow the integration of a proper plant control system. To be precise, pump must be able to vary its rotational speed in order to maintain the required liquid level in the cold drum, placed downstream of the condenser and working as accumulator for the ORC. This parameter will depend on the off-design conditions of the vessel engines. For this reason, the pump model presents also a tuning variable that is function of travel conditions, the rotational speed ω. It will be presented in Paragraph 3.4.1.1, where the off-design model is discussed.

Design model of the pump allows to evaluate all parameters that off-design model requires in order to simulate the component behaviour whenever is out of nominal conditions. Main equations adopted in this model are shown below. Given that operating conditions are nominal for this calculation, all parameters refer to design point.

- *Mass balance equations*:

They describe the continuity equation inside this component, index of no internal mass storage.

$$\dot{m}_{in} = \dot{m}_{DP} \tag{3.8}$$

$$\dot{m}_{out} = \dot{m}_{DP} \tag{3.9}$$

- *Energy conservation equation*:

This relation consists in the product between the mass flow rate crossing the pump and its enthalpy variation, from entrance to exit, and gives out the required mechanical power.

$$\dot{W}_{mec,DP} = \dot{m}_{DP}(h_{out,DP} - h_{in,DP}) \tag{3.10}$$

- *State equations*:

To calculate the needed properties for the model, inlet and outlet pressure and inlet enthalpy and entropy are employed.

$$\left[\rho_{in,DP}, s_{in,DP}\right] = f\left(p_{in,DP}, h_{in,DP}\right) \tag{3.11}$$

$$h_{out,is,DP} = f\left(p_{out,DP}, s_{in,DP}\right) \tag{3.12}$$

- *Additional equations*:

The pump's characteristic map is function of inlet volumetric flow rate $\dot{V}$ and processed specific energy. The necessary additional equations are reported here, in particular regarding the head of the pump *y* and isentropic efficiency $\eta_{is,P}$ calculation. There is also the relation describing the required electric power, as function of the mechanical one and of the pump electric efficiency, representing the electrical consumption.

$$y_{DP} = \frac{p_{out,DP} - p_{in,DP}}{\rho_{in,DP}} \tag{3.13}$$

$$\dot{V}_{DP} = \frac{\dot{m}_{DP}}{\rho_{in,DP}} \tag{3.14}$$

$$\eta_{is,P,DP} = \frac{h_{out,is,DP} - h_{in,DP}}{h_{out,DP} - h_{in,DP}} \tag{3.15}$$

$$\dot{W}_{e,DP} = \dot{W}_{mec,DP}\, \eta_{el} \tag{3.16}$$

To complete the design model, two other variables must be defined:

- ω_{DP}: rotational speed at design point;
- $y_{0,DP}$: head of the pump without flow rate allowed, at design point; it defines the maximum pressure increase at nominal speed.

In the following, a list of the involved variables and parameters in this pump design model will be presented, arranging them as physical quantities, dependent variables, independent variables (that are fixed before the simulation by the user), state variables and output variables. It is worth noting that the sum of the dependent and independent variables, the fixed parameters and eventual constants must be equal to the number of physical quantities, all the last of which are applied into the equations shown until now. The fixed parameters are all the design values that are previously decided by the user, depending on the selected pump device for the ORC plant model.

Variables and parameters

N° of equations: 10 *from Eq.* (3.8) *to* (3.16)

Physical quantities: 6

$\dot{m}_{in}$ $\dot{m}_{out}$ $\dot{m}_{DP}$ $h_{in,DP}$ $h_{out,is,DP}$ $h_{out,DP}$ $p_{in,DP}$ $p_{out,DP}$
$\rho_{in,DP}$ $s_{in,DP}$ y_{DP} $\dot{V}_{DP}$ $\eta_{is,P,DP}$ η_{el} $\dot{W}_{mec,DP}$ $\dot{W}_{e,DP}$

Fixed parameters: 5

$\dot{m}_{DP}$ $p_{in,DP}$ $p_{out,DP}$ $\eta_{is,P,DP}$ η_{el}

Dependent variables: 9

$\dot{m}_{out}$ $h_{out,is,DP}$ $h_{out,DP}$ $\rho_{in,DP}$ $s_{in,DP}$ y_{DP} $\dot{V}_{DP}$ $\dot{W}_{mec,DP}$
$\dot{W}_{e,DP}$

Independent variables: 2

$\dot{m}_{in}$ $h_{in,DP}$

Among the 16 physical quantities there are the following state and output variables.

State variables: 4

$p_{in,DP}$ $h_{in,DP}$ $p_{out,DP}$ $s_{in,DP}$

Output variables: 4

$\dot{m}_{out}$ $h_{out,DP}$ $p_{out,DP}$ $\dot{W}_{e,DP}$

3.2.1.2 Turbine

Vapour turbine design model is quite similar to the pump's one. Most equations are analogous, and the modelling approach is the same. The chosen expander is a single stage axial vapour turbine, whose rotational speed is assumed to be fixed.

As for the case of pump, here all the main adopted equations are presented, relations that give out the parameters needed by the off-design turbine model. Also in this case, all parameters refer to nominal conditions.

- *Mass balance equations*:

They are the same presented for the design model of the pump, Eqs. (3.8) and (3.9).

- *Energy conservation equation*:

This relation gives out the produced mechanical power and is analogous to the pump's one, where the result is the required power. The difference consists in decreasing the working fluid enthalpy from entrance to exit, instead of increasing it, as happens in the pump.

$$\dot{W}_{mec,DP} = \dot{m}_{DP}(h_{in,DP} - h_{out,DP}) \tag{3.17}$$

- *State equations*:

$$\left[T_{in,DP}, \rho_{in,DP}, s_{in,DP}\right] = f\left(p_{in,DP}, h_{in,DP}\right) \tag{3.18}$$

$$h_{out,is,DP} = f\left(p_{out,DP}, s_{in,DP}\right) \tag{3.19}$$

- *Additional equations*:

To calculate the mass flow rate crossing the vapour turbine, useful for implementation of the characteristic map, Stodola equation is applied here. K parameter is included in this relation, and it strongly influences the flow rate processed by this component. K is evaluated in this case by imposing inlet and outlet pressures, density and mass flow rate, as it can be seen below.

$$K = \frac{\dot{m}_{DP}}{\left(\rho_{in,DP}\, p_{in,DP}\left[1-\left(\frac{1}{\varepsilon_{DP}}\right)^2\right]\right)^{\frac{1}{2}}} \tag{3.20}$$

$$\varepsilon_{DP} = \frac{p_{in,DP}}{p_{out,DP}} \tag{3.21}$$

The other necessary additional equations are reported here, in particular regarding nominal isentropic efficiency and reduced mass flow rate calculation. *Reduced mass flow rate* is an input parameter for the off-design model. There is also in this case the relation describing the electric power, to represent this time electric production.

$$\eta_{is,T,DP} = \frac{h_{in,DP} - h_{out,DP}}{h_{in,DP} - h_{out,is,DP}} \tag{3.22}$$

$$\dot{m}_{R,DP} = \frac{\dot{m}_{DP}\left(T_{in,DP}\right)^{\frac{1}{2}}}{p_{in,DP}} \tag{3.23}$$

$$\dot{W}_{el,DP} = \dot{W}_{mec,DP}\, \eta_{el} \tag{3.24}$$

Variables and parameters

N° of equations: 12 *Eqs. (3.8)-(3.9) and from Eq.* (3.17) *to* (3.24)

Physical quantities: 18

$\dot{m}_{in}$ $\dot{m}_{out}$ $\dot{m}_{DP}$ $h_{in,DP}$ $h_{out,is,DP}$ $h_{out,DP}$ $p_{in,DP}$ $p_{out,DP}$
$T_{in,DP}$ $\rho_{in,DP}$ $s_{in,DP}$ K ε_{DP} $\dot{m}_{R,DP}$ $\eta_{is,T,DP}$ η_{el}
$\dot{W}_{mec,DP}$ $\dot{W}_{e,DP}$

Fixed parameters: 6

$\dot{m}_{DP}$ $p_{in,DP}$ $p_{out,DP}$ $T_{in,DP}$ $\eta_{is,T,DP}$ η_{el}

Dependent variables: 10

$\dot{m}_{out}$ $h_{out,is,DP}$ $h_{out,DP}$ $\rho_{in,DP}$ $s_{in,DP}$ K ε_{DP} $\dot{m}_{R,DP}$
$\dot{W}_{mec,DP}$ $\dot{W}_{e,DP}$

Independent variables: 2

$\dot{m}_{in}$ $h_{in,DP}$

Among the 18 physical quantities there are the following state and output variables.

State variables: 4

$p_{in,DP}$ $h_{in,DP}$ $p_{out,DP}$ $s_{in,DP}$

Output variables: 4

$\dot{m}_{out}$ $h_{out,DP}$ $p_{out,DP}$ $\dot{W}_{e,DP}$

3.2.2 Heat exchangers

For the ORC system of study shell and tube heat exchangers are adopted, in particular the types E and F. Fluids are always sent in counter-current, and the selected configurations are:

- one pass shell-side, one pass tube-side (1-1, perfect counter-current);
- one pass shell-side, two passes tube-side (1-2);
- two passes shell-side, four passes tube-side (2-4).

Regarding the tube layout, for these heat exchangers the possible choices are reported here:

- triangular pitch (θ = 30°);
- square pitch (θ = 90°);
- rotated square pitch (θ = 45°).

The selected choice for all the shell and tube heat exchangers in this work is the triangular tube layout.

An example of shell and tube type E, configuration 1-1, is schematically shown in Figure 3.9.

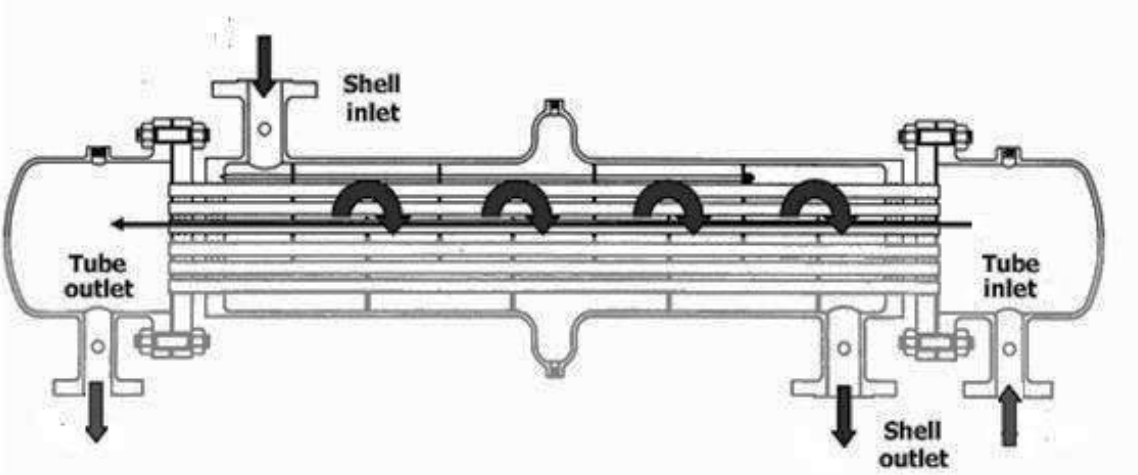

Figure 3.9 *Scheme of Shell and Tube type E, configuration 1-1, perfect counter-current.*

Significant assumptions have been adopted for modelling purpose and are presented below:

- without any phase change, both fluids are treated as incompressible and no mass accumulation is considered;
- pressure losses are accounted;
- thermal capacitance of the metal pipe is neglected (only convective heat flux between fluids and pipe are considered);
- axial conductive heat flux is not considered for both fluids;
- all components are considered adiabatic;

- thermodynamic properties of both fluids are constant and evaluated at mean temperature.

State variables are employed in this kind of components, in order to define the system behaviour during simulation and to check all necessary properties in the various thermodynamic states of the cycle. To summarize, design models are useful for geometry calculation and for parameters evaluation at design point (global heat exchange coefficient U_e, pressure drops Δp, heat flux q, outlet working fluid temperature T_u), while off-design models are employed then to simulate the behaviour of the component starting from the obtained nominal parameters.

3.2.2.1 Preheater

In the preheater the two fluids exchange heat flux maintaining their own phase, that here must be liquid. Adopted state variables in single-phase heat exchangers are pressure and absolute temperature.

As mentioned above, a shell and tube heat exchanger is adopted. The working fluid is sent shell-side and the hot fluid tube-side as design choice, to allow continuity with the successive evaporator where the same choice has been done. This component operates as economizer, it increases the working fluid's temperature in order to lead it as close as possible to the evaporation's one. In Simulink modelling, the evaporation temperature is usually assumed as the target one, while in the real economizer component it is necessary to fix a small ΔT for safety issue, to avoid phase change inside it that could lead to higher pressure drops, inefficient exchange and overheating of the tubes' material.

In the analysed configurations the ORC system receives the hot fluxes by the low temperature and high temperature cooling circuits, as shown in Figure 2.18. For this reason, the cycle requires two heat exchangers to rise the working fluid temperature and evaporate it:

- one low temperature preheater, in order to exploit the residual heat coming from the LT cooling circuits to increase the operative fluid temperature;
- one evaporator, in which preheating and subcritical evaporation happen to the organic fluid, the heat flux provided by the HT cooling circuits.

The available hot source for the LT preheater is hence the low temperature cooling stream that receives the heat flux by exchanging with Diesel engines charge air and lubricating oil and then releases it to the organic fluid, on the tube side of the heat exchanger. The evaporator's hot source, instead, is the high temperature cooling stream that collects the heat flux from the engines cooling water and charge air.

For the first heat exchanger, LT preheater, corresponding to HE2 in the figure, the available heat is not sufficient to lead the refrigerant to evaporation but only to increase its temperature, helping in this way to enhance the cycle's efficiency. Regarding the successive heat exchanger (HE1), where both preheating and evaporation are carried out, the Simulink

model has been split into two parts, the first that simulates the preheating and the second the evaporation. This component will be presented in detail in the next section, however the main concept to keep in mind is that low temperature preheater and the preheating part of evaporator are modelled almost in the same way, in particular with the very same design and off-design equations, that will be described in the following.

In this ORC application, the configuration choice about the LT preheater is the 1-2. The reason is the necessity to keep the working fluid pressure drops below a certain level, in order not to lose too much producible work in the vapour turbine.

The design model of the preheater provides all required geometric parameters, to be used to define heat exchange area and then by off-design model in order to perform the dynamic behaviour. For the single phase heat exchange, for design purposes Gnielinski correlation [28] is adopted to calculate the convective hot fluid heat exchange coefficient α', Bell-Delaware method [25] for the cold fluid's one α'' and for pressure drops for both flows. Main equations are shown below [26], while for correlations, see appendix.

- *Mass balance equations*:

They describe continuity equations inside this component and show no mass storage.

$$\dot{m}'_{in,DP} = \dot{m}'_{out,DP} \tag{3.25}$$

$$\dot{m}''_{in,DP} = \dot{m}''_{out,DP} \tag{3.26}$$

- *Energy conservation equations*:

The heat flux exchanged by fluids is expressed as follows, remembering that for the hypothesis made specific heat at constant pressure is evaluated at mean temperature [26].

$$\dot{Q}_{DP} = \dot{m}' c'_p \left(T'_{in,DP} - T'_{out,DP}\right) \tag{3.27}$$

$$\dot{Q}_{DP} = \dot{m}'' c''_p \left(T''_{out,DP} - T''_{in,DP}\right) \tag{3.28}$$

- *State equations*:

The necessary fluid properties for the model, in particular density ρ, heat capacity c_p, thermal conductivity λ and viscosity μ, are evaluated at the mean temperatures (T'_m, T''_m).

$$\left[\rho',\ c'_p, \lambda', \mu'\right] = f(p', T'_m) \tag{3.29}$$

$$\left[\rho'',\ c''_p, \lambda'', \mu''\right] = f(p'', T''_m) \tag{3.30}$$

- *Additional equations*:

The heat flux is function of the global heat exchange coefficient U_e at design point, of external exchange area A_e and of logarithmic mean difference temperature ΔT_{ml} multiplied by temperature factor F_t, as shown in the following simple relation [26].

$$\dot{Q_{DP}} = U_{e,DP} A_e \, \Delta T_{ml,CC} \, F_t \tag{3.31}$$

Global coefficient U_e is function of five thermal resistances:

I. Shell-side fluid convective resistance $\frac{1}{\alpha''}$
II. Tube-side fluid convective resistance $\frac{A_e}{A_i \alpha'}$
III. Metal pipe conductive resistance $\frac{D_e \ln\left(\frac{D_e}{D_i}\right)}{2\,\lambda_{pipe}}$
IV. Shell-side fouling resistance f_e
V. Tube-side fouling resistance f_i

The two fouling resistances are incorporated into the global fouling resistance R_{sp} [26].

$$U_{e,DP} = \frac{1}{\frac{1}{\alpha''} + \frac{A_e}{A_i \alpha'} + \frac{D_e \ln\left(\frac{D_e}{D_i}\right)}{2\,\lambda_{pipe}} + R_{sp}} \tag{3.32}$$

$$R_{sp} = f_i \left(\frac{D_e}{D_i}\right) + f_e \tag{3.33}$$

Adopted heat exchange correlations, that can be found in their entire form in the appendix, will appear with the following dependence relations:

- Gnielinski:

$$\alpha' = f(\dot{m}', T'_m, p', v', D_i, L, N_{tt}, configuration) \tag{3.34}$$

- Delaware:

$$\alpha'' = f\left(\dot{m}'', T''_m, p'', T_{m,wall}, D_e, L, pitch, N_b, B_c, B/D_s, N_{tt}, N_{ss}, layout, configuration\right) \tag{3.35}$$

$$[\Delta p'_{DP}, \Delta p''_{DP}\,] = f\left(\dot{m}'', f, s_g, \varphi, \rho'', geometry, configuration\right) \tag{3.36}$$

$$T_{m,wall} = f(\alpha', f_i, A_i, T'_m) \tag{3.37}$$

Internal and external heat exchange surfaces and volumes are evaluated by the following equations, where L is the tubes length and N_{tt} the number of tubes in the bundle.

$$A_i = \pi \, D_i \, L \, N_{tt} \tag{3.38}$$

$$\mathrm{A_e} = \pi \, \mathrm{D_e} \, \mathrm{L} \, \mathrm{N_{tt}} \tag{3.39}$$

$$\mathrm{V_i} = \frac{\pi \mathrm{D_i^2}}{4} \mathrm{L} \, \mathrm{N_{tt}} \tag{3.40}$$

$$\mathrm{V_e} = \left(\frac{\pi \mathrm{D_s^2}}{4} \mathrm{L}\right) - \left(\frac{\pi \mathrm{D_e^2}}{4} \mathrm{L} \, \mathrm{N_{tt}}\right) \tag{3.41}$$

Logarithmic mean temperature difference $\Delta T_{ml,CC}$ is evaluated by the following equation. For temperature factor F_t the dependence relation is presented, while for the complete form [27] see appendix.

$$\Delta T_{ml,CC} = \frac{(T'_{in} - T''_{out}) - (T'_{out} - T''_{in})}{\ln\left(\frac{T'_{in} - T''_{out}}{T'_{out} - T''_{in}}\right)} \quad (3.42)$$

$$F_t = f(T'_{in}, T'_{out}, T''_{in}, T''_{out}, configuration) \quad (3.43)$$

$$\Delta T_{eff\,,DP} = \Delta T_{ml,CC}\, F_t \quad (3.44)$$

$$T'_m = \frac{T'_{in} - T'_{out}}{2} \quad (3.45)$$

$$T''_m = \frac{T''_{in} - T''_{out}}{2} \quad (3.46)$$

Variables and parameters

N° of equations: 29 *from Eq.* (3.25) *to* (3.46)

N° of physical quantities: 49

$\dot{m}'_{in,DP}$	$\dot{m}'_{out,DP}$	$\dot{m}''_{in,DP}$	$\dot{m}''_{out,DP}$	$T'_{in,DP}$	$T'_{out,DP}$	$T''_{in,DP}$	$T''_{out,DP}$
c'_p	c''_p	ρ'	ρ''	λ'	λ''	μ'	μ''
T'_m	T''_m	$\Delta T_{ml,CC}$	F_t	$\Delta T_{eff\,,DP}$	p'	p''	D_i
D_e	D_s	L	N_{tt}	A_i	A_e	V_i	V_e
λ_{pipe}	α'	α''	f_i	f_e	R_{sp}	$U_{e,DP}$	$T_{m,wall}$
$\dot{Q}_{DP}$	v'	$pitch$	N_b	B_c	B/D_s	N_{ss}	$\Delta p'_{DP}$
$\Delta p''_{DP}$							

N° of fixed parameters: 16

$\dot{m}'_{in,DP}$	$\dot{m}'_{out,DP}$	$\dot{m}''_{in,DP}$	$\dot{m}''_{out,DP}$	$T'_{in,DP}$	$T'_{out,DP}$	$T''_{in,DP}$	v'
D_i	D_e	$pitch$	B/D_s	B_c	N_{ss}	p'	p''

N° of dependent variables: 33

$T''_{out,DP}$	T'_m	T''_m	$\Delta T_{ml,CC}$	F_t	$\Delta T_{eff\,,DP}$	c'_p	c''_p
ρ'	ρ''	λ'	λ''	μ'	μ''	D_s	L
N_{tt}	A_i	A_e	V_i	V_e	λ_{pipe}	α'	α''
f_i	f_e	R_{sp}	$U_{e,DP}$	$T_{m,wall}$	N_b	$\dot{Q}_{DP}$	$\Delta p'_{DP}$
$\Delta p''_{DP}$							

N° of independent variables: 0

Among the 49 physical quantities there are the following state and output variables.

N° of state variables: 4

p'	p''	T'_m	T''_m

N° of output variables: 6

$\dot{Q}_{DP}$	$U_{e,DP}$	$\Delta p'_{DP}$	$\Delta p''_{DP}$	A_e	$\Delta T_{eff\,,DP}$

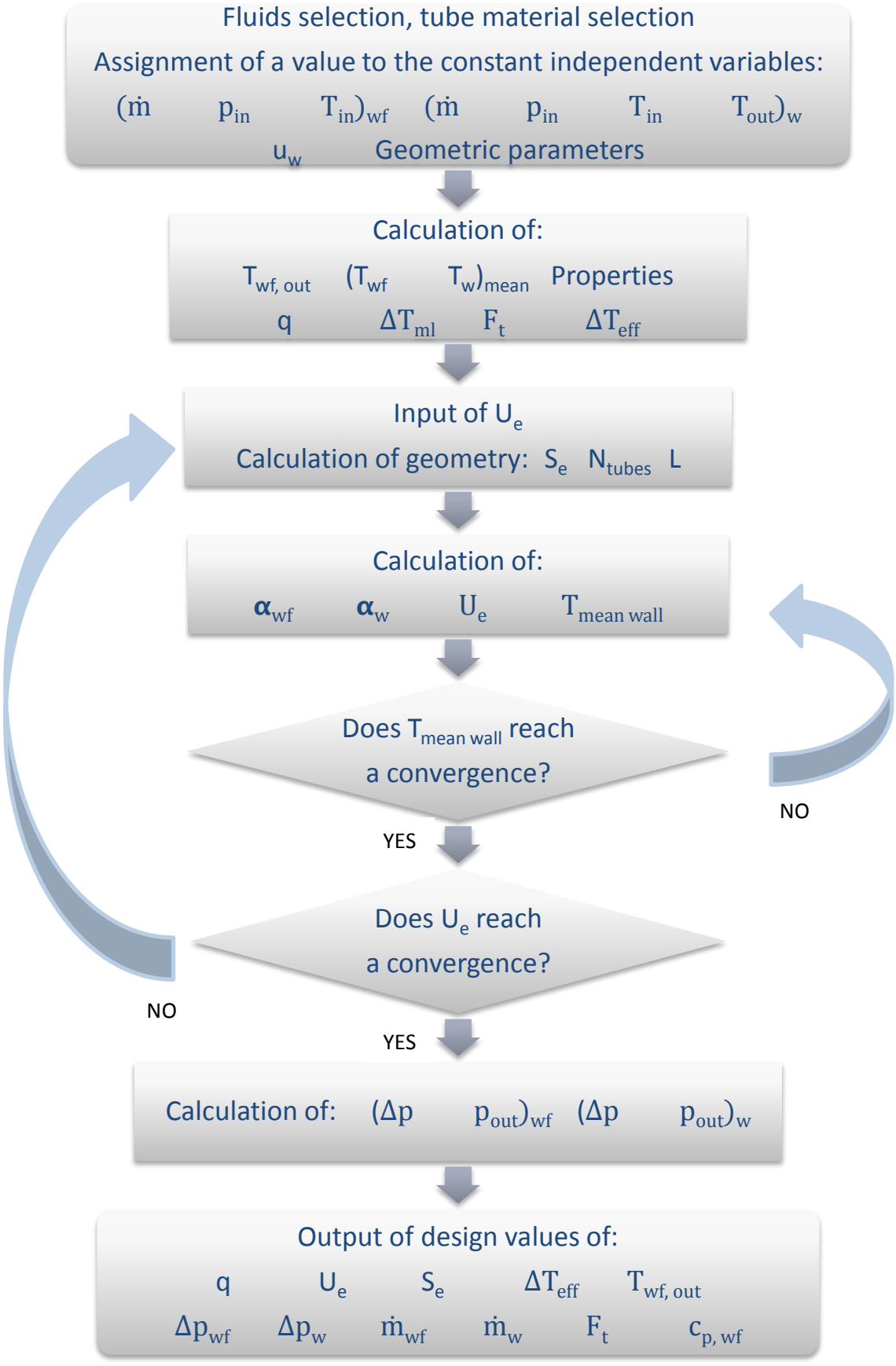

Figure 3.10 *Flowchart of the design procedure for preheater.*

3.2.2.2 Subcritical evaporator

This component pursues the subcritical evaporation of working fluid while it exchanges heat with the hot source, phenomenon that is characterized by a phase separation in its operating thermodynamic conditions. This is a very typical application in power industry, that can be found in many different plants using Rankine cycles, where the main examples are steam plants of various sizes, from the low size version of 20 MW to the standard 320 MW steam group, and LWRs (Light Water Reactor), the most diffused nuclear plants in the world.

In our case study, subcritical evaporator is adopted to change the operative fluid's phase from liquid to vapour, in order to exploit it in the last form into the vapour turbine to produce mechanical and then electric energy at the generator. The choice made about the heat exchanger are the shell and tube type E and F, the standard typology with insertion in the latter case of a longitudinal baffle for an additional shell-side pass, a very well-known technology suitable for ship applications. This solution is feasible because of the geometry of the evaporator, hence for the way in which hot and cold fluids are sent inside. For example, a kettle evaporator, the shell and tube type K, could not be applied because of the nonstationary position of the ship during the travel, caused by the natural oscillations given by the movements on the sea. The kettle evaporator's operation is depending in fact on the fluid level inside the exchanger, that must assure the bundle of inner tubes to be flooded and be stable inside the component, goal that is not achievable if the system where it is inserted is not motionless.

The chosen configuration for the adopted shell and tube the 2-4, the hot fluid being sent through the bundle of tubes and the cold operative fluid externally. The reason for this choice is again the necessity to reduce the working fluid pressure drops at an acceptable level, in order not to lose too much producible power in the vapour turbine.

As it can be seen in Figure 2.18, the hot source corresponds to the high temperature cooling water that comes from the operating engines and the charge air exchange sections. For the selected configuration of the whole Diesel engines – ORC system, the heat exchanger employed for the subcritical evaporation is called HE1 and has the double function of high temperature preheater and evaporator. Indeed, the working fluid coming from HE2, the low temperature preheater, is still subcooled liquid as seen in the previous section. This is caused by the fact that the available hot source for HE2 is not sufficient to lead the refrigerant to saturation point, hence in HE1 the fluid is continued to be heated and then it evaporates.

In the Simulink model, these two incorporated functions are divided into two different model blocks, the first representing the surface portion where the operative fluid only warms up, the second describing the remaining part where evaporation is pursued. The first block is so modelled right as a preheater, with the same equations shown in the previous section, while the main relations for the second block are presented in the following.

Some assumptions have been considered in order to simplify the modelling of the evaporator:

- outlet flux is physically sent to the vapour turbine in saturated conditions;
- the evaporating fluid in the component, shell-side, is in perfect equilibrium between liquid and vapour phase; hence the working fluid's temperature is only function of shell-side pressure;
- in the part of heat exchanger where evaporation manifests, it is supposed not to find subcooled liquid or superheated vapour;
- tube-side, the hot fluid is assumed not to change its phase;
- thermodynamic properties of hot fluid are constant and evaluated at mean temperature, while for cold evaporating fluid they are evaluated at saturated liquid phase and saturated vapour phase conditions.

At last, it is worth stating that in this case study there is no need for the single stage ORC of an hot drum downstream of the evaporator, but for modelling purposes it will be added a block, called actually *hot drum*, not representing a real device of this typology but only simulating the pressure trend inside the heat exchanger. This block will be characterised by a volume equal to the evaporator's one and it will be placed downstream. This choice is made because its presence is fundamental to reach the whole model stability: here differential equations that make the model dynamic and manage time dependent parameters can be found. This kind of blocks belongs to the category "Capacities", and will be explained in the next sections.

The design model of the subcritical evaporator, where both preheating and evaporation happen for the working fluid, has the aim of determining the geometric parameters. The particularity of this component is that, by using two different Simulink blocks to describe preheating part and evaporation part, there must be a constraint regarding design choices in order to maintain the same geometry for the two sections, given that they actually characterize one single heat exchanger. The only two design geometric parameters that should be different each other are exchange surface and the corresponding tube length, because both of them describe the ideal section in which you can find preheating and evaporation of the operative fluid inside the heat exchanger. These two parameters are also the only ones that will change during off-design conditions, simply because varying the heat grade of the external source, and consequently the heat flux between the two fluids, more or less exchange surface will be necessary to achieve evaporation, hence with a different remaining surface useful for vapour production.

Global heat transfer coefficient U_e is calculated in nominal conditions by using different correlations for preheating and evaporation sections, in the former Bell-Delaware is used in the same manner of the preheater modelling, while in the latter Mostinski and Palen are adopted to calculate the convective cold fluid's heat exchange coefficient α" and Chisholm for pressure drops [25]. Gnielinski is still the chosen correlation for the convective hot fluid's heat exchange coefficient α', tube side.

Excluding the heat transfer equations, the design procedure is very similar for the evaporator to the preheater's one. In the following, its main equations are presented, while for correlations see appendix.

- *Mass balance equations*:

They are the same presented for preheater, Eqs. (3.25) and (3.26).

- *Energy conservation equations*:

Heat flux exchanged by fluids is expressed as in the case of the preheater, but for the cold fluid, shell-side, it is not possible to express the balance by mean of the average specific heat because of the phase change, therefore the enthalpy drop between inlet and outlet flows is utilized [26].

$$\dot{Q} = \dot{m}' c_p' \left(T_{in}' - T_{out}'\right) \tag{3.47}$$

$$\dot{Q} = \dot{m}'' \left(h_{out}'' - h_{in}''\right) \tag{3.48}$$

- *State equations*:

The necessary properties for the model are evaluated at the mean temperature T_m' for the hot flux, that is assumed not to change its phase, while for the cold flux the same properties are obtained both for liquid phase (x = 0) and for vapour phase (x = 1).

$$\left[\rho',\ c_p', \lambda', \mu'\right] = f(p', T_m') \tag{3.49}$$

$$\left[\rho'',\ c_p'', \lambda'', \mu'', h''\right]_l = f(p'', x = 0) \tag{3.50}$$

$$\left[\rho'',\ c_p'', \lambda'', \mu'', h''\right]_v = f(p'', x = 1) \tag{3.51}$$

- *Additional equations*:

Adopted equations are the same ones used for preheater, regarding convective heat flux $\dot{Q}$, global heat exchange coefficient $U_{e,DP}$, global fouling resistance R_{sp}, exchange surfaces and volumes and at last logarithmic mean temperature difference $\Delta T_{ml,CC}$ and temperature factor F_t. Involved relations are: from Eq. (3.31) to (3.33) and from Eq. (3.38) to (3.44).

Adopted heat exchange correlations for the subcritical evaporator, completely defined in the appendix, are here expressed by the following dependence relations:

- Gnielinski:

$$\alpha' = f(\dot{m}', T_m', p', D_i, L, N_{tt}, configuration) \tag{3.52}$$

- Delaware:

$$\Delta p' = f\left(\dot{m}, f, s_g, \varphi, D_i, L, A, A_n, N_{pass}, N_s, configuration\right) \tag{3.53}$$

$$T_{m,wall} = f(\alpha', f_i, A_i, T_m') \tag{3.54}$$

- Mostinski and Palen:

$$\alpha'' = f\left(\dot{m}'', p'', p_{cr}'', T_{m,wall}, T_{sat}'', D_e, pitch, L, B_c, \frac{B}{D_s}, N_{tt}, \rho'', \mu'', \lambda'', g, layout, config\right) \tag{3.55}$$

- Müller-Steinhagen and Heck:

$$\Delta p'' = f(\dot{m}'', x, f, s, \varphi, \rho'', geometry, configuration) \quad (3.56)$$

Variables and parameters

N° of equations: 32 *Eqs. (3.25)-(3.26), from Eq.* (3.31) *to* (3.33), *from Eq. (3.38) to (3.44), from Eq. (3.47) to (3.56)*

N° of physical quantities: 62

$\dot{m}'_{in,DP}$	$\dot{m}'_{out,DP}$	$\dot{m}''_{in,DP}$	$\dot{m}''_{out,DP}$	$T'_{in,DP}$	$T'_{out,DP}$	$h''_{in,DP}$	$h''_{out,DP}$
$T''_{in,DP}$	$T''_{out,DP}$	c'_p	c''_{p_l}	c''_{p_v}	ρ'	ρ_l''	ρ_v''
λ'	λ_l''	λ_v''	μ'	μ_l''	μ_v''	T'_m	x
$\Delta T_{ml,CC}$	F_t	$\Delta T_{eff,DP}$	p'	p''	D_i	D_e	D_s
L	N_{tt}	A_i	A_e	V_i	V_e	λ_{pipe}	α'
α''	f_i	f_e	R_{sp}	$U_{e,DP}$	$T_{m,wall}$	$\dot{Q}_{DP}$	v'
f	s	φ	A_n	N_{pass}	N_s	p_{cr}''	$pitch$
g	B/D_s	B_c	N_{ss}	$\Delta p'_{DP}$	$\Delta p''_{DP}$		

N° of fixed parameters: 21

$\dot{m}'_{in,DP}$	$\dot{m}'_{out,DP}$	$\dot{m}''_{in,DP}$	$\dot{m}''_{out,DP}$	$T'_{in,DP}$	$T'_{out,DP}$	$T''_{in,DP}$	v'
D_i	D_e	$pitch$	B/D_s	B_c	N_{ss}	x	N_{pass}
N_s	p_{cr}''	g	p'	p''			

N° of dependent variables: 41

$h''_{out,DP}$	$h''_{in,DP}$	$T''_{out,DP}$	c'_p	c''_{p_l}	c''_{p_v}	ρ'	ρ_l''
ρ_v''	λ'	λ_l''	λ_v''	μ'	μ_l''	μ_v''	T'_m
$\Delta T_{ml,CC}$	F_t	$\Delta T_{eff,DP}$	D_s	L	N_{tt}	A_i	A_e
V_i	V_e	λ_{pipe}	α'	α''	f_i	f_e	R_{sp}
$U_{e,DP}$	$T_{m,wall}$	$\dot{Q}_{DP}$	f	s	φ	A_n	$\Delta p'_{DP}$
$\Delta p''_{DP}$							

N° of independent variables: 0

Among the 62 physical quantities there are the following state and output variables.

N° of state variables: 4

p'	p''	T'_m	x

N° of output variables: 6

$\dot{Q}_{DP}$	$U_{e,DP}$	$\Delta p'_{DP}$	$\Delta p''_{DP}$	A_e	$\Delta T_{eff,DP}$

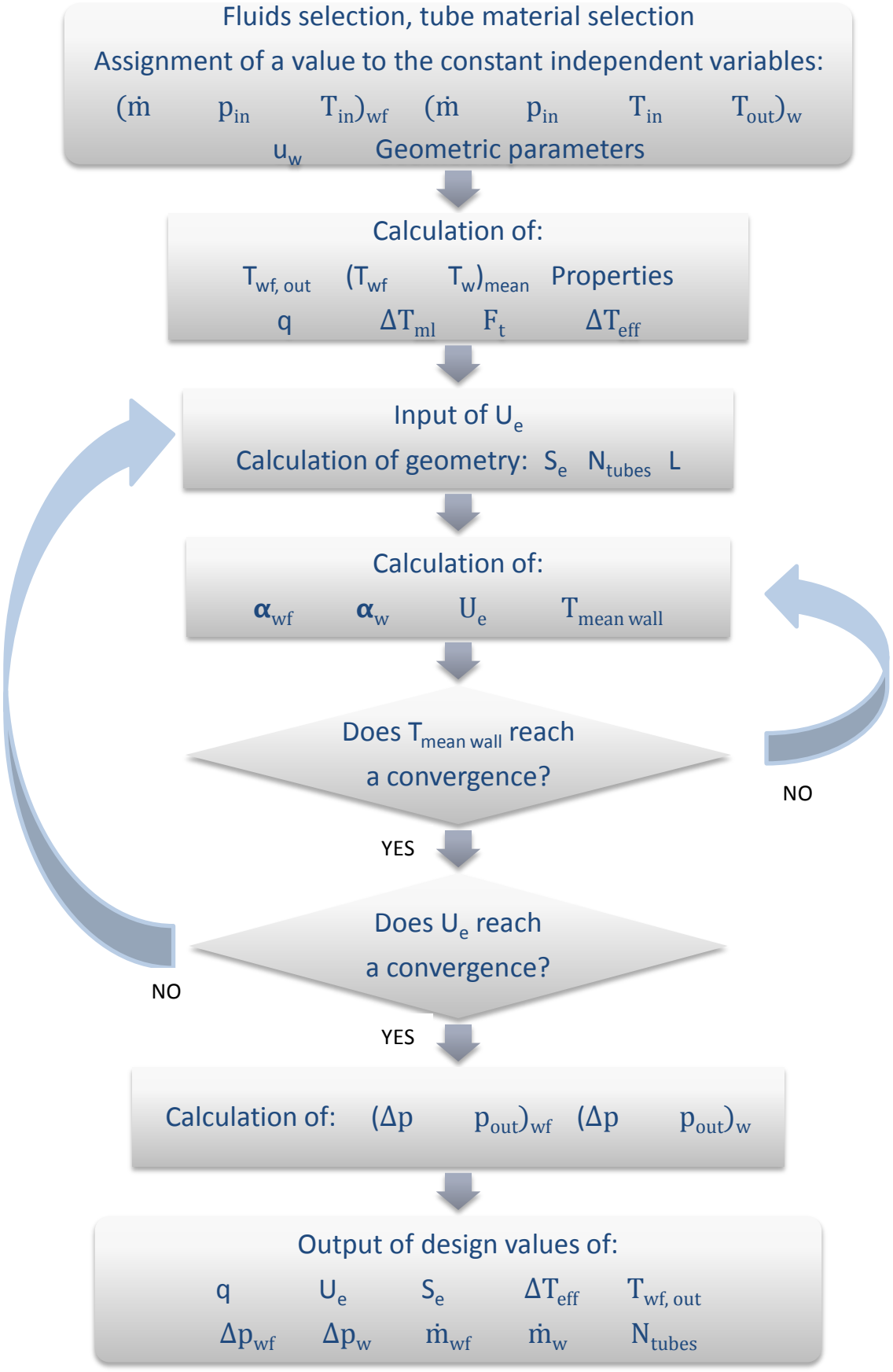

Figure 3.11 *Flowchart of the design procedure for subcritical evaporator (preheating).*

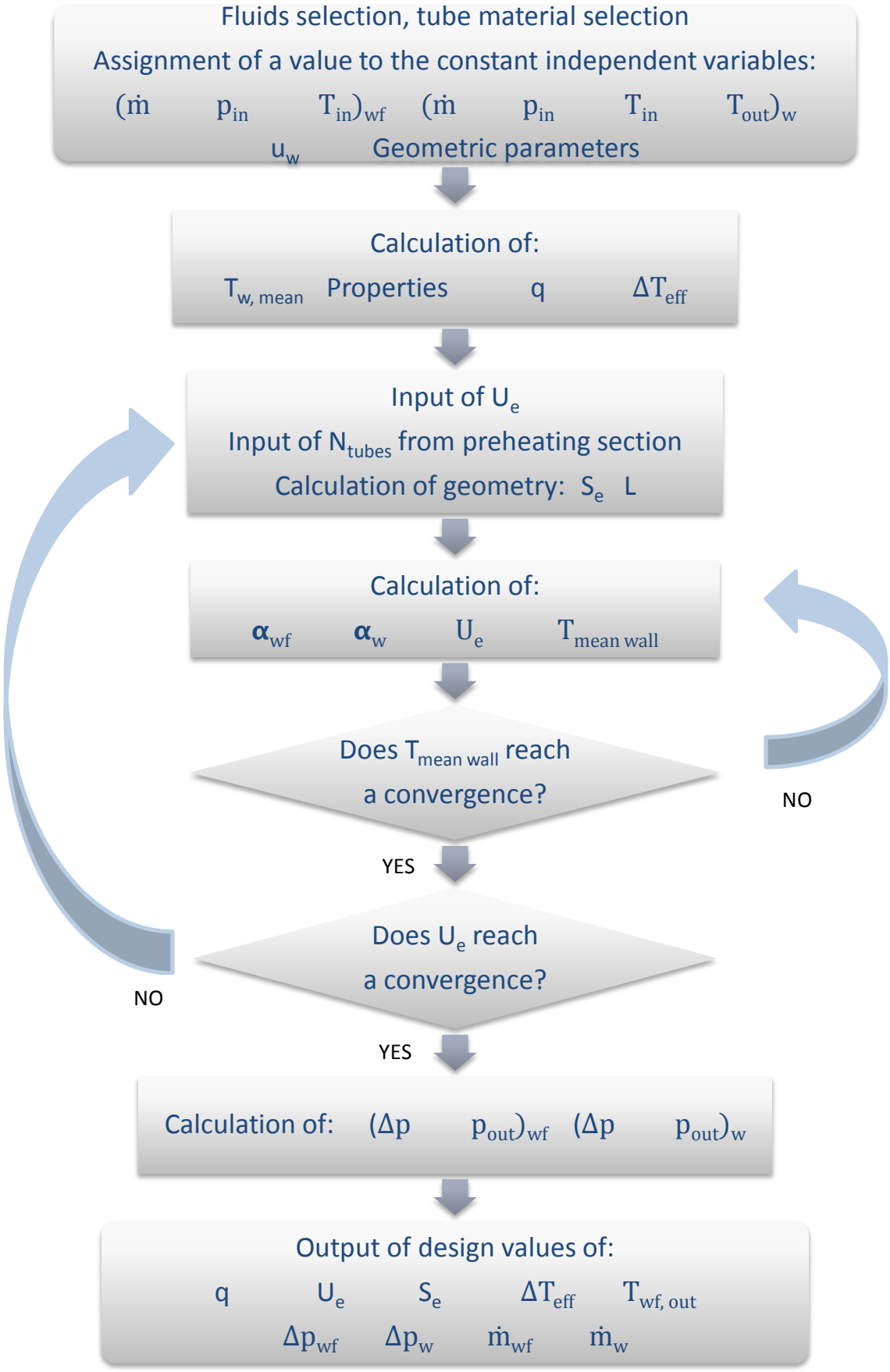

Figure 3.12 *Flowchart of the design procedure for subcritical evaporator (evaporation).*

3.2.2.3 Supercritical evaporator

The supercritical evaporation, contrarily to the subcritical one, manifests through a continuous transformation of the fluid along the component, from liquid to vapour state, without a clear phase separation. In the thermodynamic diagram, as shown in Figure 2.24, for the same reason there is not a specific region where to recognize the phase change. It is only conceivable that evaporation manifests mainly around the critical point, hence in the upper part of the Andrews curve, close to the top. The main characteristic of the supercritical evaporation is that the two phases cannot be distinguished: liquid and vapour coexist presenting the very same thermodynamic properties, until the phase change is completed.

The first step to obtain this kind of evaporation consists in increasing the fluid pressure to supercritical values. The second step requires the use of an hot source which temperature is higher than the critical one of the evaporating fluid, with an additional margin to allow the heat exchange. In this way, it is possible to pass from the subcooled liquid state to the superheated vapour state avoiding to enter inside the two phase region of thermodynamic diagram. It is worth noting that in this case, without a liquid-vapour phase transition, there are not phenomena to consider as critical heat flux and dry-out for the heat exchange.

In power industry, the first works and applications date back to the 1950s, about the use of supercritical water for steam generators and turbines in order to increase the thermal efficiency of coal fired power plants. Current applications are mainly supercritical and ultra-supercritical thermal power plants, which efficiency overcomes 50%, and SCWR (Super-Critical Water Reactor) nuclear power plants [29].

In our case study, supercritical evaporator is useful to implement a second pressure level for the ORC system, with the goal of an higher electric energy production, thanks to the addition of a second vapour turbine and the increase of the thermodynamic values of the vapour entering to the first level turbine after mixing in a three way valve.

The selected heat exchanger is again the shell and tube type F. Available hot source for the second pressure level is charge air, as shown in Figure 2.18. The 2-4 configuration is chosen for this component, in order to keep at acceptable values both the R245fa and the air pressure drops. Moreover, given the lack of correlations for supercritical evaporation, the available relation is the one provided by Mokry et al. [29], referred to fluid evaporating inside vertical tubes (to know more, see appendix A.1). Hence, in this context a vertical shell and tube heat exchanger is adopted, with working fluid sent into tubes from the bottom and charge air shell side from the top. It must be remarked that this choice is unusual in naval applications, where typically only horizontal shell and tube exchangers are employed. A limitation on the height is hence imposed, because of the necessity of installation inside the ship's machine room, resulting in a constraint on the tube length of the heat exchanger.

Some assumptions, useful to simplify modelling, are here presented:

- outlet flux is physically sent to the vapour turbine in superheated conditions;
- shell-side, the hot fluid is assumed not to change its phase;

- thermodynamic properties are constant and evaluated at mean temperature.

The outlet working fluid is considered being only vapour: the heat exchanger will be sized in order to insure complete evaporation for every possible off-design condition. Contrarily to the subcritical phase change, here the drum is not needed, right because there is not a clear distinction between phases. It is hence assumed outlet flux to be always in only vapour phase.

At last, to keep pressure higher than the critical one, not taking the risk to go down too much and enter inside the two phase region, the selected R245fa pressure for the second pressure level of the ORC system is fixed at the value of 37 bar, above the critical value of 36.4 bar, taking into account of pressure drops as well. In this way, given that the outlet pressure value of the second pump is fixed, there is no need of a control system for the model to vary the pump's rotational speed, as instead happens for the first pressure level.

As for the previous heat exchangers, the design model of the supercritical evaporator consists in determining geometric parameters, evaporation surface, global heat transfer coefficient U_e in nominal conditions and R245fa pressure drops. Bell-Delaware method is used for shell side modelling, to calculate the convective hot fluid heat exchange coefficient α' [25]. Delaware is used as well for tube side pressure drops calculation, where working fluid is sent. As mentioned above, Mokry correlation is adopted for the convective cold fluid heat exchange coefficient α', tube side. In this case, the charge air pressure drops are not calculated, because they are not a parameter of interest for this work and they are assumed to be equal to the ones already estimated for the original energy system's layout. In the following, main equations are presented, while for correlations see appendix. Note that some of the equations are expressed in the same way of preheater or subcritical evaporator.

- *Mass balance equations*:
  See Eqs. (3.25) and (3.26).

- *Energy conservation equations*:
  See Eqs. (3.47) and (3.48).

- *State equations*:
  See Eqs. (3.29) and (3.30).

- *Additional equations*:

Adopted heat exchange correlations, that can be found in the entire form in the appendix, will appear with the following dependence relations:

- Delaware:

$$\alpha' = f\left(\dot{m}', T'_m, p', T_{m,wall}, D_e, L, pitch, N_b, B_c, B/D_s, N_{tt}, N_{ss}, layout, configuration\right) \quad (3.57)$$

$$\Delta p'' = f\left(\dot{m}, f, s, \varphi, D_i, L, A, A_n, N_{pass}, N_s, configuration\right) \quad (3.58)$$

$$T_{m,wall} = f(\alpha', f_i, A_i, T'_m) \tag{3.59}$$

- Mokry:

$$\alpha'' = f\left(v'', \rho_{wall}, \rho'', c''_p, \mu'', \lambda''\right) \tag{3.60}$$

Variables and parameters

N° of equations: 25 *Eqs.* (3.25)-(3.26), *from Eqs.* (3.29) *to* (3.33),

from Eq. (3.38) *to* (3.44), Eqs. (3.47)-(3.48), *from Eq.* (3.57) *to* (3.60)

N° of physical quantities: 56

$\dot{m}'_{in,DP}$	$\dot{m}'_{out,DP}$	$\dot{m}''_{in,DP}$	$\dot{m}''_{out,DP}$	$T'_{in,DP}$	$T'_{out,DP}$	$h''_{in,DP}$	$h''_{out,DP}$
$T''_{in,DP}$	$T''_{out,DP}$	c'_p	c''_p	ρ'	ρ''	λ'	λ''
μ'	μ''	T'_m	T''_m	$\Delta T_{ml,CC}$	F_t	$\Delta T_{eff,DP}$	p'
p''	D_i	D_e	D_s	L	N_{tt}	A_i	A_e
V_i	V_e	λ_{pipe}	α'	α''	f_i	f_e	R_{sp}
$U_{e,DP}$	$T_{m,wall}$	$\dot{Q}_{DP}$	v''	f	s	φ	A_n
N_{pass}	N_s	$pitch$	ρ''_{wall}	B/D_s	B_c	N_{ss}	$\Delta p''_{DP}$

N° of fixed parameters: 18

$\dot{m}'_{in,DP}$	$\dot{m}'_{out,DP}$	$\dot{m}''_{in,DP}$	$\dot{m}''_{out,DP}$	$T'_{in,DP}$	$T'_{out,DP}$	$T''_{in,DP}$	v''
D_i	D_e	$pitch$	B/D_s	B_c	N_{ss}	N_s	N_{pass}
p'	p''						

N° of dependent variables: 38

$h''_{out,DP}$	$h''_{in,DP}$	$T''_{out,DP}$	c'_p	c''_p	ρ'	ρ''	ρ''_{wall}
λ'	λ''	μ'	μ''	T'_m	T''_m	$\Delta T_{ml,CC}$	F_t
$\Delta T_{eff,DP}$	D_s	L	N_{tt}	A_i	A_e	V_i	V_e
λ_{pipe}	α'	α''	f_i	f_e	R_{sp}	$U_{e,DP}$	$T_{m,wall}$
$\dot{Q}_{DP}$	f	s	φ	A_n	$\Delta p''_{DP}$		

N° of independent variables: 0

Among the 56 physical quantities there are the following state and output variables.

N° of state variables: 4

p'	p''	T'_m	T''_m

N° of output variables: 6

$\dot{Q}_{DP}$	$U_{e,DP}$	$\Delta p'_{DP}$	$\Delta p''_{DP}$	A_e	$\Delta T_{eff,DP}$

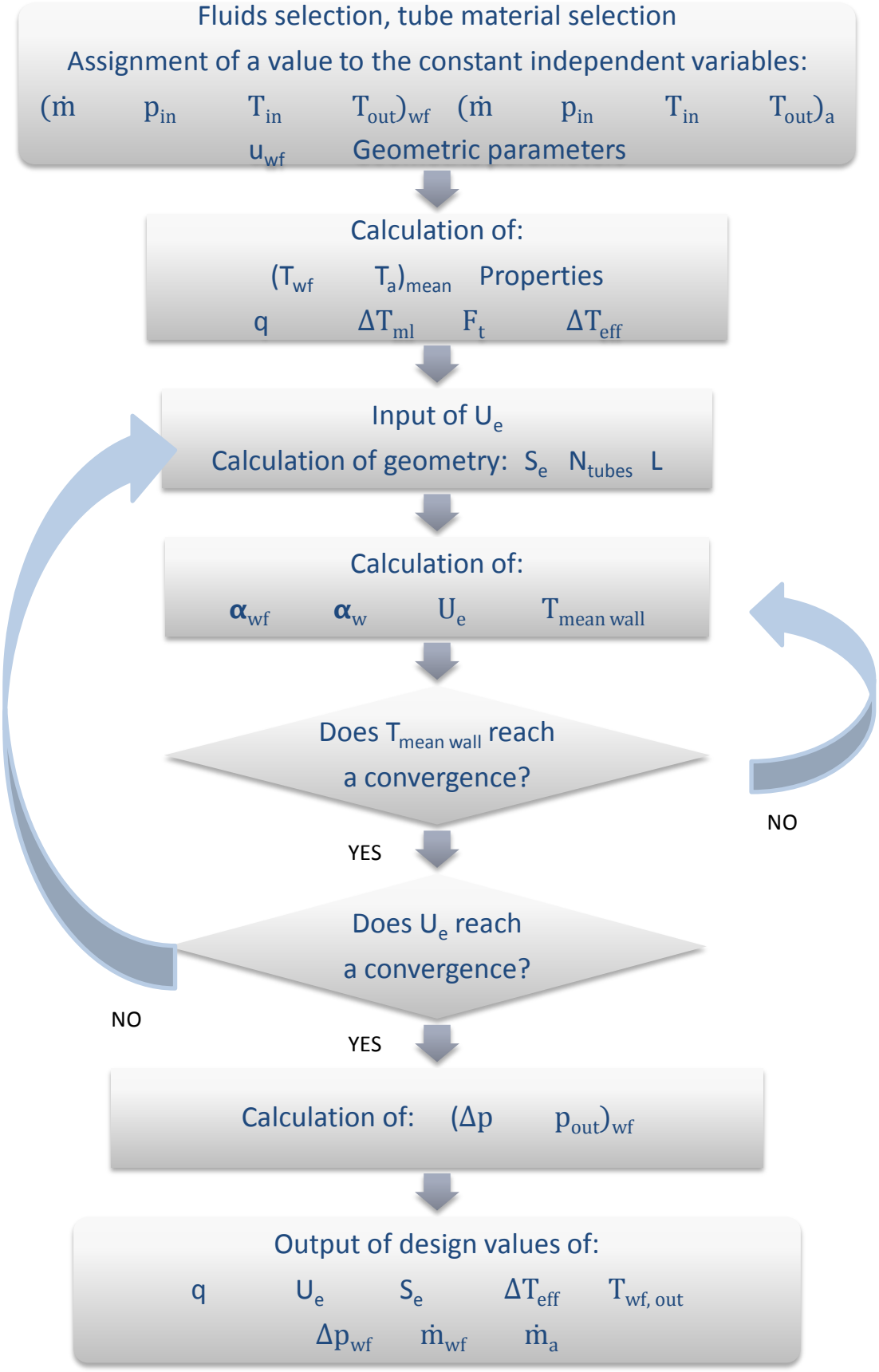

Figure 3.13 *Flowchart of the design procedure for supercritical evaporator.*

3.2.2.4 Condenser

This is the second and last presented heat exchanger where a subcritical phase change happens, used in the ORC system to condense the operative fluid after its expansion through the vapour turbine. As for the subcritical evaporator, this component is widely used in the power industry, being a fundamental element to allow the Rankine cycle to work, both for water and for organic operative fluids. Condenser, indeed, has the function of changing the phase of the working fluid from vapour to liquid, in order to allow the successive pump, placed downstream of the condenser and the cold drum, to circulate it and win pressure drops, making the cycle reliable.

In this case of study, the chosen heat exchanger for condensation is a shell and tube type F, where the working fluid is first desuperheated and then condensed. Outlet fluid is supposed to be saturated liquid and is sent to a drum, called cold drum, a real device with the function of accumulator for the whole ORC cycle. From this component only saturated liquid is supposed to be taken in order to avoid sending to the pump also vapour bubbles. Cold drum will be presented at detail in the next sections.

The chosen configuration for the condenser is the 2-4 because of the high operative fluid pressure drops, that this layout is able to reduce enough. The hot working fluid is sent shell side and the cold fluid tube side. The cold source consists in cooling water coming from central cooler, at the supposed constant temperature of 15°C.

The assumptions for the model of this component are similar to the evaporator's ones:

- outlet flux is physically sent to the cold drum in conditions of saturated liquid;
- inlet fluid is in superheated conditions, so in an early part of the heat exchanger the vapour is desuperheated and then condensed;
- condensing fluid in the shell side is in perfect equilibrium for both liquid and vapour phase; hence the working fluid's temperature is only function of shell-side pressure;
- tube-side, the cold fluid is assumed not to change its phase;
- thermodynamic properties of cold fluid are constant and evaluated at mean temperature, while for hot evaporating fluid they are evaluated at saturated liquid phase and saturated vapour phase conditions;
- inlet cooling water temperature is supposed constant (it comes from the central cooler that is not influenced by the ship's travelling conditions).

Differently from the case of evaporator, here desuperheating and condensation are treated together, thanks to the appropriate correlations found in literature, allowing to avoid splitting the model of this component into two parts as instead necessary for the HE1. In this way, condenser's modelling results much simpler.

The design model of the condenser consists in determining the geometric parameters, evaporation surfaces, the global heat transfer coefficient U_e and pressure drops Δp, calculated in nominal conditions. Adopted correlations are Gnielinski for the convective cold fluid's heat exchange coefficient α" and Bell-Delaware for pressure drops Δp", tube side,

Nusselt and Kern in case of smooth tubes or Beatty-Katz in case of finned tubes for the hot fluid α' and Chisholm for $\Delta p'$, shell side [25]. The main equations are presented below, while for correlations see appendix.

- *Mass balance equations*:
  See Eqs. (3.25) and (3.26).

- *Energy conservation equations*:
  As in the evaporator's case, heat flux is expressed using the enthalpy drop between inlet and outlet flows for the hot condensing fluid instead of the average specific heat, because of the phase change [26].

$$\dot{Q} = \dot{m}' \left(h'_{out} - h'_{in} \right) \tag{3.61}$$

$$\dot{Q} = \dot{m}'' c''_p \left(T''_{in} - T''_{out} \right) \tag{3.62}$$

- *State equations*:
  The properties necessary for the model are evaluated at the mean temperature T''_m for the cold flux, that is assumed not to change its phase, while for the hot flux the same properties are obtained both for liquid phase (x = 0) and for vapour phase (x = 1).

$$\left[\rho',\ c'_p, \lambda', \mu', h'\right]_l = f(p', x = 0) \tag{3.63}$$

$$\left[\rho',\ c'_p, \lambda', \mu', h'\right]_v = f(p', x = 1) \tag{3.64}$$

$$\left[\rho'',\ c''_p, \lambda'', \mu''\right] = f(p'', T''_m) \tag{3.65}$$

- *Additional equations*:

  - Gnielinski:

$$\alpha'' = f(\dot{m}'', T''_m, p'', D_i, L, N_{tt}, configuration) \tag{3.66}$$

  - Delaware:

$$\Delta p'' = f\left(\dot{m}'', f, s, \varphi, D_i, L, A, A_n, N_{pass}, N_s, configuration\right) \tag{3.67}$$

$$T_{m,wall} = f(\alpha', f_i, A_i, T'_m) \tag{3.68}$$

  - Nusselt and Kern:

$$\alpha' = f\left(\dot{m}'_v, p', T'_{sat}, L, N_{tt}, B_c, \frac{B}{D_s}, \rho'_v, \rho'_l, \mu'_l, \lambda'_l, g, layout, configuration\right) \tag{3.69}$$

  - Beatty-Katz:

$$\alpha' = f\left(\dot{m}'_v, p', T'_{sat}, T_{m,wall}, D_e, L, N_{tt}, B_c, \frac{B}{D_s}, \rho'_v, \rho'_l, \mu'_l, \lambda'_l, r', g, layout, configuration\right) \tag{3.70}$$

  - Chisholm:

$$\Delta p' = f(\dot{m}', x, f, s, \varphi, \rho', geometry, configuration) \quad (3.71)$$

Variables and parameters

N° of equations: 32 *Eqs.* (3.25)-(3.26), *from Eq.* (3.61) *to* (3.71)

N° of physical quantities: 61

$\dot{m}'_{in,DP}$	$\dot{m}'_{out,DP}$	$\dot{m}''_{in,DP}$	$\dot{m}''_{out,DP}$	$T''_{in,DP}$	$T''_{out,DP}$	$h'_{in,DP}$	$h'_{out,DP}$
$T'_{in,DP}$	$T'_{out,DP}$	c''_p	c'_{p_l}	c'_{p_v}	ρ''	ρ'_l	ρ'_v
λ''	$\lambda_l{}'$	$\lambda_v{}'$	μ''	$\mu_l{}'$	$\mu_v{}'$	T''_m	x
$\Delta T_{ml,CC}$	F_t	$\Delta T_{eff,DP}$	p'	p''	D_i	D_e	D_s
L	N_{tt}	A_i	A_e	V_i	V_e	λ_{pipe}	α'
α''	f_i	f_e	R_{sp}	$U_{e,DP}$	$T_{m,wall}$	$\dot{Q}_{DP}$	v''
f	s	φ	A_n	N_{pass}	N_s	$pitch$	g
B/D_s	B_c	N_{ss}	$\Delta p'_{DP}$	$\Delta p''_{DP}$			

N° of fixed parameters: 20

$\dot{m}'_{in,DP}$	$\dot{m}'_{out,DP}$	$\dot{m}''_{in,DP}$	$\dot{m}''_{out,DP}$	$T''_{in,DP}$	$T''_{out,DP}$	$T'_{in,DP}$	v''
D_i	D_e	$pitch$	B/D_s	B_c	N_{ss}	x	N_{pass}
N_s	g	p'	p''				

N° of dependent variables: 41

$h''_{out,DP}$	$h''_{in,DP}$	$T''_{out,DP}$	c'_p	c''_{p_l}	c''_{p_v}	ρ'	ρ''_l
ρ''_v	λ'	$\lambda_l{}''$	$\lambda_v{}''$	μ'	$\mu_l{}''$	$\mu_v{}''$	T'_m
$\Delta T_{ml,CC}$	F_t	$\Delta T_{eff,DP}$	D_s	L	N_{tt}	A_i	A_e
V_i	V_e	λ_{pipe}	α'	α''	f_i	f_e	R_{sp}
$U_{e,DP}$	$T_{m,wall}$	$\dot{Q}_{DP}$	f	s	φ	A_n	$\Delta p'_{DP}$
$\Delta p''_{DP}$							

N° of independent variables: 0

Among the 61 physical quantities there are the following state and output variables.

N° of state variables: 4

p'	p''	T''_m	x

N° of output variables: 6

$\dot{Q}_{DP}$	$U_{e,DP}$	$\Delta p'_{DP}$	$\Delta p''_{DP}$	A_e	$\Delta T_{eff,DP}$

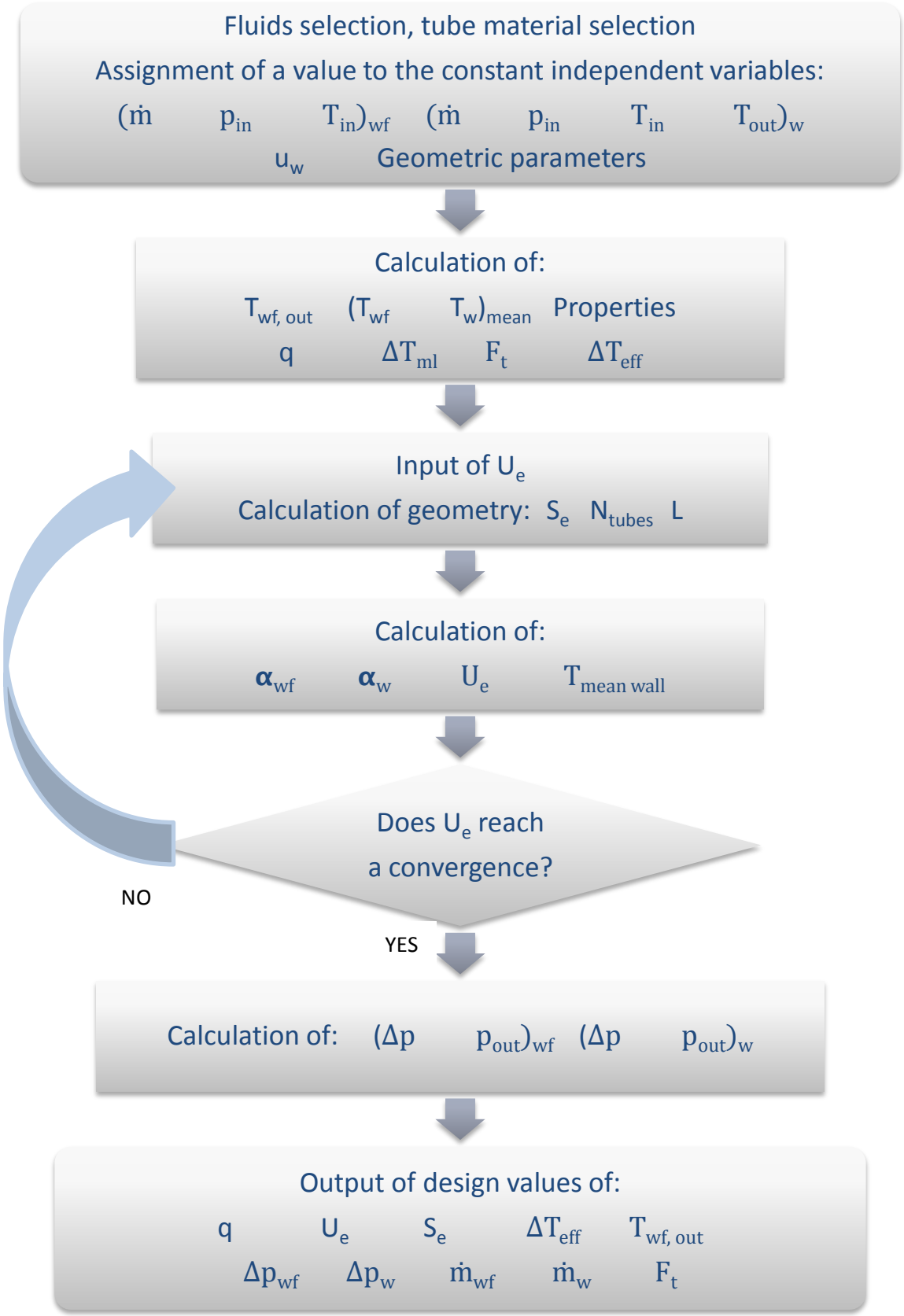

Figure 3.14 *Flowchart of the design procedure for condenser.*

3.2.3 Design operating characteristics

In this paragraph, all main design choices about the selected components for the ORC systems are presented. The shown values refer to the chosen operating points for the three ORC layouts, determined and exposed in Chapter 2. *EES* (Engineering Equation Solver) software has been used to find main design thermodynamic values for the three cycles.

A ΔT_{min} of 10°C has been imposed for the design of preheaters, subcritical evaporators and condensers, while a higher ΔT_{min} of 35°C was necessary for sizing supercritical evaporator.

Fluid velocities inside tubes of the heat exchangers are set at 2 m/s, that is considered the optimal economical speed for the material of the tubes, in this case carbon steel, except for the supercritical evaporator.

A mention has to be made about supercritical evaporator. The best available correlation for this phenomenon inside a heat exchanger, determined by Mokry et al. [29], refers to tube side exchange, where the tube is vertical. Given that the available hot source for the second pressure level of the studied ORC system is charge air, a gaseous fluid with a sufficient but not high quality level of the heat rejected, looking at its temperatures an optimal design would lead to a high exchange surface with a consequent very high length of the single tubes. A constraint must be taken into consideration at this point, about the feasibility of the installation inside LNG carrier. For this reason, a limit of 2.5 meters of highness is defined for the supercritical evaporator. To respect this constraint, only for this heat exchanger the tube side fluid velocity has been reduced.

In case of subcritical second pressure level there is not this problem, given that a horizontal shell and tube type E is selected. However, for this heat exchanger different design choices have been made about geometry, in particular about size of the tubes and pitch distance. Moreover, the number of tubes has been fixed to 1250, in order not to design a too large and too short heat exchanger, again with the constraint of 2.5 meters in the vertical direction. Due to the thermodynamic characteristics of charge air, hot source also in this case, the volume of this subcritical evaporator is much higher than the same exchanger adopted for the first pressure level. The eventual possibility of installation inside the ship should be verified at first.

In the following, tables containing gathered all design choices are reported, relative to selected operating points. The selected types of heat exchangers are also indicated, following the recommendations proposed by T.E.M.A. (Tubular Exchanger Manufacturers Association). *AspenONE* has been used to verify and support these choices, in particular thanks to its tool *Aspen Exchanger Design and Rating*.

About turbomachinery, it is reminded that rotational speed is fixed and constant for the vapour turbines, while it is variable and imposed by the ORC control system in off-design conditions for the pump. Given the relatively low head of the pump selected for the first pressure level, rotational speed is imposed by the chosen four poles electric motor, in this case 1450 rounds per minute. For the pumps considered for the second pressure level, the

higher head requires higher rotational speed: an indirect connection through speed reducer has been assumed, disengaging the pump from the constraint of rotational speed imposed by the mains frequency.

At last, nominal pressures for pumps and turbines take into account of pressure drops of the working fluid through heat exchangers.

Table 3.1 *Preheater design datasheets, first pressure level.*

PROCESS				
ORC layout		**1PL**	**2PL sub**	**2PL sup**
Tube side	*Hot fluid*	*Water*		
Mass flow rate	kg/s	53.2	39.9	39.9
Pressure	bar	3.15	3.15	3.15
Inlet temperature	°C	51.46	52.47	52.47
Outlet temperature	°C	49.48	49.52	49.52
Shell side	*Cold fluid*	*R245fa*		
Mass flow rate	kg/s	28.00	28.35	28.35
Pressure	bar	5.236	4.612	4.612
Inlet temperature	°C	29.92	29.72	29.72
Outlet temperature	°C	41.46	42.47	42.47

GEOMETRY				
ORC layout		**1PL**	**2PL sub**	**2PL sup**
Shell / tube passes	-	1-2	1-2	1-2
Exchanger type (T.E.M.A.)	-	AES	AES	AES
F_t	-	0.9806	0.9681	0.9681
Tube side velocity	m/s	2	2	2
External tube diameter	mm	15.875	15.875	15.875
Internal tube diameter	mm	13.385	13.385	13.385
Tube length	m	2.282	3.228	3.228
Pitch distance	mm	21.11	21.11	21.11
Layout angle	°	30	30	30
Number of tubes	-	383	288	288
Internal shell diameter	mm	479.8	422.1	422.1
Inlet / outlet baffle spacing	mm	361.3	432.3	432.3
Central baffle spacing	mm	311.8	295.5	295.5

Number of baffles	-	6	9	9
Baffle cut	%	25	25	25
Pairs of sealing strips	-	1	1	1

HEAT EXCHANGE				
ORC layout		**1PL**	**2PL sub**	**2PL sup**
External exchange surface	m^2	43.59	46.37	46.37
Tube side exchange coefficient	W/m^2K	12091	12055	12055
Shell side exchange coefficient	W/m^2K	1007	1093	1093
Total fouling resistance	m^2K/W	0.00026	0.00026	0.00026
Global heat transfer coefficient	W/m^2K	721.3	763.8	763.8
Heat flux	kW	439.5	492.1	492.1

Table 3.2 *Subcritical evaporator design datasheets, first pressure level.*

PROCESS				
ORC layout		**1PL**	**2PL sub**	**2PL sup**
Tube side	*Hot fluid*	*Water*		
Mass flow rate	kg/s	137.8	106.1	106.1
Pressure	bar	3.15	3.15	3.15
Inlet temperature	°C	82.41	80.65	79.70
Outlet temperature	°C	72.84	68.36	67.41
Shell side	*Cold fluid*	*R245fa*		
Mass flow rate	kg/s	28.00	28.35	28.35
Pressure	bar	5.236	4.612	4.612
Inlet temperature	°C	41.46	42.57	42.47
Outlet temperature	°C	64.36	59.82	59.82

GEOMETRY				
ORC layout		**1PL**	**2PL sub**	**2PL sup**
Shell / tube passes	-	2-4	2-4	2-4
Exchanger type (T.E.M.A.)	-	AFM	AFM	AFM
F_t	-	0.9957 - 1	0.9959 - 1	0.9954 - 1

Tube side velocity	m/s	2	2	2
External tube diameter	mm	15.875	15.875	15.875
Internal tube diameter	mm	13.385	13.385	13.385
Tube length	m	2.872	3.250	3.600
Pitch distance	mm	21.11	21.11	21.11
Layout angle	°	30	30	30
Number of tubes	-	2014	1548	1547
Internal shell diameter	mm	1051.0	928.5	928.2
Inlet / outlet baffle spacing	mm	510.3	423.4	453.0
Central baffle spacing	mm	473.1	371.4	417.7
Number of baffles	-	6	8	8
Baffle cut	%	25	25	25
Pairs of sealing strips	-	2	2	2

HEAT EXCHANGE				
ORC layout		**1PL**	**2PL sub**	**2PL sup**
External exchange surface	m^2	293.5	249.9	276.7
Tube side exchange coefficient	W/m^2K	14044	13797	13711
Shell side exchange coefficient	W/m^2K	577.7 - 5420	844.4 - 5230	835.4 - 4616
Total fouling resistance	m^2K/W	0.00026	0.00026	0.00026
Global heat transfer coefficient	W/m^2K	473.7 - 1771	638.7 - 1746	633.3 - 1670
Heat flux	kW	5531.3	5468.8	5468.2

Table 3.3 *Condenser design datasheets.*

PROCESS				
ORC layout		**1PL**	**2PL sub**	**2PL sup**
Tube side	*Cold fluid*	*Water*		
Mass flow rate	kg/s	242.55	242.55	242.55
Pressure	bar	3.15	3.15	3.15
Inlet temperature	°C	15.00	15.00	15.00
Outlet temperature	°C	20.43	21.53	21.95

Shell side	*Hot fluid*	*R245fa*		
Mass flow rate	kg/s	28.00	28.35	28.35
Pressure	bar	1.778	1.766	1.766
Inlet temperature	°C	39.23	40.29	41.31
Outlet temperature	°C	29.80	29.61	29.61

GEOMETRY				
ORC layout		**1PL**	**2PL sub**	**2PL sup**
Shell / tube passes	-	2-4	2-4	2-4
Exchanger type (T.E.M.A.)	-	AFM	AFM	AFM
F_t	-	0.9923	0.9894	0.9880
Tube side velocity	m/s	2	2	2
External tube diameter	mm	15.875	15.875	15.875
Internal tube diameter	mm	13.385	13.385	13.385
Tube length	m	3.007	3.636	3.818
Pitch distance	mm	21.11	21.11	21.11
Layout angle	°	30	30	30
Number of tubes	-	3452	3452	3452
Internal shell diameter	mm	1366	1366	1366
Inlet / outlet baffle spacing	mm	820.3	929.9	751.7
Central baffle spacing	mm	683.2	888.3	781.5
Number of baffles	-	3	3	4
Baffle cut	%	25	25	25
Pairs of sealing strips	-	2	2	2

HEAT EXCHANGE				
ORC layout		**1PL**	**2PL sub**	**2PL sup**
External exchange surface	m^2	517.7	626.2	657.2
Tube side exchange coefficient	W/m^2K	8852	8885	8902
Shell side exchange coefficient	W/m^2K	885.1	890.1	888.5
Total fouling resistance	m^2K/W	0.00026	0.00026	0.00026
Global heat transfer coefficient	W/m^2K	641.2	644.1	643.3
Heat flux	kW	5509	6626	7053

Table 3.4 *Evaporator design datasheets for the second pressure level.*

PROCESS			
ORC layout		**2PL sub**	**2PL sup**
Tube side	*Hot fluid*	*Air*	*R245fa*
Mass flow rate	kg/s	24.61	7.10
Pressure	bar	3.14	37.00
Inlet temperature	°C	175.70	30.84
Outlet temperature	°C	124.47	158.16
Shell side	*Cold fluid*	*R245fa*	*Air*
Mass flow rate	kg/s	5.11	24.61
Pressure	bar	25.85	3.14
Inlet temperature	°C	30.46	175.70
Outlet temperature	°C	135.37	103.22

GEOMETRY			
ORC layout		**2PL sub**	**2PL sup**
Shell / tube passes	-	1-1	2-4
Exchanger type (T.E.M.A.)	-	AES	AFM
F_t	-	1	0.6125
Tube side velocity	m/s	2	0.45
External tube diameter	mm	50.08	9.525
Internal tube diameter	mm	44.54	7.035
Tube length	m	8.774	2.355
Pitch distance	mm	62.60	11.91
Layout angle	°	30	30
Number of tubes	-	1250	1425
Internal shell diameter	mm	2440.0	511.5
Inlet / outlet baffle spacing	mm	270.9	103.4
Central baffle spacing	mm	488.0	102.3
Number of baffles	-	17	22
Baffle cut	%	25	25
Pairs of sealing strips	-	2	1

HEAT EXCHANGE			
ORC layout		**2PL sub**	**2PL sup**
External exchange surface	m^2	1725.3	100.4
Tube side exchange coefficient	W/m^2K	25.67	20980
Shell side exchange coefficient	W/m^2K	5220.4	1377
Total fouling resistance	m^2K/W	0.00026	0.00026
Global heat transfer coefficient	W/m^2K	22.65	752.3
Heat flux	kW	1284.6	1816.0

Table 3.5 *Pump design datasheets.*

PROCESS						
ORC layout		**1PL**	**2PL sub**		**2PL sup**	
			1PL	**2PL**	**1PL**	**2PL**
Mass flow rate	kg/s	28.00	28.35	5.11	28.35	7.10
Inlet enthalpy	J/kg	239.34	239.08	239.08	239.08	239.08
Inlet pressure	bar	1.778	1.766	1.766	1.766	1.766
Outlet pressure	bar	5.428	5.345	25.850	5.282	37.000

DESIGN PARAMETERS						
ORC layout		**1PL**	**2PL sub**		**2PL sup**	
			1PL	**2PL**	**1PL**	**2PL**
Volumetric flow rate	m^3/s	0.021	0.021	0.004	0.021	0.005
Head	J/kg	275.3	269.9	1816	265.1	2651
Head at 0 kg/s	J/kg	397.2	389.4	2620	382.5	3833
Rotational speed	rpm	1450	1450	14227.50	1450	16306.09
Isentropic efficiency	-	0.7	0.7	0.7	0.7	0.7
Electric efficiency	-	0.9	0.9	0.9	0.9	0.9

Table 3.6 *Turbine design datasheets.*

PROCESS						
ORC layout		**1PL**	**2PL sub**		**2PL sup**	
			1PL	**2PL**	**1PL**	**2PL**
Mass flow rate	kg/s	28.00	28.35	28.35	28.35	28.35
Inlet enthalpy	J/K	452.18	449.56	492.35	449.56	497.52
Inlet pressure	bar	5.108	4.612	25.850	4.612	36.820
Outlet pressure	bar	1.950	1.955	4.612	2.090	4.612

DESIGN PARAMETERS						
ORC layout		**1PL**	**2PL sub**		**2PL sup**	
			1PL	**2PL**	**1PL**	**2PL**
Reduced flow rate	$m \cdot s \cdot K^{0.5}$	0.0010	0.0013	0.00004	0.0014	0.00004
Stodola coefficient	m^2	0.0080	0.0092	0.0002	0.0093	0.0002
Isentropic efficiency	-	0.85	0.85	0.85	0.85	0.85
Electric efficiency	-	0.9	0.9	0.9	0.9	0.9

Table 3.7 *Drums design datasheets.*

DESIGN PARAMETERS						
ORC layout		**1PL**	**2PL sub**		**2PL sup**	
			1PL	**2PL**	**1PL**	**2PL**
Shape	-	Cylinder	Cylinder	Cylinder	Cylinder	-
Internal volume	m^3	2.5	2.5	2.5	2.5	-
Base diameter	m	0.728	0.728	0.728	0.728	-
Height	m	1.5	1.5	1.5	1.5	-
Wall thickness	m	0.08	0.08	0.08	0.08	-

3.2.4 Simulink design model

To allow the MATLAB Simulink dynamic model to work, the first step consists in providing it all necessary design values that describe geometry and performance at nominal conditions of the heat exchangers. Substantially, a first Simulink model simulates the design procedure for the selected shell and tubes, by making use of the equations that have been exposed in section 3.3 about design models. In this way, useful data regarding geometry, global heat transfer coefficient U_e and pressure drops Δp are saved in the MATLAB workspace, from where they are successively called by the main dynamic model, which purpose is to simulate the off-design behaviour of the whole ORC system.

This *ORC design model* is briefly introduced in order to explain how the main nominal values are provided to the dynamic model. It is composed by separate blocks, each of them representing design model of the single heat exchangers. The structure of these blocks is the same for every component:

- the first hierarchical level of the Simulink model consists in a single block, which flowchart corresponds to the one referred to the relative heat exchanger, for example the one in Figure 3.10 about preheater; there are no variable inputs, inlet values are only the ones that must be previously defined by the user in order to make the initial design choices about geometry and to provide the nominal thermodynamic conditions of the exchanging fluids;
- the second hierarchical level is formed by seven blocks, each of them representing a design step and inside of which it is findable the third and last hierarchical level; the model runs in the following precise order:
    I. in the first block, the working fluid's missing outlet temperature and the mean temperatures are calculated; by the use of them and the fluids' pressures all useful thermodynamic properties are obtained, by calling them from NIST Refprop; at last, temperature factor F_t and logarithmic mean temperature difference ΔT_{ml} are determined; the nominal heat flux is here calculated as well;
    II. the second block allows to define the first important geometric parameters, in particular number of tubes N_{tt}, external and internal exchange surfaces S_e and S_i, tube length L, diameter of shell D_s, pitch distance p and baffle spacing B; here an input of design global heat transfer coefficient U_e is introduced;
    III. the third block presents the selected correlations for calculating tube side fluid convective heat exchange coefficient α;
    IV. the fourth block has the same purpose of the third one, in this case for calculation of the shell side fluid convective heat exchange coefficient by use of the proper correlations;
    V. the fifth block receives all main previously determined parameters, in particular convective coefficients, geometric parameters and properties to

define the global heat transfer coefficient U_e, and nominal heat flux together with logarithmic mean temperature difference and temperature factor to calculate again the external exchange surface S_e and the tube length L; the mean wall temperature T_{mp} is also calculated in this block; finally, the last geometric parameters are determined, the heat exchanger volume V, the number of baffles N_b and the first and last baffle spacing B_{in} and B_{out};

VI. the sixth block makes use of the set correlations to calculate tube side fluid pressure drops;

VII. the seventh and last block utilizes different correlations to determine shell side fluid pressure drops.

Iterations are carried out in order to define the final values of T_{wall}, U_e, S_e and L. In particular, the value of the mean wall temperature is sent back to *block IV* to be used into the interested correlation, and it is calculated again inside *block V*. A similar path is followed by U_e, that is sent back from *block V* to *block II* and then recalculated, determining also new values for S_e and L. These iterations stop when the difference between the last calculated value of the parameter in question and the previous one is smaller than a predefined "error", that is directly set by MATLAB.

These model blocks, ordered in the presented way, are able to carry out the design procedure shown in the previous paragraphs. In particular, main steps are explained in the reported flowcharts at the end of every paragraph above, about the heat exchangers. The complete design procedure for a shell and tube heat exchanger is presented in appendix A.4, while adopted correlations are shown in A.1, A.2 and A.3.

A mention has to be made about design model of the subcritical evaporator. In this case, given that the adopted heat exchangers in this ORC system of study, *HE1* and *HE3* when subcritical, pursue both preheating and evaporation of the working fluid, the design procedure is split into two parts, everyone represented by a first hierarchical level block. The first step is the design of the preheating part, the second one of the evaporation part. It must be reminded that these two phenomena happen in the same heat exchanger, that obviously cannot change its geometry passing from a section to the other. To maintain the same geometry in this design procedure, a key geometric parameter is sent from the first block where it is calculated for preheating, to the second block referred to the evaporation. The selected key parameter is the number of tubes. In this way, the constraint about geometry is respected. The only two geometric parameters that can be different are the exchange surfaces and the corresponding length, because they are related to the heat exchange and not to the shell and tube sizing.

In the following, a figure of the main structure of the Simulink design model is shown, reporting the example of the preheater, followed by a figure that shows the *Parameter Dialog Box* where the initial design choices are set by the user. The blocks are marked with the roman numeral corresponding to the seven presented design steps. It is worth noting

that Figure 3.15 refers to the second Simulink hierarchical level, the first of which being only the single representative block of the heat exchanger.

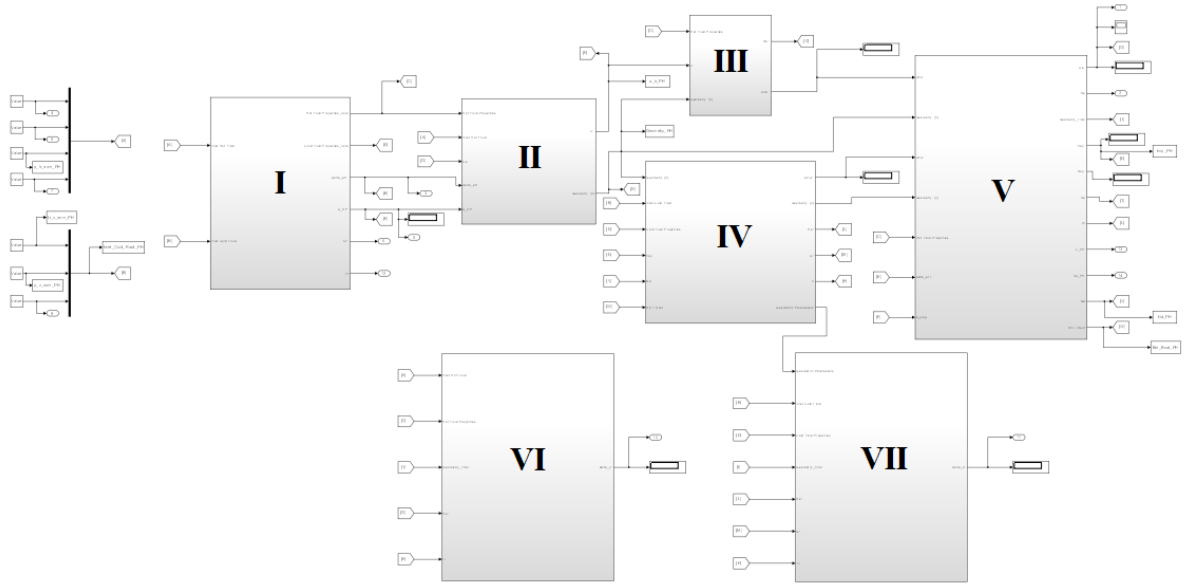

Figure 3.15 *Flowchart of the off-design procedure for preheater.*

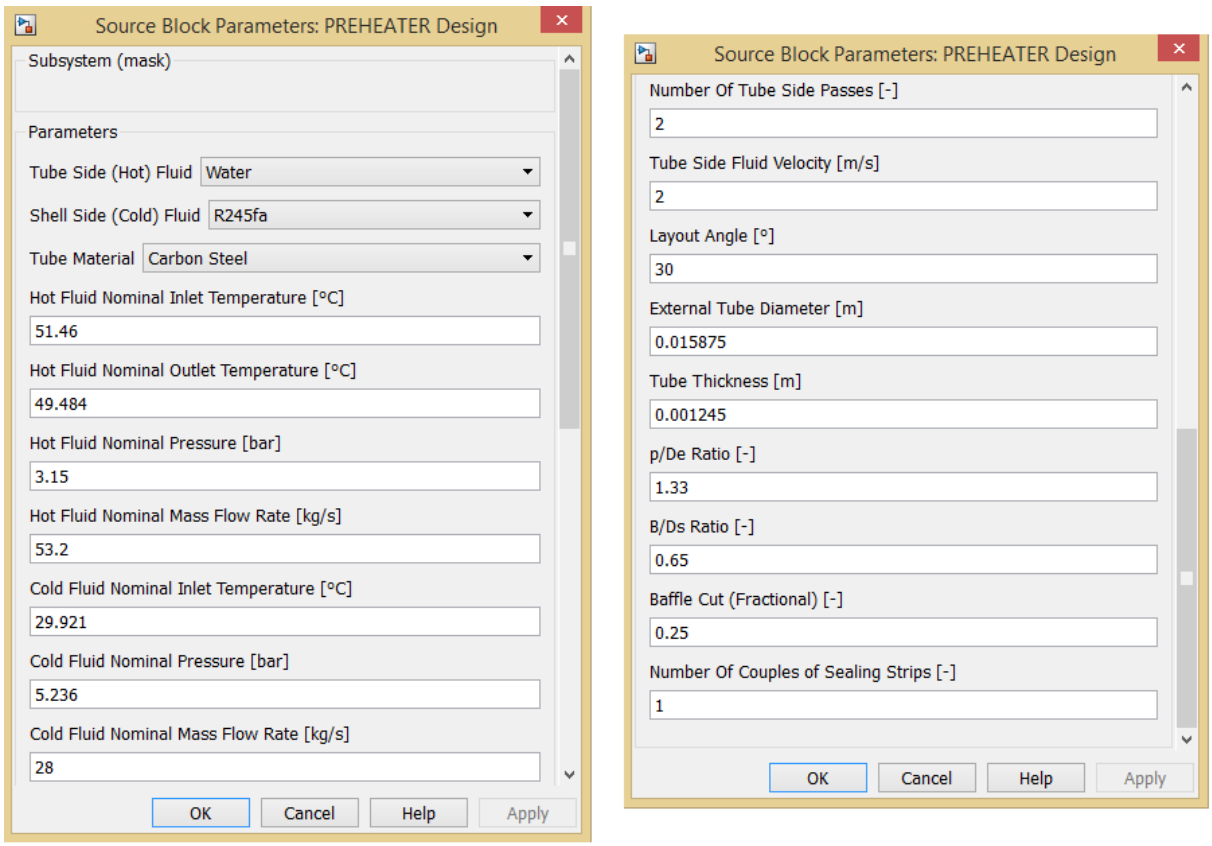

Figure 3.16 *Parameter Dialog Box for the design model of the preheater.*

3.3 OFF-DESIGN DYNAMIC MODEL OF THE ORC SYSTEM

3.3.1 Turbomachinery

In the following, dynamic models of pump and vapour turbine are presented. This kind of components is characterised by a faster dynamic response and a simpler modelling approach if compared to heat exchangers. A quasi-stationary approach is adopted for these not-state determined components, hence time behaviour is described as sequence of stationary conditions. For modelling purposes, only the parameters needed to perform off-design operation are defined, therefore for these components geometric parameters are not included in the calculation because not useful for the final aim. It is worth noting that these dynamic models make use of characteristic maps coming from literature, adopted here in order to quickly simulate the off-design performance.

3.3.1.1 Pump

The off-design model of the pump allows to describe its behaviour when the system is not in nominal conditions. In particular, changing the input parameters such as pressure, enthalpy or rotational speed leads to a variation in the mass flow rate that leaves the pump and in the outlet enthalpy. The way used here to manage these varying conditions to obtain an appropriate off-design behaviour is the adoption of characteristic maps, found in literature. A mention must be made for the defined tuning variable, rotational speed ω, that is allowed to vary according to the chosen type of pump. Rotational speed variation leads to a characteristic map translation, as described by the equations. In the following, main adopted relations are presented.

- *Mass balance equations*:

$$\dot{m}_{in}^{t} = \dot{m}_{out}^{t} \tag{3.72}$$

- *Energy balance equations*:

$$\dot{W}_{mec}^{t} = \dot{m}_{in}^{t}(h_{out}^{t} - h_{in}^{t}) \tag{3.73}$$

- *State equations:*

$$[\rho_{in}^{t}, s_{in}^{t}] = f(p_{in}^{t}, h_{in}^{t}) \tag{3.74}$$

$$\rho_{in,DP} = f\left(p_{in,DP}, x\right) \tag{3.75}$$

$$h_{out,is}^{t} = f(p_{out}^{t}, s_{in}^{t}) \tag{3.76}$$

- *Additional equations*:

These reported relations are necessary to implement the characteristic equation for the pump.

$$y^t = \frac{p_{out}^t - p_{in}^t}{\rho_{in}^t} \tag{3.77}$$

$$\dot{V}^t = \frac{\dot{m}_{in}^t}{\rho_{in}^t} \tag{3.78}$$

$$y_{DP}'^t = y_{DP} \left(\frac{\omega^t}{\omega_{DP}}\right)^2 \tag{3.79}$$

$$y_{DP} = \frac{p_{out,DP} - p_{in,DP}}{\rho_{in,DP}} \tag{3.80}$$

$$y_0'^t = y_{0,DP} \left(\frac{\omega^t}{\omega_{DP}}\right)^2 \tag{3.81}$$

$$\dot{V}_{DP}'^t = \dot{V}_{DP} \left(\frac{\omega^t}{\omega_{DP}}\right)^2 \tag{3.82}$$

$$\dot{V}_{DP} = \frac{\dot{m}_{DP}}{\rho_{in,DP}} \tag{3.83}$$

$$\eta_{is,P}^t = \frac{h_{out,is}^t - h_{in}^t}{h_{out}^t - h_{in}^t} \tag{3.84}$$

$$\dot{W}_e^t = \dot{W}_{mec}^t \, \eta_{el} \tag{3.85}$$

- *Characteristic equations*:

The characteristic maps adopted for this off-design model presents a second degree dependence from volumetric flow rate $\dot{V}$, according to Vaja [14].

$$y^t = \frac{y_{DP}'^t - y_0'^t{}_{,DP}}{\dot{V}_{DP}'^{t\,2}} \dot{V}^{t\,2} + y_0'^t{}_{,DP} \tag{3.86}$$

$$\eta_{is,P}^t = 2 \frac{\eta_{is,P,DP}}{\dot{V}_{DP}'^t} \dot{V}^t - \frac{\eta_{is,P,DP}}{\dot{V}_{DP}'^{t\,2}} \dot{V}^{t\,2} \tag{3.87}$$

Variables and parameters

N° of equations: 17 *from Eq.* (3.72) *to* (3.87)

Physical quantities: 28

$\dot{m}_{in}^t$	$\dot{m}_{out}^t$	h_{in}^t	$h_{out,is}^t$	h_{out}^t	p_{in}^t	p_{out}^t	$p_{in,DP}$
$p_{out,DP}$	ρ_{in}^t	$\rho_{in,DP}$	s_{in}^t	x	y^t	$y_{DP}'^t$	y_{DP}
$y_0'^t$	$y_{0,DP}$	$\dot{V}^t$	$\dot{V}_{DP}'^t$	$\dot{V}_{DP}$	$\dot{m}_{DP}$	ω^t	ω_{DP}
$\eta_{is,P}^t$	$\eta_{is,P,DP}$	η_{el}	$\dot{W}_{mec}^t$	$\dot{W}_e^t$			

Fixed parameters: 7

$p_{in,DP}$ $p_{out,DP}$ $y_{0,DP}$ $\dot{m}_{DP}$ ω_{DP} $\eta_{is,P,DP}$ η_{el}

Dependent variables: 15

$\dot{m}_{out}^{t}$ $h_{out,is}^{t}$ h_{out}^{t} ρ_{in}^{t} $\rho_{in,DP}$ s_{in}^{t} y^{t} $y_{DP}^{\prime t}$

y_{DP} $y_{0}^{\prime t}$ $\dot{V}^{t}$ $\dot{V}_{DP}^{\prime t}$ $\eta_{is,P}^{t}$ $\dot{W}_{mec}^{t}$ $\dot{W}_{e}^{t}$

Independent variables: 6

$\dot{m}_{in}^{t}$ h_{in}^{t} p_{in}^{t} p_{out}^{t} x ω^{t}

Among the 28 physical quantities there are the following state and output variables.

State variables: 5

p_{in}^{t} h_{in}^{t} p_{out}^{t} s_{in}^{t} x

Output variables: 4

$\dot{m}_{out}$ h_{out}^{t} p_{out}^{t} $\dot{W}_{e}^{t}$

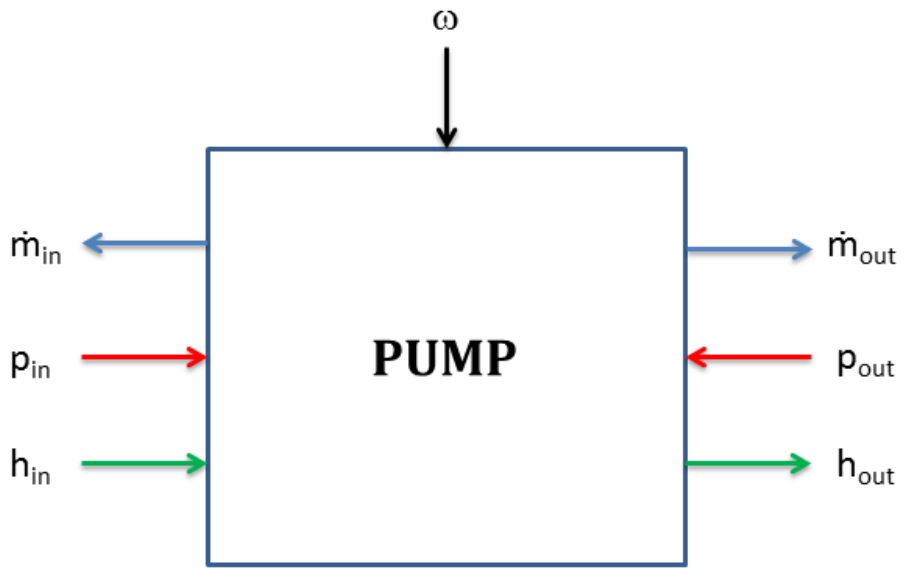

Figure 3.17 *Input output diagram of dynamic model for pumps.*

3.3.1.2 Turbine

Also in this case, characteristic maps are employed in order to describe the dynamic behaviour of vapour turbine. Contrarily to the pump, the turbine's characteristic map consists in a single curve, given that rotational speed is fixed for this component, therefore

depending only on the mains frequency. Main equations adopted in this model are reported below.

- *Mass balance equations*:

$$\dot{m}_{in}^{t} = \dot{m}_{out}^{t} \tag{3.88}$$

- *Energy balance equations*:

$$\dot{W}_{mec}^{t} = \dot{m}_{in}^{t}(h_{in}^{t} - h_{out}^{t}) \tag{3.89}$$

- *State equations:*

$$[T_{in}^{t}, \rho_{in}^{t}, s_{in}^{t}] = f(p_{in}^{t}, h_{in}^{t}) \tag{3.90}$$

$$\rho_{in,DP} = f\left(p_{in,DP}, x\right) \tag{3.91}$$

$$h_{out,is}^{t} = f(p_{out}^{t}, s_{in}^{t}) \tag{3.92}$$

- *Additional equations*:

The following relations are necessary to implement the characteristic equation for the vapour turbine. To calculate mass flow rate, Stodola equation has been applied [14].

$$\dot{m}_{in}^{t} = K\left(\rho_{in}^{t}\, p_{in}^{t}\left[1 - \left(\frac{1}{\varepsilon^{t}}\right)^{2}\right]\right)^{\frac{1}{2}} \tag{3.93}$$

$$\varepsilon^{t} = \frac{p_{in}^{t}}{p_{out}^{t}} \tag{3.94}$$

$$K = \frac{\dot{m}_{DP}}{\left(\rho_{in,DP}\, p_{in,DP}\left[1-\left(\frac{1}{\varepsilon_{DP}}\right)^{2}\right]\right)^{\frac{1}{2}}} \tag{3.95}$$

$$\varepsilon_{DP} = \frac{p_{in,DP}}{p_{out,DP}} \tag{3.96}$$

$$\eta_{is,T}^{t} = \frac{h_{in}^{t} - h_{out}^{t}}{h_{in}^{t} - h_{out,is}^{t}} \tag{3.97}$$

$$\dot{W}_{el}^{t} = \dot{W}_{mec}^{t}\, \eta_{el} \tag{3.98}$$

- *Characteristic equation*:

The adopted characteristic map for this off-design model presents a second degree dependence from the reduced mass flow rate $\dot{m}_R$, according to Mazzi [23].

$$\eta_{is,T}^{t} = \eta_{is,T,DP}\left[2\frac{\dot{m}_{R}^{t}}{\dot{m}_{R,DP}} - \left(\frac{\dot{m}_{R}^{t}}{\dot{m}_{R,DP}}\right)^{2}\right] \tag{3.99}$$

$$\dot{m}_{R,DP} = \frac{\dot{m}_{DP}\left(T_{in,DP}\right)^{\frac{1}{2}}}{p_{in,DP}} \tag{3.100}$$

$$\dot{m}_{R}^{t} = \frac{\dot{m}_{in}^{t}\left(T_{in}^{t}\right)^{\frac{1}{2}}}{p_{in}^{t}} \tag{3.101}$$

Variables and parameters

N° of equations: 16 *from Eq.* (3.88) *to* (3.101)

Physical quantities: 26

$\dot{m}_{in}^{t}$	$\dot{m}_{out}^{t}$	h_{in}^{t}	$h_{out,is}^{t}$	h_{out}^{t}	p_{in}^{t}	p_{out}^{t}	$p_{in,DP}$
$p_{out,DP}$	T_{in}^{t}	$T_{in,DP}$	ρ_{in}^{t}	$\rho_{in,DP}$	s_{in}^{t}	x	K
ε^{t}	ε_{DP}	$\dot{m}_{DP}$	$\dot{m}_{R}^{t}$	$\dot{m}_{R,DP}$	$\eta_{is,T}^{t}$	$\eta_{is,T,DP}$	η_{el}
$\dot{W}_{mec}^{t}$	$\dot{W}_{e}^{t}$						

Fixed parameters: 6

$p_{in,DP}$	$p_{out,DP}$	$\dot{m}_{DP}$	$T_{in,DP}$	$\eta_{is,T,DP}$	η_{el}

Dependent variables: 15

$\dot{m}_{out}^{t}$	$h_{out,is}^{t}$	h_{out}^{t}	ρ_{in}^{t}	s_{in}^{t}	T_{in}^{t}	$\rho_{in,DP}$	K
ε^{t}	ε_{DP}	$\dot{m}_{R}^{t}$	$\dot{m}_{R,DP}$	$\eta_{is,T}^{t}$	$\dot{W}_{mec}^{t}$	$\dot{W}_{e}^{t}$	

Independent variables: 5

$\dot{m}_{in}^{t}$	h_{in}^{t}	p_{in}^{t}	p_{out}^{t}	x

Among the 26 physical quantities there are the following state and output variables.

State variables: 5

p_{in}^{t}	h_{in}^{t}	p_{out}^{t}	s_{in}^{t}	x

Output variables: 4

$\dot{m}_{out}$	h_{out}^{t}	p_{out}^{t}	$\dot{W}_{e}^{t}$

Figure 3.18 *Input output diagram of dynamic model for vapour turbines.*

3.3.2 Heat exchangers

Dynamic models of heat exchangers are here presented. Dynamic response is significant for this kind of components, more than the turbomachinery's one. For this reason heat exchangers, especially when characterised by phase change of the inlet fluid, are the critical elements for this ORC model, and they need particular attention in the choice of modelling strategy.

Differential equations are also adopted, in conservation laws: the chosen ones are of time differential type (δt). These equations refer to the dynamics of the model, which represents the main purpose of the capacity models that will be exposed in Section 3.4.3.

It must be noticed that the two parameters that will be presented in the following, l_{11} and l_{12}, exponents of the selected off-design law for heat exchangers synthesized by Eq. (3.1), have been previously fixed and are constant. Their values have been determined by carrying out several simulations of the single components in various off-design conditions, by the use of the design tool of *AspenONE*, *Heat Exchanger Design and Rating*, obtaining in this way an off-design behaviour that is described by the law presented in Eqs. (3.109) to (3.111). In particular, l_{11} defines the dependence of global heat transfer coefficient with the hot fluid mass flow rate in off-design, while l_{12} determines the same dependence referred to the cold fluid mass flow rate variation.

In the same way, l_2 and l_3 provide the dependence relation of pressure drops with the respective fluid's mass flow rate variation. They have been previously determined by the use of the Aspen tool as well.

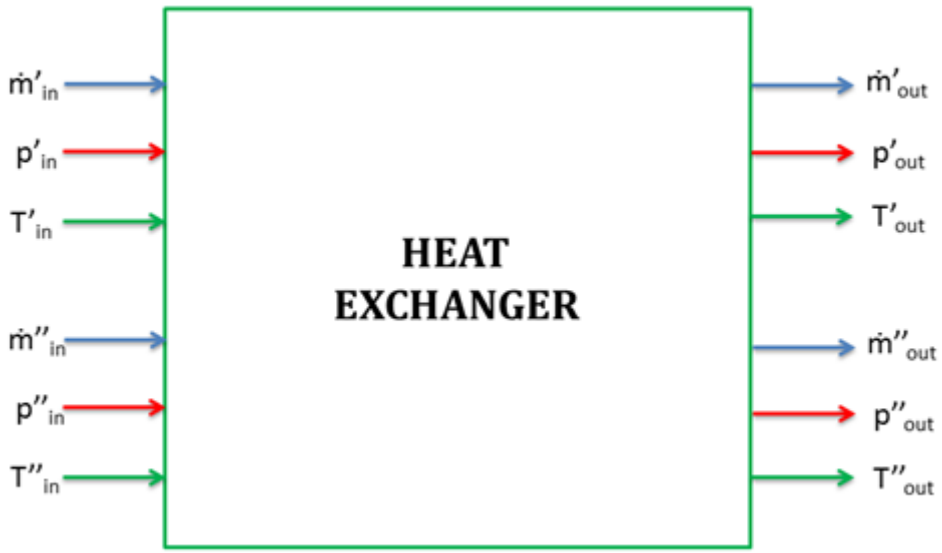

Figure 3.19 *Input output diagram of dynamic model for heat exchangers.*

3.3.2.1 Preheater

The off-design model allows to perform the dynamic behaviour of this component by a simple variation law of global heat exchange coefficient U_e and pressure drops Δp. From inlet design values and geometry, with the heat exchange surface that was already determined and fixed, it calculates the main off-design values in a fast way, due to the assumptions made.

- *Mass balance equations*:

$$\dot{m}'^{t}_{in} = \dot{m}'^{t}_{out} \tag{3.102}$$

$$\dot{m}''^{t}_{in} = \dot{m}''^{t}_{out} \tag{3.103}$$

- *Energy conservation equations*:

$$\dot{Q}^{t} = \dot{m}'^{t}(h'^{t}_{in} - h'^{t}_{out}) \tag{3.104}$$

$$\dot{Q}^{t} = \dot{m}''^{t}(h''^{t}_{out} - h''^{t}_{in}) \tag{3.105}$$

- *State equation:*

$$c_p''^{t} = f(p''^{t}, T_m''^{t}) \tag{3.106}$$

$$h''^{t} = f(p''^{t}, T''^{t}) \tag{3.107}$$

$$h'^{t} = f(p'^{t}, T'^{t}) \tag{3.108}$$

- *Additional equations*:

A simple variation law is applied here in order to calculate global coefficient U_e and pressure drops Δp at off-design conditions, to use them to obtain the related heat flux. It must be noticed that the heat exchange surface is obviously fixed because coming from design model, hence the first following equation can be simplified by eliminating A_{ext}. Parameters l_1 and l_2 are characteristic values of the type of exchanging fluids, to be obtained experimentally or analytically.

$$U_e^t A_{e,DP} = (U_e A_e)_{DP} \left(\frac{\dot{m}'^t}{\dot{m}'_{DP}}\right)^{l_{11}} \left(\frac{\dot{m}''^t}{\dot{m}''_{DP}}\right)^{l_{12}} \tag{3.109}$$

$$\Delta p'^t = \Delta p'_{DP} \left(\frac{\dot{m}'^t}{\dot{m}'_{DP}}\right)^{l_2} \tag{3.110}$$

$$\Delta p''^t = \Delta p''_{DP} \left(\frac{\dot{m}''^t}{\dot{m}''_{DP}}\right)^{l_3} \tag{3.111}$$

$$\dot{Q}^t = U_e^t A_e \, \Delta T_{ml,CC}^t \, F_t \tag{3.112}$$

Variables and parameters

N° of equations: 11 *from Eq.* (3.102) *to* (3.112)

Physical quantities: 25

$\dot{m}'^t_{in}$	$\dot{m}'^t_{out}$	$\dot{m}''^t_{in}$	$\dot{m}''^t_{out}$	$\dot{m}'_{DP}$	$\dot{m}''_{DP}$	$c_p''^t$	p''^t
$T_m''^t$	$A_{e,DP}$	U_e^t	$U_{e,DP}$	$\Delta p'^t$	$\Delta p''^t$	$\Delta p'_{DP}$	$\Delta p''_{DP}$
$\Delta T_{ml,CC}^t$	F_t	l_{11}	l_{12}	l_2	l_3	$\dot{Q}^t$	h'^t
h''^t							

Fixed parameters: 2

$\dot{m}'_{DP}$ $\dot{m}''_{DP}$

Dependent variables: 7

$c_p''^t$ U_e^t $\dot{Q}^t$ $\Delta p'^t$ $\Delta p''^t$

Independent variables: 12

$\dot{m}'^t_{in}$	$\dot{m}'^t_{out}$	$\dot{m}''^t_{in}$	$\dot{m}''^t_{out}$	p''^t	$T_m''^t$	$\Delta T_{ml,CC}^t$	F_t
$A_{e,DP}$	$U_{e,DP}$	$\Delta p'_{DP}$	$\Delta p''_{DP}$				

Constants: 4

l_{11} l_{12} l_2 l_3

Among the 25 physical quantities there are the following state and output variables.

State variables: 2

p''^t $T_m''^t$

Output variables: 4

$\dot{Q}^t$ U_e^t $\Delta p'^t$ $\Delta p''^t$

Two other output variables are given out by this model: the cold fluid's outlet temperature $t_u''^t$ and the value of ΔT_{eff}^t, both calculated by a MATLAB script.

In the following, the flowchart for the off-design calculation of preheater is reported. It is worth noting that it corresponds to the flowcharts of supercritical evaporator and condenser, while for the subcritical evaporator ulterior passages must be added in order to take into account of phenomena like preheating, evaporating and superheating inside the same heat exchanger.

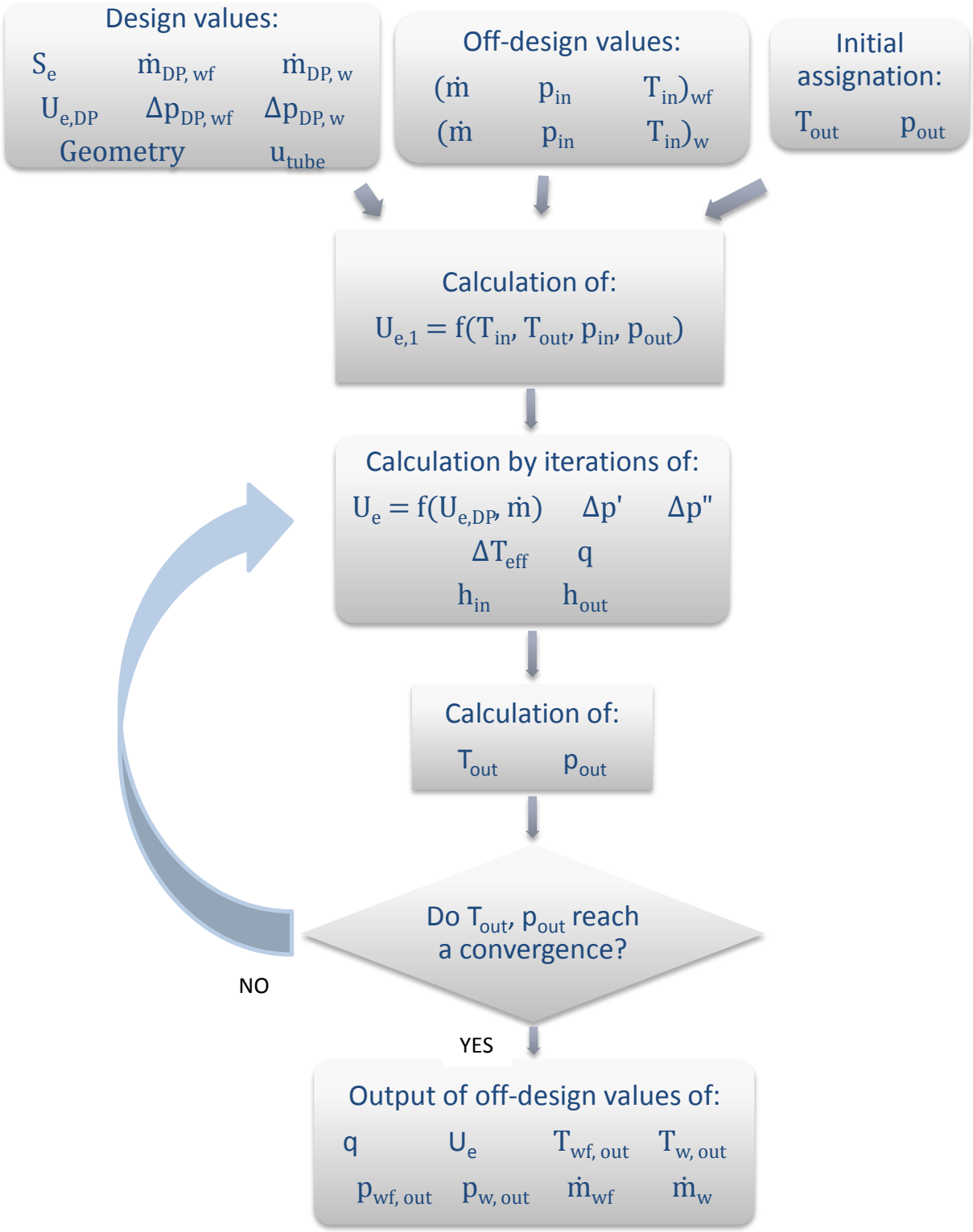

Figure 3.20 *Flowchart of the off-design procedure for preheater, supercritical evaporator and condenser.*

3.3.2.2 Subcritical evaporator

Also in the case of this heat exchanger, as for preheater, the off-design model allows to perform the dynamic behaviour, by executing the same simple variation law presented for the previous component. Global heat transfer coefficient U_e and pressure drops Δp are determined in off-design conditions in the same manner, by using the inlet design values and geometry, not forgetting that the calculated heat exchange surface remains fixed. In the whole component, considering both preheating and evaporation parts, the total values of U_e and Δp consist in the sum of the calculated terms in the two model blocks. To read more about, the modelling procedure regarding the whole heat exchanger will be presented at detail in the next chapter. The main off-design relations are the same adopted for preheater, thanks to the use of the same kind of off-design behaviour law.

Variables and parameters

N° of equations: 10 *from Eq.* (3.102) *to* (3.105), *from Eq.* (3.107) *to* (3.112)

Physical quantities: 22

$\dot{m}'^{t}_{in}$ $\dot{m}'^{t}_{out}$ $\dot{m}''^{t}_{in}$ $\dot{m}''^{t}_{out}$ $\dot{m}'_{DP}$ $\dot{m}''_{DP}$ $A_{e,DP}$ U_e^t
$U_{e,DP}$ $\Delta p'^t$ $\Delta p''^t$ $\Delta p'^t_{DP}$ $\Delta p''^t_{DP}$ $\Delta T^t_{ml,CC}$ F_t l_{11}
l_{12} l_2 l_3 $\dot{Q}^t$ h'^t h''^t

Fixed parameters: 2

$\dot{m}'_{DP}$ $\dot{m}''_{DP}$

Dependent variables: 4

U_e^t $\dot{Q}^t$ $\Delta p'^t$ $\Delta p''^t$

Independent variables: 12

$\dot{m}'^{t}_{in}$ $\dot{m}'^{t}_{out}$ $\dot{m}''^{t}_{in}$ $\dot{m}''^{t}_{out}$ $\Delta T^t_{ml,CC}$ F_t $A_{e,DP}$ $U_{e,DP}$
$\Delta p'^t_{DP}$ $\Delta p''^t_{DP}$

Constants: 2

l_{11} l_{12} l_2 l_3

Among the 22 physical quantities there are the following state and output variables.

State variables: 0

Output variables: 4

$\dot{Q}^t$ U_e^t $\Delta p'^t$ $\Delta p''^t$

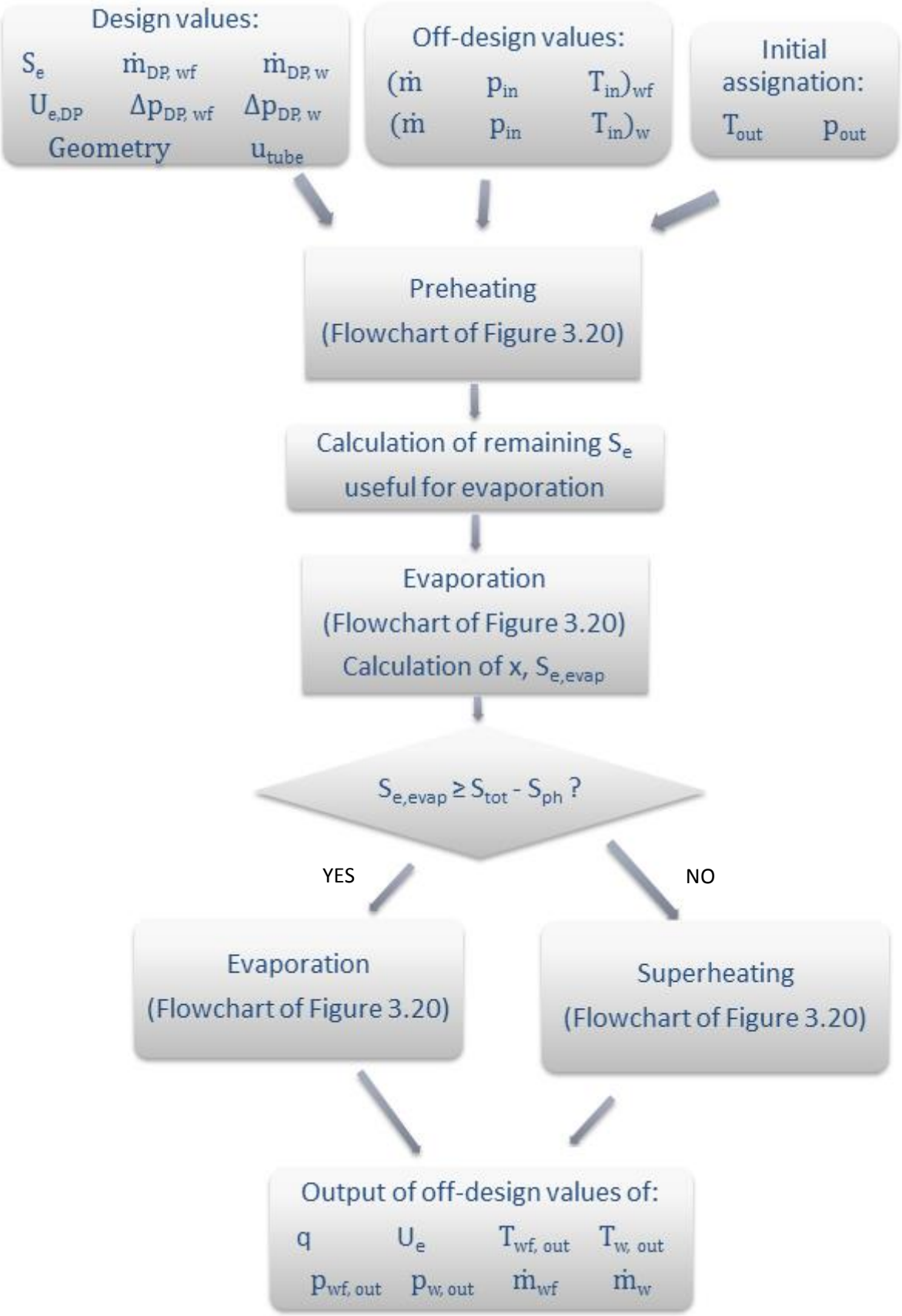

Figure 3.21 *Flowchart of the off-design procedure for subcritical evaporator.*

3.3.2.3 Supercritical evaporator

The off-design model allows to perform the dynamic behaviour, by adopting the same simple variation law presented for the previous component. Global heat transfer coefficient U_e and pressure drops Δp are determined in off-design conditions in the same manner, by using the inlet design values and geometry, with the calculated heat exchange surface that remains fixed.

To see the flowchart of supercritical evaporator, see Figure 3.20.

Variables and parameters

N° of equations: 10 *from Eq.* (3.102) *to* (3.105), *from Eq.* (3.107) *to* (3.112)

Physical quantities: 22

$\dot{m}'^{t}_{in}$ $\dot{m}'^{t}_{out}$ $\dot{m}''^{t}_{in}$ $\dot{m}''^{t}_{out}$ $\dot{m}'_{DP}$ $\dot{m}''_{DP}$ $A_{e,DP}$ U_e^t
$U_{e,DP}$ $\Delta p'^{t}$ $\Delta p''^{t}$ $\Delta p'^{t}_{DP}$ $\Delta p''^{t}_{DP}$ $\Delta T^{t}_{ml,CC}$ F_t l_{11}
l_{12} l_2 l_3 $\dot{Q}^t$

Fixed parameters: 2

$\dot{m}'_{DP}$ $\dot{m}''_{DP}$

Dependent variables: 4

U_e^t $\dot{Q}^t$ $\Delta p'^{t}$ $\Delta p''^{t}$

Independent variables: 12

$\dot{m}'^{t}_{in}$ $\dot{m}'^{t}_{out}$ $\dot{m}''^{t}_{in}$ $\dot{m}''^{t}_{out}$ $\Delta T^{t}_{ml,CC}$ F_t $A_{e,DP}$ $U_{e,DP}$
$\Delta p'^{t}_{DP}$ $\Delta p''^{t}_{DP}$

Constants: 2

l_{11} l_{12} l_2 l_3

Among the 22 physical quantities there are the following state and output variables.

State variables: 0

Output variables: 4

$\dot{Q}^t$ U_e^t $\Delta p'^{t}$ $\Delta p''^{t}$

3.3.2.4 Condenser

Off-design model is almost the same of the evaporators' ones. The adopted main equations are the same, and they are shown below. The goal is still to calculate the global heat transfer coefficient U_e and pressure drops Δp in off-design conditions, by using the inlet design values and geometry, with the heat exchange surface that is fixed by the design model.

To see the flowchart of condenser, see Figure 3.20. It is worth noting that in this case the cold source is cooling water, supposed constant in temperature, pressure and mass flow rate for all off-design conditions of the ship energy system.

Variables and parameters

N° of equations: 10 *from Eq.* (3.102) *to* (3.105), *from Eq.* (3.107) *to* (3.112)

Physical quantities: 22

$\dot{m}'^{t}_{in}$ $\dot{m}'^{t}_{out}$ $\dot{m}''^{t}_{in}$ $\dot{m}''^{t}_{out}$ $\dot{m}'_{DP}$ $\dot{m}''_{DP}$ $A_{e,DP}$ U_e^t
$U_{e,DP}$ $\Delta p'^{t}$ $\Delta p''^{t}$ $\Delta p'^{t}_{DP}$ $\Delta p''_{DP}$ $\Delta T^t_{ml,CC}$ F_t l_{11}
l_{12} l_2 l_3 $\dot{Q}^t$

Fixed parameters: 2

$\dot{m}'_{DP}$ $\dot{m}''_{DP}$

Dependent variables: 4

U_e^t $\dot{Q}^t$ $\Delta p'^{t}$ $\Delta p''^{t}$

Independent variables: 12

$\dot{m}'^{t}_{in}$ $\dot{m}'^{t}_{out}$ $\dot{m}''^{t}_{in}$ $\dot{m}''^{t}_{out}$ $\Delta T^t_{ml,CC}$ F_t $A_{e,DP}$ $U_{e,DP}$
$\Delta p'^{t}_{DP}$ $\Delta p''^{t}_{DP}$

Constants: 2

l_{11} l_{12} l_2 l_3

Among the 22 physical quantities there are the following state and output variables.

State variables: 0

Output variables: 4

$\dot{Q}^t$ U_e^t $\Delta p'^{t}$ $\Delta p''^{t}$

3.3.3 Capacities

Here dynamic models of the components belonging to the category called “Capacities” are presented. These devices take both mass and energy storage of the working fluid and are associated to a subcritical phase change, where there is a clear separation between vapour and liquid. There are two phase changes in the Rankine cycle, one evaporation and one condensation, the former characterised by upper temperatures and pressures with respect of the latter. The two capacities are called “hot drum” and “cold drum”. The hot drum Simulink model is placed downstream of the evaporator, while the cold drum is downstream of the condenser.

In our case study, for single stage ORC only cold drum represents a real device inside of the cycle, operating as an accumulator for the cycle itself. Regarding the hot drum, it appears in the model only for modelling purposes, in order to manage the dynamic of the ORC system by applying the required balances, described by differential equations. Without the hot drum model, dynamics could not be implemented. To maintain the correspondence between the ORC model and the described real system, the hot drum block represents the dynamic variation of pressure and temperature during transients towards off-design conditions, and it is possible by assigning as total volume of the drum the same one of the evaporator, the so called HE1. In this way, the hot drum model fits in the overall one only as an addition block to describe dynamics of the working fluid inside evaporator, hence it does not represent a real device in the studied ORC system.

The case of cold drum is different, because its Simulink model actually describes a real system component, with the double function of an accumulator for the ORC, making stable the cycle pressures, and a tank from where to take saturated liquid to send to the pump, avoiding in this way to leave any vapour bubbles in the working fluid. In the cold drum Simulink model hence there are no constraints about the volume, except the fact that obviously it must be compatible for the application in this ship. For this reason, the cold drum’s volume must be chosen both to lead to a good ORC working and to be allowed to be installed in the LNG carrier in question.

Hot drum and cold drum models are characterised by the application of mass and energy balances, the only two kind of equations in the whole ORC model to present derivatives, being both differential equations. For this reason, their presence allows to implement dynamics in the model. The same problem was studied by Åström and Bell [27], who presented a nonlinear dynamic model for natural circulation drum-boilers. This is a second order model that is able to describe drum pressure and total volume of liquid in the system, using them as state variables into the two mentioned mass and energy balances. According to the authors, it is possible to implement a third or fourth order model for these devices, able to capture also the vapour dynamics in the risers and the dynamics of vapour below the liquid surface in the drum. This possibility goes far beyond the purposes of this study, because of the too high detail level respect of the requested one, moreover at cost of increasing of simulation time that is against the search of rapidity and simplicity for the

overall ORC model. For these reasons, in this work the second order model is employed, as right compromise for the demanded level of detail and simulation speed.

Dynamics is managed by a control system block, which purpose is to regulate the pump's rotational speed in order to lead the model to converge to reliable simulation results. To make possible the control system to work, an additional parameter must be provided by the cold drum block, the ratio between the operative fluid's liquid volume inside the component and its total volume, to send it to the control block allowing it to evaluate the pump's rotational speed. To be precise, the mentioned information provided by the drum model represents the liquid level. During transients the control system must impose the right pump's rotational velocity, increasing it if the liquid level tends to drop, decreasing it if liquid level tries to grow up. To provide this required ratio between liquid volume and total volume, V_l/V_{tot}, the cold drum model must present a third equation, the volume conservation. The same equations are applied to the hot drum, with the only difference that it does not correspond to a real device in the energy system.

The cold drum, representing a real component in which mass and energy storage are carried out, performs as accumulator to manage:

- transient between two off-design states, leading to a filling or an emptying of the drum, to maintain stable pressures inside the cycle;
- thermal expansion of operative fluid from nonworking cold plant to nominal operations.

The cold drum device is substantially a tank in which liquid and vapour coexist in saturation conditions, the liquid laying in the bottom and the vapour occupying the top. The outflow duct is placed on the lower side of this tank, in order to take only saturated liquid to send to the successive pump.

In the following, the main equations adopted for the capacities are shown [27].

- *Mass and energy balance equations*:

$$\begin{cases} \dot{m}_{in}^{t} - \dot{m}_{out}^{t} = a_{11}\dfrac{dp}{dt} + a_{12}\dfrac{dT}{dt} & (3.113) \\ \dot{m}_{in}^{t} h_{in}^{t} - \dot{m}_{out}^{t} h_{out}^{t} = a_{21}\dfrac{dp}{dt} + a_{22}\dfrac{dT}{dt} & (3.114) \end{cases}$$

It can be noticed that the drum Simulink block requires as input both the inlet and outlet working fluid's mass flow rates, considering for example for the hot drum the inlet one as saturated liquid and the outlet one as saturated vapour and vice versa for the cold drum, plus the inlet fluid enthalpy. The equations system is solved by isolating the two derivatives of pressure and temperature, which are then integrated in time after calculation. In this way, the model gives out pressure and temperature of the operative fluid inside the studied component, be it evaporator or cold drum device. These differential equations allow to determine pressure and temperature variations when there is a transient between two off-design states, or between the design and an off-design state. As mentioned before, these

variations could lead to a filling or an emptying of the drum, as the result of the modification of the pump's rotational speed imposed by the control system in order to restore the predefined liquid level in the cold drum, in order to reach an equilibrium point for pressure in the particular off-design condition.

To solve the drum mass and energy balances, the coefficients a_{11}, a_{12}, a_{21}, a_{22} must be determined. In the system presented below these coefficients are expressed in their complete form, according to the notation adopted in [27].

- *Coefficients*:

$$\begin{cases} a_{11} = V_v \frac{d\rho_v}{dp} + V_l \frac{d\rho_l}{dp} & (3.115) \\ a_{12} = V_v \frac{d\rho_v}{dT} + V_l \frac{d\rho_l}{dT} & (3.116) \\ a_{21} = V_v u_v \frac{d\rho_v}{dp} + V_l u_l \frac{d\rho_l}{dp} & (3.117) \\ a_{22} = \left(V_v u_v \frac{d\rho_v}{dT} + V_l u_l \frac{d\rho_l}{dT} \right) + \left(V_v \rho_v c_{v,v} + V_l \rho_l c_{v,l} \right) & (3.118) \end{cases}$$

Required parameters are substantially the volumes of vapour phase and liquid phase, in an equilibrium condition inside the drum, and fluid properties at the two saturated conditions. To obtain these needed values, the main properties are called by the *NIST Refprop* program through the next relations.

- *State equations (hot drum)*:

$$\left[u, \rho, c_v, \frac{d\rho}{dp}, \frac{d\rho}{dT} \right]_l = f(p, x = 0) \quad (3.119)$$

$$\left[h, u, \rho, c_v, \frac{d\rho}{dp}, \frac{d\rho}{dT} \right]_v = f(p, x = 1) \quad (3.120)$$

- *State equations (cold drum)*:

$$\left[h, u, \rho, c_v, \frac{d\rho}{dp}, \frac{d\rho}{dT} \right]_l = f(p, x = 0) \quad (3.121)$$

$$\left[u, \rho, c_v, \frac{d\rho}{dp}, \frac{d\rho}{dT} \right]_v = f(p, x = 1) \quad (3.122)$$

It is worth noting that the two derivatives of density, on pressure and on temperature, are equivalent to the following relations:

$$\frac{d\rho}{dp} = \frac{1}{R\,T} \quad (3.123)$$

$$\frac{d\rho}{dT} = -\frac{p}{R\,T^2} \quad (3.124)$$

where R is the specific gas constant, given from the ratio between ideal gas constant and molar mass of the fluid in question, in our case R245fa.

To determine the remaining requested values, which are the volumes of liquid and vapour phases inside drum, another parameter is necessary. The chosen one is the ratio between liquid volume of the working fluid and total volume of the drum, which is the evaporator for the hot drum Simulink block and the cold drum device for the cold drum block. This parameter describes the liquid level inside the component in question and it helps to determine the two required volumes, starting from a predefined initial value of this V_l/V_t.

By knowing volumes and densities of vapour and liquid phases, it is easy to obtain the masses of the two phases contained in the drum at a certain time during simulation. To complete the model of these devices that work as capacities, it is now necessary to add a physical constraint, that consists in imposing the volumes of the two phases to be equal to the total volume of the drum in question. This constraint is described by the following equation.

- *Volume conservation equation*:

$$\frac{m_v^{t+dt}}{\rho_v^{t+dt}} + \frac{m_l^{t+dt}}{\rho_l^{t+dt}} = V_{tot} \tag{3.125}$$

At last, to determine the liquid level inside the component at the time *t + dt*, id est $\left(V_l/V_{tot}\right)^{t+dt}$, to send it back to calculate the new vapour and liquid volumes and at the same time to the control system block, the equation presented below is necessary to obtain the total mass at *t + dt*, useful for the next calculations:

$$m_{tot}^{t+dt} = m_l^t + m_v^t + \int_t^{t+dt} (\dot{m}_{in} - \dot{m}_{out})\, dt \tag{3.126}$$

Variables and parameters (hot drum)

N° of equations: 21 *from Eq.* (3.113) *to* (3.120) *and from Eq.* (3.123) *to* (3.126)

Physical quantities: 25

$\dot{m}_{in}^t$	$\dot{m}_{out}^t$	h_{in}^t	h_{out}^t	p^t	T	a_{11}	a_{12}
a_{21}	a_{22}	V_v	V_l	u_v	u_l	ρ_v	ρ_l
$c_{v,v}$	$c_{v,l}$	R	m_v	m_l	m_{tot}	V_{tot}	x
t							

Fixed parameters: 0

Dependent variables: 21

h_{out}^t	p^t	T	a_{11}	a_{12}	a_{21}	a_{22}	V_v
V_l	u_v	u_l	ρ_v	ρ_l	$c_{v,v}$	$c_{v,l}$	R
m_v	m_l	m_{tot}	x	t			

Independent variables: 4

$\dot{m}'^{t}_{in}$ $\dot{m}'^{t}_{out}$ h^{t}_{in} V_{tot}

Among the 25 physical quantities there are the following state and output variables.

State variables: 2

p^t x

Output variables: 3

p^t h^{t}_{out} $\left(\frac{V_l}{V_{tot}}\right)^t$

Variables and parameters (cold drum)

N° of equations: 21 *from Eq.* (3.113) *to* (3.118) *and from Eq.* (3.121) *to* (3.126)

Physical quantities: 25

$\dot{m}^{t}_{in}$	$\dot{m}^{t}_{out}$	h^{t}_{in}	h^{t}_{out}	p^t	T	a_{11}	a_{12}
a_{21}	a_{22}	V_v	V_l	u_v	u_l	ρ_v	ρ_l
$c_{v,v}$	$c_{v,l}$	R	m_v	m_l	m_{tot}	V_{tot}	x
t							

Fixed parameters: 1

V_{tot}

Dependent variables: 21

h^{t}_{out}	p^t	T	a_{11}	a_{12}	a_{21}	a_{22}	V_v
V_l	u_v	u_l	ρ_v	ρ_l	$c_{v,v}$	$c_{v,l}$	R
m_v	m_l	m_{tot}	x	t			

Independent variables: 3

$\dot{m}'^{t}_{in}$ $\dot{m}'^{t}_{out}$ h^{t}_{in}

Among the 25 physical quantities there are the following state and output variables.

State variables: 2

p^t x

Output variables: 3

p^t h^{t}_{out} $\left(\frac{V_l}{V_{tot}}\right)^t$

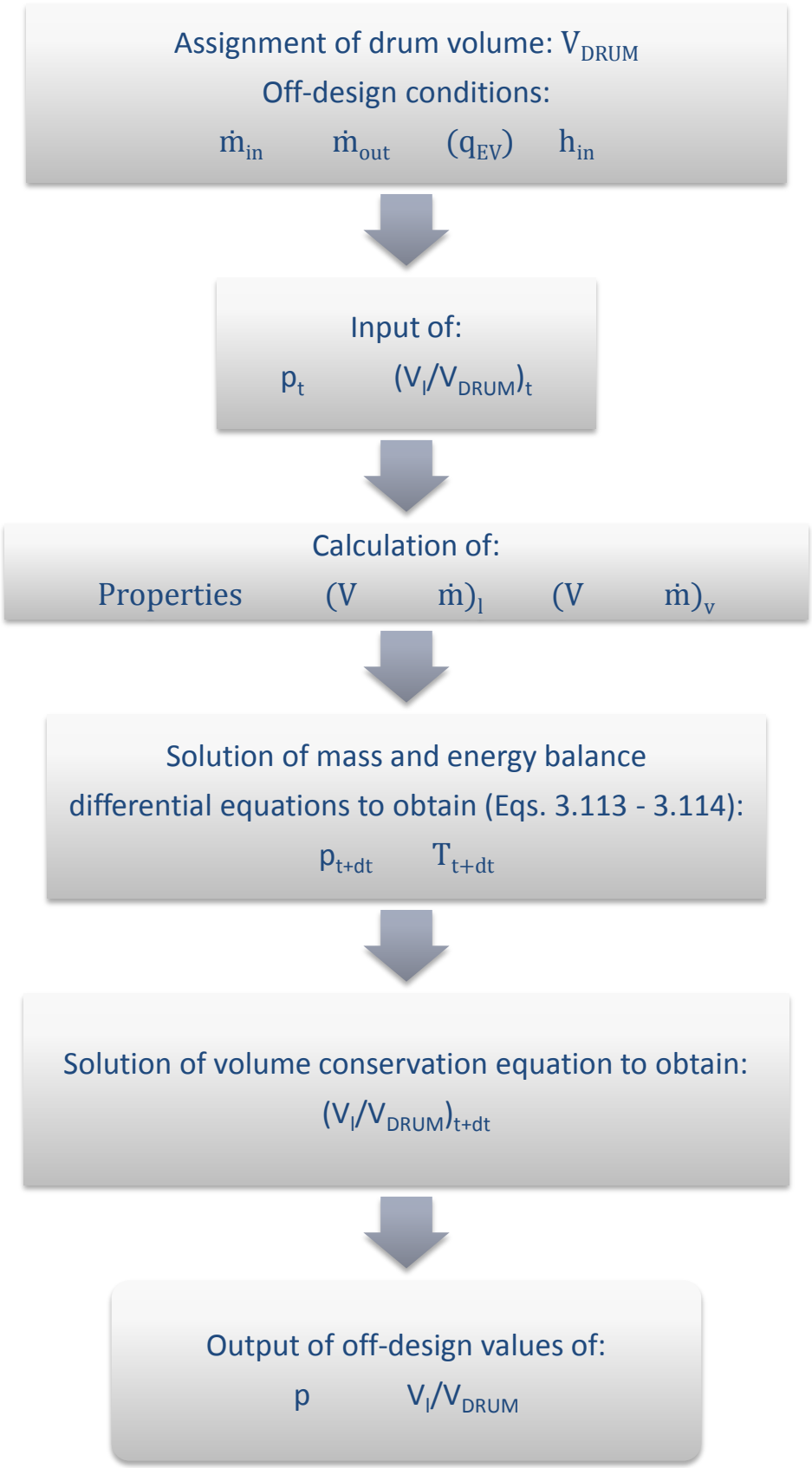

Figure 3.22 *Flowchart of the dynamic operations of hot and cold drum.*

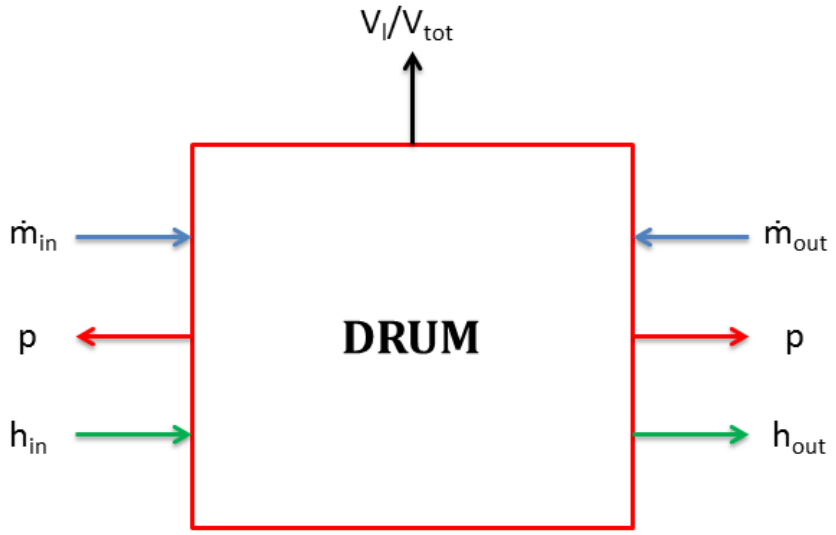

Figure 3.23 *Input output diagram of dynamic model for capacities / drums.*

3.3.4 Single stage ORC system

The dynamic model of the whole ORC system is applied to the presented LNG carrier. The result is an ICEs-ORC combined cycle, where the four internal combustion engines represent the *topping cycle*, which available waste heat is recovered by the ORC system, the *bottoming cycle*, in order to produce additional electric energy without any fuel cost. This extra energy is exploitable to integrate the ship's engines production, leading upstream to an engine fuel saving, with the relative economic advantages.

The aim of the dynamic model consists in studying various possible solutions for this application, starting from the available data about the ship's travels. By the use of this model, indeed, many different configurations for the ORC system can be set and evaluated, in order to obtain the best one, relatively to the chosen final objective. The evaluation consists in analysing two different system behaviours:

1. the plant dynamics, by the study of the transient during a changing of the ship's travel speed between predefined values;
2. the ORC electric production, related to the test reference year.

In the first case, the behaviour of all main parameters is examined by the use of a fully detailed MATLAB Simulink model, while in the second case a faster version is employed to calculate the final value of the parameters of interest, e. g. work production or efficiency, over a period of one year.

The main advantage about this model is its versatility, indeed the easiness to study a high number of different configurations, the results of which to compare each other. Given the determined operating points in chapter 2, the feasible off-design conditions for all designed ORC systems include ship velocities between 14.5 kn and 19.5 kn for laden voyage, 15.5 kn and 18.5 kn for ballast voyage. The reason of this is the too low available heat for lower speeds because of the use of only one engine type A and one type B, that do not provide enough hot fluid mass flow rate to the Rankine cycle. Substantially, the ORC system would work at a too partial load, in particular below 70% of the nominal power, inconvenient for this application. In these conditions, an equilibrium point for evaporation and condensation pressures is not reached inside the designed heat exchangers, which surfaces are hence undersized. With these selected operating points anyway the most frequent ship's velocities and the highest ones are exploited, with the utilization of the ORC system for 4381.3 hours of the total amount of 6528.1. ORC is hence supposed to work with a load factor of 67.11%, result that is considered acceptable for this kind of application.

In this paragraph, the single stage ORC layout will be presented. A summary of the built Simulink models used to pursue the mentioned objectives is presented, explaining also the main operations carried out during the simulations. Special attention will be dedicated to the adopted control systems.

3.3.4.1 Dynamic model for transient simulations

The MATLAB Simulink dynamic model mainly consists in six blocks, each one representing a real ORC component, with addition of two blocks which main purpose is to complete the dynamic operation. To be more precise, this group of Simulink blocks is composed by:

- the *pump*, a flow control device that receives level variables and gives out flow variables. The involved level variables are the operative fluid inlet pressure from the cold drum and the outlet pressure imposed by the hot drum block, the latter with addition of the pressure drops related to preheater and evaporator. The only provided flow variable is the outlet mass flow rate, that is physically sent to the preheater downstream, and only as a signal to the cold drum. This block receives also a tuning variable from the control system, rotational speed. The last treated quantity is the fluid enthalpy, which value is taken from the cold drum, recalculated according to the presented equations and sent to the preheater;
- the *preheater*, a component classified for modelling purposes only as *heat exchanger*, which receives inlet values of mass flow rate, pressure and temperature related to the hot and cold fluid, to provide to the next component, the evaporator, outlet values about the same quantities of the working fluid;
- the *subcritical evaporator*, that belongs to the category *heat exchanger*, with the same modelling function of the preheater. The main difference with the previous component is that here different equations are adopted, in particular because the model of this component is split into two, the first one adopting preheating correlations, the second one evaporation correlations. From this block, mass flow rate and enthalpy of the working fluid are provided to the hot drum model, together with the evaporator volume and the evaporative heat flux;
- the *hot drum*, that is a capacity block. It is reminded that it is not a real component in the ORC system, but it represents again the subcritical evaporator to which it refers in order to apply its mass and energy balances and the volume conservation, by application of Eqs. (3.113), (3.114) and (3.125). The hot drum volume is so fixed at the value of the evaporator's one, and also the evaporative heat flux is taken to count in the energy balance, given that phase change happens inside this component. The Simulink block receives also the enthalpy referred to the liquid phase, to give out the one referred to the vapour phase, eventually with a little superheating. The hot drum, as capacity, receives flow variables as inlet working fluid mass flow rate from the subcritical evaporator block and outlet mass flow rate that is imposed by the vapour turbine downstream. This block provides to the same turbine the operative fluid pressure and enthalpy. The pressure signal is also sent to the pump and to the preheater models, with addition of pressure drops of the two "hot exchangers";

- the *vapour turbine*, the other flow control device. It operates in the whole model similarly to the pump block, with as main difference the absence of a tuning variable as rotational speed, because it is assumed fixed for this component. The turbine block receives enthalpy from the hot drum and provides the new enthalpy after expansion to the condenser. The incoming level variables are inlet pressure from hot drum and outlet pressure from cold drum, the last one with addition of pressure drops of the condenser, while the provided flow variable is the outlet mass flow rate, physically sent to the condenser and as signal to the hot drum block;
- the *condenser*, another model classified as *heat exchanger*, that receives inlet mass flow rate, temperature and pressure of the hot and cold fluids and gives out the same outlet quantities of the working fluid, to send to the cold drum;
- the *cold drum*, the second and last capacity block of this single stage ORC model. It works as the hot drum model, but in this case it represents a physical component, an accumulator that receives the liquid phase exiting from the condenser. Inside drum there is not heat exchange, therefore the condensation heat flux is not necessary to solve the energy balance equation. The volume is fixed by design to 2.5 m^2, a little higher than the condenser's volume. The cold drum block receives enthalpy referred to the liquid phase from condenser, enthalpy that is recalculated and sent to the pump. The incoming flow variables are inlet mass flow rate from the condenser and outlet flow rate from the pump. The provided level variables are pressure to the pump's model and the liquid level inside the drum that is sent to the control system, which elaborates it to define the pump's rotational speed;
- The *control system*, a PID controller block that receives the value of the liquid level from the cold drum and determines the pump's rotational speed by application of a differential equation that presents one proportional term, one integrative term and one derivative term. The elaborated variable is the difference between a predefined liquid level value, set at $\frac{V_l}{V_{CD}} = 0.5$ as goal, and the real calculated liquid level coming from the condenser block. When the two values are equal, the provided rotational speed corresponds to the predefined one, that is for example the design velocity at design conditions of the ORC system.

An additional block, necessary to calculate input values for the Simulink dynamic model, must be defined. This model block is built in order to provide data about the hot sources depending on the number of working Diesel engines and their current load. As stated in chapter 2, the assumption of equal load for the active engines is made. There are two parameters that determine the operating conditions of the energy system: the voyage mode, laden or ballast, and the current velocity of the vessel. The aim of the data block is to elaborate these two incoming parameters in order to calculate, by evaluation of the

corresponding number and load of working engines, mass flow rate, pressure and temperature of all inlet hot fluids into the ORC's heat exchangers. In case of single ORC system, the provided data are related to the hot water of LT and HT cooling system respectively entering into the ORC preheater and evaporator.

The available statistical data of loads and number of operative engines are only referred to the mean vessel velocity in a range of 1 kn, as shown in Tables 2.3 and 2.4. Furthermore, once the information is known, to obtain the relative values of mass flow rates, pressures and temperatures of the hot fluids Table 2.2 has been used to define interpolating equations among the desired values. At this point, by making use of the determined relations, it is possible to calculate all needed data referred to the particular number of working Diesel engines and their load. These equations are gathered in a MATLAB script, each of them related to the own vessel velocity range and the conditions of the voyage. Summarizing, the data block receives as input the voyage mode and the ship velocity, finds the corresponding number and load of the working engines and makes use of predefined interpolating equations to give out mass flow rate, pressure and inlet temperature of all hot fluids that are involved in heat exchange with the ORC's operative fluid. Next figure shows how this data block is modelled, in particular about the second Simulink hierarchical level.

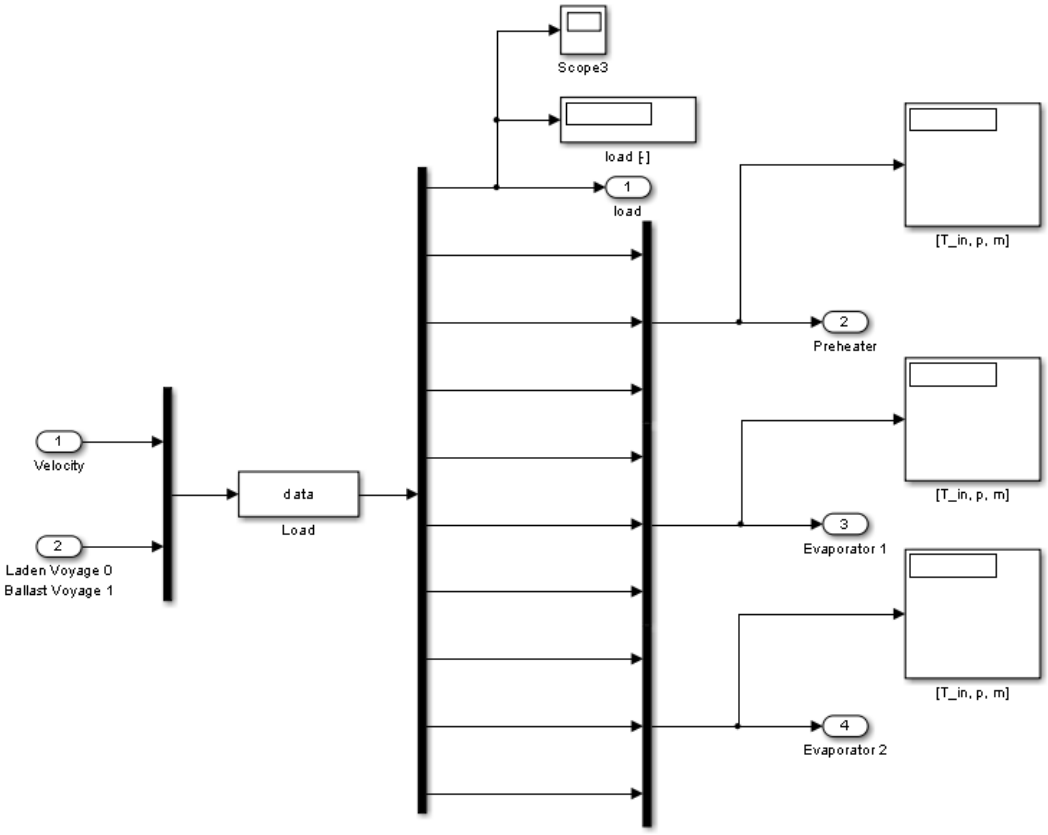

Figure 3.24 *Simulink model that provides data to the main ORC model, hierarchical level 2.*

In the following figure, the whole single stage ORC model is presented. It represents the first hierarchical level of the Simulink model.

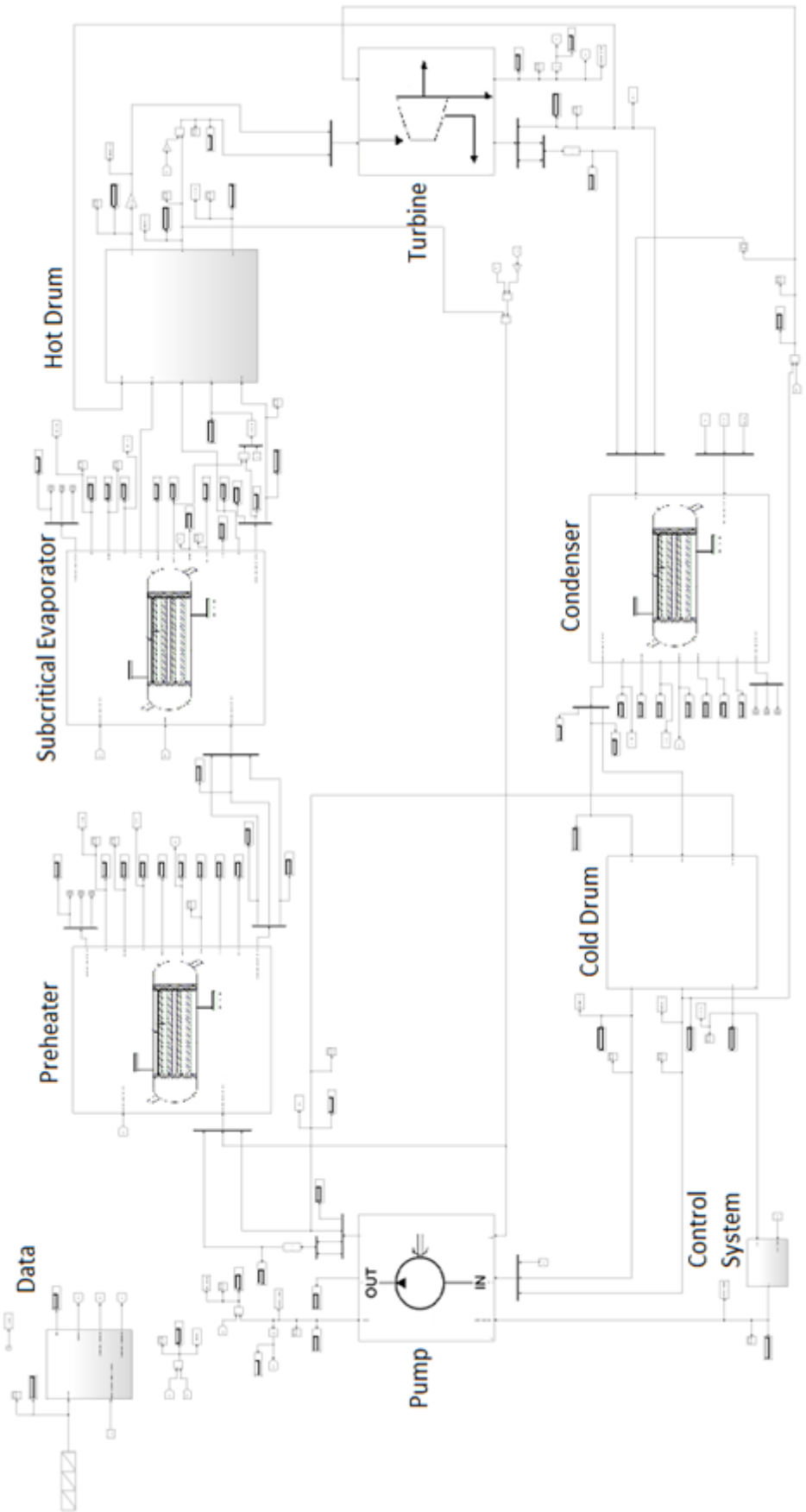

Figure 3.25 *Simulink model of the single stage ORC system, hierarchical level 1.*

To examine now the second Simulink hierarchical level, dynamic model of pump is here reported. At first, all needed values of design parameters must be set by the user, as it is shown in Figure 3.27 reporting an example of *Parameter Dialog Box*. For this component there is no need of defining the geometry for modelling purposes. The pump model is composed by five blocks, each one containing the third hierarchical level, characterised by the following functions:

I. in the first block, the correlation given by Eq. (3.86) is applied in order to obtain the volumetric flow rate and the mass flow rate of the working fluid;
II. in the second block, the correlation corresponding to Eq. (3.87) is used to calculate the isentropic efficiency;
III. in the third block, the outlet enthalpy is determined starting from inlet enthalpy, that is obtained by making use of state equations;
IV. in the fourth and last block, the pump power is obtained by utilizing the previously calculated mass flow rate and enthalpy.

An auxiliary block is also built to convert the pump's rotational speed from radians per second to rounds per minute. One figure representing the Simulink model of the pump is reported below, with marked blocks with roman numeral that refers to the four presented steps.

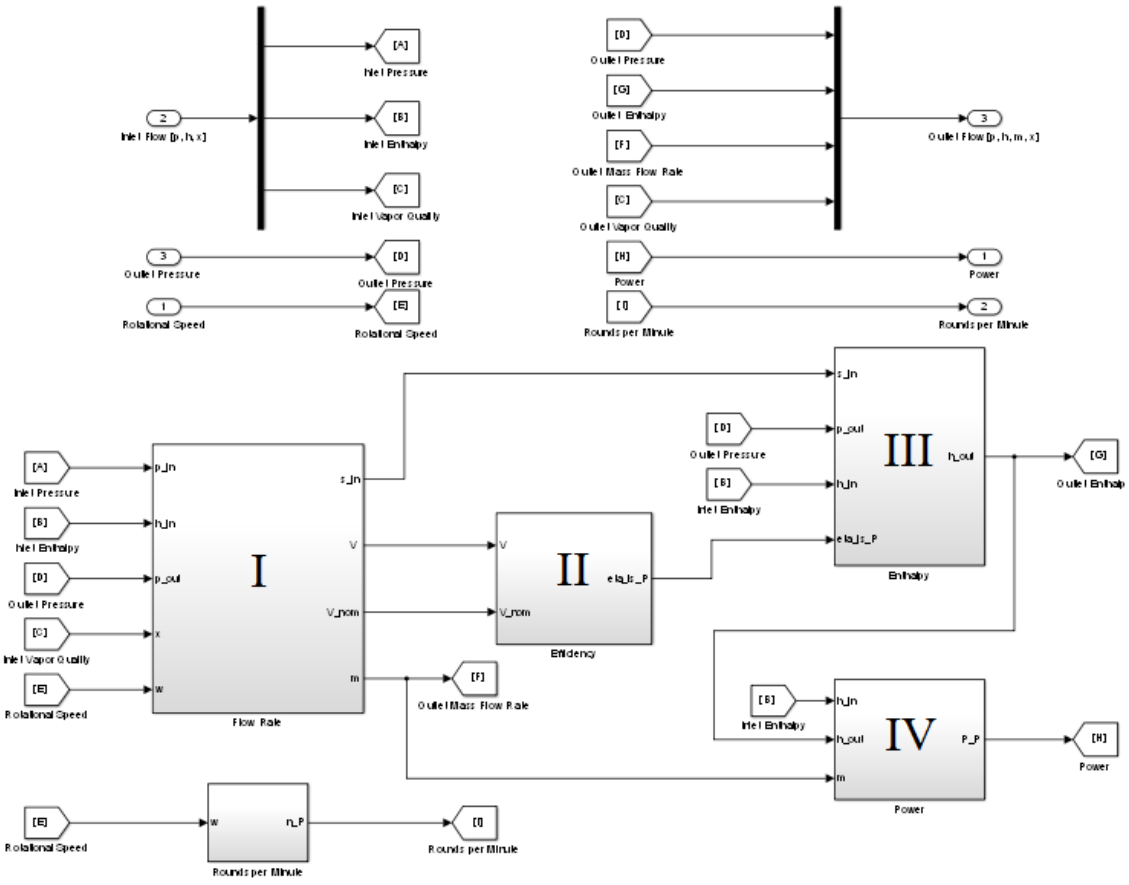

Figure 3.26 *Simulink block of the pump, hierarchical level 2.*

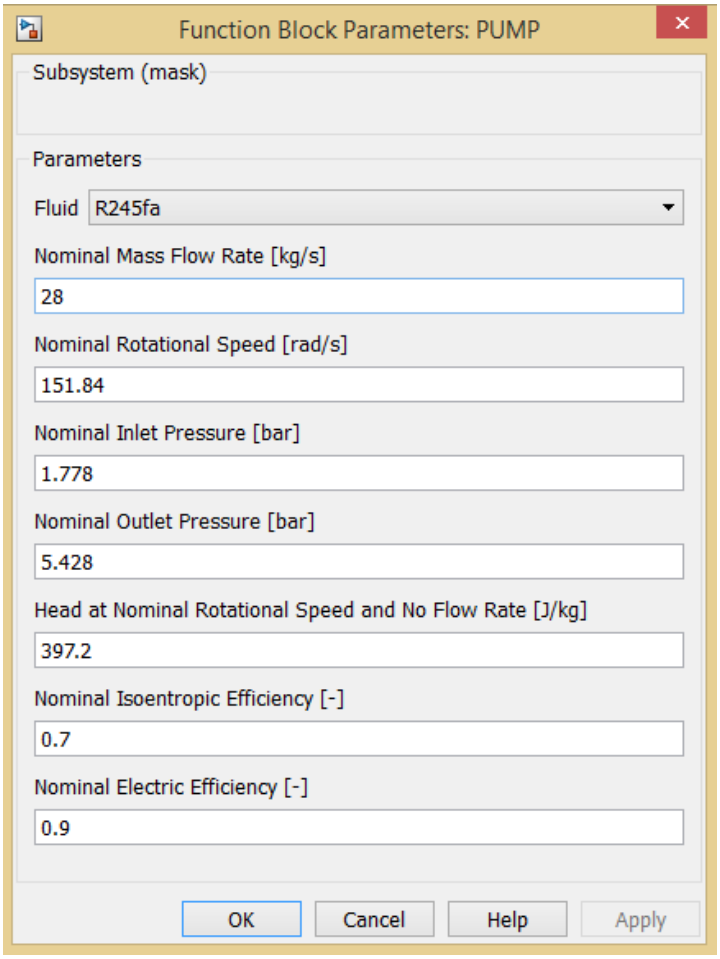

Figure 3.27 *Parameter Dialog Box for the model of the pump.*

The dynamic model of vapour turbine is similar to the pump's one, because both of them are flow control devices with similar modelling purposes. Design values, not related to geometry, must be fixed by the user as well. The turbine model consists in four blocks:

I. in the first block, Stodola equation is applied to define the working fluid outlet mass flow rate;
II. in the second block, the correlation given by Eq. (3.99) is adopted to calculate the isentropic efficiency;
III. in the third block, outlet enthalpy is determined by knowing the inlet enthalpy and the previously defined isentropic efficiency;
IV. in the fourth and last block, the turbine power is obtained by making use of the calculated mass flow rate and enthalpy.

As for the pump, in the following one figure reporting the *Parameter Dialog Box* and the turbine model are presented.

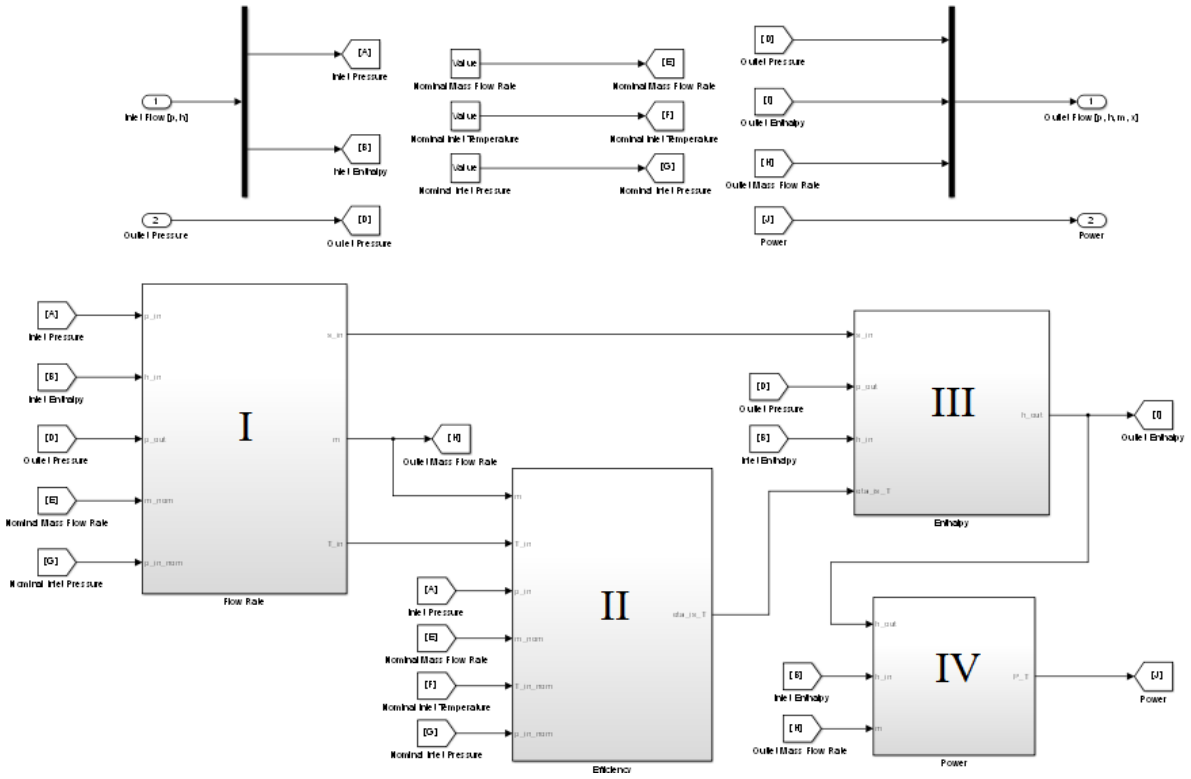

Figure 3.28 *Simulink block of the turbine, hierarchical level 2.*

The dynamic model of the heat exchangers is simple, because of the chosen simplified off-design law, given by Eq. (3.1). In the Simulink blocks of every heat exchanger, nominal values calculated by the design model, that has been presented in paragraph 3.3.4, are called from the workspace. The off-design values of mass flow rate, pressure and temperature of the working fluid come from the previous model block, while the values of the same parameters of the hot fluid are provided by the data block. In case of condenser, the cooling fluid parameters are constant for every off-design condition of the ship, hence their values are provided by simple constant blocks. Inside every heat exchanger block there is the calculation in off-design conditions of the global heat transfer coefficient U_e, the heat flux q and the outlet temperatures of the exchanging fluids.

The hot drum and cold drum Simulink models are fundamental to manage the dynamics of the whole ORC model, as mentioned above. In these blocks, differential equations are included in order to perform mass and energy balances and volume conservation. The two blocks are analogous, their operations are collected in the next four steps, corresponding to four blocks of the second Simulink hierarchical level:

I. in the first block, the cold drum pressure and the vapour quality are used to determine the working fluid's properties;

II. in the second block, the ratio $\frac{V_l}{V_{tot}}$ is used together with the previously defined total volume and fluid densities to obtain volume and mass of liquid and vapour phases;

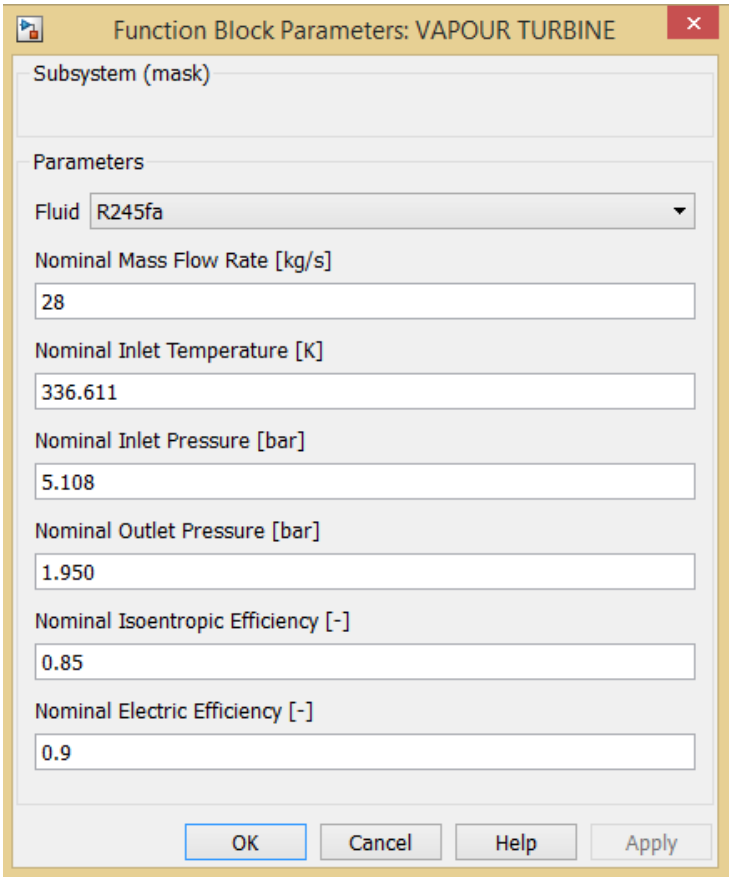

Figure 3.29 *Parameter Dialog Box for the model of the turbine.*

III. in the third block, energy balance is performed by use of Eqs. (3.113) and (3.114) to determine $\frac{dp}{dt}$ and $\frac{dT}{dt}$, to integrate then to obtain pressure and temperature of the working fluid inside the cold drum at the successive time interval, p_{t+dt} and T_{t+dt}. In particular, the new value of pressure is used to define the new densities and it is sent back to the first block, to calculate all new needed properties;

IV. in the fourth and last block, volume conservation is performed by use of Eq. (3.125), giving out the volume ratio at the next time interval, $\left(\frac{V_l}{V_{tot}}\right)_{t+dt}$ that is successively sent to *block II*.

In the following, hot drum Simulink model is reported. The cold drum model is analogous.

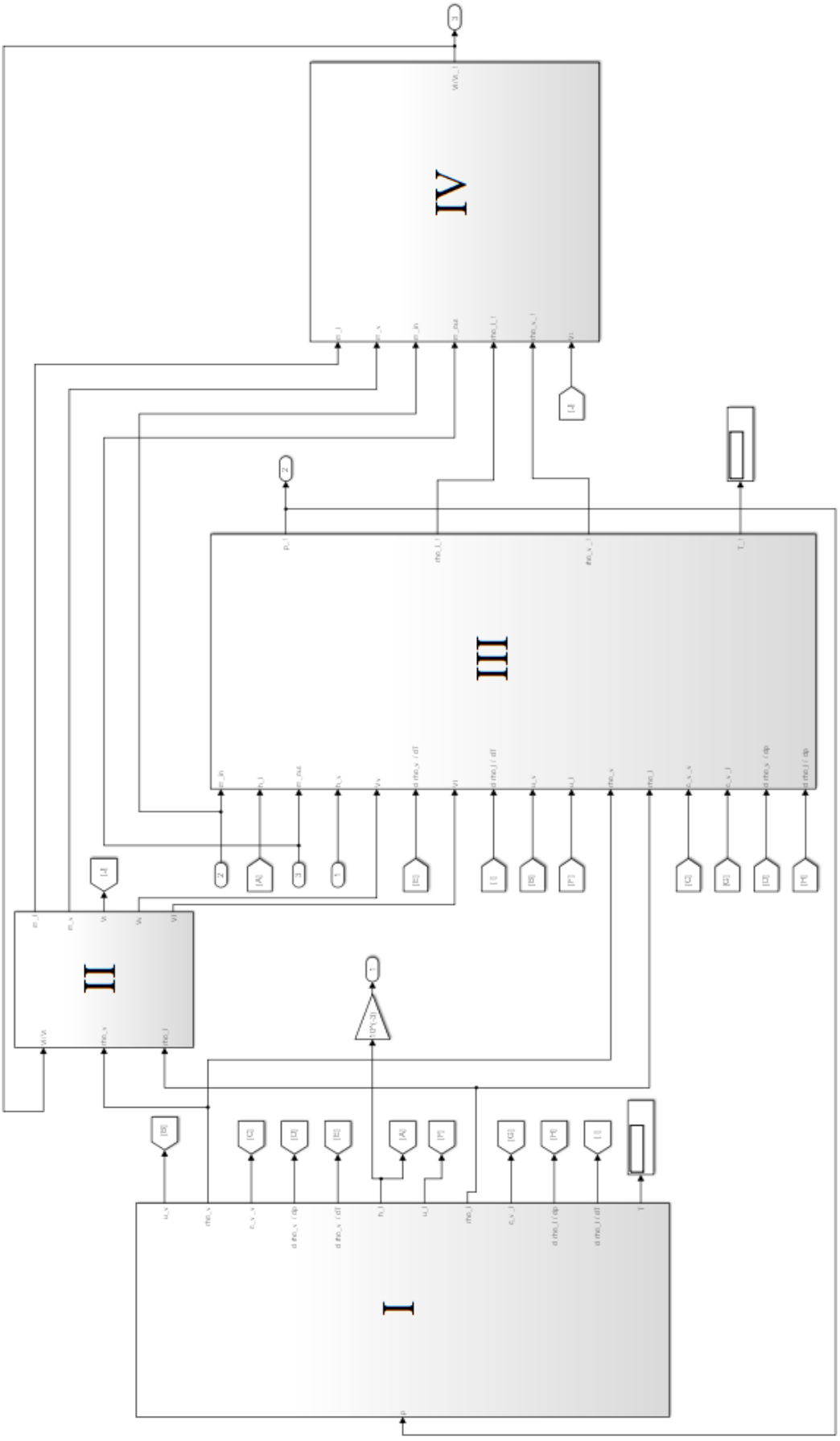

Figure 3.30 *Simulink block of the cold drum, hierarchical level 2.*

The last model to examine is the control system block. It operates as PID controller, performing an equation that appears in the following form:

$$P + I\frac{1}{s} + D\frac{N}{1+N\frac{1}{s}} \tag{3.127}$$

The presented relation is in form of Laplace transform. It presents a proportional term *P*, an integral term *I* and a derivative term *D*. *N* is a filter coefficient that in this case is imposed equal to 1. The control system receives as input the algebraic sum of the goal value of a certain quantity and its real calculated value at time *t*. Depending on the resulting value and if it is positive or negative, the PID controller provides a quantity to associate to an output that is related to the input. In case of the single stage ORC system, the control system's function consists in determining as output the pump's rotational speed by evaluating the liquid level of the working fluid inside the cold drum. The input value is hence the difference between the goal liquid level, set as $\frac{V_l}{V_{CD}} = 0.5$, that means a liquid level corresponding to half the cold drum's height, and the real value of this level in off-design conditions. The output value is the pump's rotational speed at time *t*, that is sent to the pump model. In this way, the pump regulates its velocity, and hence the mass flow rate, in order to restore the goal liquid level inside the cold drum. In the following, a figure representing the PID controller is reported.

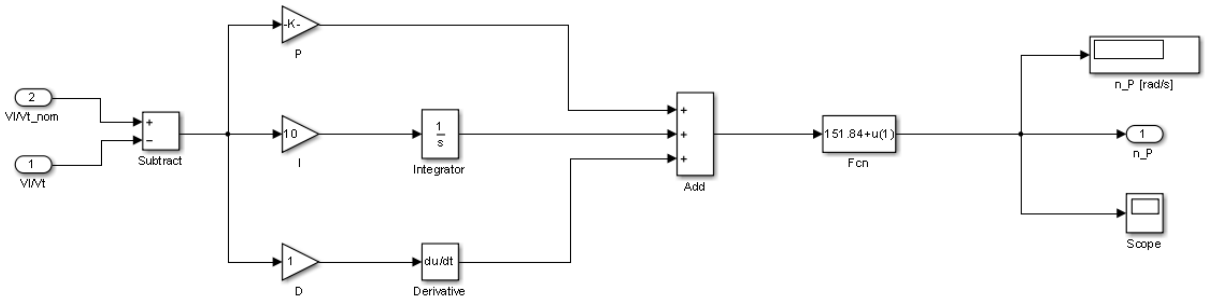

Figure 3.31 *Simulink block of the control system, hierarchical level 2.*

3.3.4.2 Steady-state model for annual production evaluation

To make long term evaluations, a simplified version of the ORC Simulink model is necessary in order to reduce simulation time. The available data about the annual vessel operation are provided by Tables 2.3 and 2.4 and refer to stationary off-design conditions, ordered from the lowest to the highest ship velocity.

The aim of the simplified model is to determine the total work production of the ORC system, by evaluations at all different stationary off-design states. The transient behaviour is not considered in this case, therefore the hot and cold drum models are not needed anymore.

The new model is hence similar to the previously presented one, with as main difference the absence of hot and cold drums and the data block. To substitute them, *Repeating Sequence* blocks are employed to set time intervals, related to all velocity ranges both for laden and ballast voyage, and the relative values of: pump's rotational speed, outlet pressure and enthalpy of the cold drum, outlet pressure and enthalpy of the hot drum. All these values have been previously obtained by carrying out simulations by making use of the already presented detailed model at the velocities and voyage modes of interest. *Integrator* blocks are also added to evaluate pump energy and turbine energy, which difference corresponds to the net energy, final aim of this simplified model. In the following, a figure reports the adopted simplified Simulink model for the single stage ORC, for annual work production evaluations.

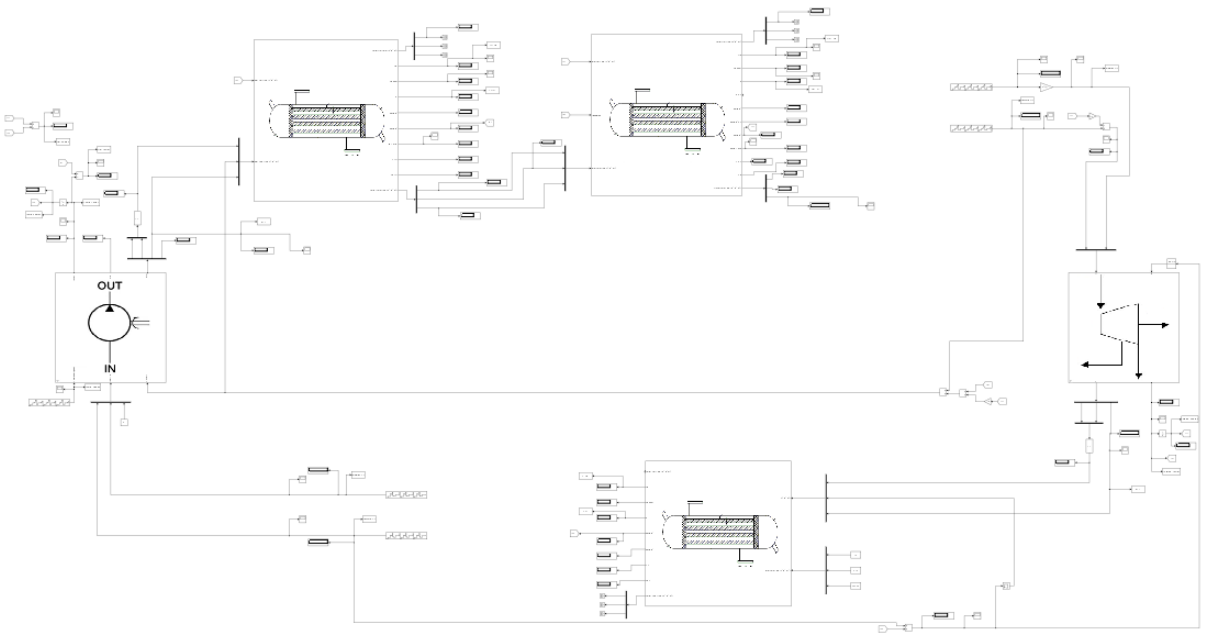

Figure 3.32 *Simulink simplified model of the single stage ORC system, hierarchical level 1.*

3.3.5 Two stage ORC system

Dynamic model of the two stage ORC system is here presented. As mentioned above, two versions have been developed for the two stage plant, one with a subcritical second pressure level and one with a supercritical second pressure level.

Also in this case, two versions of the Simulink model have been built, the first one to simulate transient behaviour, the second one to make annual work production evaluations. The design choice for both the ORC systems is the operating point corresponding to a vessel velocity of about 15.5 kn, laden voyage.

The available hot fluid for the second pressure level, charge air at point *a2* of Figure 2.18, imposes for the supercritical case the two levels to work together only for certain loads of the Diesel engines, because of the thermodynamic properties. At certain vessel velocities, indeed, the hot fluid temperature is not sufficient to lead to the evaporation: for this reason, the ORC system is set by making use of valves to work as two stage in the operative ranges in which it is possible, while in the remaining travel conditions it works as single stage, with the only first pressure level.

It is worth noting that to obtain cycle stability, namely equilibrium points at the various design and off-design stationary conditions, the ORC layout must present a real hot drum device for the first pressure level, downstream of the evaporator, and another one in case of subcritical second pressure level, again downstream of the evaporator. Without these solutions, it has been demonstrated the inability of the model to achieve thermodynamic equilibrium, with a continuous increasing or decreasing of the dynamic values of pressure and liquid volume of the drum models. To solve this problem, addition of real hot drums is necessary in order to be able to control their liquid levels by varying the two pumps' rotational speeds. In case of supercritical second stage, given that a hot drum cannot be installed due to this kind of evaporation without clear separation between phases, rotational speed of the second pump is imposed equal to the value that satisfies the following constraint

$$\dot{m}_{P,2PL} = \dot{m}_{T,2PL} \tag{3.128}$$

obtaining in this way also a good control of the liquid volume inside cold drum, by respecting all mass balances.

3.3.5.1 Dynamic model for transient simulations

The MATLAB Simulink dynamic model of the first pressure level presents the same component blocks of the single stage version. The second pressure level is implemented by addition of the models of pump and turbine, with different design assignments, and of the subcritical evaporator and hot drum, equal to the first stage ones, or of the supercritical

evaporator. Two three way valves are also added, each one represented by a single simple block:

- a *diverter valve*, downstream of the cold drum, which function is to provide to both the pumps the same pressure and enthalpy of the working fluid that enters into the valve;
- a *mixer valve*, downstream of the first pressure level hot drum and the second pressure level vapour turbine, where the two mass flow rates of the operative fluids are summed and the energy balance provides the outlet enthalpy as follows.

$$h_{out} = \frac{\dot{m}_{1PL} h_{1PL} + \dot{m}_{2PL} h_{2PL}}{\dot{m}_{1PL} + \dot{m}_{2PL}} \tag{3.129}$$

The model of the supercritical evaporator is structured in the same way of the previously presented heat exchangers. In this versions of the ORC model, data block must also provide mass flow rate, pressure and temperature of the hot charge air incoming into the evaporator of the second stage.

For the second stage of the ORC model, another control system is implemented in order to define the second pump's rotational speed. The PID controllers elaborate the following inputs:

- in the subcritical second pressure level of the ORC system, the evaluated incoming variable is the liquid level of the second hot drum, to keep the related ratio V_l/V_{tot} to the design value of 0.5;
- in the supercritical second pressure level, the rotational speed of the pump is set in order to cancel the difference between the mass flow rates given out by pump and turbine. In supercritical evaporation, indeed, there is not phase separation, therefore the outlet vapour mass flow rate must be equal to the inlet liquid mass flow rate. The control system is here simply defined by a constant block, with the predetermined correct rotational speed as assigned value;
- for both versions of the ORC system, in the first pressure level the control system operates with the liquid level of the first hot drum, to maintain its V_l/V_{tot} to the design value of 0.5.

In this way the cold drum is never controlled, but its thermodynamic parameters and volume ratio always remain in the right ranges, thanks to operations on the other drums.

In the following, two figures representing the two developed models are shown.

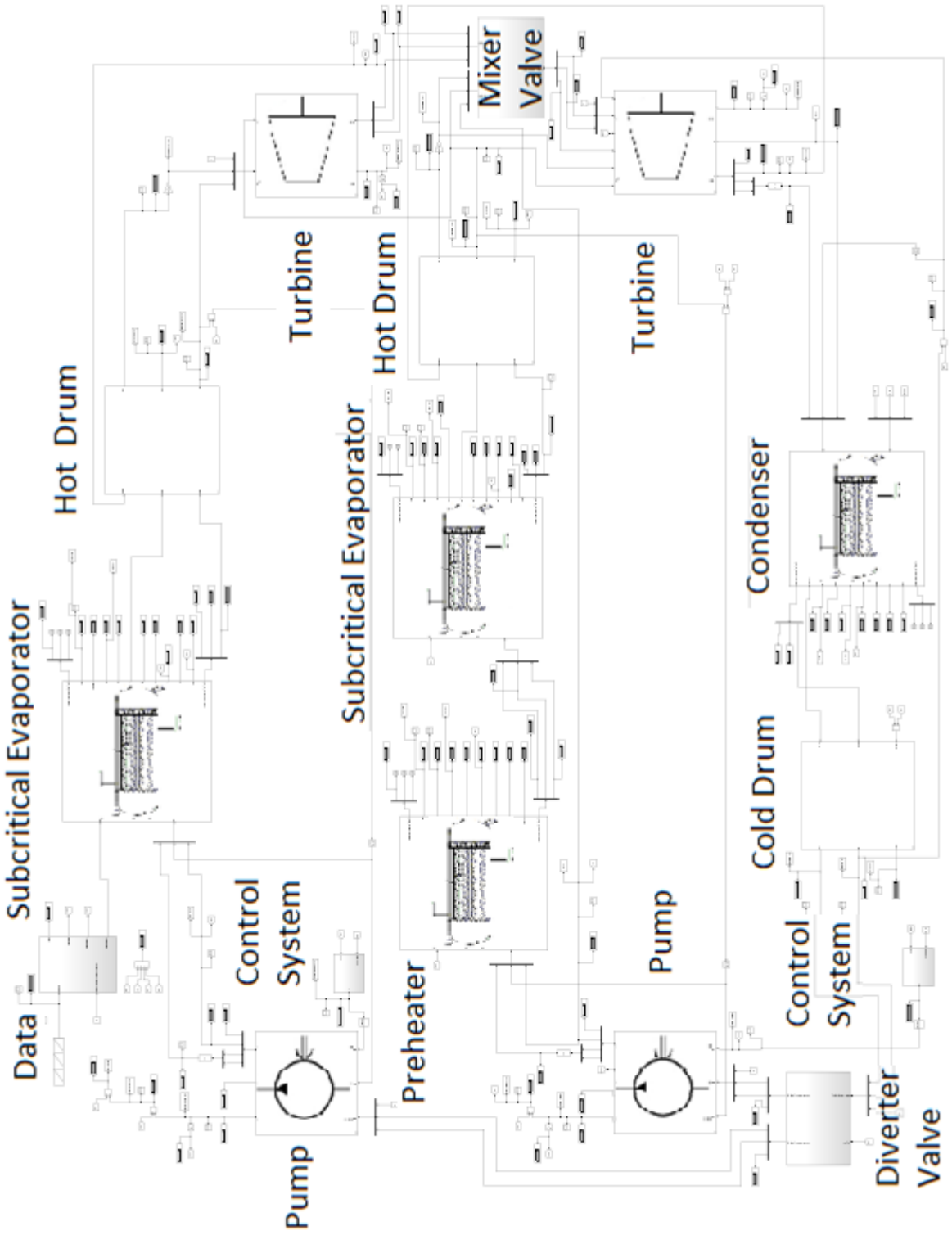

Figure 3.33 *Simulink model of the two stage ORC system, subcritical second pressure level, hierarchical level 1.*

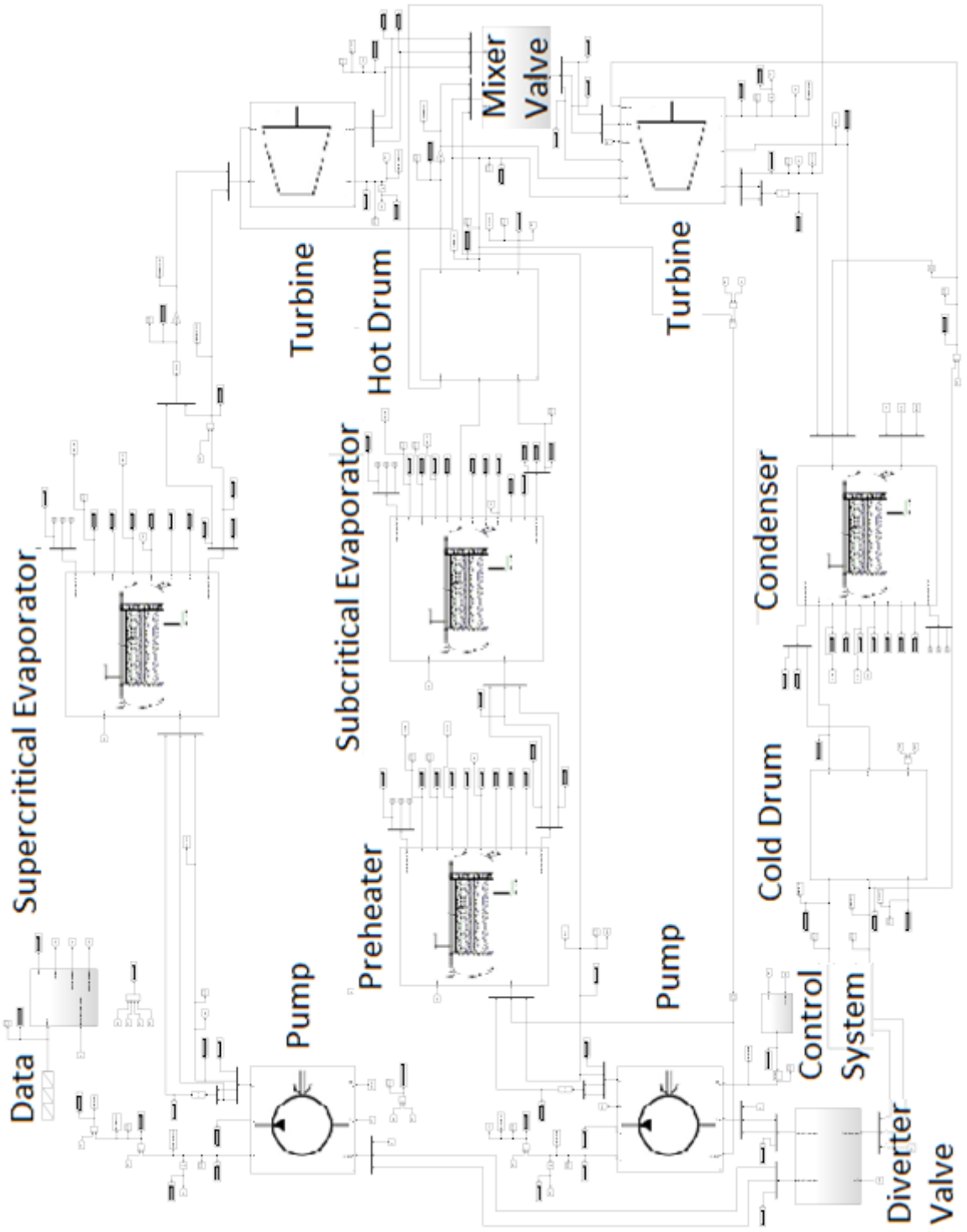

Figure 3.34 *Simulink model of the two stage ORC system, supercritical second pressure level, hierarchical level 1.*

3.3.5.2 Steady-state model for annual production evaluation

The steady-state two stage ORC model is developed in the same way of the single stage one, hence by substituting the drum models and setting all needed values at stationary off-design conditions and the corresponding time intervals. A figure is reported below to show how the simplified model appears.

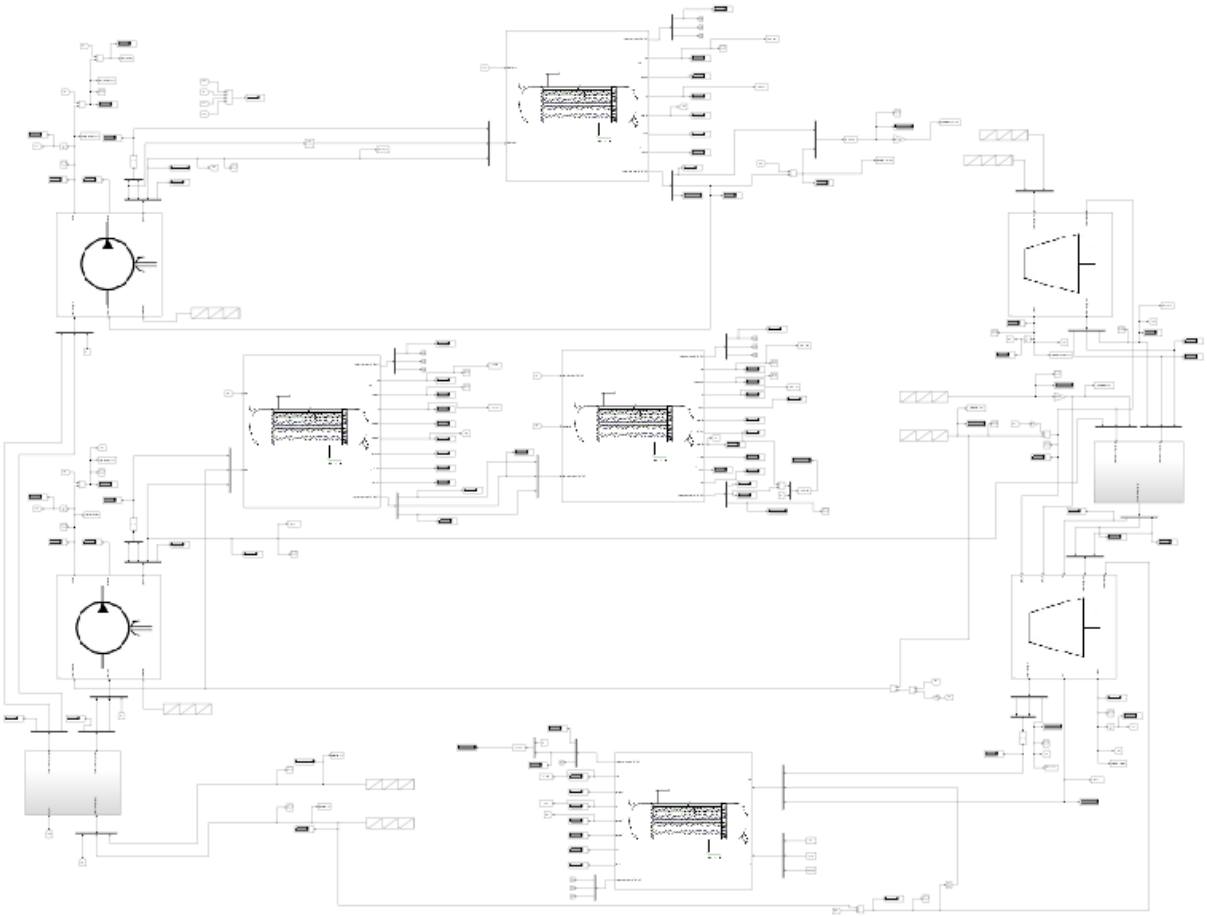

Figure 3.35 *Simulink simplified model of the two stage ORC system, hierarchical level 1.*

3.4 CONCLUSIONS

In this chapter dynamic modelling approach for the ORC system of this study is presented. At first, generalities about modelling are introduced, by listing types of approach and main available classifications, together with software suitable for the purpose. The choice made about modelling strategy is briefly presented, by defining peculiarities and main concepts. MATLAB Simulink is the chosen software for this work, with the support in design and off-design procedures of EES and Aspen Exchanger Design And Rating.

Selected modelling approach is then applied to this case study, with classification of components and variables, and arrangement of the connections within the plant model by the use of signals and physical fluxes. At first, adopted strategy about design and off-design modelling of components and ORC plant is introduced, after that proceeding with a deeper analysis of both.

Design models of the various components are discussed, by reporting useful equations, a list of involved variables and parameters, and flowcharts. Datasheets, collecting all design choices, are proposed after presentation of the components. Off-design models are then presented, again by reporting equations, variables, flowcharts and input output diagrams, with a deep analysis of the capacities, involved in the dynamic of the whole ORC model.

Simulink models of the three selected layouts for the ORC system are introduced, both for design and off-design simulations. Main features are described, in order to explain the operation of the models, especially with the introduction of control systems useful for searching of equilibrium points for the thermodynamic cycle. Comprehension of the models is important to deeply understand the results of simulations, which will be exposed in the next chapter.

4 SIMULATIONS AND RESULTS

In this chapter, simulations of the ORC dynamic and steady-state models, introduced in chapter 3, are presented. At first, stationary off-design simulations are reported to verify the annual work production. In case of single stage ORC system, the relative best design model is selected to implement the related nominal values into the dynamic model, to simulate the transient behaviour of the power plant. Several simulation results are presented, in order to show the dynamic operation of the ORC system in significant ranges of velocities, comparing also the different behaviour in laden and ballast voyage. In case of two stage ORC system, steady-state and dynamic simulation results are introduced to compare the transient behaviour of the two stage ORC systems and the single stage.

4.1 SINGLE STAGE ORC SYSTEM

Four different operating points are considered for the work production, in order to compare the possible energy savings for the Diesel engines of the ship. Four tables describing the relative design conditions are shown. For each of them the annual work production has been performed, to select the most convenient one in terms of energy saving for the LNG carrier of study.

Table 4.1 *Operating point for the engines in design conditions (case 1, 15.5 kn laden voyage).*

$\dot{W}_e$	12V50DF No.1	6L50DF No.2	GL50DF No.3	12V50DF No.4	Load
kW	kW	kW	kW	kW	%
14741	0	0	4914	9827	89

Table 4.2 *Operating point for the engines in design conditions (case 2, 16.5 kn laden voyage).*

$\dot{W}_e$	12V50DF No.1	6L50DF No.2	GL50DF No.3	12V50DF No.4	Load
kW	kW	kW	kW	kW	%
17514	0	4378	4378	8757	80

Table 4.3 *Operating point for the engines in design conditions (case 3, 16.5 kn ballast voyage).*

$\dot{W}_e$	12V50DF No.1	6L50DF No.2	GL50DF No.3	12V50DF No.4	Load
kW	kW	kW	kW	kW	%
16573	8287	0	0	8287	75

Table 4.4 *Operating point for the engines in design conditions (case 4, 17.5 kn laden voyage).*

$\dot{W}_e$	12V50DF No.1	6L50DF No.2	GL50DF No.3	12V50DF No.4	Load
kW	kW	kW	kW	kW	%
20711	0	5178	5178	10355	94

4.1.1 Work production

The simplified single stage ORC model has been used to carry out simulations referred to the annual ship operation for the four presented operating points. The available statistical data have been set as input into the model as discussed in chapter 3. Here, the simulations results are shown for the four cases, reporting energy saving E_{saved}, the mean net power $\dot{W}_{m,net}$, the load factor f_{load} and the percent of the energy coverable by the ORC system with respect to the total annual energy demand of the ship, E. The mean net power is defined as ratio between saved energy E_{saved} and the total ORC operation time, while the load factor f_{load} is the percentage of the time during a year in which the ORC system is working during the vessel operation.

Table 4.5 *Work production and energy saving at the four presented operating points.*

Parameter	Unit	Operating point 1	Operating point 2	Operating point 3	Operating point 4
E_{saved}	MWh	1546.9	1665.8	1582.5	1578.9
$\dot{W}_{m,net}$	kW	353.1	380.2	361.2	360.4
f_{load}	%	67.1	67.1	67.1	67.1
E	%	1.657	1.785	1.696	1.692

It can be noticed that the highest work production is performed by the second presented operating point, referred to a design vessel velocity of 16.5 kn, even if the load factor is smaller than two other cases. This phenomenon can be explained by the annual speed distribution of the studied LNG carrier: most of the time the ship travels between 15 and 17 kn, as Figure 2.17 shows. Hence, given that the choice of this design point provides higher net power in that range, the production increases respect to the other three performed configurations. This result proves that an off-design model can be very useful also in finding the adequate design point for an energy system.

About the load factor, for all cases the exploited ranges of velocities are between 14 and 20 kn in laden voyage, 15 and 19 kn in ballast voyage, for an amount of 4381.3 hours in which ORC is working, of the total 6528.1 hours of ship operation. Under these ranges, as previously explained, the available waste heat provided by the LNG carrier is too little for a good ORC operation, mainly because of the reduction of hot mass flow rates. Below 14 kn, indeed, only one Diesel engine operates, consequently with an insufficient heat grade provided to preheater and evaporator of the ORC system, which tries to find a thermodynamic equilibrium for a too low evaporating pressure, impeding the cycle to work. The alternative would be to select a design operating point for lower velocities, but in this case the major potential relative the most performed speeds of the ship would not be completely exploited. For these reasons, in this work it has been chosen to design the ORC system on the most frequent operating conditions of the LNG carrier.

The mean net power and the percentage of saved energy confirm the convenience of the adoption of the design point relative to case 2. This operating point is hence chosen to

perform the dynamic simulation, to study the off-design behaviour of the ORC system set with this configuration. In the following, the results obtained by Soffiato [18] about the annual energy saving, related to the operating point described by Table 2.5 and six different working fluids, are reported.

Table 4.6 *Work production and energy saving at the operating point defined by Soffiato [18].*

Par.	Unit	R-134a	R-125	R-236fa	R-245ca	R-245fa	R-227ea
E_{saved}	MWh	1387	1110	1418	1464	1456	1361
$\bar{\dot{W}}_{net}$	kW	219	175	224	231	229	214
f_{load}	%	54	54	54	54	54	54
E	%	1.49	1.19	1.52	1.57	1.56	1.46

4.1.2 Transient simulations

The operating point that provides the highest annual work production, among the studied ones, according to the available statistical data on the vessel speed distribution and the relative engines' loads, has been determined and presented in the previous paragraph. This design has been then selected for the single stage ORC system to perform its transient behaviour during velocity changes of the ship, with the consequent modification in the working conditions of the Diesel engines energy system. The simulations have the purpose of determining the behaviour of the ORC system during transitions from a stationary off-design condition of the topping cycle, the engines energy system of the ship, to another. The adopted Simulink model is the fully detailed version of the single stage ORC system, that has been presented in paragraph 3.4.4.1.

The assumption of 10 minutes required by the LNG carrier to change its velocity of 1 kn has been made, and a simulation time step of 0.1 seconds has been fixed.

In this paragraph, executed simulations and relative results are discussed, presenting also several diagrams showing the interesting outcomes and the behaviour of the most significant parameters during the simulation time.

At first, evolution in time of main characteristics of the external sources, precisely exchanged heat fluxes, temperatures and mass flow rates, are presented. They are followed by diagrams reporting the behaviour of main ORC parameters during simulation, in particular evaporation and condensation pressures and liquid volume ratios V_l/V_{tot} for the capacities. At last, evolution in time of working fluid's mass flow rate, enthalpy at the inlet of the turbine, pump's rotational speed, produced and absorbed electric power is presented. An increase of speed for the vessel of 1 kn has been performed.

- **CASE A:** operating point 2, transition of ship velocity from 16.5 kn to 17.5 kn, laden voyage.

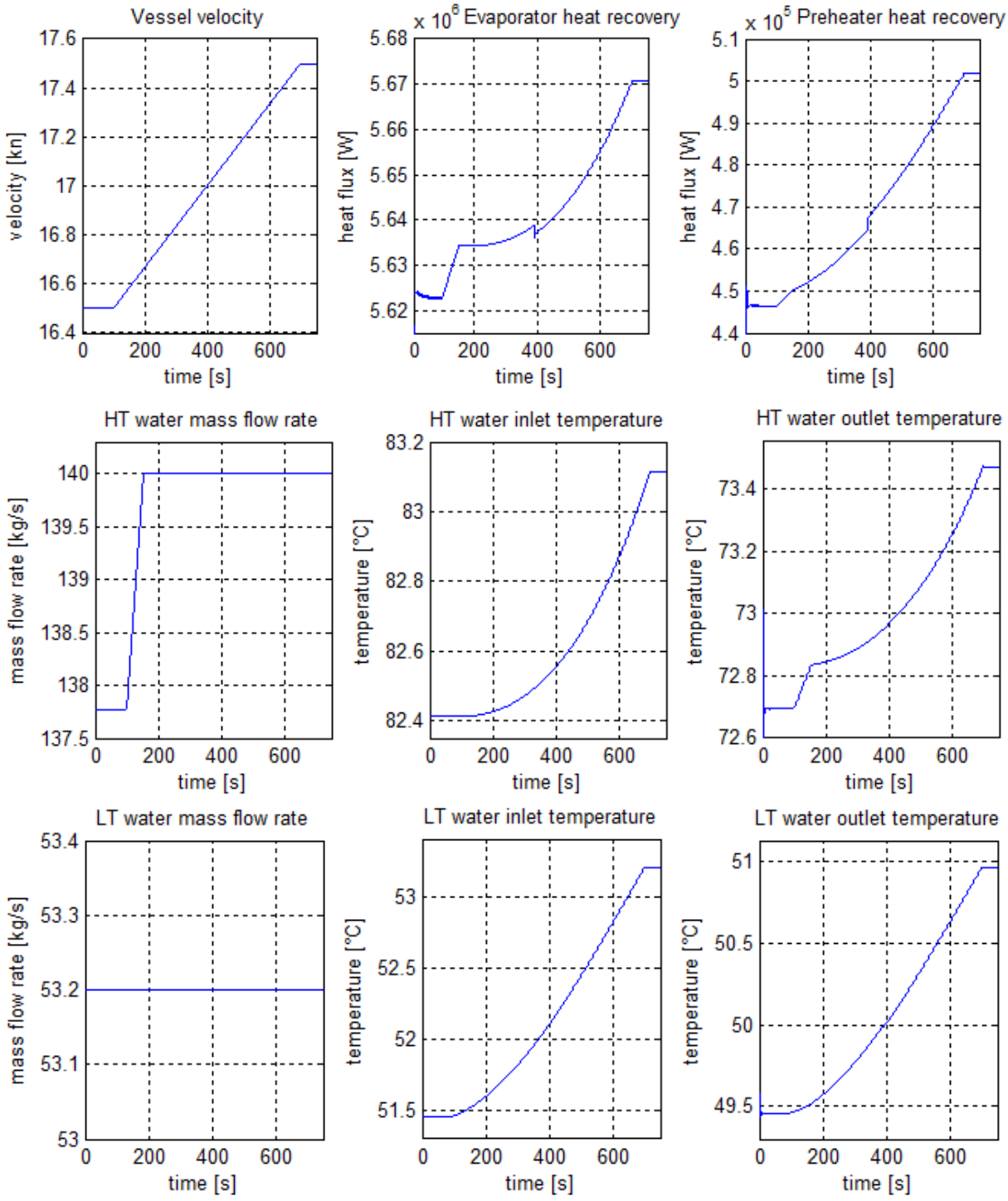

Figure 4.1(a) *Hot sources heat exchanged, mass flow rates, inlet and outlet temperatures.*

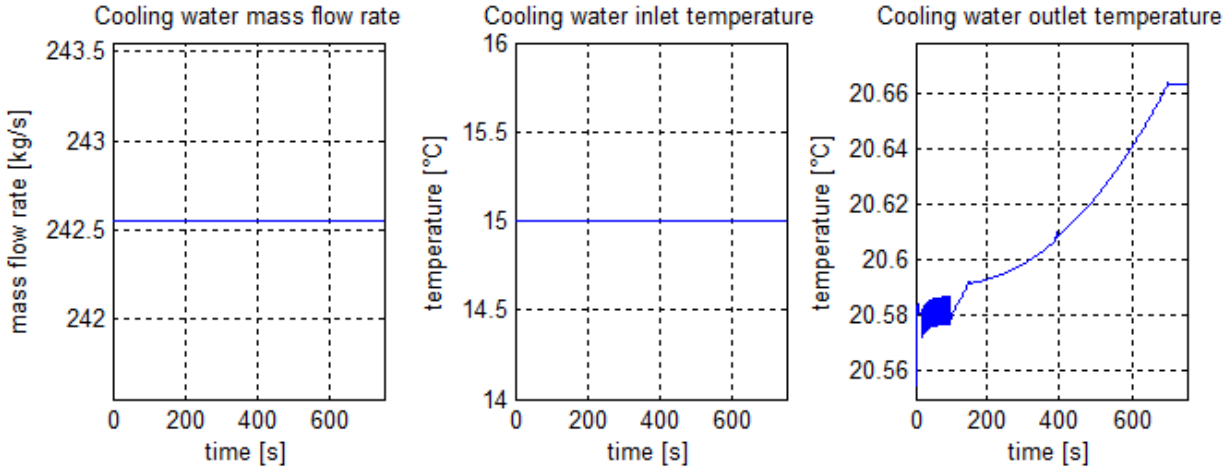

Figure 4.1(b) *Cold source mass flow rate, inlet and outlet temperatures.*

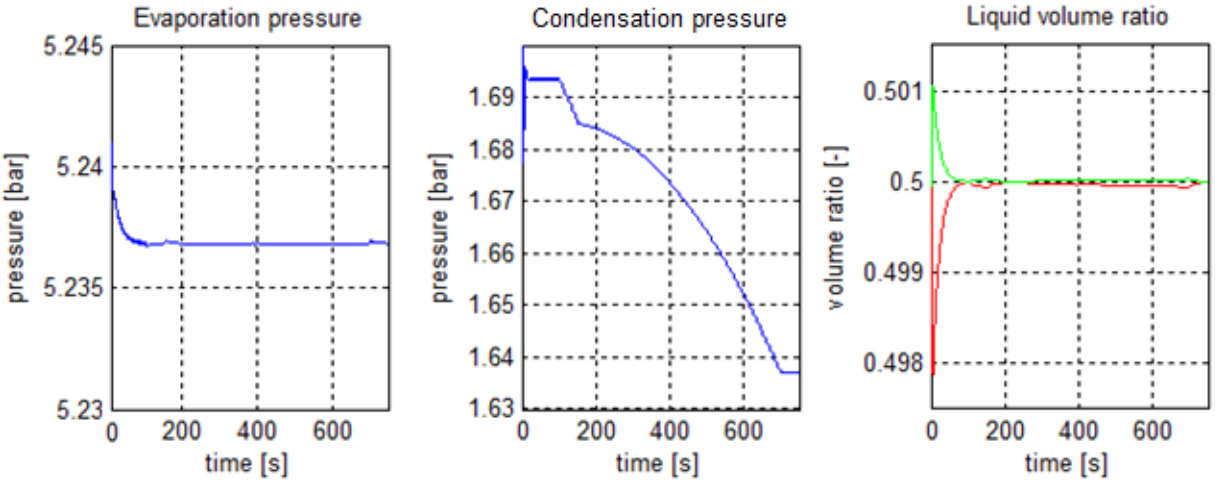

Figure 4.1(c) *Evaporation and condensation pressures, liquid volume ratios (red: hot drum, green: cold drum).*

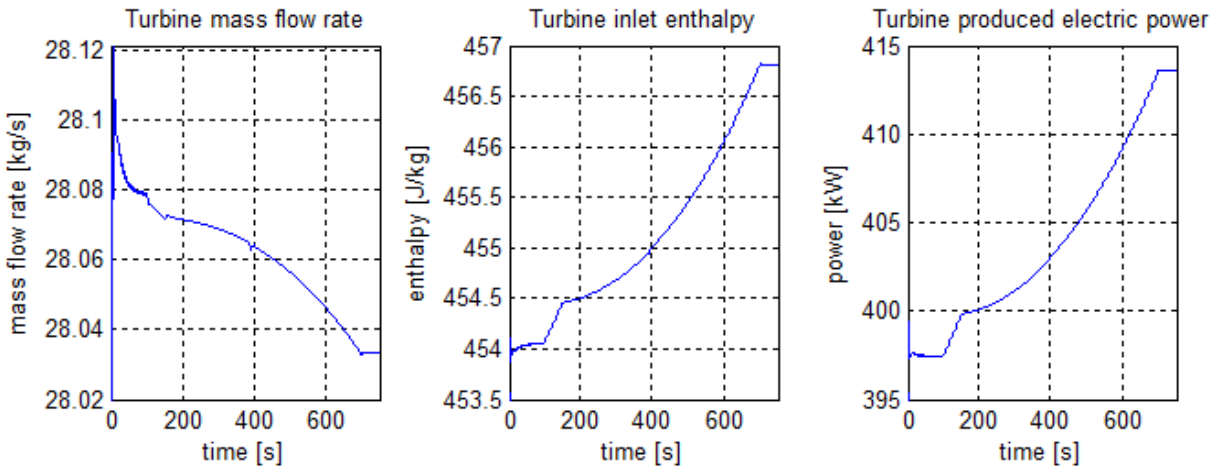

Figure 4.1(d) *Turbine mass flow rate, inlet enthalpy and produced electric power.*

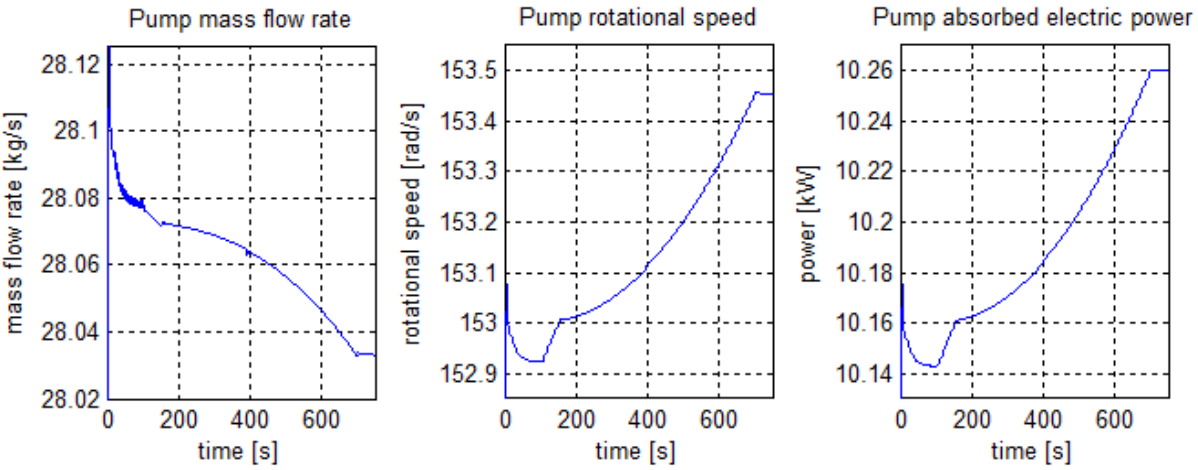

Figure 4.1(e) *Pump mass flow rate, rotational speed and absorbed electric power.*

It is worth noting that a limit of 140 kg/s has been imposed for the HT water mass flow rate to keep the received heat flux at the evaporator within an acceptable range, in order to avoid a too high superheating that would lead to an unsustainable increase of the vapour temperature inside the component. Heat exchange and outlet temperature relative to the evaporator are hence influenced by this operative choice, with a variation in the curve slope during the simulation.

Another interesting aspect is the variation of the condensation pressure during transient between the first equilibrium point to the second one, while evaporation pressure remains approximatively constant for all simulation. This happens because of the operative choice about the control system: it operates by varying the pump's rotational speed depending on the liquid level inside cold drum. A modification on the rotational speed implies variations in both liquid level and condensation pressure of the cold drum. In particular, the increase of received heat flux at the evaporator, with the consequent increase of evaporation rate and temperature at the inlet of the turbine, leads to a higher condensation rate at the cold drum to achieve equilibrium. The liquid level starts to go up, inducing the control system to impose a higher rotational speed for the pump. In this way, liquid mass flow rate leaving cold drum is more than the inlet one, with the consequent reduction of the required fluid pressure for condensation.

About the model of hot drum, a change on the liquid level inside cold drum comports an opposite change on the liquid level inside hot drum, but without a modification on the evaporation pressure. However, the increase of difference between the two pressures results in a higher electric power production at the vapour turbine.

For both capacities, the initial variation of the liquid levels during the first 100 seconds depends on the initial conditions of the ORC model, a change in main parameters which set to equilibrium values that leads to an initial strong modification on drum volume ratios. Pump's rotational speed stabilizes than to a value that allow to restore the predefined condition V_l/V_{tot}=0.5. It is worth noting the different thermal inertias, caused by the different volumes of cold drum and evaporator (on which the fictitious hot drum is modelled).

Looking at the working fluid's mass flow rates, the ones relative to pump and turbine are substantially equal, but their evolution in time is opposite with respect to the pump's rotational speed. The mass flow rate elaborated by this component is indeed strongly influenced by the condensation pressure decrease. The evolution in time is hence analogous between mass flow rate and condensation pressure, instead of pump's rotational speed.

- **CASE B:** operating point 2, transition of ship velocity from 16.5 kn to 17.5 kn, ballast voyage.

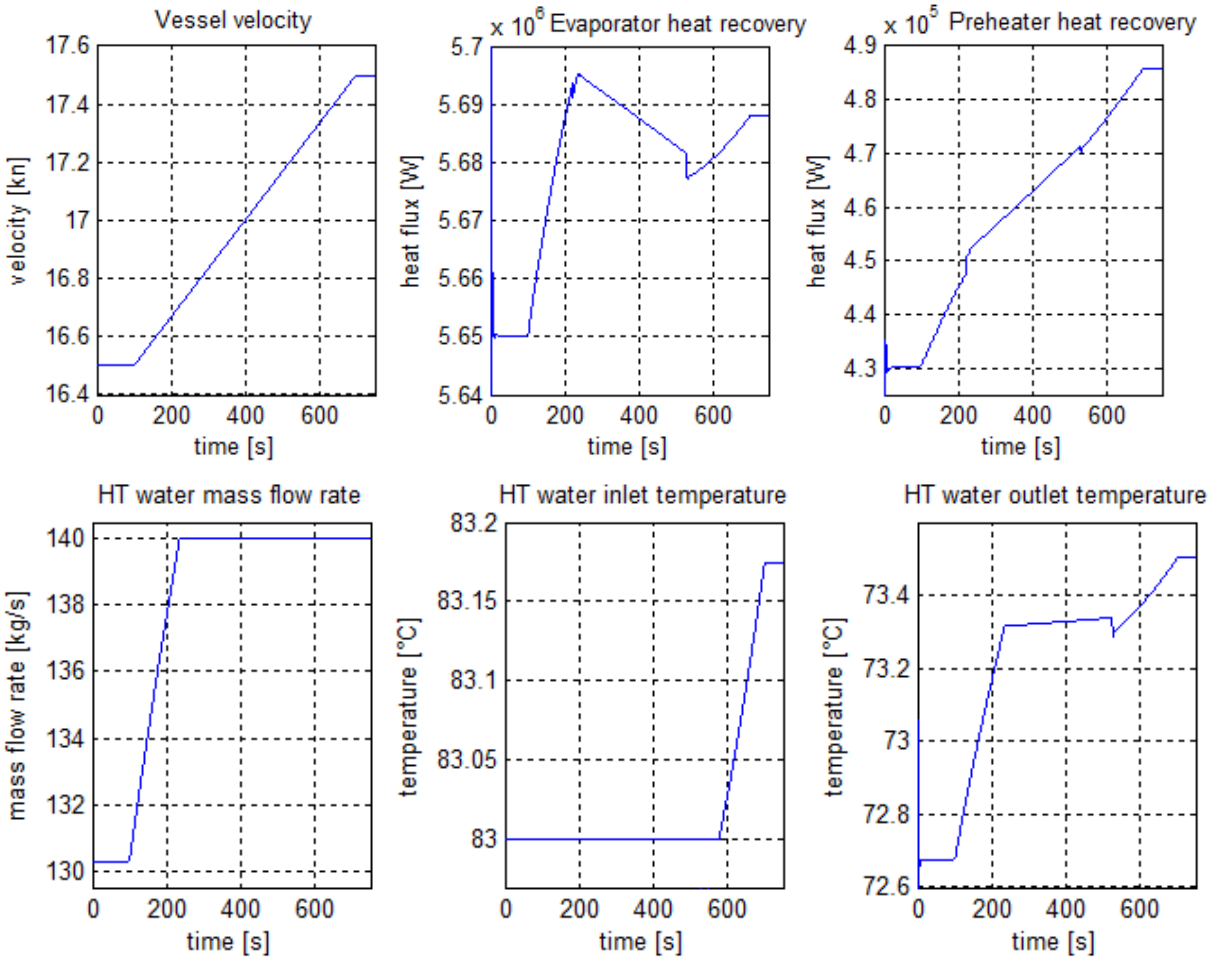

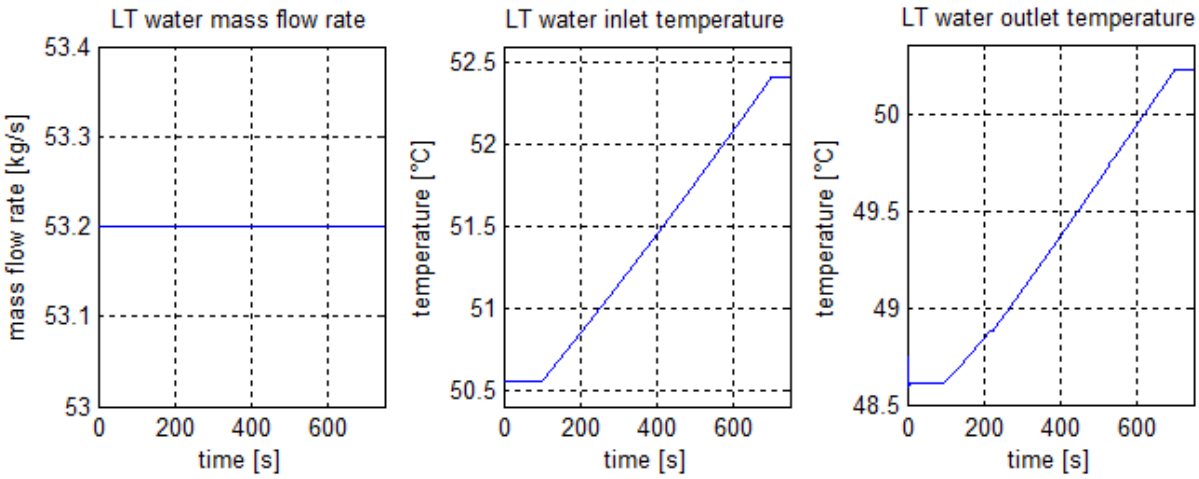

Figure 4.2(a) *Hot sources heat exchanged, mass flow rates, inlet and outlet temperatures.*

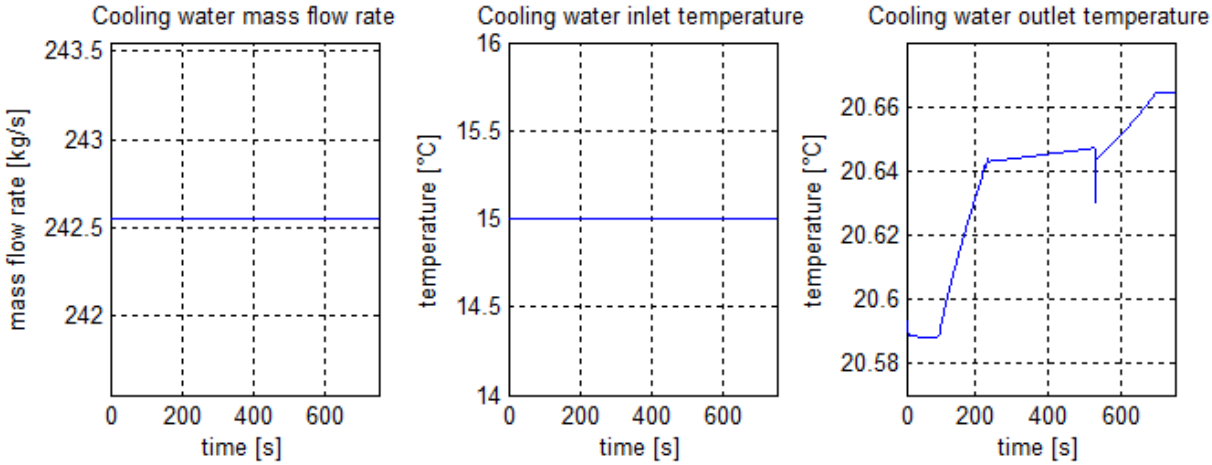

Figure 4.2(b) *Cold source mass flow rate, inlet and outlet temperatures.*

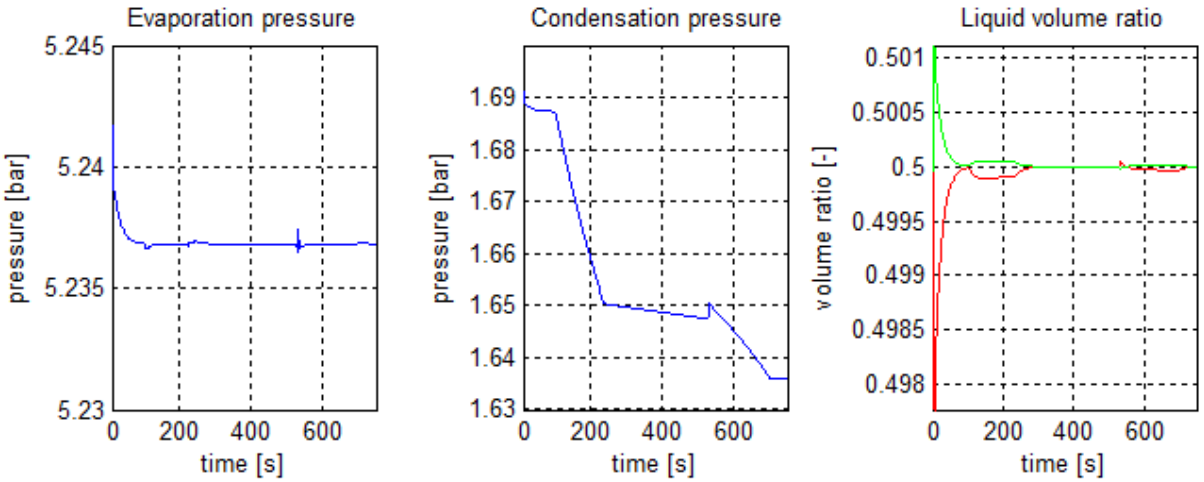

Figure 4.2(c) *Evaporation and condensation pressures, liquid volume ratios (red: hot drum, green: cold drum).*

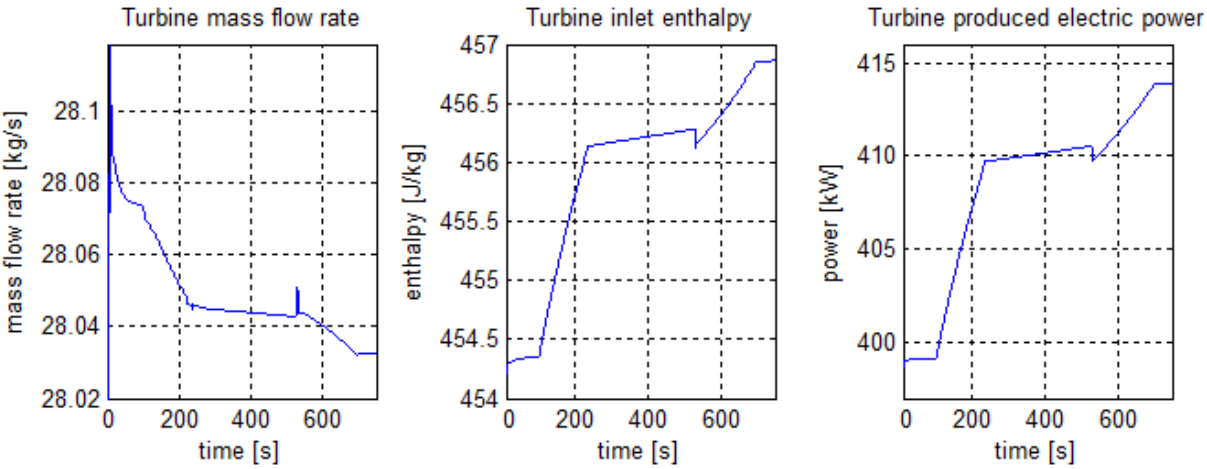

Figure 4.2(d) *Turbine mass flow rate, inlet enthalpy and produced electric power.*

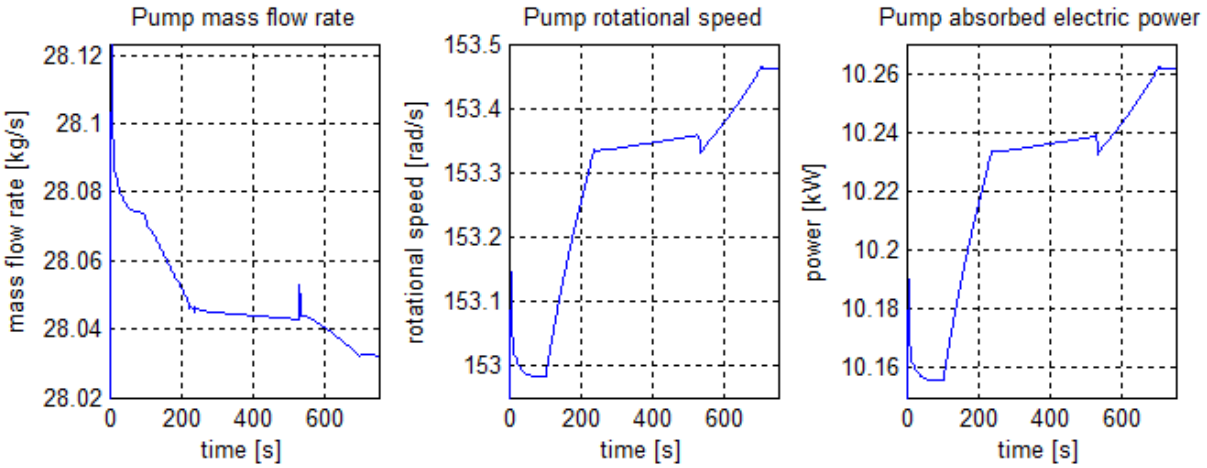

Figure 4.2(e) *Pump mass flow rate, rotational speed and absorbed electric power.*

In this case, the simulation is carried out with a different load condition of the vessel. A different behaviour of the heat sources is observed, together with a different evolution in time of main thermodynamic parameters. A limitation of 140 kg/s is imposed again to the HT water mass flow rate.

- **CASE C:** operating point 2, transition of ship velocity from 17.5 kn to 16.5 kn, laden voyage.

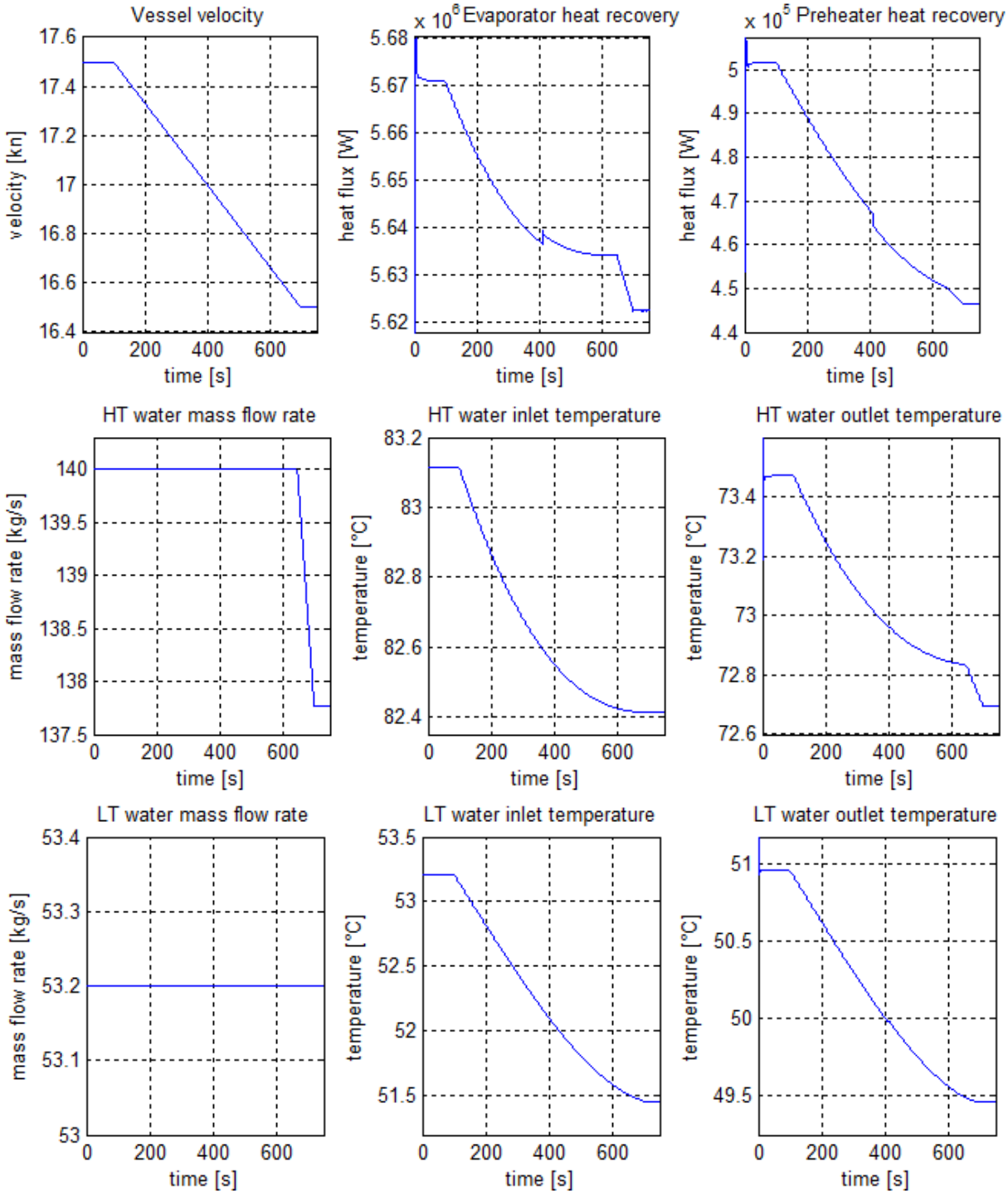

Figure 4.3(a) *Hot sources heat exchanged, mass flow rates, inlet and outlet temperatures.*

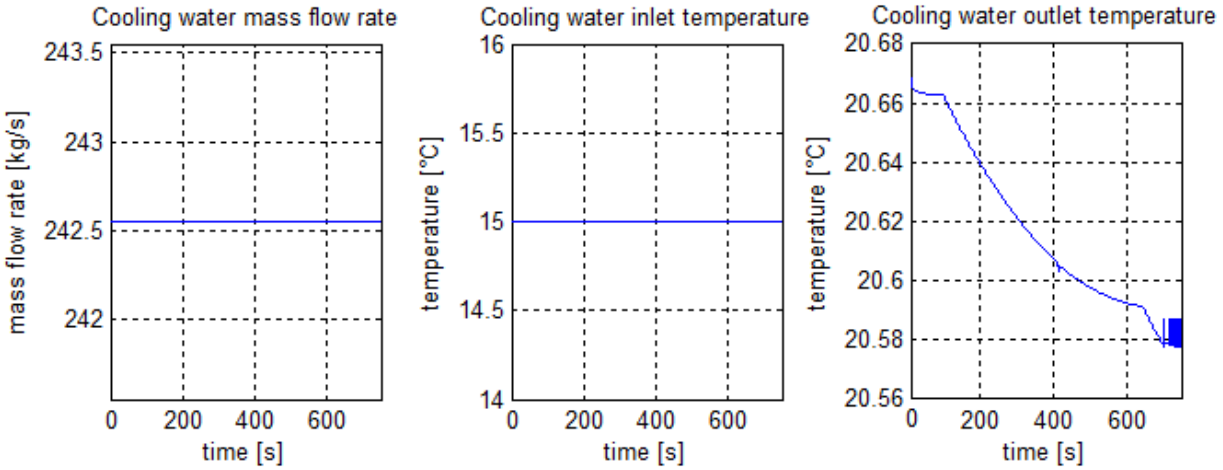

Figure 4.3(b) *Cold source mass flow rate, inlet and outlet temperatures.*

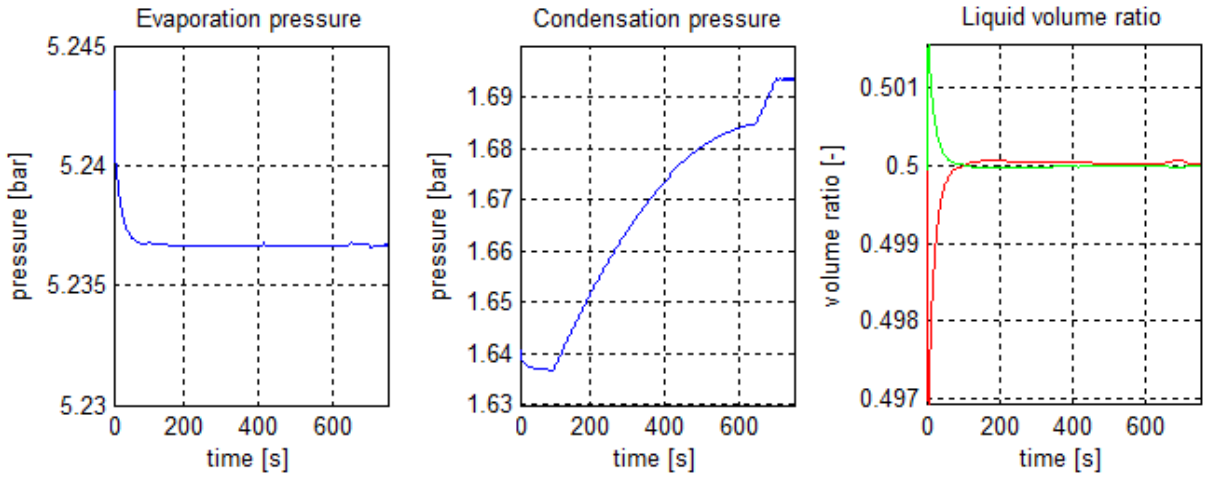

Figure 4.3(c) *Evaporation and condensation pressures, liquid volume ratios (red: hot drum, green: cold drum).*

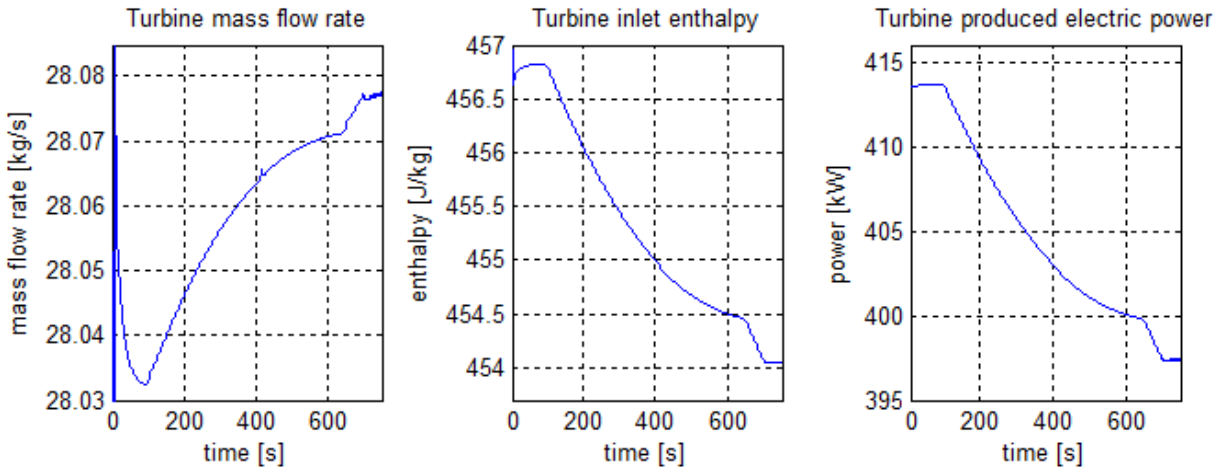

Figure 4.3(d) *Turbine mass flow rate, inlet enthalpy and produced electric power.*

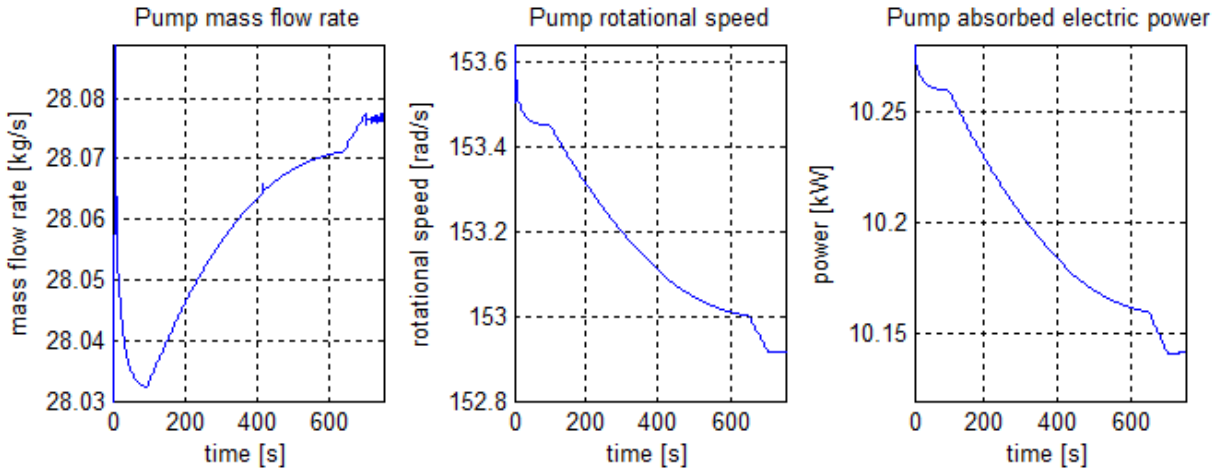

Figure 4.3(e) *Pump mass flow rate, rotational speed and absorbed electric power.*

From the presented diagrams, an opposite behaviour of all parameters has been observed during a decrease of the vessel velocity. It is worth noting looking at the results that the two equilibrium points, once inverted, are very similar between case A and C, where the same two velocities with the same load of the ship are performed.

- **CASE D:** operating point 2, transition of ship velocity from 14.5 kn to 15.5 kn, laden voyage.

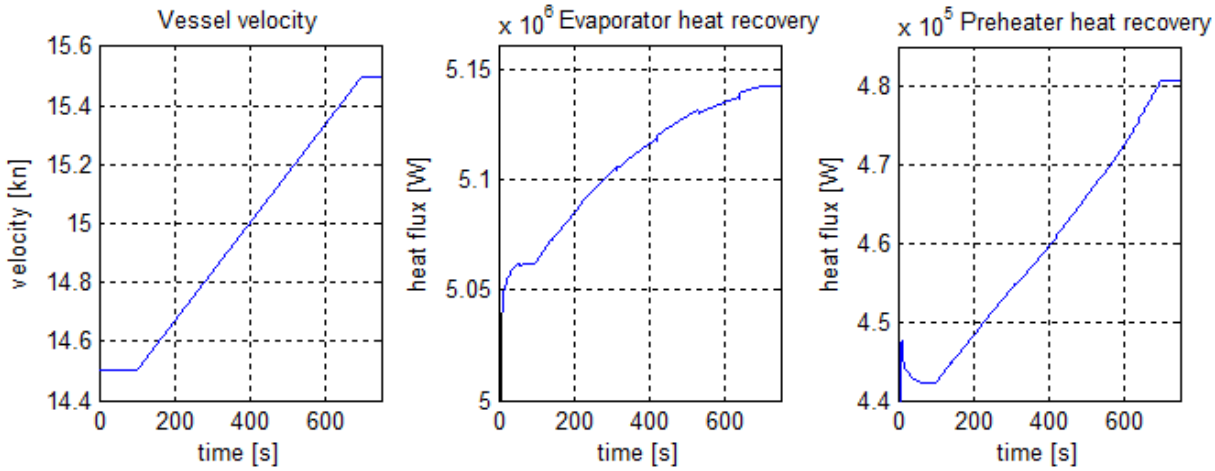

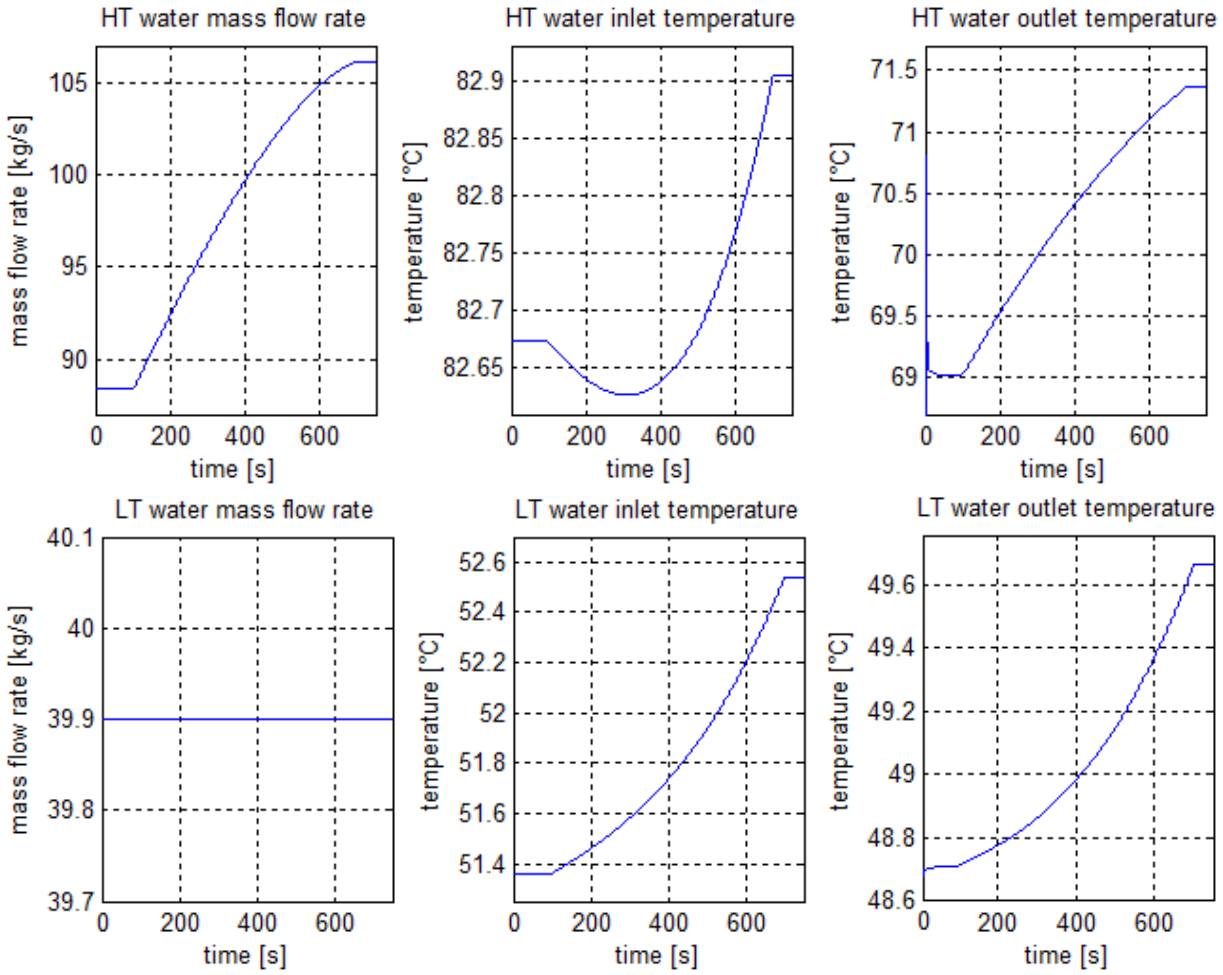

Figure 4.4(a) *Hot sources heat exchanged, mass flow rates, inlet and outlet temperatures.*

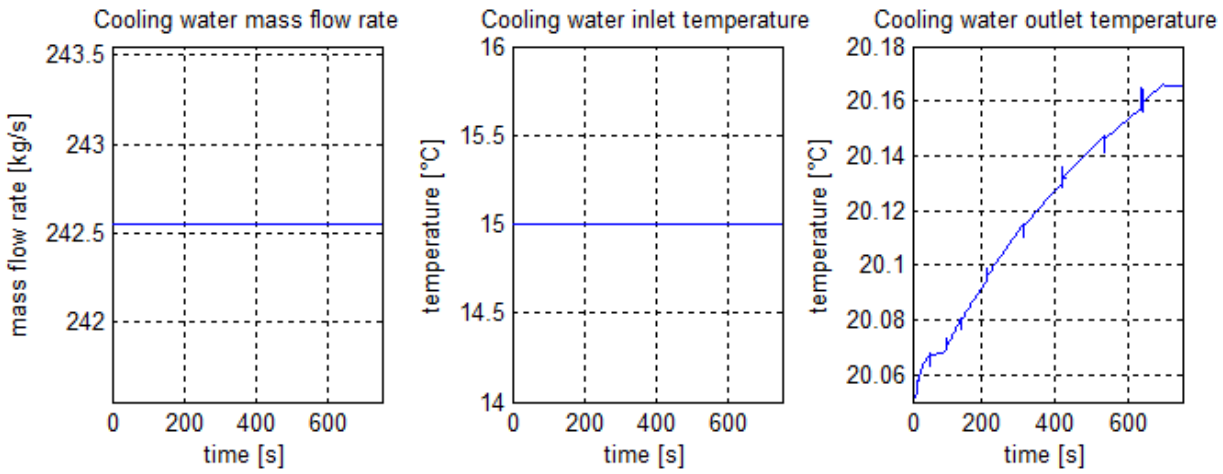

Figure 4.4(b) *Cold source mass flow rate, inlet and outlet temperatures.*

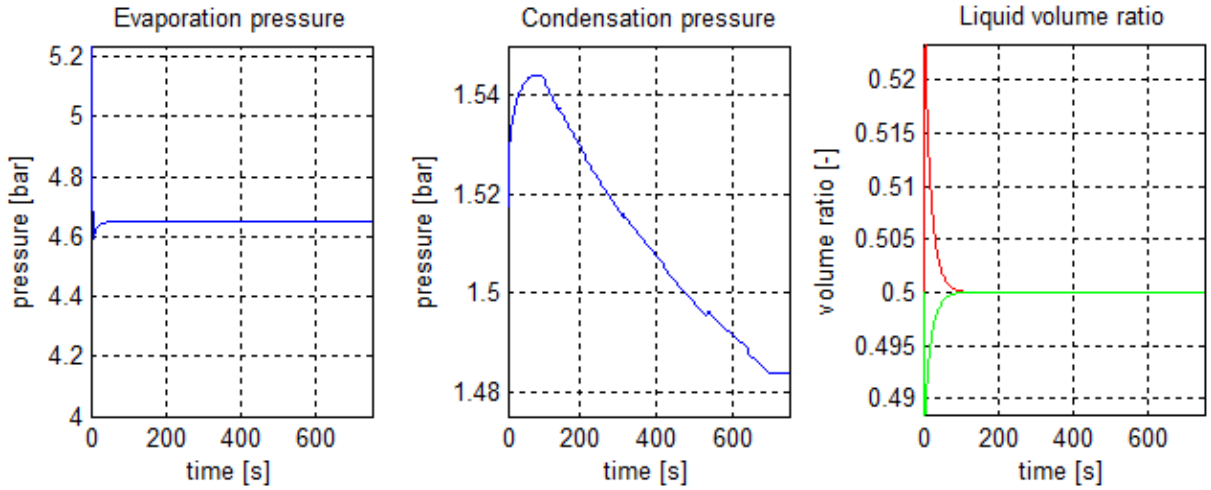

Figure 4.4(c) *Evaporation and condensation pressures, liquid volume ratios (red: hot drum, green: cold drum).*

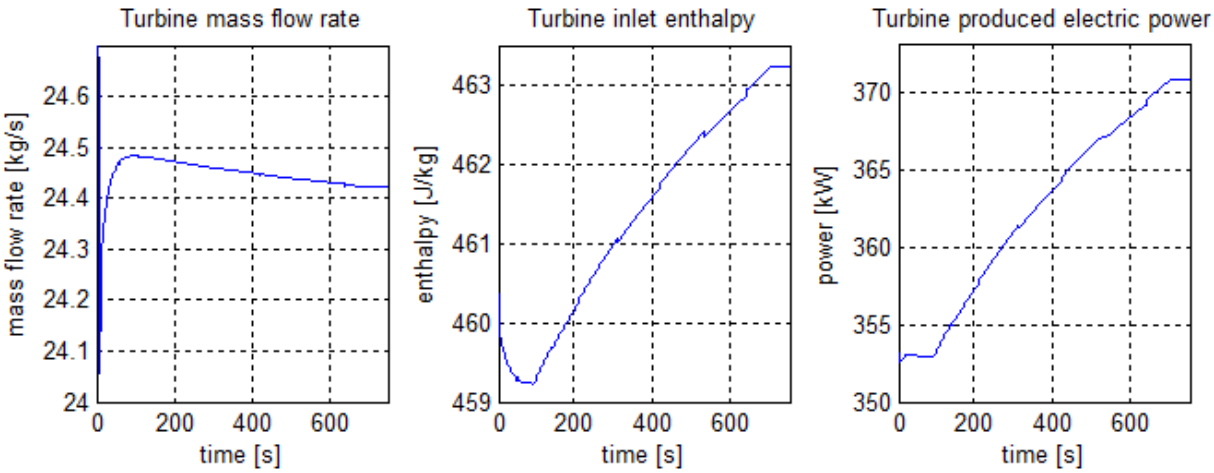

Figure 4.4(d) *Turbine mass flow rate, inlet enthalpy and produced electric power.*

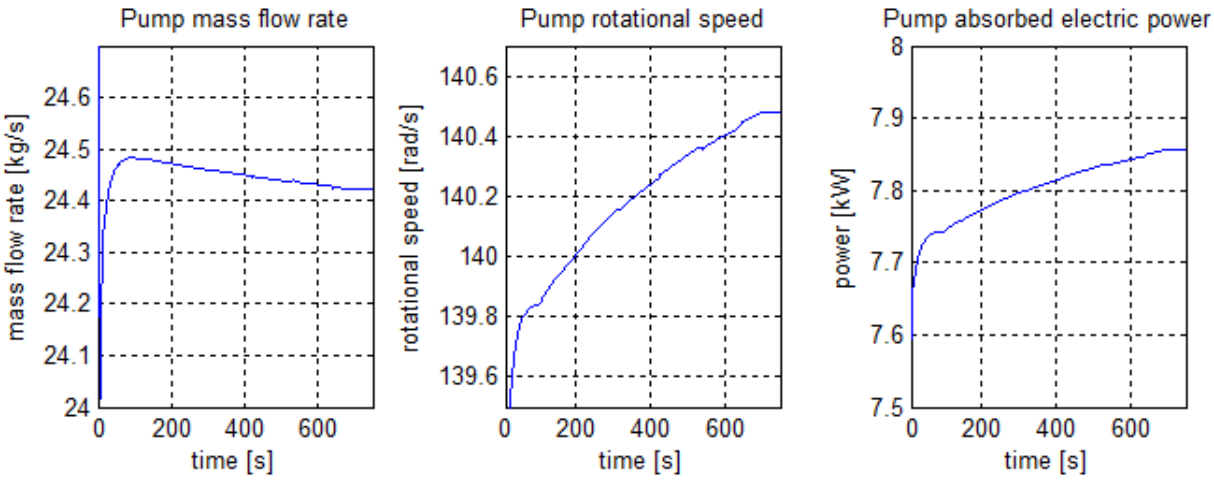

Figure 4.4(e) *Pump mass flow rate, rotational speed and absorbed electric power.*

In this case, a transition in a different velocity range is performed. Again, different conditions of the heat sources lead to a different transient behaviour of thermodynamic parameters, as it can be noticed by reported diagrams. In particular, lower evaporation and condensation pressures are observed due to the lower load of the Diesel engines, especially for the reduced HT water mass flow rate and consequently the reduced heat flux at the evaporator.

- **CASE E:** operating point 4, transition of ship velocity from 16.5 kn to 17.5 kn, laden voyage.

In this last case, a comparison between the behaviours of two different configurations of the single stage ORC system is presented. For this purpose, a simulation in the same working conditions of the ship, related to case A, has been performed.

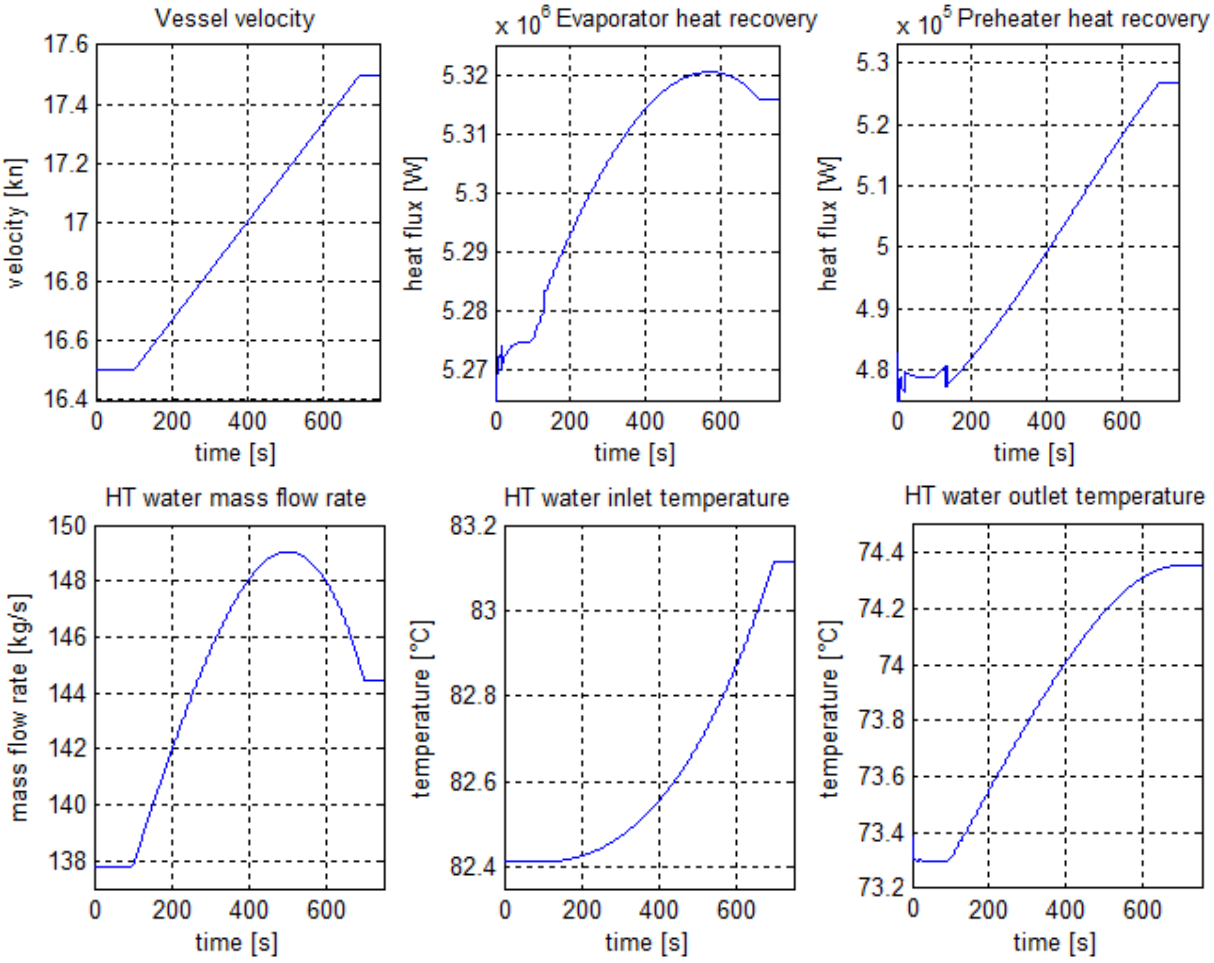

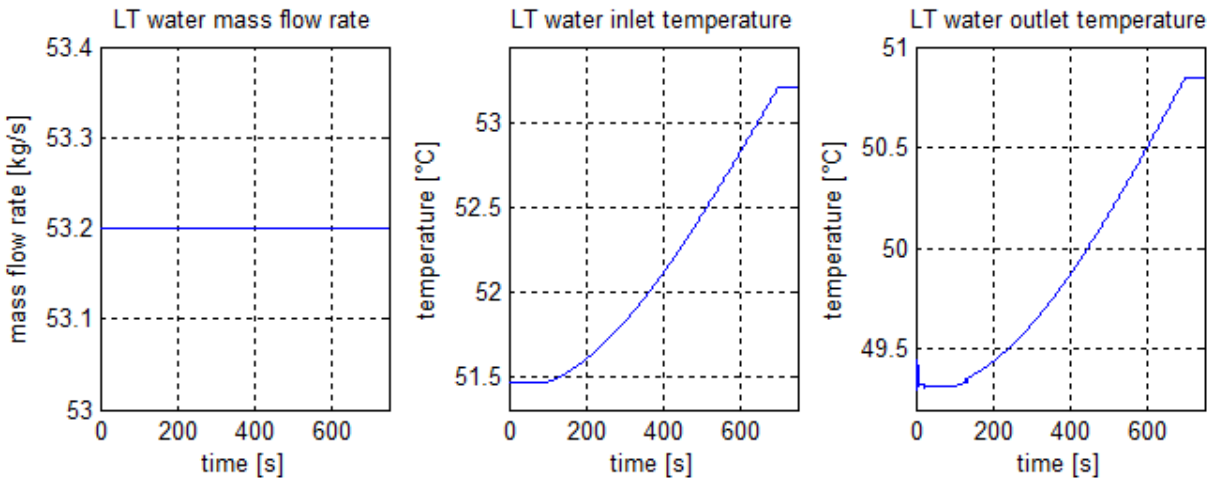

Figure 4.5(a) *Hot sources heat exchanged, mass flow rates, inlet and outlet temperatures.*

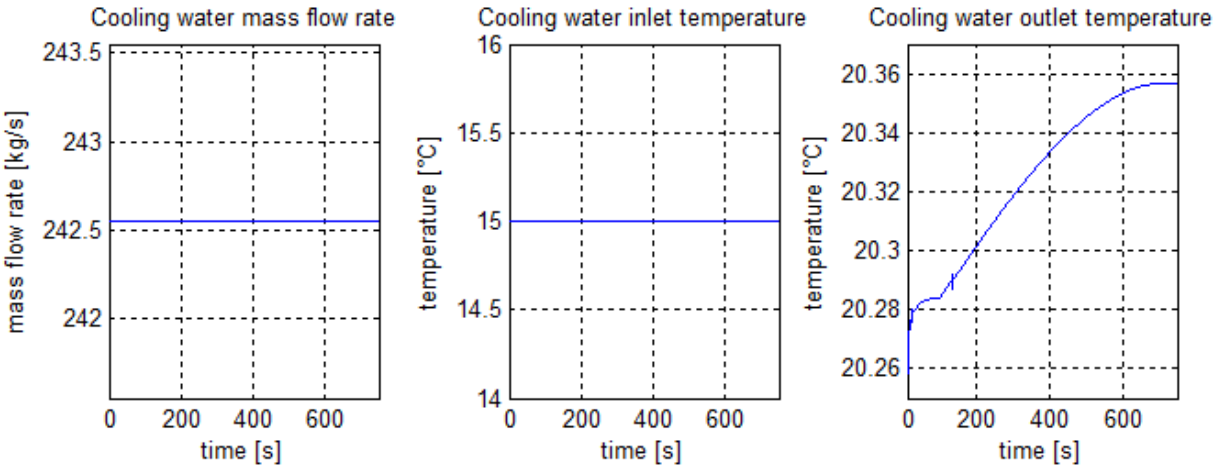

Figure 4.5(b) *Cold source mass flow rate, inlet and outlet temperatures.*

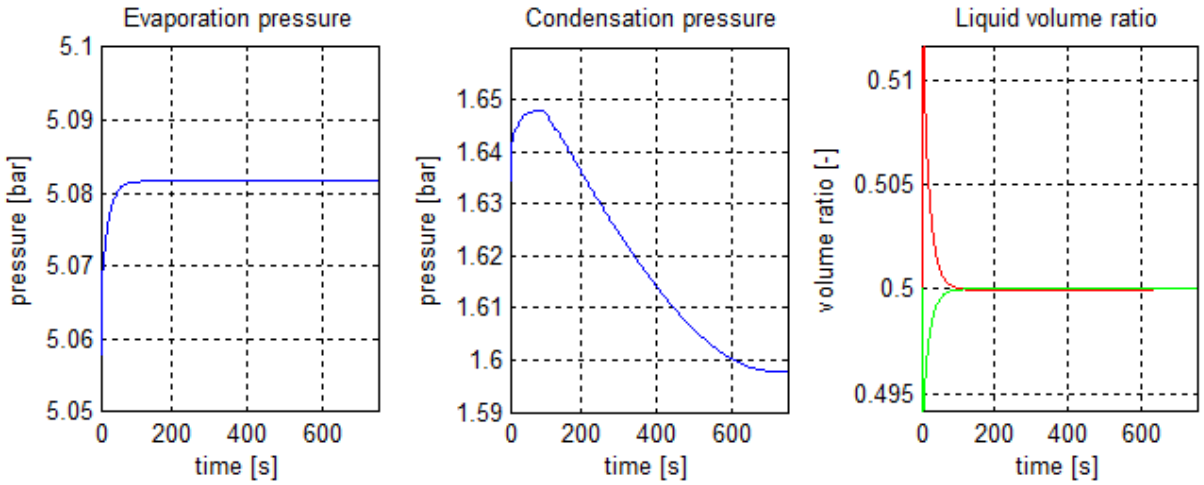

Figure 4.5(c) *Evaporation and condensation pressures, liquid volume ratios (red: hot drum, green: cold drum).*

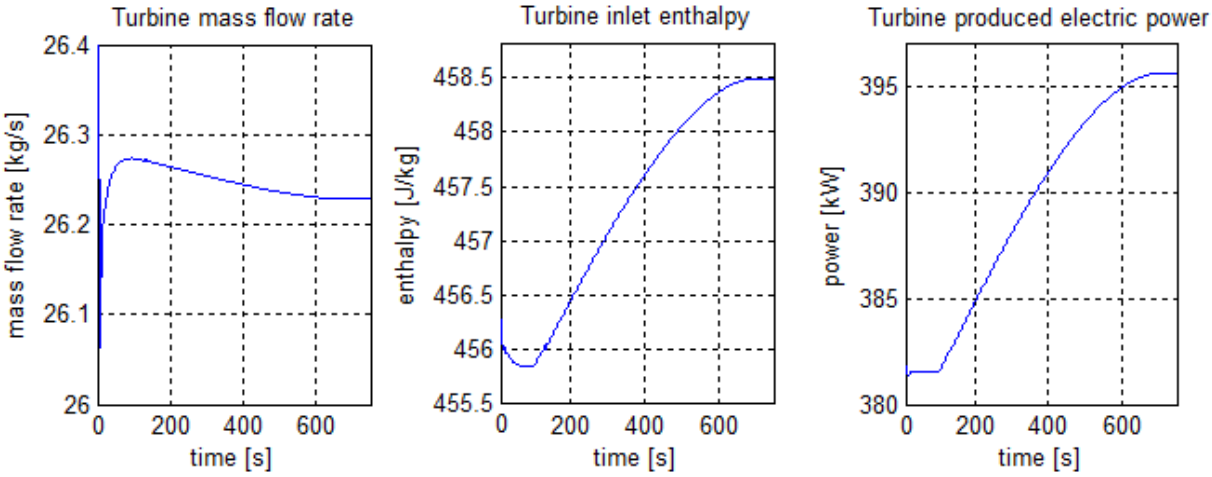

Figure 4.5(d) *Turbine mass flow rate, inlet enthalpy and produced electric power.*

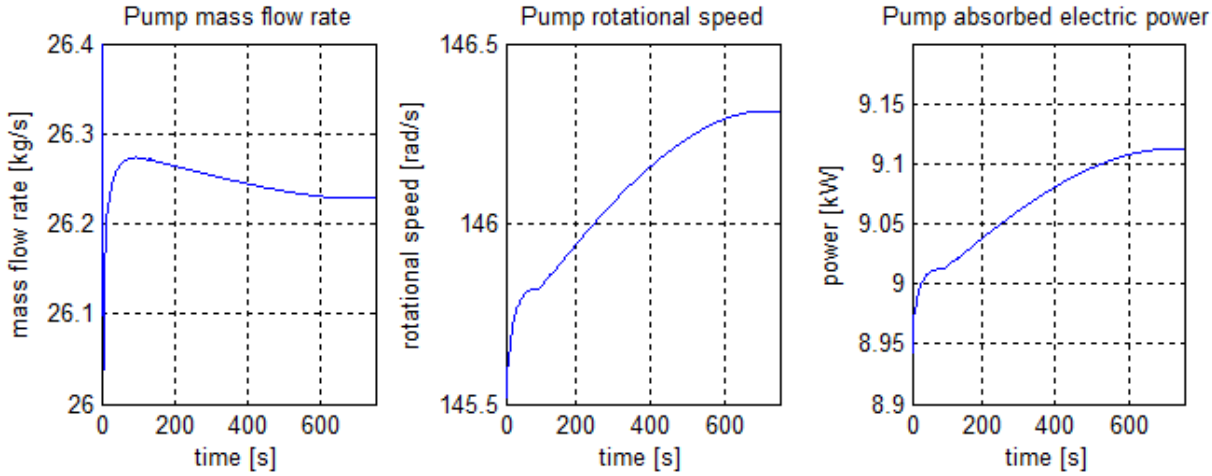

Figure 4.5(e) *Pump mass flow rate, rotational speed and absorbed electric power.*

4.2 TWO STAGE ORC SYSTEM

The selected design conditions for the two stage ORC systems are the ones relative to the *operating point 1*, reported in Table 4.1. For the two power plant versions, the annual work production has been performed by making use of the Simulink models. For each of them, dynamic simulations have been carried out in order to determine all main values at the various off-design conditions, in order to allow the simplified model to perform the annual work production evaluation.

4.2.1 Work production

The simplified two stage ORC models, presented in chapter 3, have been used to evaluate the annual work production, starting from the available statistical data about the ship operation referred to the test reference year.

It must be noticed that the subcritical second pressure level can work in a higher range of vessel operation with respect to the supercritical stage, because of the lower evaporation pressure and temperature of the working fluid. A bigger range of thermodynamic conditions of the relative hot fluid, charge air, is hence exploitable, resulting in a higher amount of time in which ORC can operate with both stages. Contrarily, in case of supercritical second pressure level the ORC system must work for a longer time as single stage, by the use of the valves designated to exclude the second stage because out of the useful operating conditions. The operative ranges of the second pressure levels are:

- in the subcritical case, for loads equal or higher than 0.78, from 14.7 to 16 kn and from 16.35 to 20 kn in laden voyage, from 15.1 to 16 kn and from 16.7 to 19 kn in ballast voyage;
- in the supercritical case, for loads equal or higher than 0.88, from 15.4 to 16 kn, 17.1 to 18 kn, 18.5 to 19 kn and 19.6 to 20 kn in laden voyage, and from 15.75 to 16 kn, 17.5 to 18 kn and 18.7 to 19 kn in ballast voyage.

Simulations results are reported below for the two cases. There are two load factors, one referred to the whole ORC system, the other one referred to the only second pressure level. It is reminded that, in case the second stage cannot work, the ORC system still operates with the only first pressure level by making use of controlled valves.

Table 4.7 *Work production and energy saving for the two stage ORCs at operating point 1.*

Parameter	Unit	Subcritical 2PL	Supercritical 2PL
E_{saved}	MWh	2218.3	2306.6
$\dot{W}_{m,net}$	kW	506.3	526.5
f_{load}	%	67.1	67.1
$f_{load,\ 2PL}$	%	48.2	19.2
E	%	2.377	2.471

Both solutions allow to significantly increase producible work and hence saved energy for the LNG carrier. This result was obviously expected, it is actually the aim of installing a second stage to an ORC system. Mean net power indicates as well an increase of performance of the plant, thanks to the use of another heat source with respect to the single stage.

Thanks to the adoption of controlled valves that allow the ORC plant to operate as single stage when the heat grade provided by charge air is insufficient, the global load factor is the same of the previous case. As aforementioned, the supercritical second stage can operate in a significantly smaller range with respect to the subcritical case. In spite of the lower load factor of the second stage, the ORC system with supercritical second pressure level presents the highest producible work, due to the much higher achievable power with respect to the other case.

The percentage of saved energy *E* makes these two solutions attractive for installation on the LNG carrier in question. The higher complexity of the plant and the additional costs are the negative aspects to take into account about the eventual choice about installation of a single stage or a two stage ORC system. The main critical issue is given by the heat source for the second pressure level: the relatively low grade of the provided heat impedes to exploit it with continuity in this stage, reducing in this way the benefits of a two stage ORC. If exhaust gases coming out from Diesel engines were available for their exploitation into this power plant, perhaps complexity and costs would be highly compensated by a continuous operation of both stages, consequently with a great increase of producible work and saved energy.

4.2.2 Transient simulations

Two test cases have been carried out, one for the first and one for the second version of the two stage ORC systems. In the previous paragraph available ranges for the two stages have been reported and discussed. Taking into account of this limitation on the operation of both pressure levels for the considered ORC plants, transient simulations have been performed by the use of the detailed Simulink model presented in paragraph 3.4.5.1. Also in this case, a time period of 10 minutes has been imposed for a change in the vessel velocity of 1 kn. A simulation time step of 0.05 seconds has been set. In the following, main diagrams and results of the two treated cases are presented.

- **CASE F:** two stage ORC with subcritical pressure levels, operating point 1, transition of ship velocity from 16.5 kn to 17.5 kn, laden voyage.

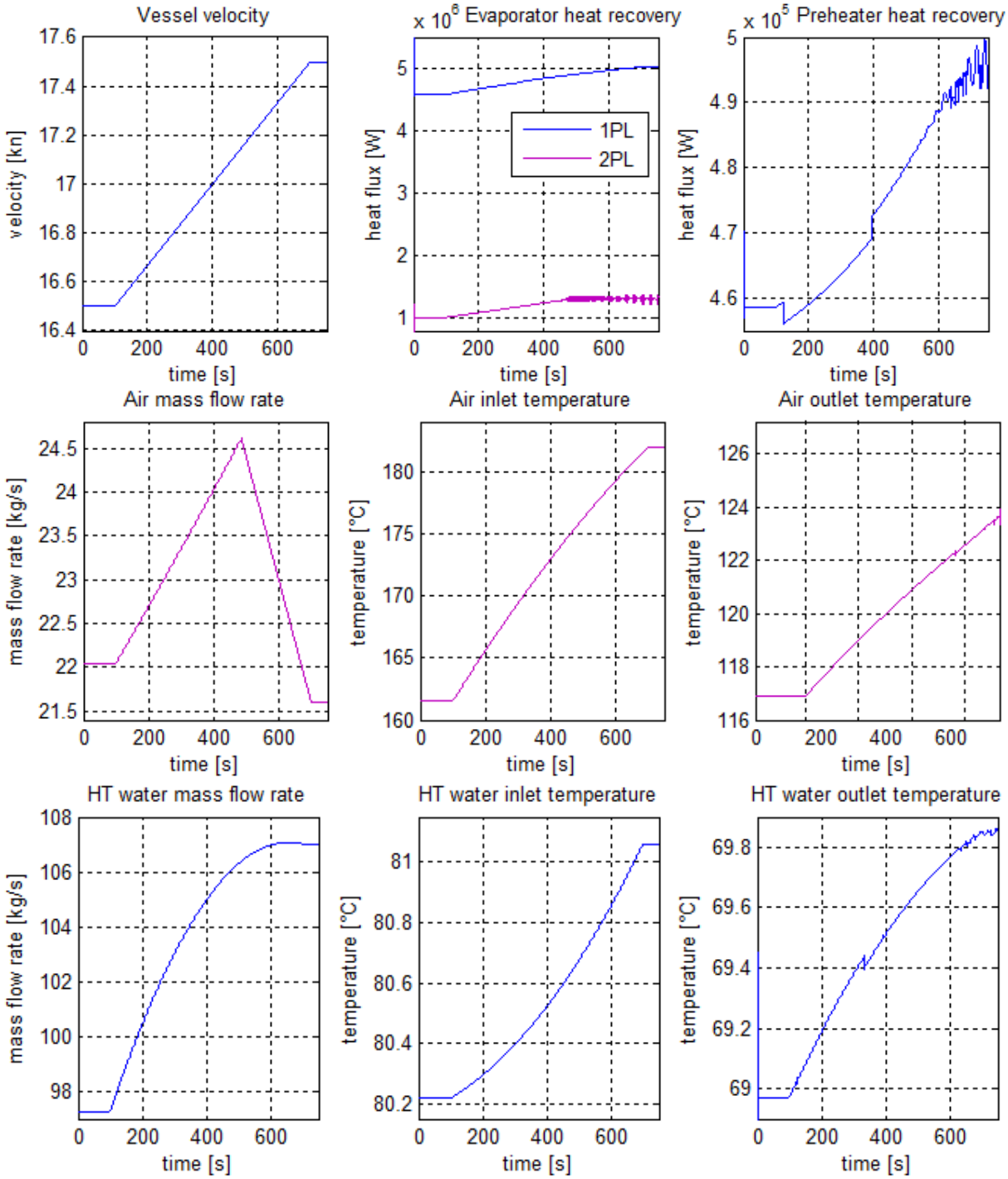

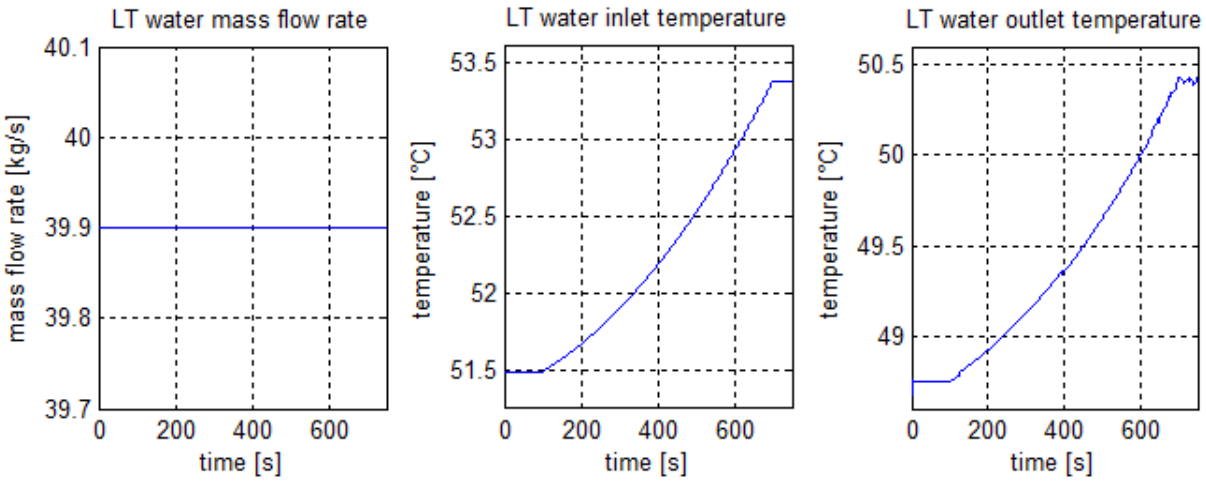

Figure 4.6(a) *Hot sources heat exchanged, mass flow rates, inlet and outlet temperatures.*

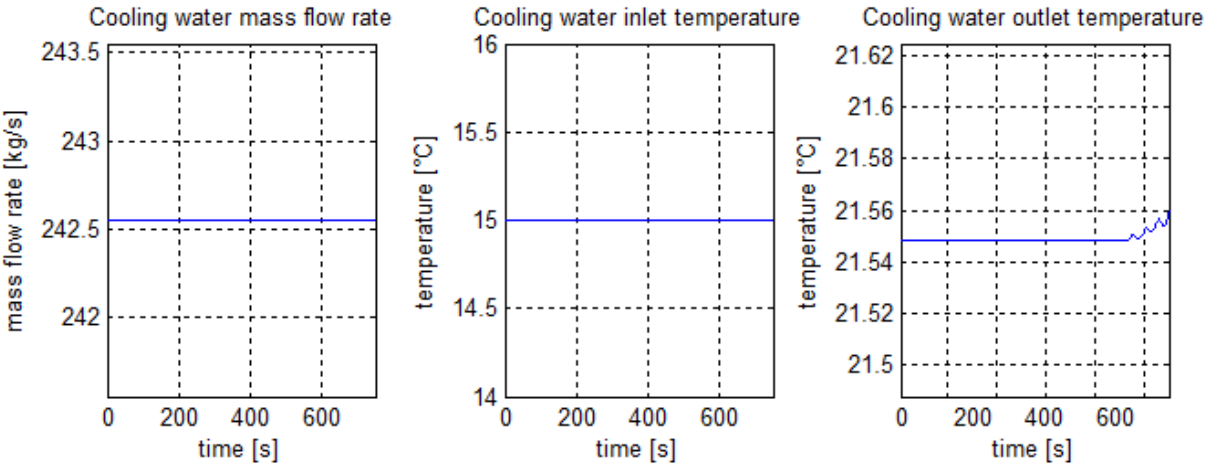

Figure 4.6(b) *Cold source mass flow rate, inlet and outlet temperatures.*

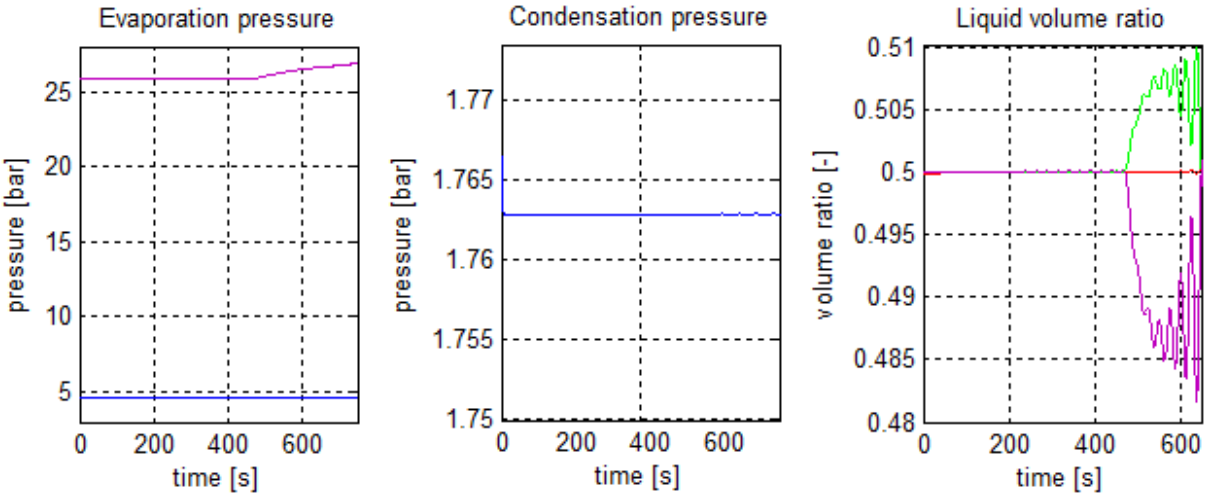

Figure 4.6(c) *Evaporation and condensation pressures, liquid volume ratios (red: hot drum 1PL, purple: hot drum 2PL, green: cold drum).*

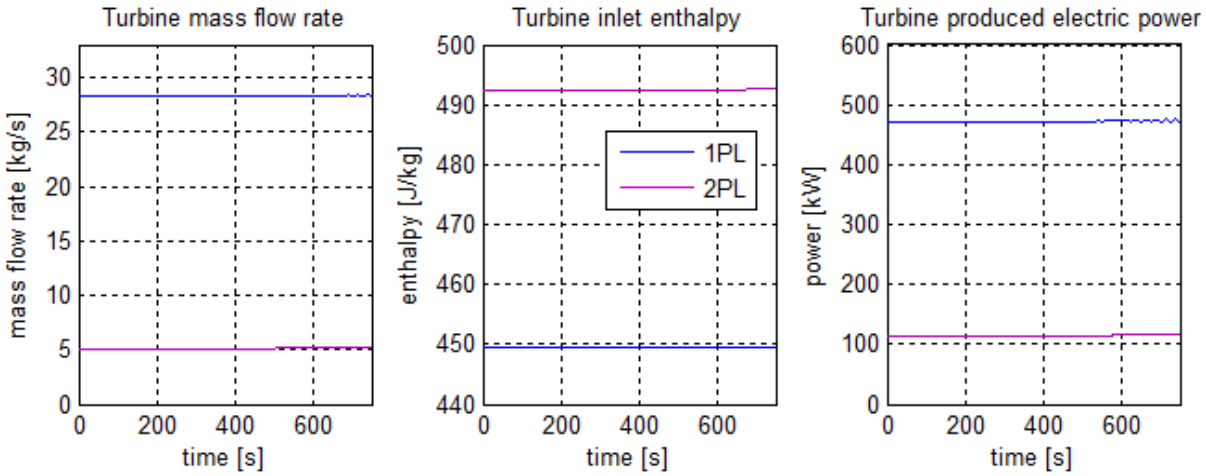

Figure 4.6(d) *Turbine mass flow rate, inlet enthalpy and produced electric power.*

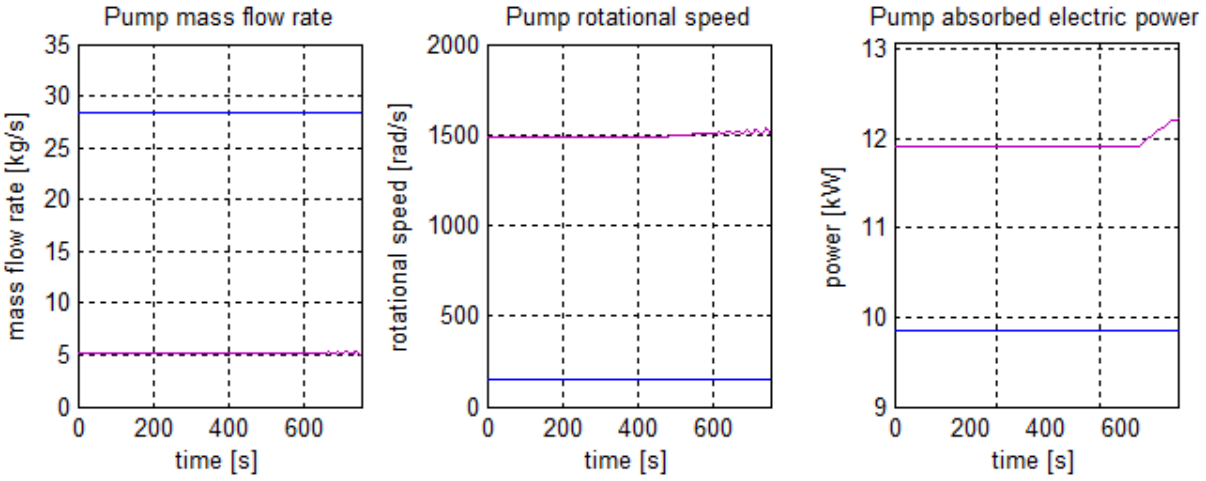

Figure 4.6(e) *Pump mass flow rate, rotational speed and absorbed electric power.*

A qualitative comparison about evolution in time of main parameters of the two stages is proposed in the reported diagrams. The main observed result is the little instability that manifests close to the end of simulation. It is basically caused by the superheating of working fluid inside the subcritical evaporator of the second pressure level: the vapour temperature quickly increases with the consequent rise of the evaporation pressure of the second stage to another equilibrium point. This causes a strong oscillation of the liquid level in the high pressure hot drum, that manifests in a lower but still observable oscillation of the liquid level inside cold drum.

About charge air, its mass flow rate is limited and progressively decreased after the design value of 24.61 kg/s, to keep the exchanged heat flux in an acceptable range in order to avoid an excessive superheating inside the evaporator of the second stage.

- **CASE G:** two stage ORC with supercritical second pressure level, operating point 1, transition of ship velocity from 17.1 kn to 18 kn, laden voyage.

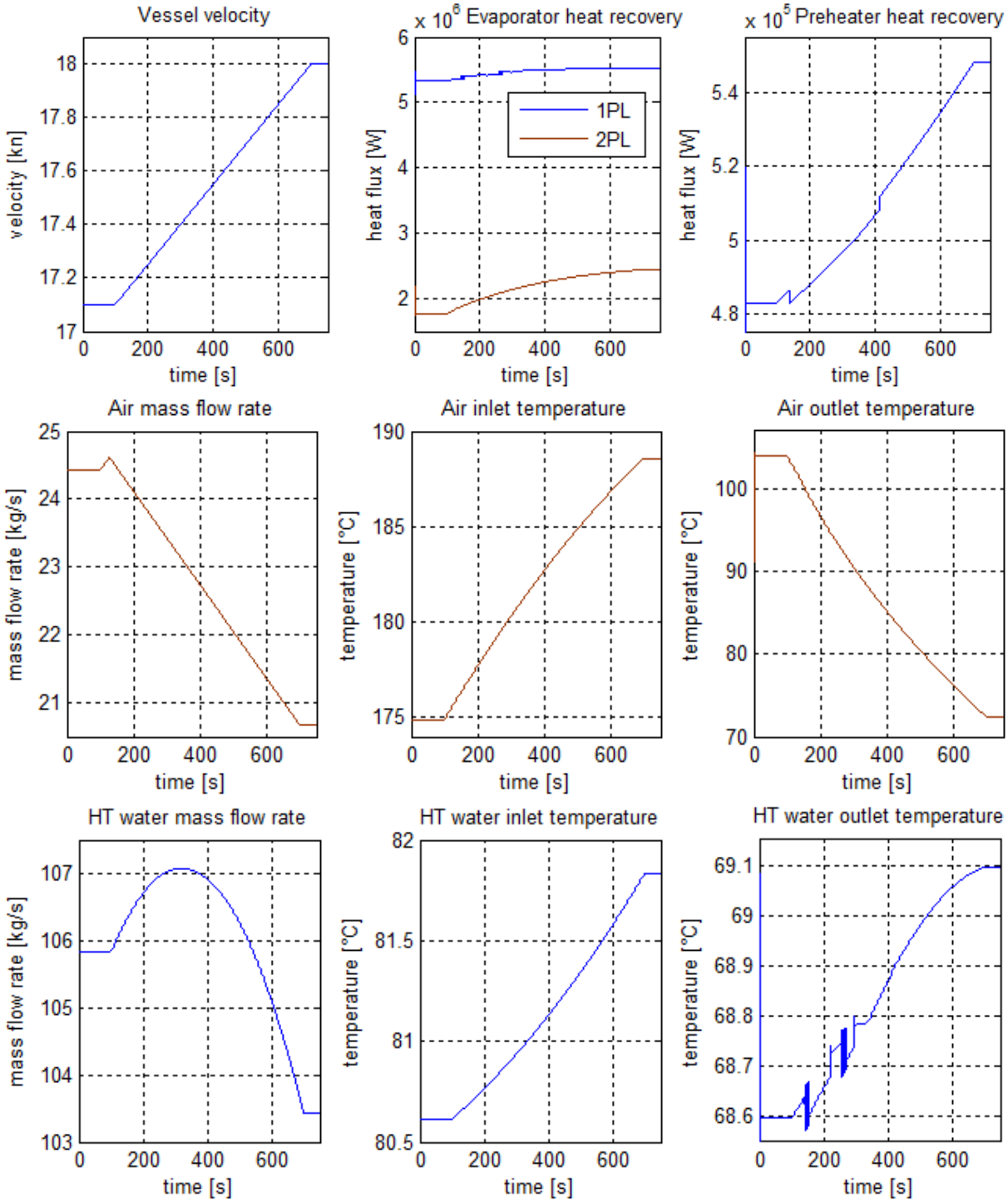

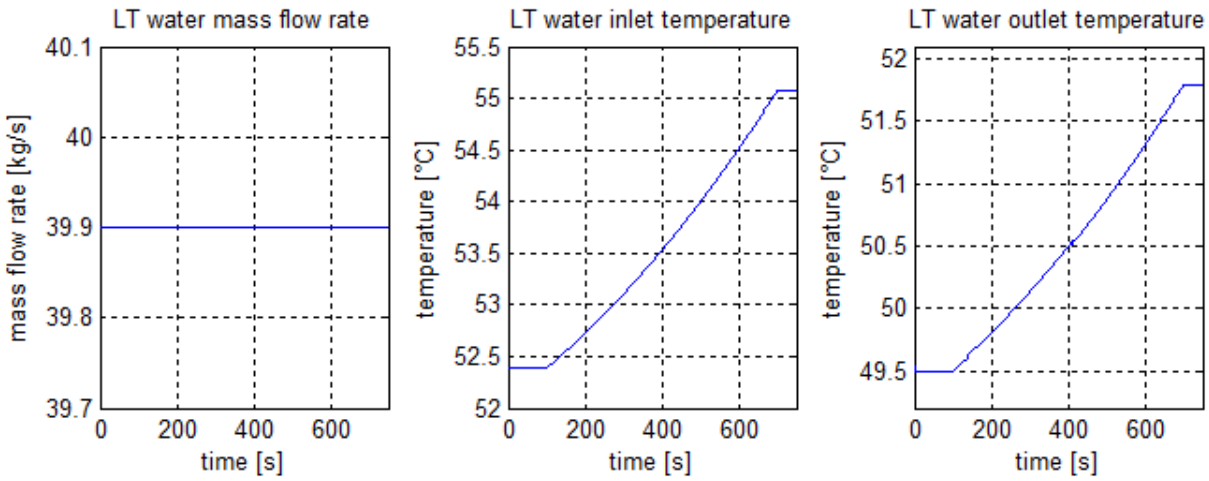

Figure 4.7(a) *Hot sources heat exchanged, mass flow rates, inlet and outlet temperatures.*

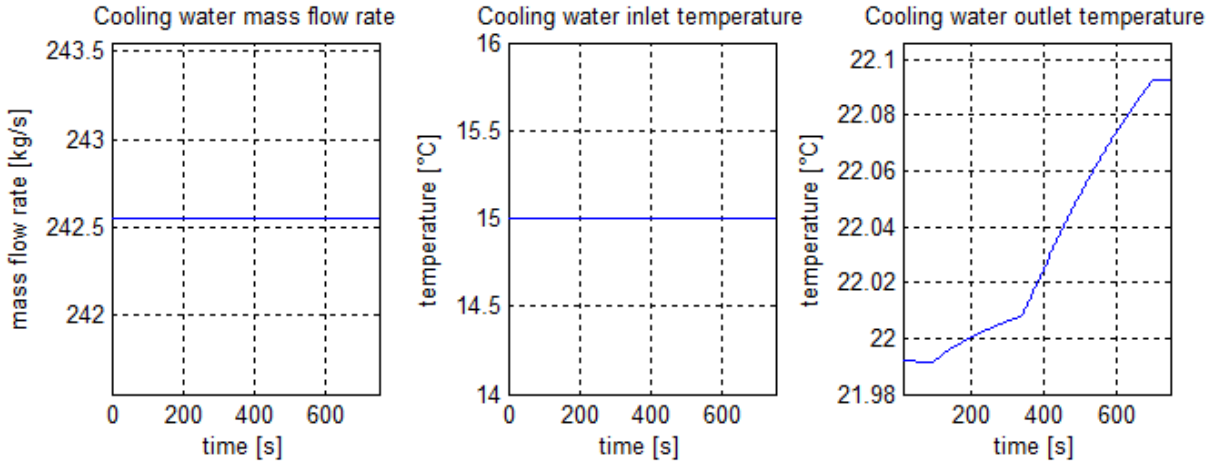

Figure 4.7(b) *Cold source mass flow rate, inlet and outlet temperatures.*

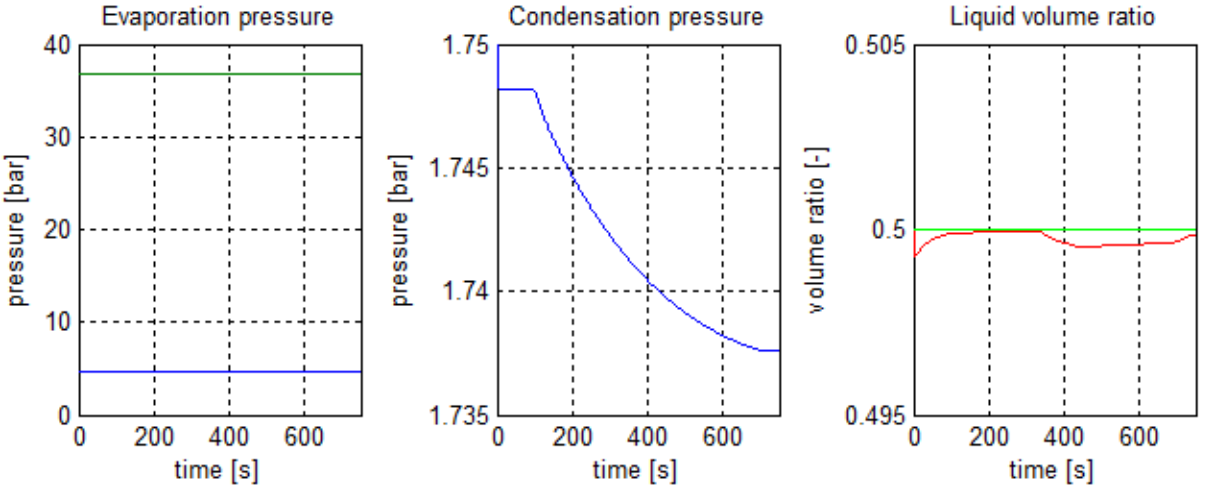

Figure 4.7(c) *Evaporation and condensation pressures, liquid volume ratios (red: hot drum 1PL, green: cold drum).*

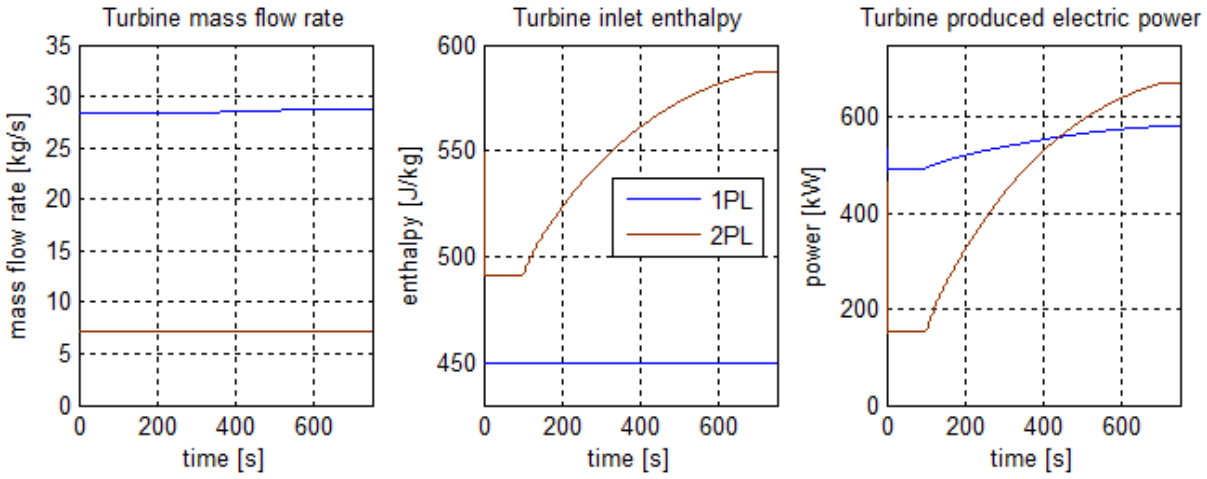

Figure 4.7(d) *Turbine mass flow rate, inlet enthalpy and produced electric power.*

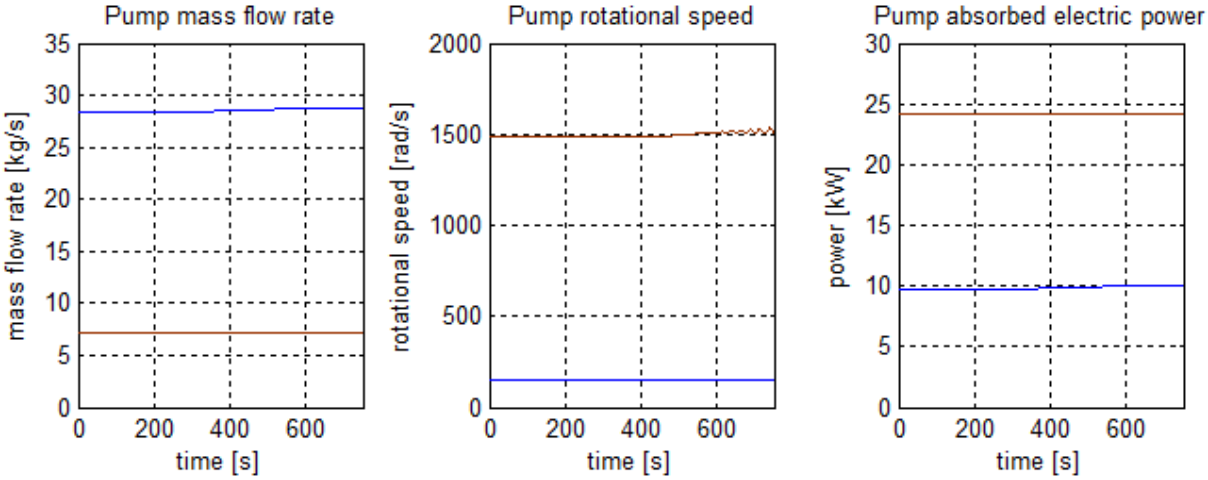

Figure 4.7(e) *Pump mass flow rate, rotational speed and absorbed electric power.*

As for case F, air mass flow rate is limited and decreased after design value of 24.61 kg/s.

The most interesting result is the evolution in time of electric power generated by the two vapour turbines: contrarily to the previous case with two subcritical evaporators, supercritical evaporation allows to achieve much higher levels of work production, even more than the work obtained by the turbine of the first stage at certain loads. This aspect suggests the great potential of supercritical evaporation, when it is possible to perform with the available heat.

Looking at the cooling water outlet temperature and liquid level inside hot drum, the sudden change in curve slope is caused by the beginning of superheating of the vapour produced by the subcritical heat exchanger. About the cold drum's liquid level, it remains constant at V_l/V_{tot}=0.5 thanks to the selected rotational speed for the second stage pump, as discussed in chapter 3.

4.3 COMPARISON BETWEEN SINGLE AND TWO-STAGE ORC SYSTEMS

A summary table of the evaluated ORC design and configurations is here proposed.

Table 4.8 *Optimized operating characteristic for considered ORC configurations and design.*

ORC layout		**1PL**				**2PL sub**	**2PL sup**
Operating point		**1**	**2**	**3**	**4**	**1**	**1**
Working fluid		R245fa	R245fa	R245fa	R245fa	R245fa	R245fa
$p_{ev,1PL}$	bar	4.955	5.236	5.256	5.393	4.612	4.612
$p_{ev,2PL}$	bar	-	-	-	-	25.850	37.000
p_{cond}	bar	1.778	1.778	1.778	1.778	1.766	1.766
T_{cond}	°C	29.80	29.80	29.80	29.80	29.72	29.72
ΔT_{sup}	°C	0.0	0.0	0.0	0.0	0.0	0.0
TIT_{1PL}	°C	62.37	64.36	64.49	65.43	59.82	59.82
TOT_{1PL}	°C	38.63	39.23	39.27	39.55	40.29	41.31
TIT_{2PL}	°C	-	-	-	-	135.37	158.16
TOT_{2PL}	°C	-	-	-	-	76.05	76.77
sub/sup	-	sub	sub	sub	sub	sub	sup
w_{exp}	kJ/kg	12.555	14.200	13.595	14.117	17.546	28.688
w_{pump}	kJ/kg	0.343	0.363	0.353	0.356	0.658	0.956
w_{net}	kJ/kg	12.212	13.837	13.242	13.761	16.888	27.732
$q_{absorbed}$	kJ/kg	210.6	213.2	213.3	214.0	217.1	219.4
q_{cond}	kJ/kg	196.2	196.7	196.8	197.0	198.0	199.0
$\dot{m}_{wf,1PL}$	kg/s	27.98	28.00	28.01	28.15	28.35	28.35
$\dot{m}_{wf,2PL}$	kg/s	-	-	-	-	5.11	7.10
$\dot{m}_{wf}$	kg/s	27.98	28.00	28.01	28.15	33.46	35.45
$W_{net,1PL}$	kW	341.7	387.4	370.9	387.4	462.9	533.3
$W_{net,2PL}$	kW	-	-	-	-	102.2	449.9
W_{net}	kW	341.7	387.4	370.9	387.4	565.1	983.2
η_{th}	%	5.80	6.49	6.21	6.43	7.78	12.64
η_t	%	3.80	4.30	4.12	4.30	5.51	9.58
ϕ	-	0.655	0.663	0.664	0.669	0.708	0.758
$\dot{Q}_{absorbed}$	kW	5892.3	5970.8	5974.4	6023.4	7265.5	7776.3
$\dot{Q}_{cond}$	kW	5489.4	5508.9	5512.0	5546.9	6625.7	7053.0

The following parameters are defined:

- *TIT* (Turbine Inlet Temperature): it represents the vapour temperature before expansion; it corresponds to the working fluid temperature at the outlet of the evaporator or eventually of the hot drum;
- *TOT* (Turbine Outlet Temperature): it is the vapour temperature after expansion, successively sent to the condenser.

For the ORC systems two kinds of cycle efficiencies are defined. *Thermal efficiency* η_{th} corresponds to the ratio between net power output and heat absorbed by the cycle, precisely by the heat exchangers receiving thermal energy from the heat source.

$$\eta_{th} = \frac{\dot{W}_{net}}{\dot{Q}_{absorbed}} \tag{4.1}$$

Total heat recovery efficiency η_t is the ratio between net power output and available heat, corresponding to the value provided by the Hot Composite Curve to the cycle.

$$\eta_t = \frac{\dot{W}_{net}}{\dot{Q}_{available}} \tag{4.2}$$

The parameter that connects the two efficiencies is the *effectiveness of heat transfer* ϕ.

$$\phi = \frac{\dot{Q}_{absorbed}}{\dot{Q}_{available}} \tag{4.3}$$

$$\eta_t = \phi\, \eta_{th} \tag{4.4}$$

The proposed table shows all values of the designed ORC systems obtained by the use of the presented Simulink models, for all considered operating points and layouts. The light-blue coloured cells indicate the three selected plant configurations that have been used for the transient simulations, presented in this chapter.

Regarding the single stage ORCs, according to the summary table the *operating point 2*, that corresponds to a design at the vessel conditions for a velocity of 16.5 kn in laden voyage, is the most performing one. Net power, thermal efficiency and total heat recovery efficiency show indeed the highest values among the four performed design. According to Table 4.6, work production and consequently saved energy are higher than the other solutions. At last, the analysis of the transient simulations among off-design stationary conditions does not report particular problems in the management of the plant within the recommended working range. All these results suggest to choose the *operating point 2* as design point for the single stage ORC system, among the four proposed possibilities.

Table 4.8 shows also interesting results about the two stage ORCs. For both versions, an increase of net power, thermal efficiency and total heat recovery efficiency is registered, with respect to the single stage ORC. According to Table 4.7, work production and saved energy are higher as well. The suggested solution is the one presenting the supercritical evaporator, in spite of the much lower load factor for the second stage. This is the overall

best solution, according to the proposed models. Further analysis are recommended to confirm obtained results and support suggested choices.

4.4 CONCLUSIONS

Simulation results have been presented in this chapter, starting from definition of design operating points for the considered solutions. An analysis of work production, relatively to the reference year for the LNG carrier of study, has been carried out in order to compare the different options, for both single stage and two stage ORCs.

Several test cases of transient behaviour have been performed and reported by presenting the evolution in time of all main system parameters.

At last, a brief comparison of the results obtained by the use of the Simulink models presented in chapter 3 has been proposed, with a summary table as support to evaluate all main outputs. The best solutions for the single stage and the two stage ORC systems, according to the simulation results, have been recommended, to possibly verify with further analysis.

5 CONCLUSIONS AND REMARKS

WHR application of an Organic Rankine Cycle (ORC) system on board a LNG carrier has been treated in this thesis. Heat is provided by jacket water, lubricating oil and charge air, while the exhaust gases are not available since they are already employed for ship internal uses. The aim of the work is to evaluate annual work production of the ORC and verify operational stability during variations of the heat sources. For this purpose, steady-state and dynamic off-design models of the ORC system have been built.

R245fa has been considered as working fluid, among a list of six fluids recommended by Soffiato [18] for the use aboard the same LNG carrier. In the models the following features related to heat exchangers are taken into account to have realistic simulations:

- Shell and tube heat exchangers have been chosen taking into account dimensional constraints deriving from the installation on the LNG carrier;
- Evaporator and condenser are type F shell and tube being Kettle not suitable for naval applications;
- Pressure drops are counted both for design and off-design operation;
- Different (and proper) heat transfer equations taken from the literature have used to model different heat transfer phenomena including subcritical and supercritical evaporation, and subcritical superheating.

Three different layouts for the ICEs-ORC combined cycle have been proposed based on a single-stage, a two-stage subcritical and a two-stage supercritical ORC and an off-design dynamic models have been developed for each solution. Four design operating points, corresponding to 15.5 kn laden, 16.5 kn laden and ballast, and 17.5 kn laden, have been considered for the single-pressure ORC, while the design point of both two-stage ORCs has been 15.5 kn laden. *EES®* (*Engineering Equation Solver*) has been used to define design parameters for the thermodynamic cycle.

The modelling approach has been modular-sequential, as suggested by Vaja [14], and the models were built using *MATLAB® Simulink*. The nominal parameters of the heat exchangers have been determined by building design models of these components. The off-design characteristic law of each heat exchanger has been obtained by several simulations of *Aspen® Exchanger Design and Rating* models for different values of hot sources and working fluid mass flow rate, has suggested by Manente et al. [13]. Characteristic maps of turbomachinery have been taken from le literature.

The control strategy has been defined by means of several simulations of the dynamic models. The stability of the single-stage solution has been achieved by a cold drum between condenser and feed pump and a control system operating on the rotational speed of the pump depending on the liquid level of the capacity. In both two-stage solutions both pumps (low pressure and high pressure ones) are directly connected to the cold drum for safety issue. The stability of the two-stage subcritical solution requires two hot drums downstream

the two evaporators and two control systems operating on the rotational speed of the two pumps depending on the liquid levels of these capacities. The stability of the two-stage supercritical solution requires only one hot drum (supercritical evaporation does not show phase separation) and one control system operating on the low pressure pump rotational speed depending on the hot drum liquid level, while the rotational speed of the high pressure pump is kept constant to the design value. In both two-stage solutions the low pressure vapour exiting the low pressure hot drum is mixed with the high pressure vapour exiting the high pressure expander in a three-way valve upstream of the low-pressure turbine.

The off-design dynamic simulations have been used also to determine the workable range of the three ORC solutions according to their transient response to variation of the ICEs load. The four single-stage ORC solutions may operate in the whole range of velocity that has been considered (14 kn to 20 kn laden and 15 kn to 19 kn ballast), while the two-stage ORC may operate with the high pressure level only in small ranges and without this pressure levels in the remaining ranges, according to the load of the engines.

Steady-state models have been developed to assess the annual work production of the proposed ORC solutions. The steady-state models have been obtained substituting the capacity blocks with a set of values at equilibrium of pressure and enthalpy in the capacities, and pump(s) rotational speed(s) corresponding to different ship speeds that have been obtained by dynamic simulations at the same ship speed.

The design velocity of 16.5 kn laden has been resulted the best design velocity for the single-pressure level. The corresponding nominal net power is 387.4 kW with a thermal efficiency of 6.49%, and an annual work production of 1665.8 MWh. It is worth noting that the off-design simulations have led to find a better design point compared to that found in a previous work [18-20] of the research group in which only the operation at design point was considered. As regards the two-stage ORC solutions, the supercritical one has reached the highest nominal net power (982.3 kW), thermal efficiency (12.64%) and annual work production (2306.6 MWh). On the other hand, the two-stage ORC may not be the best recommended option, because of an increase of system complexity and the very low load factor of the second stage due to the available heat source.

Recommendations for future works may be the use of the proposed ORC models with different design operating points, and different fluids. Moreover, the available data of vessel operation could be updated, to have better findings with the real off-design behaviour of the energy system. Another configuration of two-stage ORCs could be studied for a better integration within the overall energy system, perhaps by using part of exhaust gases if available. The solution of the supercritical evaporator would be interesting to develop, in particular the search of the most suitable heat transfer correlations and the expansion of the working range to increase the load factor are the priorities. Different ICEs-ORC configurations or a different working fluids could be useful for this purpose. Finally, an economic analysis could give more information about the profitability of the solutions proposed in this work.

REFERENCES

1. S. Quoilin, M. Van Den Broek, S. Declaye, P. Dewallef, V. Lemort, *Techno-economic survey of Organic Rankine Cycle (ORC) systems*, Renewable and Sustainable Energy Reviews, Vol. 22, pp. 168-186, 2013.

2. F. Vélez, J. Segovia, M. C. Martin, G. Antolin, F. Chejne, *A technical, economical and market review of organic Rankine cycles for conversion of low-grade heat for power generation*, Renewable and Sustainable Energy Reviews, Vol. 16, pp. 4175-4169, 2012.

3. B. Tchanche, G. Lambrinos, A. Frangoudakis, G. Papadakis, *Low-grade heat conversion into power using organic Rankine cycles – A review of various applications*, Renewable and Sustainable Energy Reviews, Vol. 15, pp. 3963-3979, 2011.

4. U. Larsen, O. Sightorsson, F. Haglind, *A comparison of advanced heat recovery power cycles in a combined cycle for large ships*, Energy, Vol. 74, pp. 260-268, 2014.

5. G. Shu, Y. Liang, H. Wei, H. Tian, J. Zhao, L. Liu, *A review of waste heat recovery on two-stroke IC engine aboard ships*, Renewable and Sustainable Energy Reviews, Vol. 19, pp. 385-401, 2013.

6. C. Sprouse, C. Depcik, *Review of organic Rankine cycles for internal combustion engine exhaust waste heat recovery*, Applied Thermal Engineering, Vol. 51, pp. 711-722, 2013.

7. T. Wang, Y. Zhang, Z. Peng, G. Shu, *A review of researches on thermal exhaust heat recovery with Rankine cycle*, Renewable and Sustainable Energy Reviews, Vol. 15, pp. 2862-2871, 2011.

8. D. Ziviani, A. Beyene, M. Venturini, *Advances and challenges in ORC systems modeling for low grade thermal energy recovery*, Applied Energy, Vol. 121, pp. 79-95, 2014.

9. S. Quoilin, S. Declaye, B. Tchanche, V. Lemort, *Techno-economic optimization of waste heat recovery Organic Rankine Cycles*, Applied Thermal Engineering, Vol. 31, pp. 2885-2893, 2011.

10. F. Calise, C. Capuozzo, A. Carotenuto, L. Vanoli, *Thermoeconomic analysis and off-design performance of an organic Rankine cycle powered by medium-temperature heat sources*, Solar Energy, Vol. 103, pp. 595-609, 2014.

11. S. Quoilin, R. Aumann, A. Grill, A. Schuster, V. Lemort, *Dynamic modeling and optimal control strategy of waste heat recovery Organic Rankine Cycles*, Applied Energy, Vol. 88, pp. 2183-2190, 2011.

12. D. Wei, X. Lu, Z. Lu, J. Gu, *Dynamic modeling and simulation of an Organic Rankine Cycle (ORC) system for waste heat recovery*, Applied Thermal Engineering, Vol. 28, pp. 1216-1224, 2008.

13. G. Manente, A. Toffolo, A. Lazzaretto, M. Paci, *An Organic Rankine Cycle off-design model for the search of the optimal control strategy*, Energy, Vol. 58, pp. 97-106, 2013.

14. I. Vaja, *Definition of an Object Oriented Library for the Dynamic Simulation of Advanced Energy Systems: Methodologies, Tools and Application to Combined ICE-ORC Power Plants*, PhD Thesis, Industrial Engineering Department, University of Parma, Italy, 2009.

15. A. Cavallini, *Notes from the lectures of "Renewable Energies"*, Padova, Italy, 2013 (in Italian).

16. D. Wang, X. Ling, H. Peng, L. Liu and L. Tao, *Efficiency and optimal performance evaluation of Organic Rankine Cycle for low grade waste heat power generation*, Energy, No. 50, pp. 343-352, 2013.

17. Z. Guzovic, P. Raskovic, Z. Blataric, *The comparison of a basic and a dual-pressure ORC (Organic Rankine Cycle): Geothermal Power Plant Velika Ciglena case study*, Energy, No. 76, pp. 175-186, 2014.

18. M. Soffiato, *Design and performance evaluation of an ORC system exploiting the waste heat of the main engines of an LNG carrier*, Master Thesis, Industrial Engineering Department, University of Padova, Italy, 2014.

19. M. Soffiato, C. A. Frangopoulos, G. Manente, S. Rech, A. Lazzaretto, *Design optimization of ORC systems for waste heat recovery on board a LNG carrier*, Energy Conversion and Management, 2014.

20. M. Soffiato, C. A. Frangopoulos, G. Manente, S. Rech and A. Lazzaretto, *Design and performance evaluation of an Organic Rankine Cycle system exploiting the low grade waste heat of the main engines in a LNG carrier*, ECOS 2014, Turku, Finland, 2014.

21. D. Malandrin, *Dynamic Model of an Organic Rankine Cycle System Exploiting Low Grade Waste Heat on board a LNG Carrier*, Master Thesis, Industrial Engineering Department, University of Padova, Italy, 2014.

22. A. Lazzaretto, *Notes from the lectures of "Energy Systems"*, Padova, Italy, 2012 (in Italian).

23. N. Mazzi, *Off-design performance model of Organic Rankine Cycle systems*, Master Thesis, Industrial Engineering Department, University of Padova, Italy, 2014.

24. L. Rossetto, *Notes from the lectures of "Applied Thermodynamics and Heat Transfer"*, Padova, Italy, 2012 (in Italian).

25. R. Serth, *Process Heat Transfer - Principles and applications*, Elsevier, 2007.

26. C. Bonacina, A. Cavallini, L. Mattarolo, *Trasmissione del calore*, Cleup Editore, Padova, Italy, 1989 (in Italian).

27. K. J. Åström, R. Bell, *Drum Boiler Dynamics*, Automatica, Vol. 36, pp. 363-378, 2000.

28. V. Gnielinski, *Capitolo Ga*, VDI-Wärmeatlas, Springer, 2006.

29. V. Anikeev, M. Fan, *Supercritical fluid technology for energy and environmental applications*, Elsevier, 2014.

30. A. R. Mumford, A. A. Markson, T. Ravese, *Characteristics of Cloth Filters on Coal Dust-Air Mixtures*, Transaction of the A.S.M.E. Vol. 62 No. 4, New York, USA, May 1940.

APPENDIX

In this work many correlations have been adopted, as mentioned in the description of the models of the power plant's components. The employed empirical equations can be divided into three correlation categories:

- heat flux;
- pressure drops;
- temperature factors.

The first ones are used to calculate the main heat exchange parameters, that are characteristic of the selected heat exchanger. Most of the necessary equations have been taken from literature, in particular they can be found in the book "Process Heat Transfer" [Serth, 10], where design procedure for the exchangers adopted in this work, all belonging to the shell and tube category, is deeply treated. The presented method is the *Bell-Delaware*: it allows to obtain the shell-side convective heat exchange coefficient and it is currently the most adopted one for shell and tubes in industrial applications [24]. In case of phase change, nucleate boiling and condensation correlations are also available in the mentioned text, for fluids that evaporate or condense into the shell side. To calculate the tube side forced convective coefficient, Gnielinski correlation [28] is employed, when there is not fluid phase change. Thanks to these equations, that allow to obtain the convective coefficients α' and α", it is possible to calculate the global heat transfer coefficient U_e, which is finally used to estimate the heat flux q exchanged by the working fluid and the hot or cold source.

The empirical equations for pressure drops that manifest into shell and tube heat exchangers are treated again by the *Delaware* method, in this case both for shell and for tube side.

At last, temperature factor's correlations are shown. For the perfect counter-current heat exchangers' configuration, the 1-1 one, this F_t factor is equal to one, right because there is the maximum possible heat exchange inside the device thanks to the selected layout. In the 1-2n and 2-4n cases, the fluid sent shell side exchanges respectively 1 and 2 times with the flow passing through the tubes respectively 2n and 4n times. For these last configurations, two proper correlations found in literature are presented, describing the reduction of the exchanged heat flux respect to the same case supposed with a layout for the device that allows the perfect counter-current for the two fluids.

One aim of this appendix is hence to define completely the equations that have been exposed in the previous chapters only as a generic function of certain variables and parameters involved in the system.

Once that all the equations have been made explicit, the design procedure for shell and tube heat exchanger is proposed.

In the last section, the way used to obtain the final form of the differential equations describing the mass and energy balances in the hot and cold drum is presented.

A.1 Heat transfer correlations

Here all the heat exchange empirical equations are presented. They refer to the *Bell-Delaware* method, developed at the University of Delaware and published in 1963, which allows to accurately design the shell and tube heat exchangers by manual calculation. This procedure is in contraposition to the *Stream Analysis* method that requires to computerize the procedure to finally obtain the geometry of the device together to the main useful coefficients. In this work, the selected version of Delaware method is the one recommended by Taborek [25], that treats the particular case of standard type E shells with single-cut segmental baffles and un-finned tubes, with different correlations about the heat exchange without and with phase change, be it nucleate boiling or condensation. Only for condensing fluid, both equations for smooth and for finned tubes can be found. The definition of the correlations is shown in the following.

A.1.1 Tube side heat transfer coefficients

Preheater, subcritical evaporator, condenser

Forced convection heat transfer correlations are adopted for the heat exchange involving the tube side flow. Given the selected design choices, according to which the fluids that represent the external sources without phase change are always sent through the pipes, except for the supercritical evaporator, Gnielinski correlation is applied for all the subcritical heat exchangers, where forced convection through the tubes is expected.

The generic function exposed in chapter 4 to develop is the next.

$$\alpha_{tube} = f(\dot{m}, T_m, p, D_i, L, N_{tt}, configuration) \tag{A.1}$$

Gnielinski proposed the following equations [10, 13] for the transition and turbulent regimes for motion inside pipes, generally accurate to within ±20%. The first presented is valid for $2300 < Re < 5.0 \cdot 10^6$ and $0.5 < Pr < 10^6$:

$$Nu = \frac{(\xi/8)(Re-1000)Pr}{1+12.7(\xi/8)^{1/2}(Pr^{2/3}-1)}\left[1 + (D_i/L)^{2/3}\right] \tag{A.2}$$

while the second one is advisable in the same range for $Re \geq 10{,}000$:

$$Nu = \frac{(\xi/8)(Re)Pr}{1+12.7(\xi/8)^{1/2}(Pr^{2/3}-1)}\left[1 + (D_i/L)^{2/3}\right] \tag{A.3}$$

The ξ term is the Darcy friction factor, expressed by the equation below:

$$\xi = (1.82 \log_{10} Re - 1.64)^{-2} \tag{A.4}$$

In order to calculate the proposed dimensionless factor, here useful equations are shown:

$$\mathrm{Pr} = \frac{c_p\,\mu}{\lambda} \tag{A.5}$$

$$Re = \frac{D_i\,\rho\,v}{\mu} \tag{A.6}$$

where v is the fluid velocity:

$$v = \frac{\dot{m}\,N_{pass}}{\rho\,\pi\,D_i\,N_{tt}} \tag{A.7}$$

N_{pass} = 1 → for 1-1 configuration (counter-current)
2 → for 1-2n configuration
4 → for 2-4n configuration

The fluid properties are evaluated by the following state equations:

$$[c_p, \mu, \lambda, \rho] = f(T, p) \tag{A.8}$$

At last, the definition of the generic Eq. (A.1) reported at the beginning of the paragraph can be completed by the following relation:

$$\alpha_{tube} = \frac{Nu\,\lambda}{D_i} \tag{A.9}$$

Supercritical evaporator

In the case of supercritical evaporator, the chosen solution consists in sending the evaporating working fluid inside tubes, instead of shell side as for the subcritical exchangers. Only few heat transfer correlations are available in literature, for the higher complexity of the supercritical phase change and its consequent fewer applications respect to the subcritical ones.

The selected correlation for our component model was developed and evaluated by Mokry et al. [29], thanks to a new set of heat transfer data and the latest thermo-physical properties of water provided by *NIST Refprop*, within the SCWRs (Super-Critical Water Reactor) nuclear power plant's operating range. The equation refers to the following working conditions: water, upward flow, vertical bare tubes with inside diameters of 3÷38 mm, pressure of 22.8÷29.4 MPa, mass flowrate of 200÷3000 kg/m^{2}s, heat flux of 70÷1250 kW/m^2. The proposed correlation can be also used for other fluids, taking into account that its accuracy might be less than the experimental conditions.

$$Nu = 0.0061\,Re^{0.904}\overline{\mathrm{Pr}}^{0.684}\left(\frac{\rho_{wall}}{\rho}\right)^{0.564} \tag{A.10}$$

The Reynolds and Prandtl numbers are obtained in the same way shown in the previous paragraph, by the Eqs. (A.5) to (A.7). In particular, Prandtl is calculated as average within the range of (t_{wall} - t_∞), which corresponds to the temperature difference between

wall and bulk. The two densities are evaluated at the evaporating fluid temperature to obtain ρ, at the wall temperature to define ρ_{wall}, by the use of state relations Eq. (A.8).

As for the subcritical cases, the forced convection heat transfer coefficient through the pipes is determined by the Eq. (A.9).

A.1.2 Shell side heat transfer coefficients

Introduction to Delaware method and equations for the geometric parameters

Bell-Delaware method has been selected for this work mainly because of the wide use in the industrial field and its applicability for hand calculation. The best alternative is the *Stream Analysis* method, which is more accurate because it is based on sound hydraulic principles that properly account for interactions among the shell side streams. This calculation procedure has not been considered because it requires a commercial software for computational calculation, with the values of many empirical parameters necessary for its implementation that are still proprietary. *Wills and Johnson* published a simplified complete version of this method, but useful only to calculate the shell side pressure drops, allowing a relatively simple solution of the hydraulic equations [25]. At last, *Kern* method has not been taken into account because of the superior accuracy of the Delaware method, at the only cost of a little major complexity, even if it has been widely used in the past years in the industrial field, mainly for its application simplicity [24].

Many versions of the Delaware method, with slight differences, have been published. In the following, the *Taborek* version [25] is reported.

To allow the resolution of the equations presented in the following paragraphs, all the relations needed for the requested geometric parameters are provided here. A simple scheme of the shell and tube exchanger's geometry is reported below, to graphically define some important parameters.

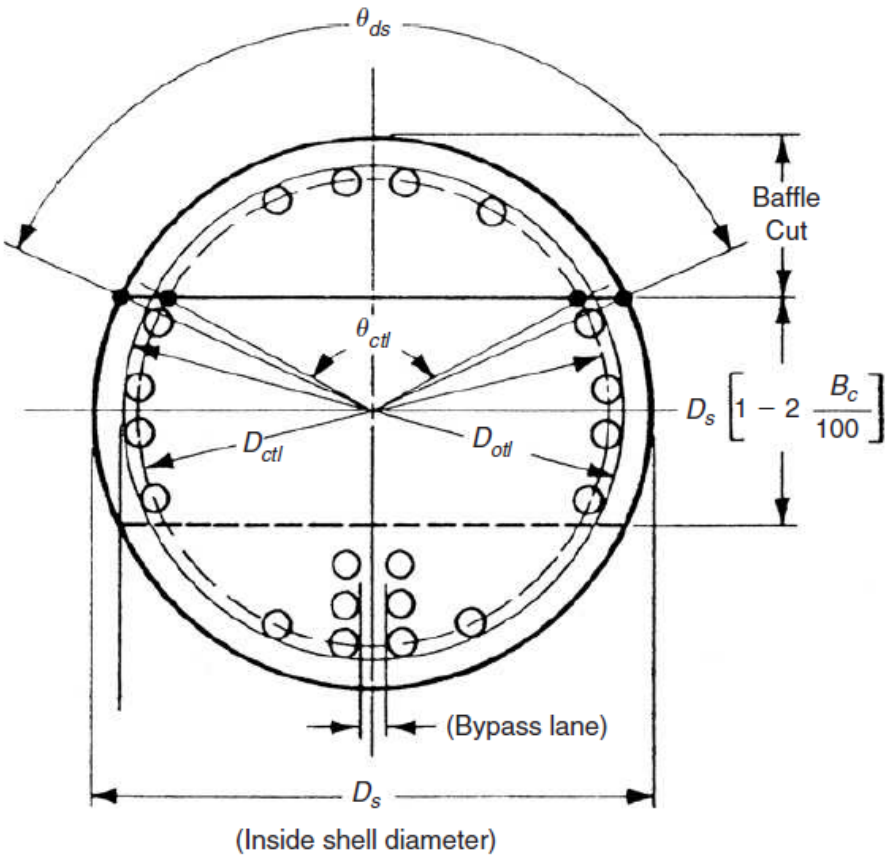

Figure A.4 *Segmental baffle geometry [25].*

In order to make more understandable the meaning of the equations, parameters are subdivided into the following five categories of geometric parameters [25].

1. The *cross-flow area* is the minimum flow area in one central baffle space at the center of the tube bundle. The related equation is the next one:

$$S_m = B\left[(D_s - D_{otl}) + \frac{(D_{otl}-D_e)}{\left(P_{T_{eff}}\right)}(P_T - D_e)\right] \quad \text{(A.11)}$$

where D_{otl} is the outer tube limit diameter, and:

$$\left(P_{T_{eff}}\right) = P_T \text{for square and triangular tube layouts}$$
$$\left(P_{T_{eff}}\right) = P_T/\sqrt{2} \text{for rotated square tube layout}$$

2. The *tube-to-baffle leakage area* is the total area of the gaps in one baffle, the holes through which the tubes pass, that are slightly larger than the pipes' diameter. Through this area, leakage fluid can pass to the next baffle space instead of crossing the tube bundle according to the defined path. Here, the total leakage area for one baffle is provided, as function of the fraction of tubes between the baffle tips, F_c, and consequently of the fraction in one baffle window, F_w.

$$S_{tb} = \frac{1}{2}\pi D_e \delta_{tb} N_{tt}(1 + F_c) \quad \text{(A.12)}$$

where

$$F_c = 1 - 2F_w \quad \text{(A.13)}$$

$$F_w = \frac{1}{2\pi}(\theta_{ctl} - sin\ \theta_{ctl}) \quad \text{(A.14)}$$

F_c is expressible also in this way:

$$F_c = 1 + \frac{1}{\pi}(sin\ \theta_{ctl} - \theta_{ctl}) \quad \text{(A.15)}$$

The fraction of tubes in one baffle window depends on the fractional area described by the circle radius D_{ctl} in the window. This is the diameter of the circle that passes through the centers of the outermost tubes in the bundle, and it is called central tube limit diameter. To deeply understand this parameter, see Figure A.4. In the following, relations about D_{ctl} and the relative angle θ_{ctl}, formed by the baffle edges and the center of the bundle, are provided.

$$D_{ctl} = D_{otl} - D_e \quad \text{(A.16)}$$

$$\theta_{ctl} = 2\arccos\left[\frac{D_s(1-2B_c)}{D_{ctl}}\right] \quad \text{(A.17)}$$

Regarding the tube-to-baffle clearance δ_{tb}, the TEMA (Tubular Exchanger Manufacturers Association) specifications are based on tube bundle assembly, tube vibration considerations and tube size. The assigned value for external diameter $D_e > 31.75$ mm is

$\delta_{tb} = 0.4$ mm, for $D_e \leq 31.75$ mm it is $\delta_{tb} = 0.4$ mm if the longest unsupported tube length in the exchanger is less of 0.9144 m, vice versa it is $\delta_{tb} = 0.2$ mm.

3. The *shell-to-baffle leakage area* is the frontal area described by the clearance between the shell, the bundle and the baffle, as shown in the next figure.

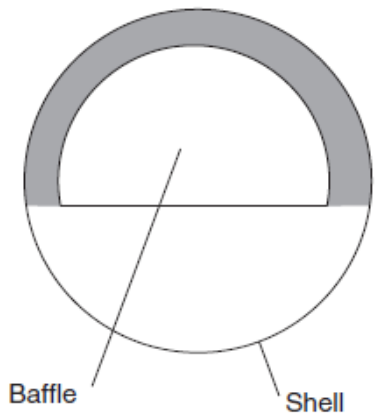

Figure A.5 *Shell-to-baffle leakage area [25].*

The relative equation is reported in the following, as function of the baffle window angle θ_{ds}, which relation is provided too, and of the shell-to-baffle clearance δ_{sb}

$$S_{sb} = D_s \delta_{sb} \left(\pi - \frac{1}{2} \theta_{ds} \right) \tag{A.18}$$

where

$$\theta_{ds} = 2 \arccos\ (1 - 2B_c) \tag{A.19}$$

The shell-to-baffle clearance is calculated by the following relation, defined by TEMA as linear function of shell diameter, according to the manufacturing tolerances for both the shell and the baffles.

$$\delta_{sb} = 0.0008 + 0.002 D_s \tag{A.20}$$

4. The *bundle bypass flow area* is the area between the outermost tubes and the shell, and it is represented by the equation that follows.

$$S_b = B(D_s - D_{otl}) \tag{A.21}$$

5. The *window flow area* is the result of the difference between the gross window area S_{wg}, between the shell and the baffle edge formed by the baffle cuts, and the surface occupied by the tubes in the window. Here the relations regarding these three quantities are reported.

$$S_{wg} = \frac{1}{8} D_s^2 (\theta_{ds} - \sin \theta_{ds}) \tag{A.22}$$

$$A_{tubes} = N_{tt} F_w \left(\frac{\pi D_e^2}{4} \right) \tag{A.23}$$

$$S_w = S_{wg} - A_{tubes} \tag{A.24}$$

Substituting into Eq. (A.24) from Eqs. (A.22) and Eqs. (A.23) gives:

$$S_w = \frac{1}{8} D_s^2 (\theta_{ds} - \sin \theta_{ds}) - \frac{1}{4} N_{tt} F_w \pi D_e^2 \tag{A.25}$$

In the following, useful ratios and combinations of the presented geometric parameters are reported, to use them into correlations for the correction factors.

$$r_s = \frac{S_{sb}}{S_{sb} + S_{tb}} \tag{A.26}$$

$$r_l = \frac{S_{sb} + S_{tb}}{S_m} \tag{A.27}$$

$$r_{ss} = N_{ss} / N_c \tag{A.28}$$

$$N_{ct} = (N_b + 1)(N_c + N_{cw}) \tag{A.29}$$

where N_{ss} is the number of pairs of sealing strips, N_c is the number of tube rows crossed between baffle tips and N_{cw} is the effective number of tube rows crossed in one baffle window. The last two geometric parameters are calculated as:

$$N_c = \frac{D_s(1-2B_c)}{P'_T} \tag{A.30}$$

$$N_{cw} = \frac{0.8\, B_c D_s}{P'_T} \tag{A.31}$$

where

$P'_T = P_T$ for square tube layout
$P'_T = P_T \cos\theta_{tp}$ for triangular tube layout (θ_{tp}=30°)
for rotated square tube layout (θ_{tp}=45°)

Preheater

Bell-Delaware method is applied to the shell side heat transfer coefficients calculation for the preheater, using the proposed correlations in order to define the following generic function, reported in chapter 4:

$$\alpha_{shell} = f\left(\dot{m}, T_m, p, T_{m,wall}, D_e, L, pitch, N_b, B_c, B/D_s, N_{tt}, N_{ss}, layout, config\right) \tag{A.32}$$

Delaware method is suitable for this component because of the behaviour of involved fluid, given that it does not change its phase inside the heat exchanger.

The calculation procedure consists in the use of empirical correlations for both heat transfer coefficient and friction factor, in the particular case of flow perpendicular to banks of tubes, approximated to the region between the baffle tips of shell and tube heat exchangers. The procedure is split into two parts:

- in the first step, the ideal heat transfer coefficient and pressure drops are obtained, by use of the ideal tube bank correlations;
- in the second step, a set of empirical correction factors allows to take into account of the deviations from ideal tube bank conditions, in particular to correct approximations about the perpendicular flux respect of the tubes, the baffle windows where the flux is totally not orthogonal, and the presence of leakage and bypass streams in the shell. There is also the possibility to differentiate the results in dependence of the fluid motion, be it laminar or turbulent.

In this work, the selected shell and tube heat exchangers are the standard type E in case of one shell-side pass, as for the preheater, type F for the two shell-side passes. All of them are characterised by single-cut segmental baffles and un-finned tubes (remember that for the condenser there is the possibility to choose between smooth and finned tubes, depending on the heat exchange requirements). For these design choices, the correlations proposed in the Taborek version of the Delaware method can be applied.

Ideal bank tube correlations

The correlations originally used in the development of the Delaware method are adopted here, recommended by Taborek. They are graphically represented by the next three figures, each of them corresponding to the most used tube bundle configurations, hence triangular pitch (θ=30°), square pitch (θ=90°), rotated square pitch (θ=45°).

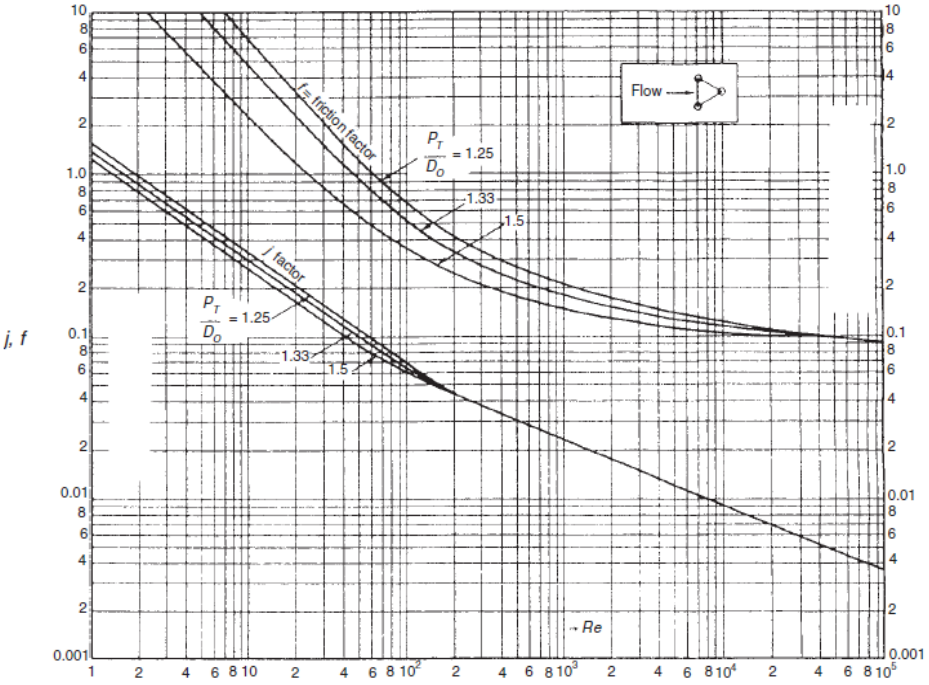

Figure A.1 *Ideal tube bank correlation for triangular pitch (θ = 30°) [25].*

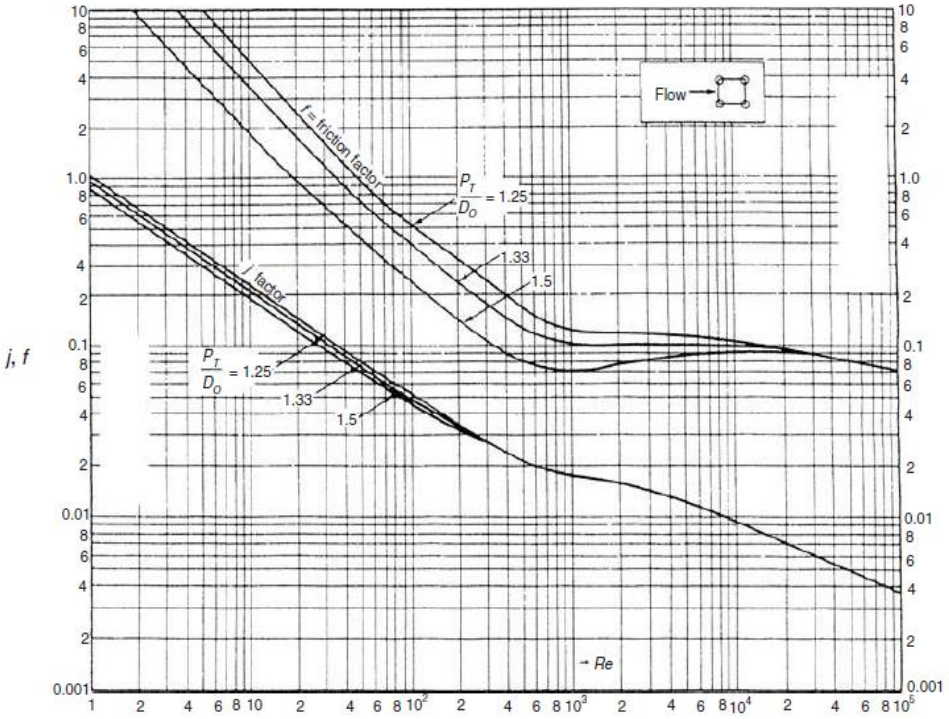

Figure A.2 *Ideal tube bank correlation for square pitch (θ = 90°) [25].*

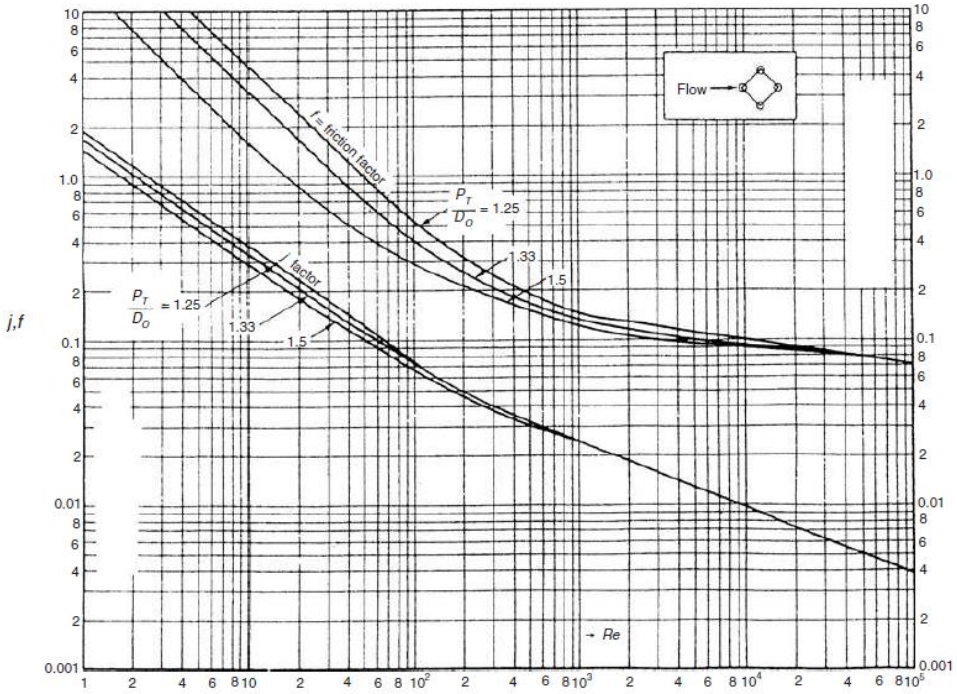

Figure A.3 *Ideal tube bank correlation for rotated square pitch (θ = 45°) [25].*

The mathematical expression of the graphically presented correlations is reported as

$$j = \frac{\alpha_{ideal} Pr^{2/3}}{c_p \, G \, \varphi} \tag{A.33}$$

which corresponds to the approximation of the curve fits from the figures shown above:

$$j = a_1 \left(\frac{1.33}{P_T/D_e}\right)^a (Re)^{a_2} \tag{A.34}$$

The approximate curve fit of the Fanning friction factor *f* is the following one:

$$f = b_1 \left(\frac{1.33}{P_T/D_e}\right)^b (Re)^{b_2} \tag{A.35}$$

The relations of the coefficients *a* and *b* are reported below:

$$a = \frac{a_3}{1+0.14(Re)^{a_4}} \tag{A.36}$$

$$b = \frac{b_3}{1+0.14(Re)^{b_4}} \tag{A.37}$$

The constants to be used in these equations are given by Table A.1.

Table A.1 *Constants for use with equations from (A.13) to (A.16) [25].*

Layout angle	Reynolds number	a_1	a_2	a_3	a_4	b_1	b_2	b_3	b_4
30°	10^5–10^4	0.321	−0.388	1.450	0.519	0.372	−0.123	7.00	0.500
	10^4–10^3	0.321	−0.388			0.486	−0.152		
	10^3–10^2	0.593	−0.477			4.570	−0.476		
	10^2–10	1.360	−0.657			45.100	−0.973		
	<10	1.400	−0.667			48.000	−1.000		
45°	10^5–10^4	0.370	−0.396	1.930	0.500	0.303	−0.126	6.59	0.520
	10^4–10^3	0.370	−0.396			0.333	−0.136		
	10^3–10^2	0.730	−0.500			3.500	−0.476		
	10^2–10	0.498	−0.656			26.200	−0.913		
	<10	1.550	−0.667			32.000	−1.000		
90°	10^5–10^4	0.370	−0.395	1.187	0.370	0.391	−0.148	6.30	0.378
	10^4–10^3	0.107	−0.266			0.0815	+0.022		
	10^3–10^2	0.408	−0.460			6.0900	−0.602		
	10^2–10	0.900	−0.631			32.1000	−0.963		
	10	0.970	−0.667			35.0000	−1.000		

Shell side heat transfer coefficients and correction factors

The forced convection heat transfer coefficient referred to the real case is obtained by the evaluation of five correction factors, to take into account of all phenomena that contribute to decrease exchange efficiency respect to a perpendicular flux through an ideal tube bank. The final form of the equation is shown here:

$$\alpha_{shell} = \alpha_{ideal}\,(J_C\,J_L\,J_B\,J_R\,J_S) \tag{A.38}$$

where the five correction factors can be grouped and expressed as *J* factor.

In the following, the main equations useful to calculate all these terms are exposed, explaining also their meaning [25]. All the geometric relations necessary to calculate the correction factors have been presented in the previous paragraph.

1. J_C is the correction factor for baffle window flow. The value 1.0 refers to the case of no tubes in the baffle windows. For very large baffle cuts the corresponding value is around 0.65, for small baffle cuts it is around 1.15. For well-designed heat exchangers the objective value should be close to 1.0. This correction factor is correlated to a single parameter, F_c, the fraction of tubes in cross flow between the baffle tips, that can be obtained by Eq. (A.27).

$$J_C = 0.55 + 0.72\,F_c \tag{A.39}$$

2. J_L is the correction factor for baffle leakage effects, it accounts for both the tube-to-baffle and the shell-to-baffle leakage fluxes. This term is inversely proportional to the leakage flowrate, and its value usually vary from 0.2 to 1.0, typically

between 0.7 and 0.8. A well designed heat exchanger should present at least 0.6 for J_L, otherwise it would be convenient to increase the baffle spacing or to think to other design solutions. This correction factor is correlated in terms of the area ratios r_s and r_l. The relations to obtain them are shown in the previous paragraph, Eqs (A.26) and (A.27).

$$J_L = 0.44\,(1 - r_s) + [1 - 0.44\,(1 - r_s)]\exp(-2.2\,r_l) \qquad \text{(A.40)}$$

3. J_B is the correction factor for bundle bypass effects, to consider the flowrate fraction that flows around the periphery of the tube bundle from one baffle window to the next, impeding a whole optimal exchange by the shell side flux and the other. The typical range of this factor's values is between 0.7 and 0.9. With lower values, it would be convenient to add a pair of sealing strips, to force the bypass stream back into the tube bundle. The correlation is expressed in terms of the presented geometric equations.

$$J_B = \exp[-C_J\,(S_b/S_m)\,(1 - (2r_{ss})^{1/3})] \qquad \text{for } r_{ss} < 0.5 \qquad \text{(A.41)}$$
$$J_B = 1.0 \qquad \text{for } r_{ss} \geq 0.5$$

where

$$C_J = 1.35 \qquad \text{for } Re < 100$$
$$C_J = 1.25 \qquad \text{for } Re \geq 100$$

4. J_R is the laminar flow correction factor. The typical range for laminar fluxes is between 0.4 and 1.0, while for $Re \geq 100$, hence for transient and turbulent flows, its value is equal to 1.0. This correction factor is correlated to the total number of tube rows crossed in the entire heat exchanger, N_{ct}, given by Eq. (A.29).

$$J_R = (10/N_{ct})^{0.18} \qquad \text{for } Re \leq 20 \qquad \text{(A.42)}$$
$$J_R = 1.0 \text{for } Re \geq 100$$

For $20<Re<100$, the factor is obtained by linear interpolation between the above values.

5. J_S is the correction factor for unequal baffle spacing in the inlet and outlet sections, where it is often larger in order to accommodate the nozzles and, in case of U-tube exchangers, the return bends. The typical range of values is between 0.85 and 1.0, the latter for equal spacing for all the baffles. The correction factor, which equation is shown below, depends so on the inlet and outlet baffle spacing, B_{in} and B_{out} respectively, the central baffle spacing, B, and the number of baffles, N_b. Note that for $B_{in}=B_{out}$ the J_S factor is equal to 1.0, according to the following relation.

$$J_S = \frac{(N_b-1)+(B_{in}/B)^{(1-n_1)}+(B_{out}/B)^{(1-n_1)}}{(N_b-1)+(B_{in}/B)+(B_{out}/B)} \qquad \text{(A.43)}$$

where

$$n_1 = 1/3 \qquad \text{for } Re < 100$$
$$n_1 = 0.6 \qquad \text{for } Re \geq 100$$

Subcritical evaporator

The design choice about the subcritical cycle of the ORC system under investigation in this work, be it characterised by one pressure level or two pressure levels where the first one is subcritical, consists in employing as evaporator a shell and tube heat exchanger type F, with horizontal tubes, operating in nucleate boiling regime. For these reasons, among the several correlations findable in literature, the ones for nucleate boiling on horizontal tubes have been selected. The generic function to be defined, exposed in chapter 4, is the following one:

$$\alpha_{shell} = f\left(\dot{m}, p, p_{cr}, T_{m,wall}, T_{sat}, D_e, pitch, L, B_c, \frac{B}{D_s}, N_{tt}, \rho, \mu, \lambda, g, layout, config\right) \quad \text{(A.44)}$$

For this component, the correlations of Mostinski and Palen [25] have been chosen, their application is suitable for this study. Monstinski correlation is expressed in the following way:

$$\alpha_{nb} = 1.167 * 10^{-8}\, P_c^{2.3} \Delta T_e^{2.333} F_P^{3.333} \quad \text{(A.45)}$$

P_c is the fluid critical pressure, in kPa, ΔT_e is the difference between the tube-wall temperature and the saturation temperature at system pressure

$$\Delta T_e = T_{wall} - T_{sat} \quad \text{(A.46)}$$

and F_P is the pressure correction factor, dimensionless, which expression has been improved by Palen:

$$F_P = 2.1\, P_r^{0.27} + [9 + (1 - P_r^2)^{-1}] P_r^2 \quad \text{(A.47)}$$

where $P_r = P/P_c$ is the reduced pressure.

The nucleate boiling is not the only phenomenon that manifests inside the subcritical evaporator, working fluid side. It is necessary to take into account also of the contribution provided by convection, therefore the following free convection correlation relative to a horizontal tube is applied.

$$Nu = \left\{0.60 + \frac{0.387(Ra)^{\frac{1}{6}}}{\left[1+(0.559/Pr)^{9/16}\right]^{8/27}}\right\}^2 \quad \text{(A.48)}$$

Ra is the dimensionless number of Rayleigh, composed by Prandtl number and Grashof number, which expressions are shown below.

$$Ra = Gr * Pr \quad \text{(A.49)}$$

$$Gr = \frac{g\beta \ |T_{wall} - T_\infty| \ L^3 \rho^2}{\mu^2} \quad \text{(A.50)}$$

where g is the gravitational acceleration, $T_\infty = T_{sat}$ in this case (it is the fluid temperature far from the solid surface), L is the characteristic length that corresponds to the tube's external diameter D_e for this heat exchanger, and β is the coefficient of volume expansion, which relation is reported here, for ideal gases.

$$\beta = \frac{1}{T_\infty} \quad \text{(A.51)}$$

The correlation (A.48) is valid in the range $10^{-5} \leq Ra \leq 10^{12}$. To obtain the free convection heat transfer coefficient, the following equation must be applied:

$$\alpha_{nc} = \frac{Nu \, \lambda}{D_e} \quad \text{(A.52)}$$

It must be noticed that the properties used to calculate α_{nc} refer to the liquid phase.

Once the two coefficients relatively to the nucleate boiling and the free convection have been calculated, they must be combined in order to obtain the global heat transfer coefficient for the evaporating fluid. For this purpose, Palen suggested the equation reported below.

$$\alpha_{evaporation} = \alpha_{nb} F_b + \alpha_{nc} \quad \text{(A.53)}$$

F_b is the factor that takes into account of the effect of the thermosyphon-type circulation in the tube bundle, correlated in terms of bundle geometry by the following empirical equation:

$$F_b = 1.0 + 0.1 \left[\frac{0.785 \, D_{otl}}{C_1 (P_T / D_e)^2 D_e} - 1.0 \right]^{0.75} \quad \text{(A.54)}$$

where

$C_1 = 1.0$ for square and rotated square tube layout
$C_1 = 0.866$ for triangular tube layout

Condenser

The heat exchanger chosen for the condensation in the investigated ORC system is the shell and tube type F, with horizontal tubes. Typically the large condensers are oriented horizontally because this allows to minimize the cost of support structures and it makes easy the maintenance operations. As for this case of study, the condensing vapour is most frequently sent shell side. The baffle E-shell and F-shell condensers are widely used and they represent the least expensive horizontal types. The baffles are cut vertically and notched at the bottom to allow the drainage of condensate. At last, an extra nozzle at the top of the shell, close to the rear head, is installed in order to vent non-condensable gases [25].

There are two possibilities for the exchanger in question, to select either smooth tubes or externally finned tubes, the latter in order to increase the heat exchange, if required by the system. Depending on this choice, the appropriate correlation will be selected.

The generic functions to define with the following equations are reported here, the first one regarding the smooth tube case, the second one for finned tubes:

$$\alpha_{shell} = f\left(\dot{m}_v, p, T_{sat}, L, N_{tt}, B_c, \frac{B}{D_s}, \rho_v, \rho_l, \mu_l, \lambda_l, g, layout, configuration\right) \quad \text{(A.55)}$$

$$\alpha_{shell} = f\left(\dot{m}_v, p, T_{sat}, T_{m,wall}, D_e, L, N_{tt}, B_c, \frac{B}{D_s}, \rho_v, \rho_l, \mu_l, \lambda_l, r, g, layout, config\right) \quad \text{(A.56)}$$

The condensate properties are evaluated at the following weighted average film temperature:

$$T_f = \beta_w T_{wall} + (1 - \beta_w) T_{sat} \quad \text{(A.57)}$$

where the weight factor β_w is recommended in literature to be between 0.5 and 0.75, the latter of which will be used in this study to obtain the final form of the equation, as follows.

$$T_f = 0.75\, T_{wall} + 0.25\, T_{sat} \quad \text{(A.58)}$$

The first presented correlation is the one relative to the smooth tubes. It comes from the modified Nusselt theory, from analysis of condensation on the external surface of a horizontal tube.

$$\alpha_{condensation,\,smooth\,tubes} = 1.52 \left[\frac{\lambda_l^3 \rho_l (\rho_l - \rho_v) g}{\mu_l^2 Re}\right]^{1/3} \quad \text{(A.59)}$$

For circular tube bundles, consisting on a number of vertical stacks of tubes, commonly used in condensers, Kern proposed the following expression of the Reynolds number, to account also for the effects of condensate drainage [25].

$$Re = \frac{4\,\Gamma^*}{\mu_l} \quad \text{(A.60)}$$

where

$$\Gamma^* = \frac{\dot{m}_v}{N_{tt}^{2/3} L} \quad \text{(A.61)}$$

The second presented correlation concerns the externally finned tubes, solution adoptable in order to increase the heat exchange in case of system necessity. Beatty and Katz proposed the next equation for this case, based on the equivalent diameter defined below, which allows the heat transfer from both fins and prime surface to be represented by a single average heat transfer coefficient [25].

$$\alpha_{condensation,\,finned\,tubes} = 0.689 \left[\frac{\lambda_l^3 \rho_l (\rho_l - \rho_v) g \eta_w (A_{tot}/L)}{\mu_l D_{eq} \Gamma^*}\right]^{1/3} \quad \text{(A.62)}$$

$$D_{eq} = \left(\frac{1.30\,\eta_f A_{fins} E^{-0.25} + A_{prime} D_e^{-0.25}}{\eta_w A_{tot}}\right)^{0.25} \quad \text{(A.63)}$$

where η_f is the fin efficiency, η_w is the weighted efficiency of finned surface, A_{fins} is the area of all fins, D_e is the root-tube diameter, and

$$A_{tot} = A_{fins} + A_{prime} \quad \text{(A.64)}$$

$$E = \pi \frac{(r_2^2 - r_1^2)}{2r_2} \quad \text{(A.65)}$$

with r_1 as root-tube radius, r_2 as fin radius.

In this work, the case of study is an Organic Rankine Cycle system which working fluid is a dry fluid, the refrigerant R245fa. The typical Rankine cycle for this kind of operating fluid is characterised by a superheated vapour exiting from the expander. Hence, the inlet vapour inside the condenser is not in saturated conditions, but it needs to be desuperheated before it is able to change its phase and condense. In this kind of systems, for this kind of fluids, this contribution to the heat exchange between cooling flux and the condensing one must be considered.

The condensation is still guaranteed for superheated vapours if the tubes' wall temperature is below the saturation temperature. To take into account of the desuperheating into the heat flux calculation the following equation must be applied, to involve both the latent heat of condensation and the sensible heat to cool the vapour from T_v to T_{sat}:

$$\dot{Q} = \dot{m}_v r + \dot{m}_v c_{p,v}(T_v - T_{sat}) = \dot{m}_v r_{global} \quad \text{(A.66)}$$

where r' is the equivalent latent heat

$$r_{global} = r\left(1 + \frac{c_{p,v}(T_v - T_{sat})}{r}\right) \quad \text{(A.67)}$$

The final expression of the condensation heat transfer coefficient hence is the following one.

$$\alpha_{desuperheating+condensation} = \alpha_{condensation}\left(\frac{r_{global}}{r}\right)^{1/4} \quad \text{(A.68)}$$

Supercritical evaporator

As mentioned above, for the supercritical evaporator the choice about where to send the two fluids is opposite respect to the other heat exchangers. In this case, the operative fluid is sent into the tubes, which are vertical in order to apply the correlation found in literature for supercritical evaporation, Eq. (A.10). Consequently, the hot fluid is sent shell side. Also in this case, the external source is different respect to the other cases: instead of

hot or cold water, respectively for hot and cold heat exchangers, here the available fluid is charge air coming from compressor and before entering the AC1 exchanger, precisely in point *a2* according to the configuration scheme in Figure (4.1). Given that the charge air pressure is higher than the atmospheric one, being absolute pressure in the range between 2.616 bar and 3.428 bar to be precise, the choice of shell and tube as adopted heat exchanger is still valid.

The adopted procedure for shell side fluid's parameters calculation is the same of the preheater. As for water in that case, indeed, here charge air does not change its phase, hence the equations proposed by Delaware method are still correct. To know more about the adopted procedure for supercritical evaporator, see the previous paragraph regarding preheater's shell side correlations.

A.2 Pressure drops correlations

In the following, empirical equations to describe pressure drops in shell and tube heat exchangers are reported. Tube side, pressure drops are calculated as function of geometry of the exchanger, of fluid density and velocity and of the *Darcy* friction factor. Shell side, the mentioned procedure is valid only for no phase change cases, therefore they fit to the preheater and to the supercritical evaporator, where cooling water and charge air are respectively sent inside and outside the bundle of tubes. In case of phase change, *Müller-Steinhagen* and *Heck* correlations are applied for the working fluid subcritical evaporation and *Chisholm* empirical equations for its condensation.

As for the heat exchange ones, pressure drops correlations are referred to standard type E shells with single-cut segmental baffles and un-finned tubes [25], but they are considered valid also for type F shells.

A.2.1 Tube side hydraulic calculations

The fluids sent tube side are water in case of preheater, subcritical evaporator and condenser, operative fluid in case of supercritical evaporator.

The generic function exposed in chapter 4 to develop is the next one.

$$\Delta p_{tube} = f\left(\dot{m}, f, s_g, \varphi, D_i, L, A, A_n, N_{pass}, N_s, configuration\right) \tag{A.69}$$

Pressure drops are calculated as sum of three terms:

1. Fluid friction pressure drop is given by the following equation, as function of the total flow path coincident to tube length multiplied by the number of tube side passes.

$$\Delta p_f = \frac{f\, N_{pass}\, L\, G^2}{2000\, D_i\, s_g\, \varphi} \tag{A.70}$$

where G is the specific mass flux in [kg/m^{2}s], s is the fluid specific gravity (equal to 1 for water) and φ the viscosity correction factor, both dimensionless:

$$G = \frac{\dot{m}}{A} \tag{A.71}$$

$$\varphi = \left(\frac{\mu}{\mu_w}\right)^x \tag{A.72}$$

with

$x = 0.14$ for turbulent flow
$x = 0.25$ for laminar flow

Darcy friction factor f is given by:

$$f = 0.4137\ Re^{-0.2585} \qquad \text{for turbulent flow, } Re \geq 3000 \text{ (A.73)}$$

$$f = \frac{64}{Re} \qquad \text{for laminar flow (A.74)}$$

It is worth noting that Eq. (A.73) fits well to commercial heat exchanger tubes, in the indicated range.

2. Pressure drop associated to tube entrance and exit and return losses are expressed by the following relation:

$$\Delta p_r = 5.0 * 10^{-4}\ \alpha_r \frac{G^2}{s} \qquad \text{(A.75)}$$

where α_r is the number of velocity heads allocated for minor losses on tube side, given in case of turbulent flow into regular tubes by:

$$\alpha_r = 2\ N_{pass} - 1.5 \qquad \text{(A.76)}$$

3. Pressure drop in inlet and outlet nozzles is calculated, for turbulent flow and $Re_n \geq 100$, as:

$$\Delta p_n = 7.5 * 10^{-4}\ N_s \frac{G_n^2}{s} \qquad \text{(A.77)}$$

where Re_n and G_n refer to the nozzle surface A_n, and N_s is the number of shells connected in series.

Finally, tube side total pressure drops, expressed in [Pa], are simply calculated as:

$$\Delta p_{tube} = \Delta p_f + \Delta p_r + \Delta p_n \qquad \text{(A.78)}$$

A.2.2 Shell side hydraulic calculations

Preheater, supercritical evaporator

The shell side fluids are working fluid in case of preheater, charge air in case of supercritical evaporator.

The generic function to make explicit is the following one:

$$\Delta p_{shell} = f\left(\dot{m}, f, s_g, \varphi, \rho, geometry, configuration\right) \qquad \text{(A.79)}$$

Also in this case, pressure drops are given by the sum of three terms. To obtain them, it is necessary to calculate as first the *Fanning* friction factor for ideal bank tube, f_{ideal} [25]. The way to estimate it is shown in the paragraph concerning preheater correlations, precisely the ideal bank tube ones. The useful relations are Eqs. (A.35) and (A.37), with the support of Table A.1 for the requested empirical coefficients.

In the following, the correlations necessary to obtain shell side pressure drops are presented, relatively to the three main pressure terms mentioned above. Given that these terms are related to precise geometric regions of the shell and tube, three simple schemes are shown before the equations in order to deeply understand which parts of the heat exchangers the different kinds of pressure drops are referred to.

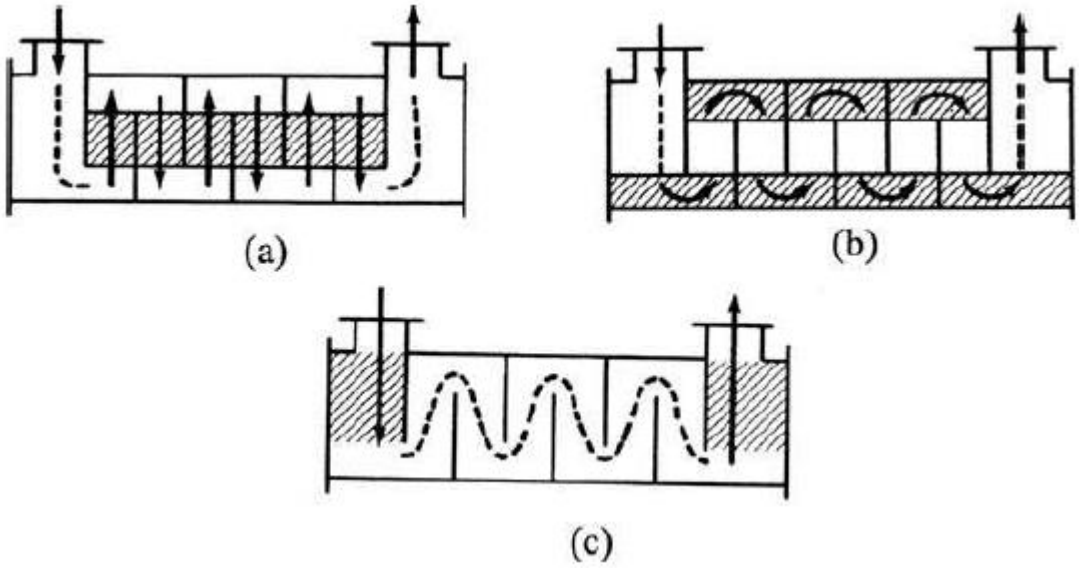

Figure A.4 *(a) Cross-flow region between baffle tips in the central baffle spaces; (b) window-flow region; (c) cross-flow region for inlet and outlet baffle spaces [25].*

Shell side correction factors for pressure drops

The adopted pressure drop correction factors are three, and they are analogous to the heat transfer ones. Here they are presented.

1. R_L is the correction factor for baffle leakage, expressed as function of the area ratios r_s and r_l, given by Eqs. (A.26) and (A.27):

$$R_L = \exp[-1.33(1 + r_s)(r_l)^p \quad \text{(A.80)}$$

where

$$p = 0.8 - 0.15(1 + r_s) \quad \text{(A.81)}$$

2. R_B is the correction factor for bundle bypass flow, depending on the ratio r_{ss} obtainable by Eq. (A.28):

$$R_B = \exp[-C_R\ (S_b/S_m)\ (1 - (2r_{ss})^{1/3})] \qquad \text{for } r_{ss} < 0.5 \quad \text{(A.82)}$$
$$R_B = 1.0 \qquad \text{for } r_{ss} \geq 0.5$$

where

$$C_R = 4.5 \qquad \text{for } Re < 100$$
$$C_R = 3.7 \qquad \text{for } Re \geq 100$$

3. R_S is the correction factor for unequal baffle spacing:

$$R_S = 0.5\left[\left(\frac{B}{B_{in}}\right)^{2-n_2} + \left(\frac{B}{B_{out}}\right)^{2-n_2}\right] \quad \text{(A.83)}$$

where

$$n_2 = 1.0 \qquad \text{for } Re < 100$$
$$n_2 = 0.2 \qquad \text{for } Re \geq 100$$

Practical ranges are: from about 0.1 to 1.0 for R_L, with typical values between 0.4 and 0.6; from about 0.3 and 1.0, typically between 0.4 and 0.7, for R_B; from about 0.3 and 1.0, with the latter corresponding to the case of perfectly equal baffle spacing, for R_S.

Shell side pressure drops calculation

As mentioned above, shell side pressure drops are calculated as sum of three terms as well:

1. The pressure drop in one central baffle space (Figure A.4 (a)) is equal to the ideal bank tube pressure drop corrected for leakage and bypass effects. This is because between baffle tips the flow pattern is considered as pure cross flow. The ideal bank tube pressure drop is the following one:

$$\Delta p_{ideal} = \frac{2\, f_{ideal}\, N_c\, G^2}{\rho\, \varphi} \quad \text{(A.84)}$$

where

$$G = \frac{\dot{m}}{S_m} \quad \text{(A.85)}$$

$$N_c = \frac{D_s(1-2\,B_c)}{P'_T} \quad \text{(A.86)}$$

with $\dot{m}$ as the total shell side mass flow rate, S_m as the cross-flow area in one central baffle space at the center of the tube bundle, given by Eq. (A.11), N_c as the number of tube rows crossed by the fluid between baffle tips (see Figure A.4), and

$$P'_T = P_T \text{ for square tube layout}$$
$$P'_T = P_T \cos\theta_{tp} \qquad \text{for triangular tube layout } (\theta_{tp} = 30°)$$
$$\text{for rotated square tube layout } (\theta_{tp} = 45°)$$

Finally, the pressure drop in all central baffle spaces is calculated by multiplying the ideal bank tube pressure drop by the number of central baffle spaces, adjusting the result by the adoption of leakage and bypass correction factors, given by Eqs. (A.80) and (A.82):

$$\Delta p_c = (N_b - 1)\Delta p_{ideal} R_L R_B \quad \text{(A.87)}$$

2. The pressure drop in baffle windows (Figure A.4 (b)), in which fluid changes its direction for 180°, is given as well as function of an ideal pressure drop for turbulent flow, hence for *Re* ≥ 100, corrected then for leakage effects.

$$\Delta p_{w,ideal} = \frac{(2+0.6N_{cw})\dot{m}^2}{2\rho\, S_m\, S_w} \tag{A.88}$$

where S_w is the window flow area, given by Eq. (A.24), and N_{cw} is the effective number of tube rows crossed in one baffle window:

$$N_{cw} = \frac{0.8\, B_c\, D_s}{P_T'} \tag{A.89}$$

The empirical factor 0.8 takes into account the fact that the flow in a baffle window is partly perpendicular and partly parallel to the tubes.

Pressure drop in all baffle windows is hence obtained, by applying the proper correction factor with the following equation:

$$\Delta p_w = N_b \Delta p_{w,ideal} R_L \tag{A.90}$$

3. The pressure drop in entrance and exit baffle spaces (Figure A.4 (c)) is not equal to the one that manifests in the central baffles of the heat exchanger, because of the different baffle spacing due to necessity to accommodate the shell side nozzles. For the same reason, the number of tubes crossed by fluid is not the same. At last, leakage effects do not affect inlet and outlet baffle spaces because not yet developed.

   Due to these several differences respect to the central baffle spaces, the pressure drop here is calculated by considering the different geometry that fluid encounters, and the corrections to the ideal case given by Eq. (A.84) are about taking into account of bypass effects and the eventual unequal spacing.

$$\Delta p_e = 2\Delta p_{ideal}\left(1 + \frac{N_{cw}}{N_c}\right) R_B R_S \tag{A.91}$$

Shell side total pressure drops, expressed in [Pa], are hence obtained as the following sum:

$$\Delta p_{shell} = \Delta p_c + \Delta p_w + \Delta p_e \tag{A.92}$$

Subcritical evaporator

In case of phase change, the correlations to adopt are different. In particular, for the subcritical evaporator, the choice made is about the Müller-Steinhagen and Heck correlation [25]. It refers to the case of two-phase flow through circular tubes, and here is given as reformulation in the Chisholm equation format, providing the following homogeneous liquid two-phase multiplier:

$$\phi_{LO}^2 = Y^2 x^3 + [1 + 2x(Y^2 - 1)](1 - x)^{\frac{1}{3}} \tag{A.93}$$

where x is the vapour mass fraction and Y is the Chisholm parameter, expressed as

$$Y = \left[\frac{\left(\frac{\Delta p_f}{L}\right)_{VO}}{\left(\frac{\Delta p_f}{L}\right)_{LO}}\right]^{0.5} \tag{A.94}$$

The Chisholm parameter can be rewritten in the following alternative form:

$$Y = \left(\frac{\rho_l}{\rho_v}\right)^{0.5} \left(\frac{\mu_v}{\mu_l}\right)^{\frac{n}{2}} \tag{A.95}$$

with n = 0.2585 for commercial tubes belonging to shell and tube heat exchangers.

It is worth noting that for x = 0, hence all liquid flow, $\phi_{LO}^2 = 1$ and the negative two-phase pressure gradient reduces to the homogeneous liquid $\left(\frac{\Delta p_f}{L}\right)_{LO}$, while for x = 1, that means all vapour flow, $\phi_{LO}^2 = Y$ and the gradient reduces to the homogeneous vapour $\left(\frac{\Delta p_f}{L}\right)_{VO}$.

Pressure drop, for subcritical evaporation case, is hence expressed by the next equation:

$$\left(\frac{\Delta p_f}{L}\right)_{tp} = \phi_{LO}^2 \left(\frac{\Delta p_f}{L}\right)_{LO} \tag{A.96}$$

where L is the heat exchanger length. Notice that, to obtain the final pressure drop, it is necessary to calculate before the pressure drops in the homogeneous liquid phase, to multiply them then by the negative pressure gradient ϕ_{LO}^2 for total flow as liquid. To do this, the procedure reported in the previous paragraph for no phase change calculation must be applied. Precisely, the homogeneous liquid phase pressure drop is obtainable by Eq. (A.92).

In recent studied cited by Serth [25], Müller-Steinhagen and Heck correlation has been compared with the Friedel one, regarded as the most reliable general method for computing two-phase pressure losses, finding superior performance despite being a simpler method.

Condenser

The choice made for condensation pressure drop is the Chisholm correlation [25], given by:

$$\phi_{LO}^2 = 1 + (Y^2 - 1)\left\{B[x(1-x)]^{\frac{2-n}{2}} + x^{2-n}\right\} \tag{A.97}$$

where B = 0.25 and n = 0.46, referring to horizontal cross flow in stratified or stratified spray flow regimes. In the same way of the subcritical evaporator, presented above, the Chisholm parameter is obtained by Eqs. (A.94) and (A.95), while the condensation pressure drop is expressed by (A.96).

A.3 Temperature factor

The heat flux calculation relatively to a heat exchanger can be pursued by two simple kinds of equations, precisely by considering the product between mass flowrate and the enthalpy variation, be them related to hot or cold fluid, or by the following simple formula:

$$\dot{Q} = UA\,\Delta T_{ml} \tag{A.98}$$

The last term of the equation, ΔT_{ml}, is the logarithmic mean temperature difference, which meaning consists in describing the temperature variation of the hot and cold fluids inside a heat exchanger, in the general case.

The best exchange conditions manifest when the two fluxes are perfectly in counter-current. If the heat exchanger has the possibility to set this kind of configuration for the fluids, the related equation to obtain the logarithmic mean temperature difference is the following one:

$$\Delta T_{ml,CC} = \frac{(T'_{in} - T''_{out}) - (T'_{out} - T''_{in})}{\log\left(\frac{T'_{in} - T''_{out}}{T'_{out} - T''_{in}}\right)} \tag{A.99}$$

To describe all the other conditions, that are all characterised by an inferior value of the heat flux because of the worse exchange between the fluids, in Eq. (A.98) the ΔT_{ml} factor is split into two: the one described by Eq. (A.99), and the temperature factor F_t. The latter is a dimensionless term, which possible values are between 0 and 1, the last one representing the perfect counter-current condition. The function of the temperature factor, indeed, is to reduce the value of $\Delta T_{ml,CC}$ in order to estimate the realistic heat exchange between the fluids, in all possible situations.

The temperature factor is defined as follows:

$$F_t = \frac{\Delta T_{ml}}{\Delta T_{ml,CC}} \tag{A.100}$$

It is worth noting that according to this relation as well the $\Delta T_{ml,CC}$ is the maximum driving force for this process. To precisely define F_t about the various heat exchangers configurations, correlations are necessary. The relations adopted in this work for shell and tube heat exchangers are findable in literature, in this case they are taken from the A.S.M.E. publication of Mumford et al. [30]. The empirical correlations are proposed as function of the two following dimensionless parameters:

$$P = \frac{T_{out,tube} - T_{in,tube}}{T_{in,shell} - T_{in,tube}} \tag{A.101}$$

$$R = \frac{T_{in,shell} - T_{out,shell}}{T_{out,tube} - T_{in,tube}} \tag{A.102}$$

Four exchange conditions, hence four shell and tube configurations, must be distinguished:

1. *Perfect counter-current*, *1-1 configuration*: with one shell side pass and one tube side pass, in this case the driving force is the maximum one, indeed ΔT_{ml} is equal to $\Delta T_{ml,CC}$, giving back the value $F_t = 1$;
2. *1-2 configuration*: characterised by one shell side pass and two tube side passes, the relative equation for the temperature factor is the next one

$$F_{t,1-2} = \frac{\frac{(R^2+1)^{\frac{1}{2}}}{R-1}\log_{10}\frac{1-P}{1-PR}}{\log_{10}\frac{\left(\frac{2}{P}\right)-1-R+(R^2+1)^{\frac{1}{2}}}{\left(\frac{2}{P}\right)-1-R-(R^2+1)^{\frac{1}{2}}}} \tag{A.103}$$

3. *2-4 configuration*: in this case the heat exchanger presents two shell side passes and four tube side passes, the relative correlation is here reported

$$F_{t,2-4} = \frac{\frac{(R^2+1)^{\frac{1}{2}}}{2(R-1)}\log_{10}\frac{1-P}{1-PR}}{\log_{10}\frac{\left(\frac{2}{P}\right)-1-R+\frac{2}{P}[(1-P)(1-PR)]^{\frac{1}{2}}+(R^2+1)^{\frac{1}{2}}}{\left(\frac{2}{P}\right)-1-R+\frac{2}{P}[(1-P)(1-PR)]^{\frac{1}{2}}-(R^2+1)^{\frac{1}{2}}}} \tag{A.104}$$

4. *1-4 configuration*: the exchanger's layout is characterised by one shell side pass and four tube side passes. Instead of the last cases, here another parameter is used, defined below as

$$V = \frac{T_{out,tube}-T_{in,tube}}{4\,T_{in,shell}-(T_{in,tube}+2\,T_i+T_{out,tube})} \tag{A.105}$$

where T_i is the intermediate temperature of the tube-side fluid when it leaves the second and enters the third tube-side pass. It is obtained by a trial and error solution of:

$$\left(\frac{T_i-T_{in,tube}}{T_{out,tube}-T_i}\right)^{(4R^2+1)^{\frac{1}{2}}} = \frac{1+V[(4R^2+1)^{\frac{1}{2}}-2R]}{1-V[(4R^2+1)^{\frac{1}{2}}+2R]} \tag{A.106}$$

Finally, the temperature factor's correlation for 1-4 shell and tube is:

$$F_{t,1-4} = \frac{\frac{(4R^2+1)^{\frac{1}{2}}}{2(R-1)}\log_{10}\frac{1-P}{1-PR}}{log\frac{1+V[(4R^2+1)^{\frac{1}{2}}-2R]}{1-V[(4R^2+1)^{\frac{1}{2}}+2R]}} \tag{A.107}$$

The three empirical relations about F_t calculation shown above, Eqs. (A.103), (A.104) and (A.107), are graphically representable as function of the used parameters P and R, as follows.

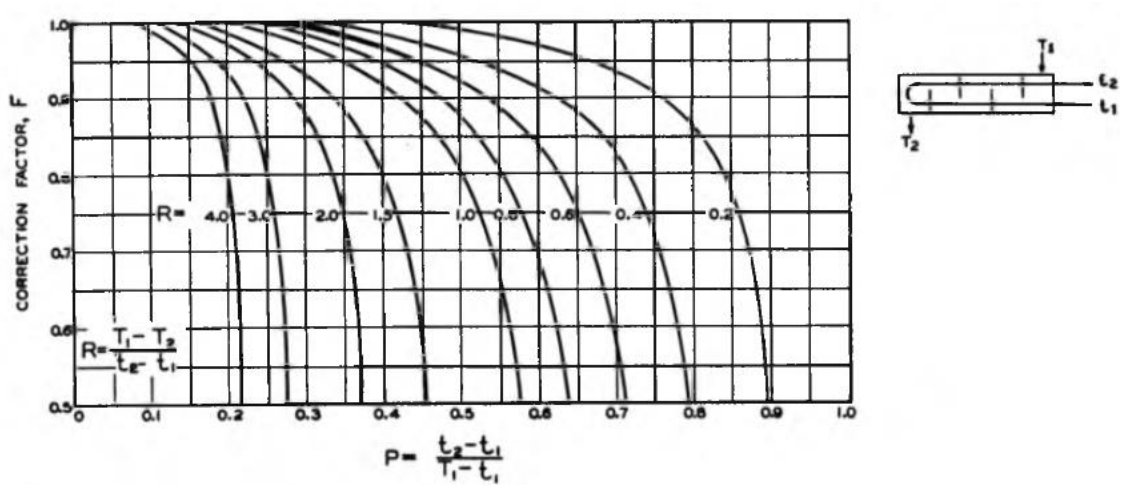

Figure A.5 *Temperature Factor plot for one shell pass and two or four tube passes (1-2, 1-4) [30].*

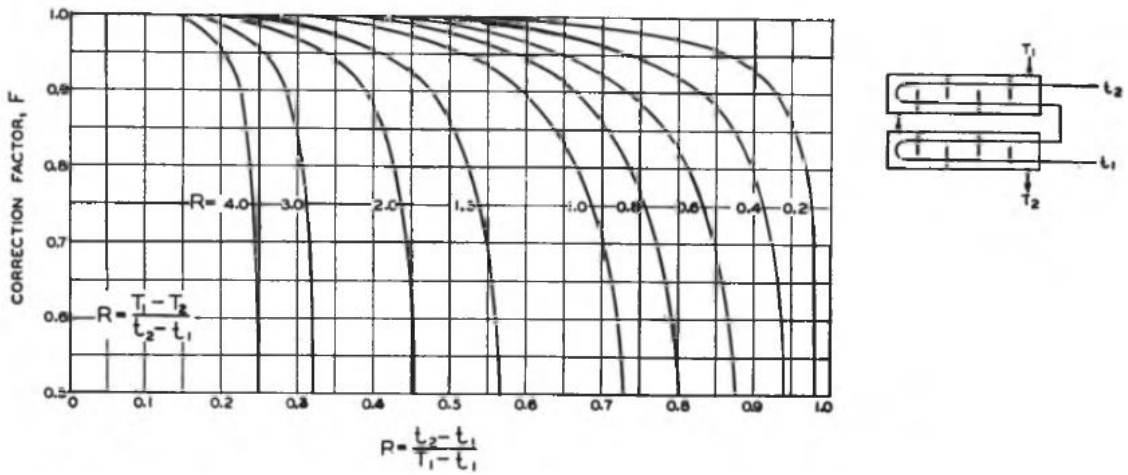

Figure A.6 *Temperature Factor plot for two shell passes and four tube passes (2-4) [30].*

The final form of the heat flux relation, represented above by Eq. (A.98), is hence the following one:

$$\dot{Q} = UA\,\Delta T_{ml,CC}\,F_t \tag{A.108}$$

A.4 Design procedure for shell and tube heat exchangers

In this appendix, the shell and tube design procedure adopted in this work is presented. The main purpose consists in determining all the geometric parameters of the heat exchanger, the effective heat flux and the pressure drops related to both fluids. One secondary aim is the achievement of the minimum of both the investment cost and the operating expense, depending more on the selected geometry than on available hot and cold sources.

There are three constraints to satisfy by the sizing of the heat exchanger:

- $\dot{Q}_{effective} \geq \dot{Q}_{required}$
- $\Delta p_{tot,tube} \leq \left(\Delta p_{tot,tube}\right)_{max}$
- $\Delta p_{tot,shell} \leq \left(\Delta p_{tot,shell}\right)_{max}$

The choice about the side where the considered flux should be sent must take into account of the main features of the fluid, such as pressure, corrosiveness, fouling and if the related cleaning is mechanical or chemical, viscosity, recommended velocities and flow regimes, available pressure drops and the achievement of the maximum heat exchange. In this work, it has been chosen to send shell side the operating fluid for preheater, subcritical evaporators and condenser because of the higher developed turbulence, which allows to reach high heat exchange coefficients. The choice regarding the supercritical evaporator is different, with the working fluid sent into tubes, in order to respect the empirical correlation determined by Mokry et al. and described by Eq. (A.10).

Known data useful for sizing are commonly the two mass flowrates, the two inlet temperatures, pressures and one of the outlet temperatures. From pressures and temperatures it is possible to evaluate the fluids' properties, here pursued by the software REFPROP that is useful also to call properties directly to MATLAB Simulink environment. The required ones are mainly specific enthalpy, specific heat at constant pressure, density, viscosity and thermal conductivity.

For the project purposes, the maximum pressure drops for both fluids are already fixed. To determine the required heat flux, the next equation is applied, before sizing:

$$\dot{Q}_{required} = \dot{m}' \left(h'_{in} - h'_{out}\right) = \dot{m}'' (h''_{out} - h''_{in}) \tag{A.109}$$

that can be easily turned, in case of no change phase for the considered fluid, into

$$\dot{Q}_{required} = \dot{m}' c'_p \left(T'_{in} - T'_{out}\right) = \dot{m}'' c''_p (T''_{out} - T''_{in}) \tag{A.110}$$

As mentioned before, usually one outlet temperature is unknown. To calculate it, the same equation is applied, making it explicit. Once all the temperatures are available, counter-current logarithmic mean difference $\Delta T_{ml,CC}$ and temperature factor F_t must be determined by the correlations shown in Appendix A.3, evaluating also if it is necessary to adopt a counter-current heat exchanger.

After that these first simple steps are completed, design procedure can be carried on. Valid methods are the so called U-ΔT and ε-NTU. The adopted method here is the first one, presented through the following simple steps.

1. The global heat transfer coefficient, external side, $U_{e,1}$ has to be estimated, as first approximation. Its value depends on the kind of exchanging fluids and the relative pressures. It is possible to find that value in literature or to set it by the experience;
2. Estimate the external exchange surface by

$$S_e = \frac{\dot{Q}_{required}}{U_e \, \Delta T_{ml}} \tag{A.111}$$

3. Select the first geometric elements, precisely the number of shell side and tube side passes, the external and internal diameters D_e and D_i of the tubes, or one of them together with the tube thickness *s*, the tube bundle layout and the pitch distance P_T (remember the constraint $1.25 \leq P_T/D_e \leq 1.50$); choose the tube material and consequently the optimal inlet fluid velocity v_i, among the suggested ones, useful to be economic and avoid fouling and erosion phenomena;
4. Calculate the internal exchange area, by the continuity equation, and the number of tubes, as follows

$$S_i = \frac{\dot{m}_i}{\rho_i v_i} \tag{A.112}$$

$$N_{tt} = N_{tube\ passes} \frac{4}{\pi D_i^2} S_i \tag{A.113}$$

5. Determine the shell diameter, through the next steps:
   a. Estimate the central tube limit diameter D_{ctl} (see Figure A.4)
   b. Use the diagram in Figure A.7 to evaluate the parameter φ_n, that is function of D_{ctl} and $N_{tube\ passes}$
   c. Calculate the number of tubes allocable in the same diameter, for one single tube side pass, by

$$(N_{tt})_1 = \frac{N_{tt}}{1-\varphi_n} \tag{A.114}$$

   d. Obtain finally the required diameter, as follows

$$D_{ctl} = \left[\frac{C P_T^2 (N_{tt})_1}{0.78}\right]^{0.5} \tag{A.115}$$

   where

$$C = 1.0 \text{for square and rotated square tube layout}$$
$$C = 0.866 \text{for triangular tube layout}$$

   If the result is different from the estimation, repeat the procedure from point a;

6. Calculate the shell internal diameter D_s, by the next simple sum

$$D_s = D_{ctl} + D_e + \delta_{stb} \tag{A.116}$$

where δ_{stb} is the shell-to-tube bundle clearance, to define by the use of the diagram shown in Figure A.8;

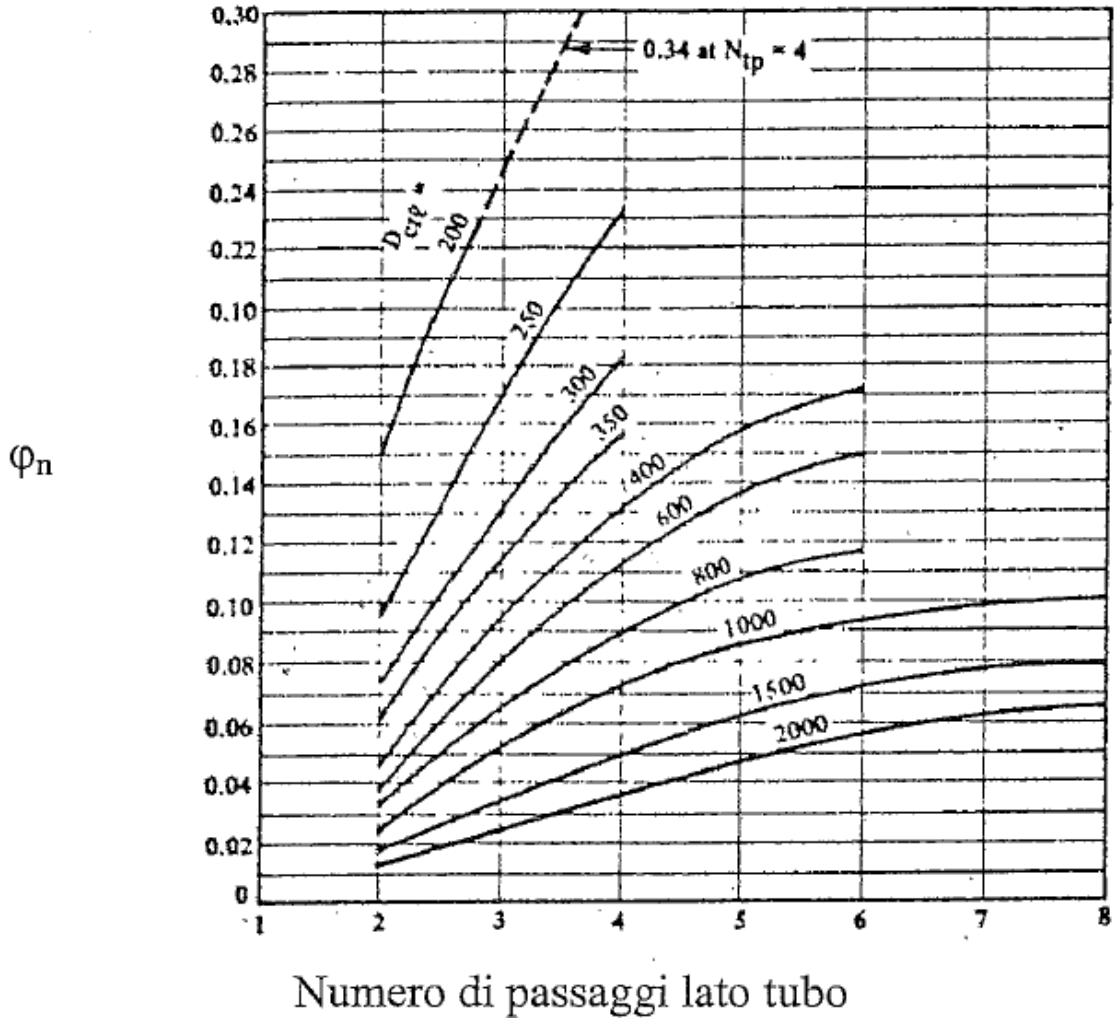

Figure A.7 φ_n *as function of* D_{ctl} *and the tube side passes [24].*

7. Set the distance q between baffles, respecting the constraint $0.2 \leq q/D_e \leq 1.0$ in order to allow them to support the tubes properly and leave enough space to the installation of inlet and outlet nozzles;
8. Determine the shell side and tube side convective heat transfer coefficients α_e and α_i, by adoption of the appropriate correlations (see Appendix A.1);
9. Calculate the effective global heat transfer coefficient U_e, and check if its value is close or far respect to the previously estimated $U_{e,1}$. In the second case, use the new value to repeat the procedure from point 1. in order to obtain better final results;

10. Finally, determine the heat flux $\dot{Q}_{effective}$ and the shell side and tube side pressure drops $\Delta p_{tot,shell}$ and $\Delta p_{tot,tube}$, the latter ones by proper correlations (see Appendix A.2). If their values do not satisfy the three constraint reported at the beginning of this Appendix A.4, the procedure must be carried out again, changing the design choices to take at point 3. and 7.
    At last, required tube length L can be calculated as follows:

$$L = \frac{S_e}{\pi D_e N_{tt}} \tag{A.117}$$

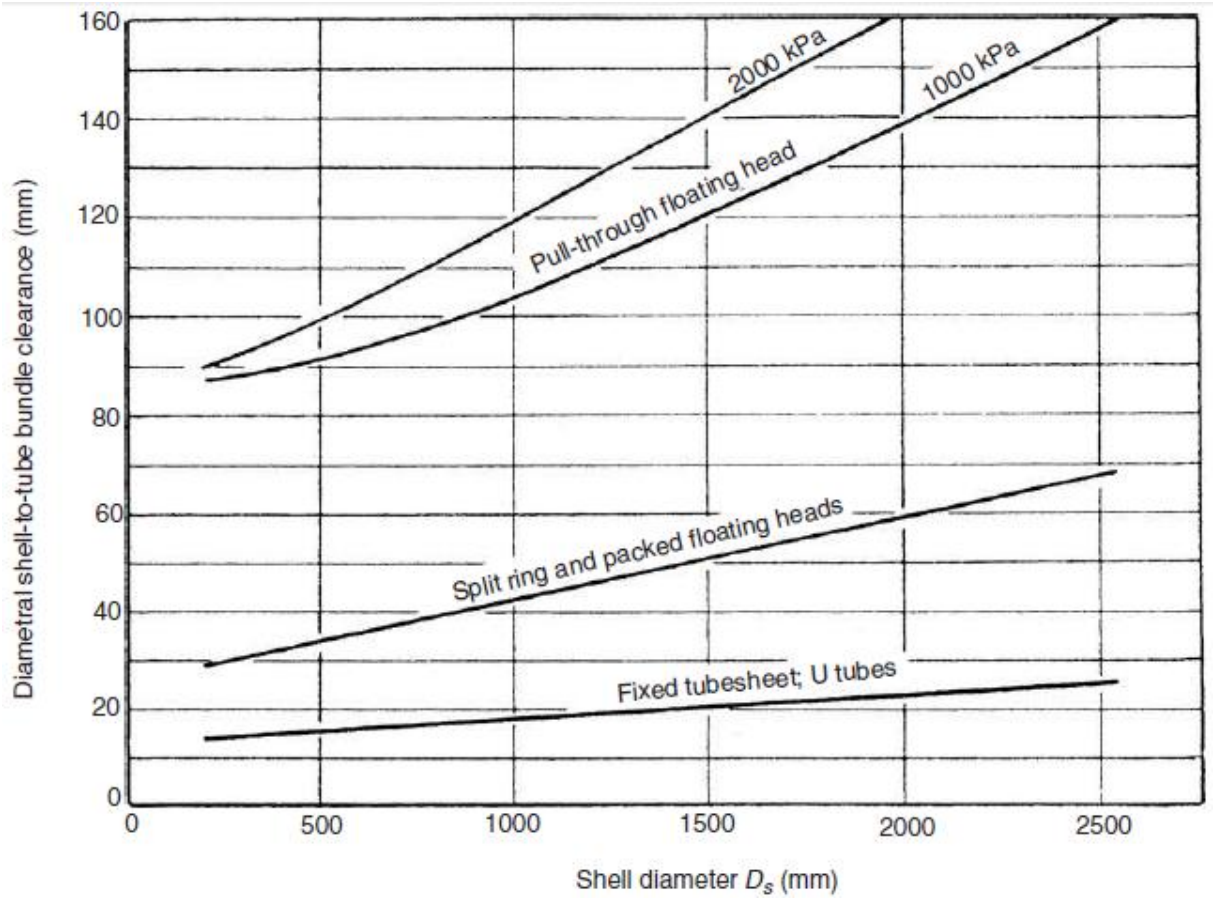

Figure A.8 *Shell-to-tube bundle clearance δ_{stb} as function of shell diameter D_s [25].*

A.5 Dynamic mass and energy balance equations

In Section 4.4, the mass and energy balances of the two capacities of the model, the hot drum and the cold drum, have been presented through their final form. In this appendix the way to obtain these mentioned equations is proposed.

The main function of the two drums, from the model viewpoint, consists in applying the balance over time of the physical quantities. To do this, inside the Capacity model there will be differential equations, which through the calculation of the parameters of interest at the successive instant will be carried out. The results can be managed then by a control system to modify tuning variables inside the model in order to reach designed goals, for example a certain liquid level inside the accumulator by the pump's rotational speed.

In order to accomplish the purposes of the model's capacities, useful properties are obtained by evaluation of pressure for all liquid phase and for all vapour phase. Pressure and temperature of the outlet fluxes are assumed to be coincident to the ones of the inlet fluxes, that is true for single phase fluids, and they are function of the inlet thermodynamic conditions and of inlet and outlet mass flowrates (the in-depth analysis of the dynamic modelling techniques is presented in Chapter 3). The required properties, called into Simulink from REFPROP, are for both phases specific enthalpy h, specific internal energy u, density ρ and specific heat at constant volume c_v. By the same program, it is also possible to call the following two useful derivatives: $\frac{d\rho}{dp}$ and $\frac{d\rho}{dT}$.

As explained above, inside a Capacity model mass and energy balances are carried on, calculating time by time the new properties and parameters of interest, taking also into consideration eventual constraints. In this case of study, given that the capacities are a hot drum that is actually represented by a subcritical evaporator and a cold drum that corresponds to an accumulator for the ORC system, the existing constraint to satisfy is the volume conservation, which is managed by Eq. (3.125). Here, the way to obtain the final form of the two balances expressed by Eqs. from (3.113) to (3.118) is shown.

- *Mass balance*:

$$\Sigma(\dot{m}_{in}) - \Sigma(\dot{m}_{out}) = \frac{dm}{dt} \tag{A.118}$$

$$m = \rho V \tag{A.119}$$

$$\frac{dm}{dt} = V\frac{d\rho}{dt} = V\left(\frac{d\rho}{dp}\frac{dp}{dt} + \frac{d\rho}{dT}\frac{dT}{dt}\right) \tag{A.120}$$

At this point, the two derivatives of density are split into the two phases, as in the equations reported in Section 4.4. Thanks to the possibility to call directly $\frac{d\rho}{dp}$ by REFPROP, Eq. (A.120) is already useful to the model. To understand the meaning of this derivative, the last equation will be rewritten by use of the ideal gases state equation, reported here

$$\rho = \frac{p}{RT} \tag{A.121}$$

which derivatives are given by Eqs. (3.123) and (3.124).

$$\Sigma(\dot{m}_{in}) - \Sigma(\dot{m}_{out}) = V\left(\frac{1}{RT}\frac{dp}{dt} - \frac{p}{RT^2}\frac{dT}{dt}\right) \tag{A.122}$$

- *Energy balance*:

$$\Sigma(\dot{m}_{in}h_{in}) - \Sigma(\dot{m}_{out}h_{out}) + \dot{Q} = \frac{d(mu)}{dt} + \dot{Q} = u\frac{dm}{dt} + m\frac{du}{dt} + \dot{Q} \tag{A.123}$$

By applying again Eq. (A.119), it follows as

$$u\frac{dm}{dt} + m\frac{du}{dt} + \dot{Q} = V\left(u\frac{d\rho}{dt} + \rho\frac{du}{dt}\right) + \dot{Q} = V\left[u\frac{d\rho}{dp}\frac{dp}{dt} + \left(u\frac{d\rho}{dT} + \rho\frac{du}{dT}\right)\frac{dT}{dt}\right] + \dot{Q} \tag{A.124}$$

The derivative of density is treated in the same way of the previous case, while the derivative of specific internal energy is represented by definition as

$$c_v = \frac{du}{dT} \tag{A.125}$$

The final form of the energy balance, expressed in Section 4.4, is rewritten as follows:

$$\Sigma(\dot{m}_{in}h_{in}) - \Sigma(\dot{m}_{out}h_{out}) + \dot{Q} = V\left[u\frac{1}{RT}\frac{dp}{dt} + \left(\rho c_v - u\frac{p}{RT^2}\right)\frac{dT}{dt}\right] + \dot{Q} \tag{A.126}$$